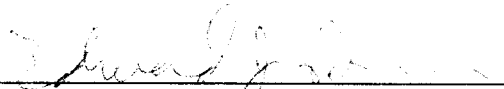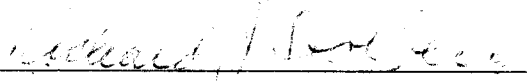THE CARBON CYCLE IN AN ANOXIC MARINE SEDIMENT:

CONCENTRATIONS, RATES, ISOTOPE RATIOS, AND DIAGENETIC MODELS

by

Marc J. Alperin

RECOMMENDED:

_____

_____

_____

_____
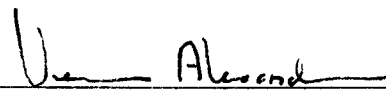
_____
Advisory Committee Chair
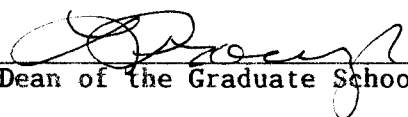
_____
Head, Graduate Program in Marine
Science and Limnology
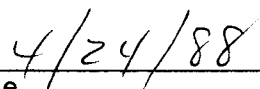
APPROVED:

_____
Dean, School of Fisheries and Ocean Sciences

_____
Dean of the Graduate School

_____
Date 4/24/88

THE CARBON CYCLE IN AN ANOXIC MARINE SEDIMENT:

CONCENTRATIONS, RATES, ISOTOPE RATIOS, AND DIAGENETIC MODELS

A

THESIS

Presented to the Faculty of the University of Alaska
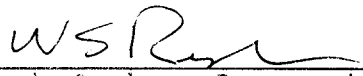
in Partial Fulfillment of the Requirements

for the Degree of

DOCTOR OF PHILOSOPHY

By

Marc J. Alperin, B. A.

Fairbanks, Alaska

May 1988

To my wife

Leslie Jean Alperin

ABSTRACT

The carbon cycle in the anoxic sediments of Skan Bay, Alaska, was investigated in order to better understand the processes that control biogeochemical transformations in an organic-rich sediment environment. Depth distributions of concentration and $\delta^{13}C$ were determined for five major carbon reservoirs: methane (CH_4), dissolved inorganic carbon (DIC), dissolved organic carbon (DOC), particulate inorganic carbon (PIC), and particulate organic carbon (POC). In addition, methane oxidation and sulfate reduction rates were measured under quasi-in situ conditions using radio-tracer techniques. Diagenetic models were applied to concentration, reaction rate, and isotope ratio depth distributions and the results were integrated into a comprehensive, depth-dependent model of the Skan Bay carbon cycle that considered advective, diffusive, and biological and chemical reactive fluxes for the five major carbon reservoirs.

The Skan Bay carbon cycle is fueled by POC, which is deposited at the sediment surface at a rate of 2290 ± 480 umol·cm^{-2}·yr^{-1}. Isotope mass-balance calculations indicate that about 60% of this material is derived from kelp while the remainder originates as phytoplankton. About 60% of the organic matter is consumed in the upper 40 cm of the sediment column. The $\delta^{13}C$-POC and $\delta^{13}C$-DOC depth distributions suggest that the material derived from kelp is more labile, accounting for greater than 60% of the total POC consumption. The products of anaerobic metabolism of POC accumulate in the DOC reservoir creating a large DOC

iv

concentration gradient at the sediment-water interface. Flux and stable carbon isotope mass-balance calculations suggest that a sizable portion (30 to 80%) of the DOC produced by degradation of POC diffuses from the sediment prior to oxidation to dissolved inorganic carbon. Methane production appears to occur primarily at depths greater than 40 cm. The CH_4 diffuses upward and is almost quantitatively oxidized to DIC in a narrow subsurface zone. Methane oxidation accounts for only 20% of the DIC production, but exerts a profound influence on the $\delta^{13}C$-DIC profile, contributing to the distinct mid-depth minimum. Pore waters are supersaturated with respect to calcite at depths greater than 10 cm, but isotope mass-balance considerations indicate that carbonate mineral formation is not occurring in these sediments.

TABLE OF CONTENTS

LIST OF FIGURES

LIST OF TABLES

The search for Truth is in one way hard and in another way easy. For it is evident that no one can master it fully nor miss it wholly. But each adds a little to our knowledge of Nature, and from all the facts assembled there arises a certain grandeur.

Aristotle

Metaphysics
a.1. 993a30-993b4

We all build more and more complicated geochemical models until no one understands anyone else's model. The only thing we do know is that our own is wrong.

R. M. Garrels

ACKNOWLEDGMENTS

The summer before moving to Alaska, I communicated with several scientists at the Institute of Marine Science regarding possible research topics. I learned of two programs with openings for a new graduate student. The first involved studying trace metal cycles in a pristine Alaskan fjord. The fjord was part of a protected national monument that happened to be the home of the world's largest deposit of molybdenum-rich ore. The federal government had given preliminary approval for mining the ore, and environmental groups were up in arms. As I understood it at the time, the research program was to gather data that would allow a rational assessment of the environmental impact of the proposed mining activity. The study promised to be controversial with important environmental, economic, and political ramifications.

In contrast, the second research program seemed to be rather arcane. Although I didn't understand the details, the study appeared to be concerned with what happens to gases in mud.

Naturally I indicated a preference for the first program. However, I received notification that I had been selected to work on the project concerned with mud-gas. As is often the case, fate had been very kind and I found myself under the auspices of Bill Reeburgh. Bill taught me the value of pure scientific inquiry, and provided an example of how the pursuit of knowledge can be every bit as exciting and rewarding as mediating man-made controversies. A graduate student is influenced by a great number of factors, but most important are the attributes of his or

her major advisor. Bill Reeburgh served as an exemplary advisor by providing inspiration, enthusiasm, advice, financial support, and a well-equipped laboratory. Most importantly, Bill provided strong, constructive guidance, but at the same time, allowed me the freedom to pursue and develop my own ideas.

I am particularly grateful to two fellow graduate students who contributed profoundly to my education. Dave Musgrave was a major influence during my initial years in graduate school. Through contact with him, I learned a great deal about the analytical approach to problem solving. Susan Sugai was always willing and able to exchange ideas, and provided steadfast support and friendship during times of frustration and discouragement.

Susan Henrichs reviewed the chapter on diagenetic modelling and her suggestions led me to modify several unfounded conclusions that I am grateful do not appear in this version. I would like to express appreciation to the members of my committee, Ed Brown, Don Schell, Dave Shaw, and Dick Stolzberg, who stuggled through the first draft of this thesis although it lacked a number of minor components (such as chapters, figures, and tables).

Ken Dunton accepted the lion's share of the responsibility for setting up and maintaining the mass spectrometer. Without his efforts, quality isotope ratio measurements would not have been possible. Steve Whalen reviewed the first draft of this thesis, and his editorial advice was responsible for trimming at least 100 pages of verbiage. John Bradbury spent a great deal of time teaching me the basics of scientific glass blowing. My experiences in the glass shop opened my eyes to a

whole world of possible applications for Pyrex tubing. Doug MacIntosh was never too busy to help me out of a jam, and I have numerous memories of his saving the day with his electronic wizardry. Chirk Chu wrote the first version of the computer programs used to solve the diagenetic equations, and provided valuable advice and assistance as the programs evolved with time.

A number of people have contributed unpublished data that appears in this thesis: Susan Sugai performed the ^{137}Cs and ^{210}Pb analyses; Susan Henrichs measured total C and N on a number of sediment and kelp samples; Al Devol provided data on alkalinity depth distributions that were useful for comparative purposes; Jeff Cornwell, Patrick Crill, and George Kipphut performed ΣH_2S analyses on the 1980, 1981, and 1982 cruises, respectively. Ken Sandbeck and Mary Lidstrom provided $^{14}CH_4$ for use in the methane oxidation rate analyses. Inter-laboratory calibration of the mass spectrometer reference gas was made possible by the efforts of Neal Blair, Dave DesMarais, and Michael Whiticar.

A very special note of appreciation is due to Chris Martens. His kindness and patience helped me through a rather protracted and somewhat awkward transition from pre-doc to post-doc.

CHAPTER 1: INTRODUCTION

Biological processes are known to have a strong influence on the chemical composition of the atmosphere, oceans, sediment, and soils. The "Gaia" hypothesis (Lovelock, 1979) extends this concept by suggesting that living organisms not only influence, but actively control, environmental conditions on earth. Elucidating the processes that regulate global chemical cycles requires abandoning traditional boundaries between scientific disciplines and adopting a holistic approach that considers biological and geological as well as chemical processes.

Biogeochemistry deals with biologically mediated interactions between the geosphere and atmosphere. Scientists generally study biogeochemical processes by quantifying mass-flow among chemical reservoirs. Broecker and Peng (1982) describe this approach as "inverse chemical engineering". According to their analogy, the earth may be viewed as a giant chemical processing plant for which blueprints do not exist. The earth incorporates many chemical reservoirs ("reactors") and mass-transfer processes ("operations") driven primarily by solar energy. The design of the processing plant can be deciphered by quantifying compositions and fluxes among reservoirs.

Carbon is the fundamental element in biological processes, representing both the "feedstock" of the global "chemical plant" and the currency of mass and energy flow. Carbon derives its predominant role from its unusual chemistry: it can form stable bonds with as many as four other carbon atoms, giving rise to an enormous number of compounds.

1

The central role of carbon in biosphere-geosphere-atmosphere interactions makes elucidation of the global carbon cycle one of the primary goals in biogeochemistry.

The global carbon cycle is so complex that it must be broken into small units for detailed examination. An area that has recently received considerable attention is the study of carbon reactions in aphotic, anoxic environments. Scientists are interested in these systems for several reasons: (a) the absence of photosynthetic carbon-fixation, aerobic respiration, and eukaryotic organisms simplifies the system making it more tractable for study, (b) they include most coastal and continental shelf sediment and therefore represent globally-significant geochemical reservoirs, and (c) they serve as models of life on ancient, anaerobic earth.

Coastal sediments that are anoxic at the sediment-water interface provide good sites for investigating the anaerobic carbon cycle. The desirable characteristics of these environments include: (a) rapid reaction rates resulting from abundant particulate material, large bacterial populations, and high substrate concentrations, (b) simplicity due to the fact that molecular diffusion, sediment accumulation, and compaction are the only physical transport processes, (c) zonation of biological processes owing to substrate depletion with depth, and (d) an intrinsic time scale (sediment depth).

Overview of the Carbon Cycle in Anoxic Marine Sediments

Carbon compounds in anoxic marine sediment may be operationally divided into five major reservoirs: methane (CH_4), dissolved inorganic

carbon (DIC), dissolved organic carbon (DOC), particulate inorganic carbon (PIC), and particulate organic carbon (POC). The carbon cycle is fuelled by sedimentation of POC of aquatic or terrestrial origin. The sediment microfauna transform this material to less complex organic and inorganic molecules which accumulate in the pore water and are recycled to the water column via diffusion. The net effect of the sediment "reactor" is conversion of POC to DOC, DIC, and CH_4.

Bacteria utilize only low molecular weight organic matter that can pass through the cell membrane. Since organic material arrives at the sediment surface as POC, it must be hydrolyzed by extracellular enzymes (exoenzymes) prior to bacterial uptake. Many exoenzymes in the natural environment are adsorbed onto mineral or organic material and thus function as immobilized enzymes (Linkins et al., 1984). Substrates produced by exoenzymatic catalysis may benefit any organism capable of utilizing the product of the depolymerization. Anaerobic POC remineralization can be considered to occur in four stages (Linkins et al., 1984; Berner, 1980):

1. **Initial metabolism.** POC is converted to high molecular weight DOC by extracellular enzymes. High molecular weight DOC is composed of biopolymers small enough to be considered "dissolved" but too large to be assimilated by bacteria.

2. **Intermediate metabolism.** High molecular weight DOC is further depolymerized by exoenzymes to intermediate molecular weight DOC. Intermediate molecular weight DOC represents monomers and

oligomers small enough to be bacterially metabolized.

3. **Fermentation.** Intermediate molecular weight DOC is converted to low molecular weight DOC, DIC, and H_2 by fermenting bacteria that use organic matter as an electron acceptor. Low molecular weight DOC consists of compounds such as short-chain fatty acids, amines, alcohols, etc.

4. **Terminal metabolism.** Low molecular weight DOC, H_2, and possibly intermediate molecular weight DOC are converted to DIC or CH_4 and H_2O by bacteria such as sulfate reducers and methanogens that use inorganic ions as electron acceptors.

Quantifying the Carbon Cycle

A quantitative description of the carbon cycle requires knowledge of material fluxes and reaction rates between major reservoirs. Two approaches have been widely used to estimate depth-dependent reaction rates in natural sediment: direct measurements and diagenetic models.

The simplest approach for direct rate measurements is the "jar experiment". The sample is isolated from the environment and the net rate of concentration change for a particular constituent is quantified by time-series analysis. Jar experiments require sample homogenization as well as long (week to month) incubation times and therefore may not provide in situ rates (Jørgensen, 1978a).

A more sensitive approach for rate measurements uses isotopically-labeled tracers. Tracers may be added directly to intact sediment and incubated for periods of only minutes to hours. The gross reaction rate

for a particular constituent is calculated from the measured pool size and fraction of tracer converted to product. Tracer experiments that employ intact sediment, short incubation times, and "trace" quantities of isotope may estimate in situ rates. However, if a portion of the measured pool is microbially "unavailable" or the added tracer is rapidly sorbed, rates estimated by tracer experiments may be erroneous.

Diagenetic models offer another approach for estimating net reaction rates in anoxic marine sediment. These models consider that concentration-depth distributions in anoxic sediment are controlled by three processes: advection, diffusion, and reaction. Since advection and diffusion are well understood physical processes, reaction rates may be estimated from concentration profiles. The advantage of models is that concentrations can be measured with relative ease and accuracy. However, models are vastly simplified, idealized representations of complex natural systems; rates predicted from models are only as valid as the assumptions used to simplify the system.

Diagenetic models may also be applied to isotope ratio depth distributions. Isotopes are nuclides having the same number of protons but a differing number of neutrons. Carbon has two stable isotopes, ^{12}C and ^{13}C, with the lighter isotope comprising 98.89% of the total carbon. Since chemical properties are primarily controlled by the number of nuclear protons, isotopes of a given element have nearly identical chemistries. However, nuclear mass does have a small effect on physical and chemical behavior. A chemical isotope effect arises primarily because molecular bonds involving different isotopes have different zero-point vibrational energies; a bond containing the lighter isotope has a

higher zero-point energy and is therefore more reactive (Hoefs, 1980).

Isotope fractionation during a chemical reaction results from equilibrium and kinetic isotope effects. Equilibrium isotope effects occur when there is isotope exchange between coexisting compounds such as AI and BI:
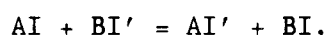
$$AI + BI' = AI' + BI,$$

where I' represents the heavy isotope of I. The equilibrium fractionation factor (α) is the same as the equilibrium constant for the isotope exchange reaction:

$$\alpha = \frac{[AI'] [BI]}{[AI] [BI']} . \qquad (1.1)$$

The general rule for equilibrium isotope effects is that the lighter isotope is concentrated in the compound containing the more stable bond (Bigeleisen, 1965).

Kinetic isotope effects occur during irreversible chemical reactions because molecules containing the lighter isotope generally react slightly faster than those containing the heavier isotope (Bigeleisen and Wolfsberg, 1958). The kinetic isotope fractionation factor (α) may be defined as the ratio of relative reaction rates of molecules containing different isotopes (Rees, 1973):

$$\alpha = \frac{RATE/[A]}{RATE'/[A']} , \qquad (1.2)$$

where RATE is the reaction rate for a particular process, A is the reacting species, and the prime represents the molecule containing the heavier isotope.

Equilibrium and kinetic isotope effects produce subtle variations

(a few percent) in carbon isotope ratios between chemical reservoirs. High-precision ratio mass spectrometers routinely resolve isotopic differences of $0.1^o/oo$ by measuring isotope ratios relative to a reference standard. The $\delta^{13}C$ value represents the relative difference in carbon isotope ratios between sample and standard:

$$\delta^{13}C \; (^o/oo) = \frac{[R(sample) - R(standard)]}{R(standard)} \; , \qquad (1.3)$$

where R is $^{13}C/^{12}C$ and the standard is belemnite carbonate from the Pee Dee formation (Craig, 1957). Samples with negative $\delta^{13}C$ values contain a greater proportion of ^{12}C than the reference material and are commonly referred to as being isotopically "light".

Natural stable isotopes of carbon serve as internal tracers of biogeochemical processes. Unlike artificial tracers, natural isotopes require no sediment manipulations or incubations thus avoiding uncertainties introduced by each. Kinetic and equilibrium isotope effects fractionate carbon isotopes in marine sediment so that most reservoirs have a distinctive range of $\delta^{13}C$ values (Fig. 1.1). Therefore, reactions between the various carbon reservoirs will leave their signatures in the $\delta^{13}C$ depth distributions.

Although models of isotope ratio depth distributions are not ideally suited for estimating reaction rates, they provide a means of constraining errors in rates estimated by other techniques. For example, diagenetic models that reproduce the basic features of the $\delta^{13}C$ depth distributions substantiate the reaction rates incorporated in the models. In addition, an isotope mass-balance provides an independent check on the accuracy of the overall carbon budget. Stable isotope
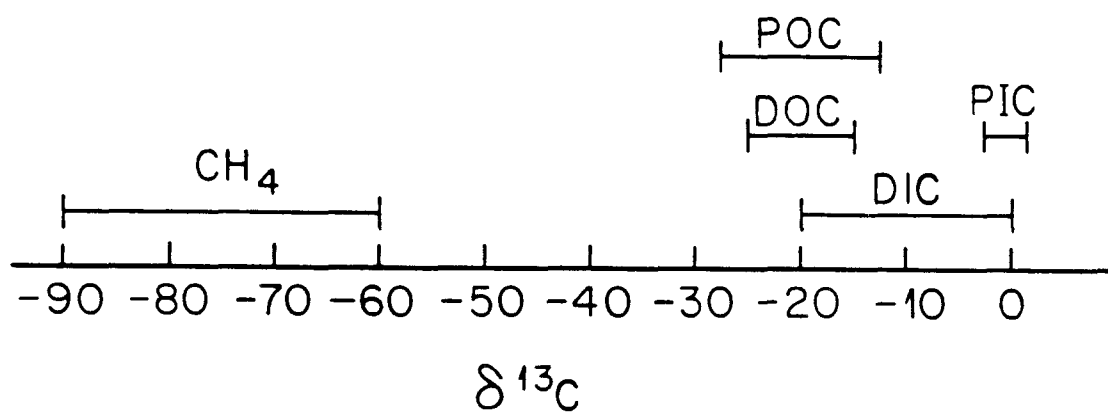
Fig. 1.1. Typical ranges of $\delta^{13}C$ values for carbon reservoirs in recently deposited anoxic marine sediments. Values are based on data from Deines (1980) and Craig (1953).

ratios also provide information as to the sources for a given reservoir, and when coupled with reaction rates, allow predictions of isotope fractionation factors in natural systems.

The two approaches for describing carbon cycling rates, direct measurements and diagenetic models, are complementary. Each provides independent and unique information regarding processes that make up the carbon cycle. No single technique is ideally suited to elucidating the complex series of reactions responsible for POC remineralization in anoxic marine sediment. Only through an eclectic approach can the details of the carbon system be resolved.

Previous Studies

Most studies of carbon cycling in anoxic marine sediment have focused on terminal metabolism (Stage 4) because it is most suited to rate estimation using tracer experiments, jar experiments, and models. Initial metabolism (Stage 1) has been quantified in a number of studies, although the mechanisms are poorly understood. A few studies have investigated fermentation processes (Stage 3) in natural anoxic marine sediment. Very little is known regarding intermediate metabolism (Stage 2), although this stage may be the rate limiting step in organic matter remineralization. (The four stages of POC remineralization were defined on pp. 3 and 4.)

The following literature review is not intended to be comprehensive. Rather, recent examples of unique or representative studies of organic matter remineralization are described. Extensive reviews of anaerobic carbon remineralization processes may be found in Capone and

Kiene (1987), Jørgensen (1983), Krumbein and Swart (1983), and Reeburgh (1983).

Initial Metabolism

Solubilization of POC is the first step in organic matter remineralization. Owing to the variety and complexity of the organic material, in situ rates of POC hydrolysis have not been directly measured. POC consumption has been studied primarily by diagenetic modelling of POC concentration profiles (Murray et al., 1978; Martens and Klump, 1984; and others). POC consumption was assumed to follow first-order kinetics with respect to "metabolizable" organic matter (defined as the difference between total POC and POC at depth, where concentration becomes constant). First-order rate constants were calculated by fitting an exponential function to the POC depth distributions. Martens (1984) showed that this model was very sensitive to the interface concentration of metabolizable POC and required "tuning" with independent rate or flux data to give reliable results.

Orem et al. (1986) analyzed solid phase organic matter from anoxic sediment using ^{13}C nuclear magnetic resonance (NMR) spectroscopy. They found that the labile fraction of the POC was primarily composed of polysaccharides, which constituted a decreasing fraction of the total POC with increasing depth.

King (1986) amended sediment with fluorescent analogs of disaccharides in order to investigate the properties of exoenzymes that catalyze polysaccharide hydrolysis. This technique is not suitable for determining in situ rates but is useful for elucidating the effects of

various environmental parameters on the exoenzyme system.

Intermediate Metabolism

The high molecular weight DOC must be decomposed to intermediate molecular weight DOC prior to bacterial uptake. However, rates of intermediate molecular weight DOC production have not been measured in anoxic marine sediment. Studies have been limited to qualitative and quantitative examinations of the high molecular weight fraction (mol wt > 500) of the DOC reservoir. Spectroscopic analyses showed that high molecular weight DOC is primarily composed of polysaccharides and peptides (Orem et al., 1986; Nissenbaum et al., 1971). The bulk of the DOC reservoir (75 to 95%) was shown to be high molecular weight material (Orem et al., 1986; Krom and Sholkovitz, 1977).

The high molecular weight DOC may also be produced by "geopolymerization" reactions, i.e. abiogenic condensation of intermediate molecular weight DOC (Nissenbaum et al., 1971; Krom and Westrich, 1980). However, there is little direct evidence that condensation reactions occur in recently deposited anoxic sediment (Orem et al., 1986).

Fermentation

Fermenting bacteria partially decompose monomers and oligomers derived from carbohydrate and protein to low molecular weight DOC, H_2, DIC, and NH_4^+. Fermentation rates in anoxic marine sediment have been studied from the perspective of substrate utilization and end-product release.

Studies of substrate utilization have used tracer experiments to determine amino acid oxidation rates. Christensen and Blackburn (1982)

found that the alanine turnover rate exceeeded the ammonia production rate suggesting that a portion of the measured alanine reservoir was microbially unavailable. No information exists regarding monosaccharide fermentation rates in anoxic marine sediment, although this process may be of extreme importance (Fenchel and Blackburn, 1979).

Studies of fermentation end-product release have focused on a variety of substrates. Numerous studies have used jar experiments, tracer experiments, or models to quantify NH_4^+ production rates in anoxic marine sediment (summarized in Reeburgh, 1983). Novelli et al. (1987) have estimated net and gross H_2 production rates with models and jar experiments. Sansone (1986) used tracer experiments to measure rates of acetate production from lactate, propionate, pyruvate, and butyrate.

Terminal Metabolism

In the final stage of anaerobic carbon remineralization, bacteria convert organic substrates to DIC and CH_4 using inorganic ions as electron acceptors. Numerous studies (reviewed in Reeburgh, 1983) have employed jar experiments, tracer experiments, and models to quantify consumption of electron acceptors (NO_3^-, Mn(IV), Fe(III), SO_4^{2-}, and HCO_3^-), consumption of organic substrates (volatile fatty acids and CH_4), and production of end products (DIC and CH_4).

Study Objectives

The goal of this study was to quantify processes involved in the carbon cycle in an anoxic marine sediment. Several approaches were used in order to over-determine the system and pinpoint deficiencies in our understanding of carbon remineralization processes. The approaches were

selected to minimize artifacts caused by sediment manipulation. Tracer experiments were used to measure CH_4 oxidation and SO_4^{2-} reduction rates; modelled reaction rates were estimated from concentration–depth distributions for the five major carbon reservoirs (CH_4, DIC, DOC, PIC, and POC); and stable isotope models were used to check the accuracy of the reaction rates, estimate source strengths for certain carbon reservoirs, and predict kinetic isotope fractionation factors for anaerobic CH_4 oxidation.

The depth-dependent concentrations and reaction rates for each of the five carbon reservoirs were combined to form a comprehensive model of the carbon cycle in an anoxic marine sediment. This model provides a framework for understanding biogeochemical processes in anoxic marine sediment and a "blueprint" for a portion of the global "chemical processing plant".

CHAPTER 2: STUDY SITE AND ANALYTICAL METHODS

This chapter describes the environment, sampling methods, and analytical techniques used in this study. The field site (Skan Bay, Ak.) is representative of frequently studied anoxic marine sediments, having comparable carbon content, temperature, and particle deposition rate (Reeburgh, 1983). Sediment was sampled using a box corer to obtain adjacent replicate cores, and a gravity corer to obtain deeper sediment. The following analyses were conducted: (a) porosity, (b) CH_4 concentrations and oxidation rates, (c) SO_4^{2-} concentrations and reduction rates, (d) concentrations and stable isotope ratios for the five major carbon reservoirs (CH_4, DIC, DOC, PIC, and POC), (e) X-radiography, (f) ^{137}Cs and ^{210}Pb dating, and (g) ΣH_2S concentrations. Estimates of analytical precision (reported as relative standard deviation) and accuracy are provided for each analytical technique.

Study Site

Skan Bay is a two-armed pristine embayment on the northwest side of Unalaska Island in the Aleutian Chain. The southwestern arm (Fig. 2.1) is relatively narrow (1.2 km at its widest point) and has a broad sill (10 m) across the inlet. The sill is vegetated with kelp of the genus _Alaria_ (K. Dunton, Univ. of Texas, Port Aransas, personal communication). The basin of the southwestern arm has steep walls and functions as a sediment trap collecting terrestrial debris, kelp fragments, and particulates from pelagic primary production.
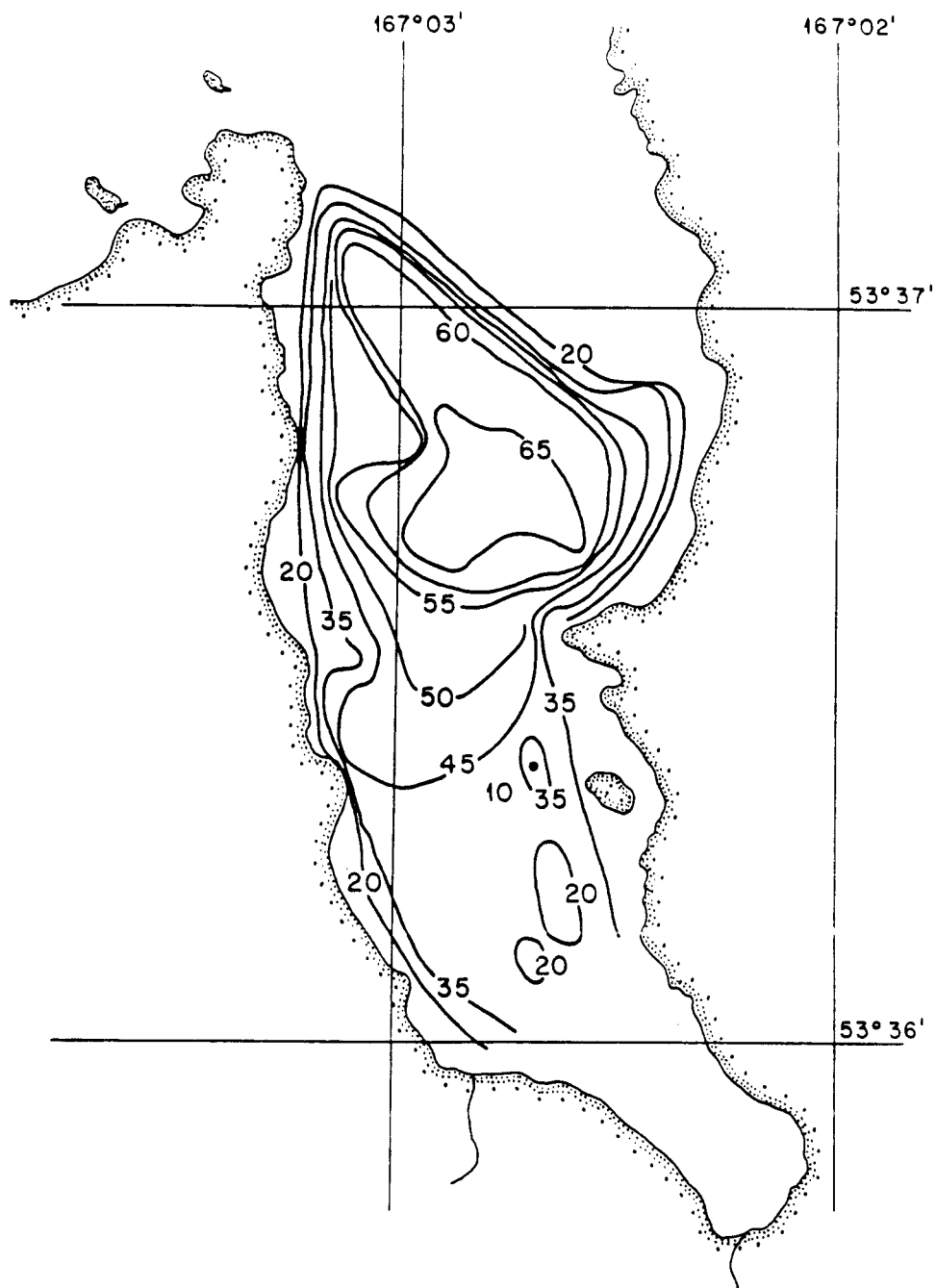
Fig. 2.1. Map of Skan Bay, Alaska. The study site is located within the 65 m isopleth.

The broad, shallow sill prevents horizontal advection of oxygen-rich Bering Sea water into the basin. During the summer months, stable temperature and salinity gradients are established in the upper 30 m (Fig. 2.2a), effectively isolating deeper water. Because of its proximity to shore and funnel-like shape, the deep basin receives a relatively high flux of organic material. This high flux of organic matter, coupled with restricted circulation, results in seasonal depletion of O_2 within the water column (Fig. 2.2b).

There were four research cruises to Skan Bay between 1980 and 1984. The cruises occurred during September in order to take advantage of maximum depletion of water column oxygen. Consequently, little is known of the seasonal variability within the basin. Water column temperature and oxygen conditions during September show interannual consistency (Table 2.1). The temperature data show a sharp thermocline extending down to 30 m with late September bottom water ranging from $2.9^{\circ}C$ in 1984 to $4.4^{\circ}C$ in 1982. By month's end, air temperatures in the Skan Bay region drop markedly (Fig. 2.3a) suggesting that September bottom water temperatures represent the annual maximum. Winter air temperatures rarely drop below $0^{\circ}C$ (Fig. 2.3a) indicating that bottom water is unlikely to cool below $1^{\circ}C$. Thus, the deep basin of Skan Bay is a relatively isothermal environment with an annual temperature range of about $3^{\circ}C$. During September, the water below 50 m has an O_2 concentration of <1 $ml \cdot l^{-1}$ (Table 2.1). Only in 1984 did the bottom water become anoxic during the sampling period. Bottom water renewal presumably occurs during the winter when high winds (Fig. 2.3b) generated by Aleutian storms mix the water column.
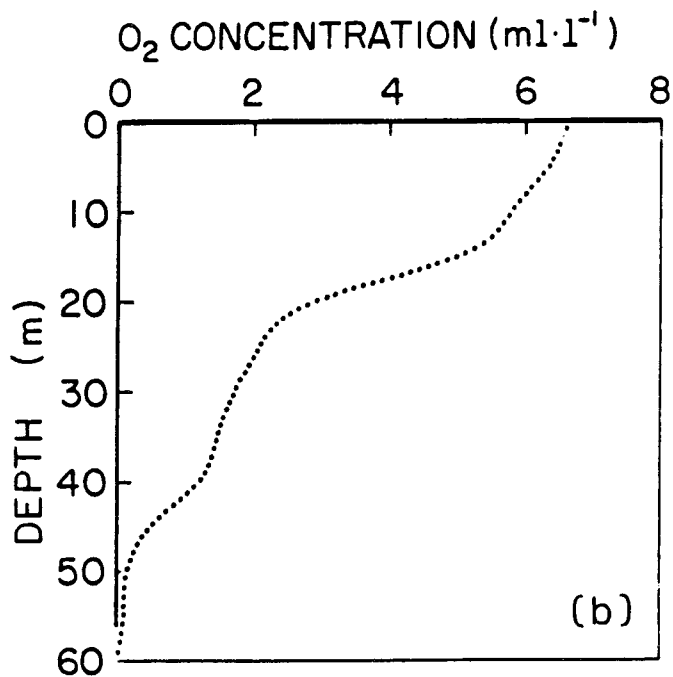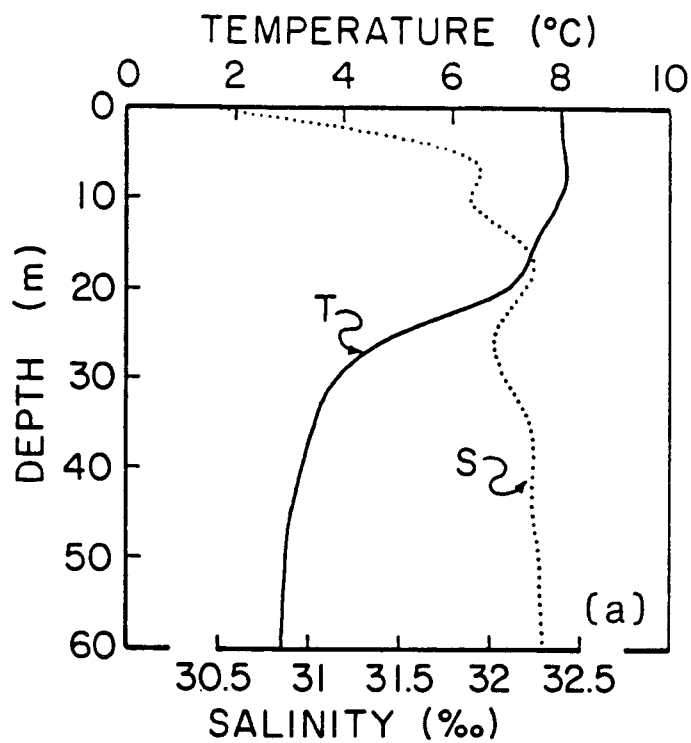
Fig. 2.2. Typical September profiles for Skan Bay water column. (a) Temperature and salinity, (b) dissolved O_2.

Table 2.1. Late September water column conditions in Skan Bay.

===

	Year			
	1980	1981	1982	1984
Approx. thermocline depth (m)	0-35	0-30	0-30	10-25
Bottom water temperature ($^\circ$C)	4.1	4.1	4.4	2.9
Bottom water O_2 (ml$\cdot$l^{-1})	0.5-0.8	NA	0.2-0.8	0-0.4

NA = data not available.
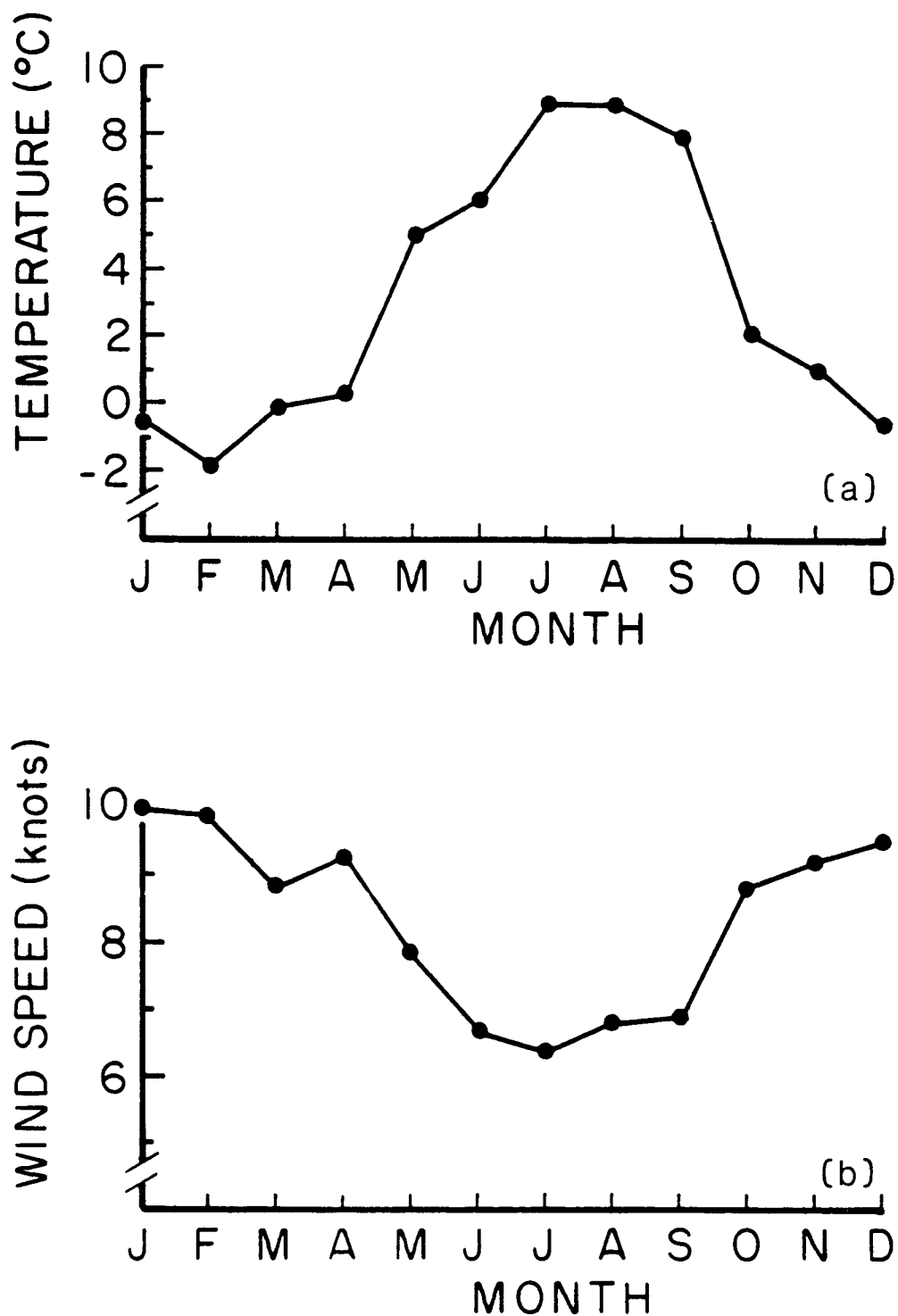
Fig. 2.3. Climatic data for the Skan Bay region. (a) Mean monthly air temperature, (b) mean monthly scalar wind speed. (Source: Climatic Atlas of Outer Continental Shelf Waters and Coastal Region of Alaska, Vol. 11, Bering Sea.)

The station occupied for the sediment studies was located in the deepest portion of the basin (65 m). The basin surface is circular with an area of about 50,000 m^2. The flocculent surface sediment has a high water content (>98% [w/w]) and a noticeable H_2S odor. The sediment is black from the surface to 40 cm, becoming dark gray thereafter.

Sediment Sampling

Sediment was obtained to a depth of 40 cm using a box corer (Ocean Instruments, Inc.) capable of sampling a 30 x 30 cm sediment section. After core retrieval, water overlying the sediment was siphoned until about 5 cm of bottom water remained. Up to nine subcores could be taken from the box core by gently inserting clear plastic core liner (6.6 cm i.d.) into the sediment. The core liner was capped on top and bottom (Caplug #45), gently removed from the box corer, and placed in a water bath in the dark at near in situ temperature. Subcores showing any sign of disturbance, i.e. turbidity at the sediment-water interface, CH_4 ebullition, etc., were discarded. Sediment to a depth of 1 m was sampled using a gravity corer (Benthos, Inc.) containing the core liner described above. The coring device, sampling date, and core designation for sediment used in each analysis are summarized in Table 2.2.

Sampling Artifacts

Any coring procedure can compress high porosity sediment causing an expulsion of pore water and an error in the depth scale. Compression may be minimized by careful insertion of core liner into sediment sampled by the box corer. Comparison of profiles for sediment sampled with the box corer and gravity corer showed that the upper 10 to 20 cm of the gravity

Table 2.2. Coring devices, sampling dates, and core designations.

```
=====================================================================
                 Coring        Sampling                   Subcore
   Analysis       Device         Date       Core #       Designation
----------------  -------------  ----------  -------  -----------------

 Porosity and    gravity corer  23 Sept. 82   82-1
Whole Sediment     box corer    27 Sept. 84   84-BC6     84-C, 84-D
   Density         box corer    27 Sept. 84   84-BC7        84-F

   Methane         box corer     8 Sept. 84   84-BC1   84-H, 84-I, 84-J
Concentrations     box corer     9 Sept. 84   84-BC2   84-K, 84-L, 84-M
                 gravity corer   9 Sept. 84    84-1
                 gravity corer  10 Sept. 84    84-2
                   box corer    10 Sept. 84   84-BC3   84-N, 84-O, 84-P
                   box corer    19 Sept. 84   84-BC4   84-Q, 84-R, 84-S

   Methane
  Oxidation        box corer    19 Sept. 84   84-BC4   84-T, 84-U, 84-V
    Rates

   Sulfate         box corer    21 Sept. 84   84-BC5   84-W, 84-X, 84-Y
Concentrations

   Sulfate
  Reduction        box corer    21 Sept. 84   84-BC5      84-Z, 84-AA,
    Rates                                                    84-BB

Stable Carbon    gravity corer  23 Sept. 82   82-1
 Isotopes and      box corer    27 Sept. 84   84-BC6     84-A, 84-B
  Pool Sizes       box corer    27 Sept. 84   84-BC7        84-E

X-radiography      box corer    16 Sept. 80   80-BC3

  137Cs            box corer       Sept. 80                 80-WP
                   box corer    27 Sept. 84   84-BC6        84-B

  210Pb            box corer       Sept. 80                 80-WP
                   box corer    27 Sept. 84   84-BC6     84-C, 84-D

  ΣH2S             box corer       Sept. 80   80-BC1     80-A, 80-B
                   box corer       Sept. 81   81-BC1        81-A
                   box corer       Sept. 82   82-BC2        82-A

---------------------------------------------------------------------
```

core were severely compressed. The depth scale for a profile measured on a gravity core was established by alignment with a similar profile from a box core. While this procedure does not ensure an accurate depth scale, it allows consistent depth correlations for all cores used in this study.

When a core was retrieved, CH_4 bubbles formed at depths greater than 25 to 30 cm, where high CH_4 concentrations led to partial pressures in excess of one atmosphere. Gentle handling of subcores sampled from the box corer usually prevented CH_4 ebullition. Retrieval of gravity cores was often accompanied by ebullition owing to deeper sediment and higher CH_4 concentrations. The bubbling resulted in loss of CH_4 from the sample and disturbance of the upper sediment.

Porosity

Porosity ($\emptyset$), the ratio of pore water volume to whole sediment volume, provides a means of relating concentrations of solid phase and pore water constituents. Porosity is calculated from solid matter density (ρ_{SM}), pore water density (ρ_{PW}), and sediment water content (WC). Solid matter density was measured by Quantachrome Corp. on two dried, finely ground sediment samples (from depths of 3-6 cm [$2.33 \, g \cdot ml^{-1}$] and 27-30 cm [$2.34 \, g \cdot ml^{-1}$]) using a gas displacement technique. The densities were corrected for the salt contribution assuming the salt's density to be the same as NaCl. Pore water density was assumed to equal bottom water density which was calculated from temperature and salinity data. Water content, defined as the ratio of pore water mass to whole sediment mass, was measured by drying a known mass of whole sediment to

constant weight (approximately 24 hours at 80°C) and reweighing. The water content was calculated as:

$$WC = \frac{(\text{mass whole sediment} - \text{mass dry sediment})}{\text{mass whole sediment}} \cdot \frac{\rho_{PW}}{\rho_{WATER}},$$

where ρ_{WATER} is the density of air saturated H_2O at 25°C. Porosity was calculated as:

$$\phi = \frac{WC \cdot \rho_{SM}}{\rho_{SM} \, WC + (1-WC)\rho_{PW}}.$$

Precision and Accuracy

Triplicate analyses for porosity had a relative standard deviation of $\leq \pm 0.5\%$. Inaccuracies caused by incomplete drying were found to be negligible by additional drying of selected samples. Violation of the implicit assumptions of constant pore water and solid matter density are not expected to introduce significant error.

Methane Concentrations

Sediment CH_4 concentrations were determined at sea by a headspace equilibration technique and later in the lab as part of the carbon concentration and stable isotope ratio analyses. The procedures for the headspace equilibration technique are described here.

Triplicate subcores from each box core were obtained using core liner with tape-covered perforations at 3 cm intervals. Gravity core 84-1 was taken using solid core liner; sediment was subsequently trans- ferred to core liner containing taped holes. However, CH_4 ebullition was stimulated by extruding sediment from one core liner into another. To avoid this problem, gravity core 84-2 was sampled using core liner

containing taped holes.

Within an hour of coring, water just above the sediment surface was sampled by piercing the tape-covered perforation with a 3 ml plastic syringe equipped with a hypodermic needle. Sediment was sub-sampled using a tip-less 3 ml plastic syringe. The tape was peeled from a perforation and the syringe barrel was inserted into the sediment while the piston was held stationary. The plastic syringe was then removed from the sediment, the exterior wiped clean, and the volume adjusted to 3.0 ml. The sample was immediately transferred to a 37.5 ml serum vial containing 5.0 ml distilled-deionized water (DDW), sealed with a gray butyl-rubber stopper, capped with an aluminum crimp, and thoroughly homogenized with a Vortex mixer. Samples were allowed to equilibrate at room temperature for 1 h during which time they were Vortex-mixed twice.

Standards were prepared while samples were equilibrating. Serum vials were filled with 8.0 ml DDW (equivalent to 5.0 ml DDW plus 3.0 ml sediment), capped with gray butyl-rubber stoppers, crimped, and injected with known volumes of pure CH_4. Six standards were prepared that spanned the range of concentrations found in the sediment (0 to 5.0 $mmol \cdot l^{-1}$ whole sediment [mM_{WS}] for the sediment obtained from a box core and 0 to 13 mM_{WS} for sediment obtained by a gravity corer). The volume of CH_4 added to the most concentrated standard was about 3% of the serum vial headspace so standard and sample pressures were similar. The standards were Vortex-mixed along with the samples and in every way treated identically. Since samples and standards were at the same temperature and had equal volumes of aqueous phase and headspace, corrections for the quantity of dissolved CH_4 were not necessary.

Methane was quantified by injecting 100 ul of headspace gas into a Hewlett-Packard 5710A gas chromatograph (GC) equipped with flame ionization detector (FID). The column, 6' x 1/8" stainless steel packed with Poropak QS, was maintained at 50°C. The carrier gas was He flowing at 40 ml min^{-1} and the retention time for CH_4 was about 0.6 min. Peak areas were quantified with an electronic integrator.

The volume of CH_4 in a sample was calculated from a least-squares, linear regression of the standard data. Two regression curves were prepared: for the few samples containing less CH_4 than the most dilute standard (equivalent to concentrations less than 0.25 mmol·l^{-1} pore water [mM$_{PW}$]), the calibration was based on the blank and the first standard; for samples containing greater quantities of CH_4, all six standards were used in the regression.

The whole sediment CH_4 concentration was calculated from the following equation:

$$[CH_4]_{WS} = \frac{P\ V_M}{V_{WS}\ R\ T}\ ,$$

where V_M is the volume of CH_4 in the serum vial, V_{WS} is the volume of whole sediment analyzed, P and T are the atmospheric pressure and temperature, respectively, at the time the standards were prepared, and R is the molar gas constant. The whole sediment CH_4 concentration is converted to pore water concentration units by:

$$[CH_4]_{PW} = \frac{[CH_4]_{WS}}{\phi}\ .$$

Precision and Accuracy

The instrumental precision of the CH_4 analysis, as measured by the relative standard deviation of triplicate GC injections of sample or standard, was always better than 3%. The accuracy depends on a number of factors including systematic errors introduced during sampling, sample preparation, and GC analysis. Methane bubble formation gave the deeper sediment a porous texture that made sampling difficult and probably resulted in some CH_4 loss. Because samples and standards were prepared and treated identically, systematic errors resulting from sample preparation were probably small. The most likely preparation error was a lack of equilibrium between the headspace and aqueous phase. Kiene and Capone (1985) have shown that for sediment treated as described above, CH_4 equilibrates between the headspace and aqueous phase within several minutes. The accuracy of the GC analysis depends on instrumental linearity and stability, and the accuracy of the standards. The calibration curves were linear ($r^2 \geq 0.9994$ [n=6], except on 10 Sept. 1984 when $r^2 = 0.978$ [n=6]) and the GC was generally very stable. Standards injected periodically throughout the analysis drifted by <3%, except on 10 Sept. when the variability averaged about 10%. Each standard was prepared independently and two or three different size syringes were used for each series of six standards. Assuming that CH_4 used to make the standards was chemically pure, the linearity of the standard calibration curves suggests that standards were accurate.

Methane Oxidation Rates

Methane oxidation rate experiments were designed to mimic natural

conditions as much as possible and to avoid disruption of microbial associations. All measurements required for the rate calculation were from the same sample, eliminating errors caused by lateral heterogeneity in the sediment. Methane oxidation rates were measured on triplicate subcores from a box corer using a modification of Reeburgh (1980); details of the modifications are described in Alperin and Reeburgh (1985).

Briefly, samples were obtained as described above, except that sediment was sub-sampled using incubation syringes constructed of Pyrex (borosilicate glass) barrels and Teflon pistons equipped with o-ring seals (Fig. 2.4). The incubation syringes were filled with sediment (6.4 ml), capped with black butyl-rubber stoppers secured with aluminum crimps, and immediately placed in a rotating rack submerged in $4^{\circ}C$ sea water. The syringes were removed from the water bath, injected with 1 uCi (50 ul) gaseous $^{14}CH_4$ (sp. act. 45 mCi·mmol^{-1}), returned to the water bath within 3 to 4 min, and allowed to incubate for 20 to 25 h. The fraction of $^{14}CH_4$ tracer oxidized during the incubation was <1.3%. The incubation was terminated by immersing the syringes in a 2-propanol bath at $-60^{\circ}C$. Samples were stored frozen until analysis (<2 d).

The stripping line is diagrammed in Fig. 2.5. Samples were transferred as frozen plugs to Pyrex stripping vessels containing NaOH solution. Methane was stripped from the slurry, dried, and collected on molecular sieve 5A at $-60^{\circ}C$. Methane was released from the molecular sieve by heating, quantified and oxidized to CO_2 with the FID, dried with a Drierite column, and collected in CO_2-trapping scintillation cocktail (Woeller, 1961). Following CH_4 collection, H_2SO_4 was injected into the reaction vessel. The acid released CO_2 was purged from solution,
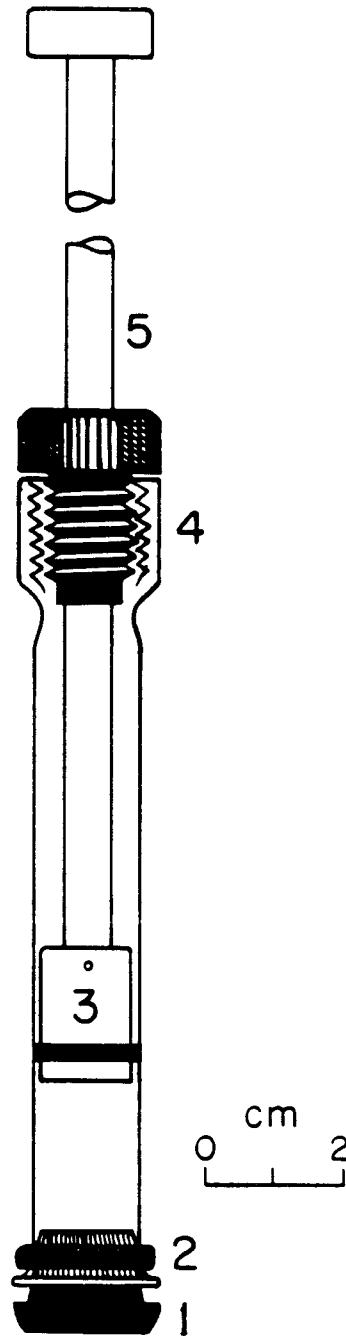
Fig. 2.4. Gas-tight syringe for sediment incubations. (1) Black butyl-rubber stopper, (2) o-ring to provide gripping surface for aluminum crimp seal, (3) Teflon piston with o-ring seal, (4) Ace Thred tubing adaptor, (5) piston handle made of Delrin.

Drierite

M.S.5A

$^{14}CH_4$

Flow Meter

$-60^{\circ}C$

Drierite

$CuSO_4-$
Chomosorb

Woellers
Solution

$^{14}CO_2$
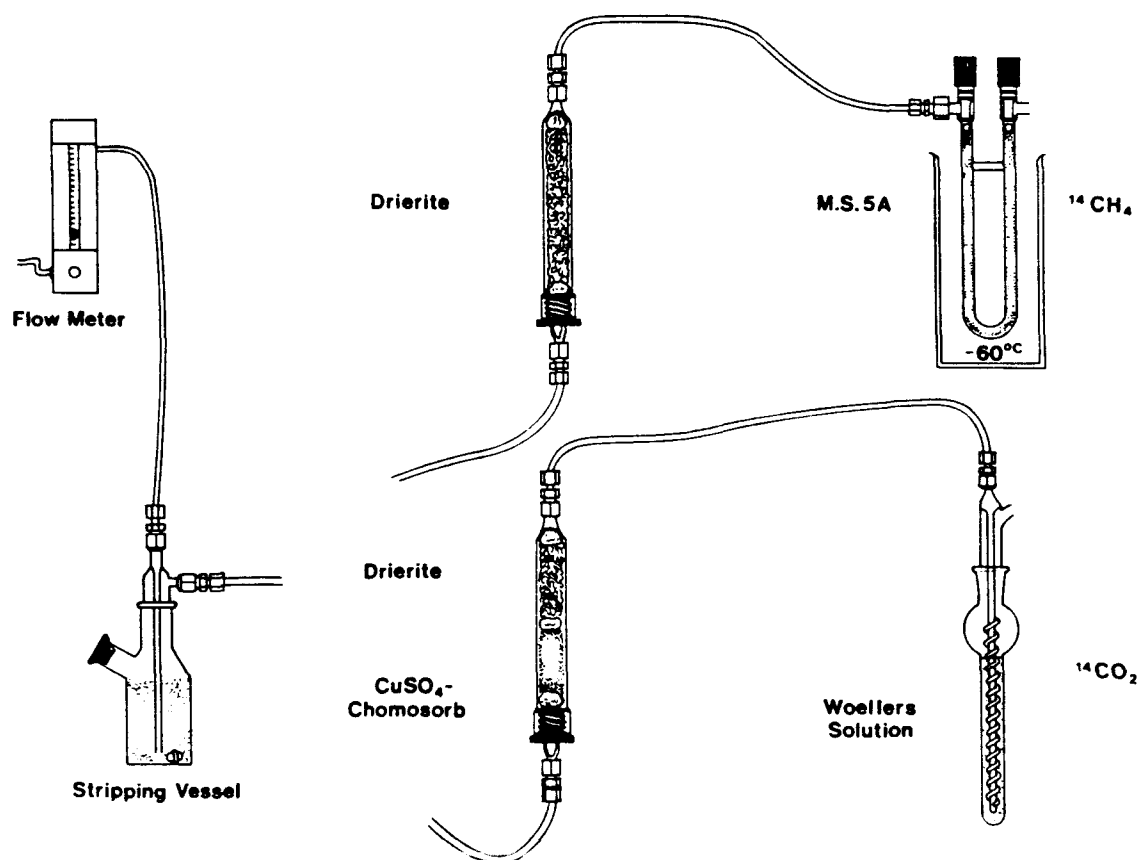
Stripping Vessel

Fig. 2.5. Stripping line for methane oxidation rate analysis. Frozen sediment was transferred to the stripping vessel. Methane was stripped from the basified sediment, dried by passage through a Drierite column, and concentrated on a molecular sieve 5A (M.S. 5A) column at low temperature. Stable and radioactive methane were quantified by warming the column, flushing the contents into an FID, and collecting the effluent in scintillation cocktail. The sediment was then acidified and carbon dioxide was stripped from the sediment and purified by a cupric sulfate-Chromosorb/Drierite column. The radioactive CO_2 was collected in scintillation cocktail (Woeller's Solution).

purged of H_2S and water by a column containing $CuSO_4$-coated Chromosorb and Drierite, and trapped in Woeller's solution. Samples were counted with a shipboard Beckman LS-100 scintillation counter; quench corrections were determined with external standard ratios.

The $^{14}CH_4$ was checked for radiochemical purity with a GC proportional counter and found to contain trace amounts of $^{14}C_2H_6$ ($^{14}C_2H_6/^{14}CH_4=0.00031$). The amount of $^{14}C_2H_6$ introduced to each sample with the $^{14}CH_4$ was too small to bias the rate measurements appreciably.

The CH_4 oxidation rate was calculated following Jørgensen (1978a):

$$RATE = \frac{[CH_4]_{PW} \, (^{14}CO_2)}{\alpha \, (^{14}CH_4) \, t} , \qquad (2.1)$$

where $[CH_4]_{PW}$ is the pore water CH_4 concentration, $(^{14}CO_2)$ and $(^{14}CH_4)$ are the activities (dpm) of recovered $^{14}CO_2$ and added $^{14}CH_4$, respectively, t is the incubation time, and α is the isotope fractionation factor. Models of stable isotope depth distributions show that $^{12}CH_4$ is oxidized 0.73 to 2.6% faster than $^{13}CH_4$ (see p. 148). Since isotope discrimination of $^{14}CH_4$ will be approximately twice that for $^{13}CH_4$ (Stern and Vogel, 1971), a value of 1.036 (1.8% x 2 = 3.6%) is used for the fractionation factor in eq. 2.1.

Uncertainty in Results

The precision and accuracy of natural rate measurements are inherently difficult to quantify. Analytical precision cannot be directly measured because the analysis consumes the entire sample and no two natural samples are identical. Methane oxidation rates measured on replicate samples homogenized by slurrying with an equal volume of

anoxic saline solution had a relative standard deviation of $\pm16\%$ (n=4). However, slurrying the sediment reduced CH_4 oxidation rates by as much as two orders of magnitude (Alperin and Reeburgh, 1985). Measurements of such slow rates are bound to be less precise than measurements of rates encountered in natural sediment.

Five quantities are required to calculate the CH_4 oxidation rate (see eq. 2.1): (a) CH_4 concentration, (b) activity of added $^{14}CH_4$, (c) activity of $^{14}CO_2$ produced, (d) incubation time, and (e) the isotope fractionation factor. An estimate of the analytical error in the overall rate measurement can be obtained by examining the error in each of these parameters. The CH_4 concentration measured in each incubation syringe agreed with profiles from the same box core measured by the headspace method, indicating that errors in this parameter were small. Uncertainty in the activity of $^{14}CH_4$ added to each incubation syringe was about $\pm10\%$ (based on the relative standard deviation of activity of tracer recovered, n=28). Preliminary experiments showed that errors in the $^{14}CO_2$ activity caused by non-quantitative retention in the NaOH solution, leakage from the stripping line, or incomplete stripping were <5%. The incubation time was known with great certainty ($\pm0.1\%$), and the isotope fractionation factor is so close to unity that a $\pm100\%$ uncertainty would not appreciably affect the rate results.

The greatest source of error in any measurement of natural biological reaction rates comes from the system manipulations necessary to conduct the experiment. Metabolic rates are extremely sensitive to environmental perturbations, hence every precaution was taken not to alter key parameters such as temperature, anaerobicity, sediment-

microbial associations, and substrate availability. Temperature was kept constant by limiting air contact of sealed syringes to <5 min. Gas-tight glass syringes and high concentrations of $\Sigma H_2 S$ maintained sediment anoxia during the 1 d incubation. Sediment-microbial associations were maintained by sampling intact sediment. Sediment was incubated under headspace-free conditions so that CH_4 remained in solution and available to bacteria. Relatively short incubation times assured that other substrates were not appreciably depleted.

Despite these precautions, it is not realistic to assume a priori that measured rates accurately represent in situ rates. As with any analysis, the best assurance of accuracy is agreement between independent methods of measurement. The other method of direct rate determination, a jar experiment, is impractical for methane oxidation as incubation times would be prohibitively long. However, rates can be estimated indirectly from diagenetic models. Modelled and measured concentration profiles were in agreement (see p. 138), indicating that experimental rates were accurate to within 25%.

Sulfate Concentrations

Pore water profiles of SO_4^{2-} concentration for triplicate subcores from a box corer were determined using ion chromatography. Sediment sampling followed the same procedure as for CH_4 concentration except that sub-sampling was done using tip-less 10 ml plastic syringes.

About 10 ml of sediment was transferred to a plastic centrifuge tube, gassed with N_2, and capped with a rubber stopper. The sediment was centrifuged for 15 min and 3.0 ml of supernatant was pipetted to a glass

scintillation vial containing 50 ul concentrated HCl. The acidified pore water was bubbled with N_2 for 5 min to remove acid volatile sulfur compounds and the vials were tightly capped and stored at $4^{o}C$ until analysis (2 to 3 months).

Sulfate was quantified using a Dionex 2000i ion chromatograph (IC) equipped with a conductivity detector. Prefiltered samples (0.45 um Millipore filter) were injected into the IC with an automated 15 ul Teflon sampling valve. Standard eluent (3.0 mM $NaHCO_3$, 2.4 mM Na_2CO_3) flowed through guard and separator columns at 2.7 ml·min^{-1}. The retention time for SO_4^{2-} was consistently 9.2 to 9.3 min. After chromatographic separation, the ions passed through a cation exchange resin and the anions were converted to their acids. This process, known as "post-column chemical supression", enhanced the conductivity associated with the anions and reduced that of the eluent. Samples were diluted 1:50 with eluent to reduce interference from the abundant chloride ion. Peak areas were measured by an integrating recorder.

Six standards were prepared which spanned the range of pore water SO_4^{2-} concentrations (0.7 to 27 mM). The standards were prepared by serial dilution of a primary SO_4^{2-} standard in a solution containing Cl^-, Br^-, and PO_4^{3-} that matched the anion matrix of the acidified pore water. Two regression lines were used to calculate SO_4^{2-} concentrations: for the few samples containing less than 2.5 mM_{PW} SO_4^{2-}, the calibration curve was based on the blank and the most dilute standard; for all other samples, all six standards were used in the regression. Concentrations were corrected for dilution resulting from addition of HCl to each sample.

Precision and Accuracy

The precision of the SO_4^{2-} concentration analysis (based on the mean relative standard deviation of triplicate determinations of 12 samples) was $\pm 1.9\%$ (range: 0.3 to 6.8%) with the relative precision best for the most concentrated samples. Instrumental drift was corrected by running standards after every second sample. Replicate analysis of three samples at different times and on different days agreed within the limits of the analytical precision. The SO_4^{2-} concentration in a blank prepared by centrifuging, acidifying, and purging DDW, was <0.05 mM. An independent standard ($[SO_4^{2-}]$=13.6 mM) was prepared to check the accuracy of the primary standard. The average measured value of the independent standard was 13.3 ± 0.2 mM (n=5), indicating that the standards were accurate to within 2.2%.

Sulfate Reduction Rates

Sulfate reduction rates were measured using a modification of the radiotracer method (Jørgensen, 1978a). The modifications were similar to those employed in the CH_4 oxidation rate analysis (described in Alperin and Reeburgh, 1985).

Three subcores from a box core were sub-sampled using the glass incubation syinges, injected with 5 uCi (50 ul) anoxic $Na^{35}SO_4$ solution (sp. act. 1.5×10^6 mCi·mmol^{-1}), and incubated at 4°C for 24 h. Maximum turnover of the SO_4^{2-} pool was <5%. The incubation was terminated by immersion in the -60°C alcohol bath, and samples were stored frozen until analysis (1 to 2 d).

The stripping line was similar to the CH_4 oxidation rate analysis.

Samples were transferred as frozen plugs into the stripping vessels containing anoxic DDW and subsequently acidified with anoxic HCl. The H_2S was stripped from the slurry using O_2-free carrier gas (N_2 passed through a Cu column at 200^oC), passed through a column packed with glass wool to trap aerosols, and collected as ZnS in a trap containing anoxic zinc acetate solution. An aliquot was counted in a gel formed with a xylene-based scintillation cocktail (Aquasol-2).

After stripping was complete, the slurries were allowed to settle and an aliquot of the aqueous phase was counted; total tracer recovery averaged $95\pm8\%$ (n=37). The SO_4^{2-} reduction rate was calculated by analogy with eq. 2.1. Sulfate concentrations were based on averages of three subcores taken from the same box core. The isotope fractionation factor (1.045) was the mean of the range of values estimated by Jørgensen (1978a).

Uncertainty in Results

The precision of the SO_4^{2-} reduction rate analysis, as determined by the relative standard deviation of 8 samples of slurried sediment, was $\pm8\%$. The difficulties of evaluating the accuracy of measured SO_4^{2-} reduction rates are similar to those for CH_4 oxidation rates and will not be restated. However, SO_4^{2-} reduction rate measurements have several unique sources of error that deserve discussion. First, the concentration and radiotracer data used to calculate the SO_4^{2-} reduction rates came from different subcores. Although all subcores were from the same box core, horizontal variability in the SO_4^{2-} concentration averaged about $\pm7\%$ (see p. 77). Second, H_2S (the product of SO_4^{2-} reduction) may

rapidly react to form elemental sulfur or pyrite, neither of which are acid volatile. Howarth and Jørgensen (1984) have shown that for subtidal marine sediments, 20 to 30% of the reduced $^{35}SO_4^{2-}$ may be converted to elemental sulfur or pyrite. Rapid pyrite or sulfur formation would lead to underestimated SO_4^{2-} reduction rates. However, modelled and measured SO_4^{2-} profiles differed significantly (see p. 151) suggesting that estimated rates may be overestimated by more than 100%.

Stable Carbon Isotopes and Pool Sizes

Concentrations and stable isotope ratios were measured on five sedimentary carbon pools: CH_4, DIC, DOC, PIC, and POC. Sediment cores were sampled at 3 cm intervals which provided a high resolution data set (13 samples per 40 cm core) and sufficient material for isotope ratio analysis. Concentrations and isotope ratios for all five reservoirs were determined for each sample.

Sediment samples were stored frozen in steel cans and analyzed in the laboratory. The analytical scheme is outlined in Fig. 2.6. Methane was removed from the can using a gas-tight headspace sampler. The gas was purified, combusted to CO_2 and H_2O, repurified, and quantified. The contents of the can were transferred to a sediment squeezer and the pore water was collected in a reaction vessel. The pore water was acidified and the DIC was stripped, purified, and quantified. The DOC in the acidified pore water was oxidized with $K_2S_2O_8$ and the resulting CO_2 extracted, purified, and quantified. The solid material was removed from the squeezer, dried, ground to a fine powder, and an aliquot was transferred to a reaction vessel. PIC was converted to CO_2 by acidification,
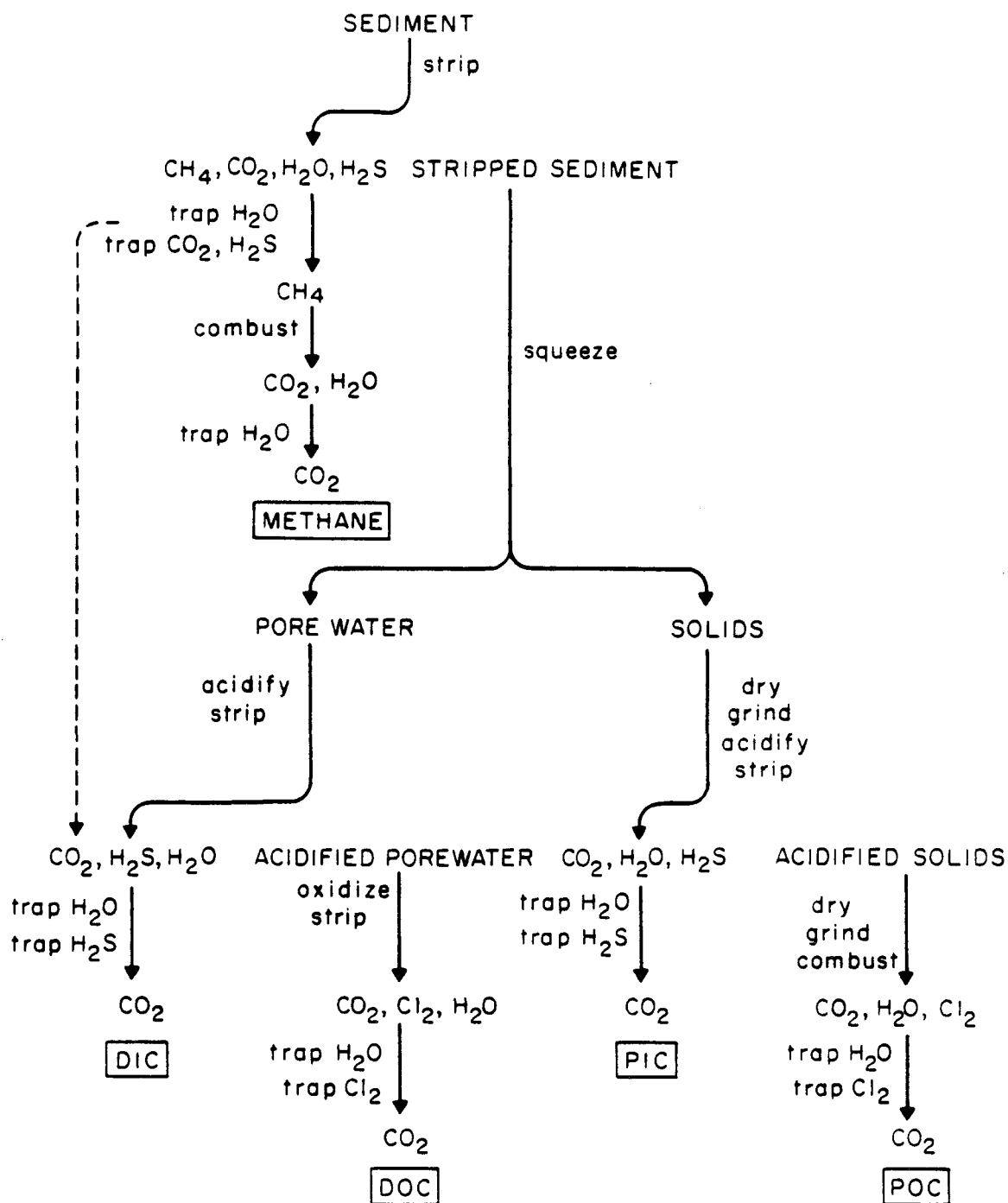
Fig. 2.6. Operational flow chart for concentration and stable isotope ratio analyses of five major carbon reservoirs: METHANE, DIC, DOC, PIC, and POC.

purified and quantified. POC was determined by combustion of the solid material in a quartz bomb using CuO as the oxidant; the resulting CO_2 was purified and quantified. For each carbon pool, an aliquot of the purified CO_2 was analyzed for $^{13}C:^{12}C$ ratios using a ratio mass spectrometer. A detailed description of the procedure is given below.

Sampling of Sediment, Bottom Water, Particulates, and Kelp

Subcores from two box cores were sampled by extruding the sediment upward into a 3 cm segment of core liner. The 0-3 cm segment, which was composed of high porosity flocculent material, was transferred to the a N_2-flushed 600 ml lacquered steel can (#303) using a 50 ml plastic syringe with the tip partially removed. For the deeper, more viscous sediment, a metal shim was inserted beneath the segment and the sediment was quickly transferred to the can. (The can had been previously cleaned with a mild detergent, rinsed with tap water, repeatedly flushed with DDW, dried, and wrapped in aluminum foil for storage.) The rim of the can was wiped clean, the lid was put in place, and the can sealed.

The cans were sealed using a manual can sealer (Ives-Way Products, Inc.). Four sealed cans were leak tested by immersion in hot soapy water. The absence of bubbles at the seams indicated a successful seal.

The entire process of sampling and canning was completed within 3 h of the time the core was taken. The cans were placed in a shipboard freezer as soon as a core was completely sampled and stored frozen until analysis (1 to 1.5 yr).

Sediment deeper than 40 cm was sampled using a gravity corer. Immediately after retrieval, the core was capped and placed upright in a

walk-in freezer. The core was sampled by extruding the frozen sediment from the core liner and slicing it at 3 cm intervals. The frozen segments were transferred to N_2-flushed steel cans (#307), sealed, and stored frozen until analysis (ca. 4 yr).

Bottom water was siphoned from a box core using Tygon tubing held about 10 cm above the sediment surface. The water was stored frozen in a glass jar until analysis (ca. 1.5 yr).

Water column particulate material was collected from 25 m with a submersible pump. Fifteen liters of seawater was filtered through a glass fiber filter. The filter was stored frozen in a plastic bag until analysis (ca. 1.5 yr).

Kelp was sampled by collecting floating fragments that had broken from the holdfast. Kelp collected in 1980 and 1981 was dried and stored at -15°C until analysis. Kelp collected in 1982 was stored frozen and divided into stipe and blade fractions prior to drying.

Vacuum Manifold Design

The manifold is a gas-tight vacuum system capable of quantitatively converting gaseous, dissolved, and particulate organic and inorganic carbon to CO_2, the carbon species required for isotope ratio analysis. The system serves to remove contaminants from the CO_2 gas, quantify the purified CO_2, and provide a sample for introduction to the mass spectrometer.

The manifold (Fig. 2.7) is composed of two main sections: the circulating loop and the reservoir section. The circulating loop contains an inlet and outlet for sample connection, an inlet and outlet
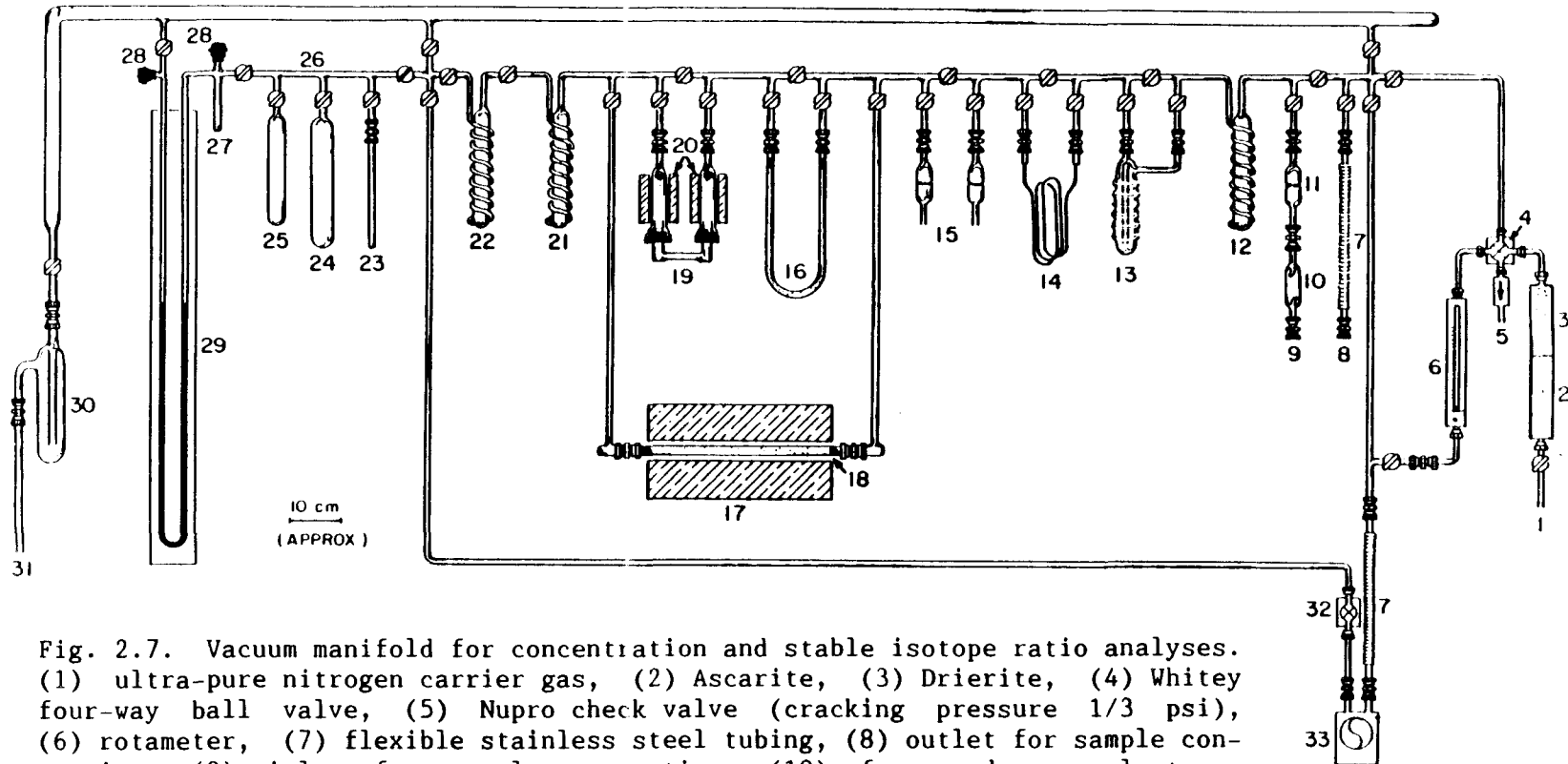
Fig. 2.7. Vacuum manifold for concentration and stable isotope ratio analyses. (1) ultra-pure nitrogen carrier gas, (2) Ascarite, (3) Drierite, (4) Whitey four-way ball valve, (5) Nupro check valve (cracking pressure 1/3 psi), (6) rotameter, (7) flexible stainless steel tubing, (8) outlet for sample connection, (9) inlet for sample connection, (10) foam and aerosol trap, (11) glass frit aerosol trap, (12) water trap, (13) carbon dioxide trap #1, (14) carbon dioxide trap #2, (15) POC evacuation ports with glass frit particulate traps, (16) hydrogen sulfide trap, (17) tube furnace, (18) methane combustion tube, (19) chlorine trap, (20) Nichrome wire heating element, (21) carbon dioxide trap #3, (22) carbon dioxide trap #4, (23) sample removal port, (24) Reservoir #4 (503.9±0.8 ml), (25) Reservoir #3 (148.5±0.2 ml), (26) Reservoir #2 (30.69±0.10 ml), (27) Reservoir #1 (13.56±0.03 ml), (28) vacuum gauge tube, (29) mercury manometer, (30) pump vapor back-streaming trap, (31) rotary vacuum pump, (32) Nupro metering bellows valve, (33) metal bellows circulating pump.

for carrier gas (ultra-pure N_2 scrubbed of CO_2 and H_2O by a column containing Ascarite and Drierite), and a series of traps and furnaces for sample preparation and purification. A circulating system was selected over a unidirectional stripping line to minimize cumulative contamination by trace impurities in the carrier gas. The reservoir section contains four calibrated volumes (approximately 14, 31, 149, and 504 ml), a mercury manometer, and a sample removal port. The volumes of the reservoirs were calibrated by acidifying $CaCO_3$ using a procedure analogous to the PIC method described below. The volume of each reservoir was known with a relative precision of $\pm0.3\%$ (n=4).

The manifold was primarily constructed of 9 mm Pyrex tubing. All stopcocks were Teflon, high vacuum valves (Kontes, model #826500-0004) suitable for vacuum applications at pressures to 5×10^{-7} mm Hg. All removable connections were made with Cajon Ultra-Torr unions. Where flexibility was needed, Cajon flexible stainless steel tubing was employed. Gases were circulated with a metal bellows pump (Metal Bellows Corp., model MB-21) and flow was metered using a Nupro bellows valve. The tube furnace (Lindberg, model #55035) had a Vycor combustion tube suitable for routine heating to $850^{o}C$. A belt-driven vacuum pump (Sargent-Welch Duo-seal, model #1400) was used to lower pressures in the manifold to 10^{-2} mm Hg. A liquid nitrogen cooled trap upstream of the vacuum pump prevented backstreaming of vapors from the pump and lowered the background pressure of condensible gases in the manifold to undetectable levels. The manometer was made from 2 mm i.d. heavy-walled capillary tubing. The height of the mercury column was read with a cathetometer (Precision Tool and Instrument Co.) capable of measuring

the distance between the two columns of mercury with a precision of ± 0.05 mm. A thermocouple vacuum gauge (Veeco, TG-70) operating in the range 10^{-3} to 1 mm Hg was used to determine pressures too low to be measured manometrically.

Material and Solution Preparation

All glassware was cleaned with detergent and tap water, and rinsed with 10% (v/v) HCl followed by DDW. Pyrex glassware was baked at $500^{o}C$ for 6 h; glass fiber filters and jars made of soft glass were baked at $450^{o}C$ for 8 h; glassware made of quartz and Vycor were baked at $850^{o}C$ for 6 h. Copper oxide used in the CH_4 and POC analyses was combusted at $850^{o}C$ for 6 h. Materials made of Teflon (stopcock shafts and magnetic stir bars) and stainless steel (Swagelok and Cajon fittings, spatulas, and tubing) were cleaned with DDW. The sediment squeezer components were completely disassembled after each use, throughly washed with tap water followed by DDW, and stored submerged in a beaker of DDW. The squeezer was dried just prior to use in a drying oven at $80^{o}C$.

All solutions were prepared using DDW stripped of DOC by refluxing through an alkaline permanganate solution. The DOC concentration in this water was about 5 uM. Solutions were purged of DIC by stripping with N_2 at 500 ml min^{-1} for several hours. The carbonate-free NaOH solution was prepared according to Kolthoff et al. (1969). Carbon-free solutions were stored in glass carboys sealed with vacuum stopcocks.

Methane Analysis

Thawing the sample. The can containing the sediment was removed from the freezer and thawed by immersion in hot water. The can was

checked for leaks by examining the seam for a stream of bubbles. Since the sediment had been preserved only by freezing, metabolic activity could resume as the sediment thawed. The first several steps of the analysis were performed as rapidly as possible to minimize the effect of post-thawing metabolism.

The **headspace sampler.** After the sediment had thawed, the can was thoroughly shaken to equilibrate CH_4 between the sediment and headspace. Methane was flushed from the can using the headspace sampler shown in Fig. 2.8. This device is composed of an upper brass plate containing a 2" x 3/16" silicone rubber o-ring, a lower aluminum plate with a recessed slot to position the can, and three threaded rods to hold the upper and lower plates together. Three wing-nuts tightened against the top of the headspace sampler pulled the brass plate against the can's lid and sealed the o-ring. Cannulae served as the inlet and outlet for the carrier gas. These were made from 1/4" stainless steel tubing sharpened to a point on the bottom and sealed on the top with toggle-operated bellows valves (Nupro, model SS-4BK). The outlet cannula had an inline filter (Nupro, model SS-4TF with 60 um sintered stainless steel element) that removed particulates from the gas stream and prevented fouling of the bellows valve. Two bored-through 1/4" o-seal straight-thread connectors (Swagelok) attached to the headspace sampler provided a seal around the cannulae. The standard conical ferrules in the straight-thread connectors were replaced with 1/4" o-rings which permitted axial movement of the cannula after the fittings were sealed.

The cans were penetrated by forcing the sharpened end of each cannula through the lid of the can. Quantitative recovery of known
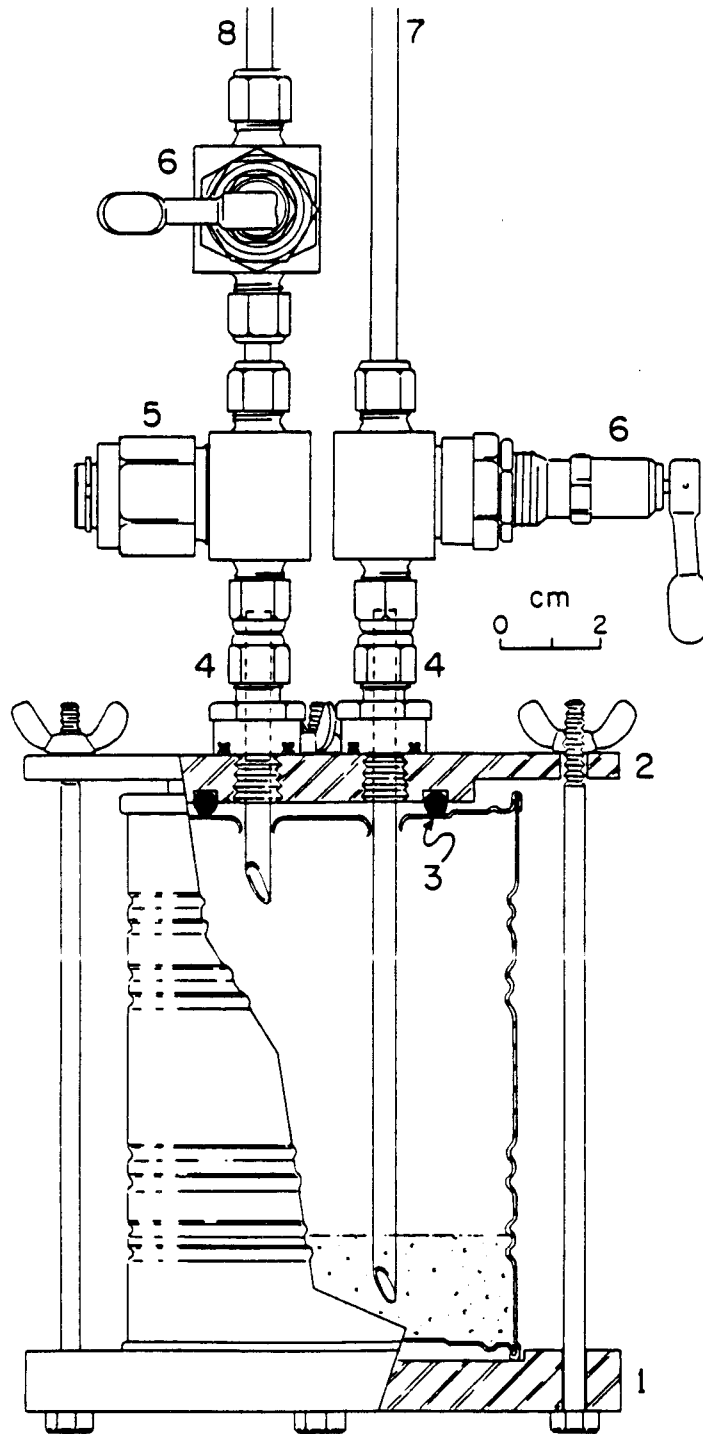
Fig. 2.8. Headspace sampler for removal of methane from the can. (1) Lower plate, (2) upper plate, (3) silicone o-ring, (4) bored-through o-seal straight thread connectors, (5) inline filter, (6) bellows valves, (7) inlet cannula, (8) outlet cannula.

amounts of CH_4 injected into the can demonstrated that the headspace sampler provided gas-tight penetration.

Stripping and combustion of CH_4. The headspace sampler was attached to the manifold and CH_4 was stripped from the sediment with N_2 flowing at 100 ml·min^{-1}. Water was removed by a trap cooled to $-89^{\circ}C$ (2-propanol slurry), and CO_2 was collected in two traps cooled to $-196^{\circ}C$ (liquid nitrogen bath).

Inside the sealed can, the fraction of CH_4 in the gas phase (f) is controlled by the headspace volume (H), the aqueous phase volume (A), and the Bunsen solubility coefficient (β) (Flett et al., 1976):

$$f = H/(H+\beta A).$$

Given the volume of the can (615 ml), the volume of sediment (103 ml), and the Bunsen solubility coefficient (0.02640 at $24^{\circ}C$, $32^{\circ}/oo$ salinity, Yamamoto et al., 1976), about 99.5% of the CH_4 equilibrated in the headspace. The characteristic stripping time (defined as the time required for the concentration of CH_4 in the headspace to decrease by a factor of 1/e) for a well mixed gas volume (V) being flushed at a flow rate (F) is $t = V/F$ (Weiss and Craig, 1973). Seven characteristic stripping times are required to remove 99.9% of the CH_4 from the can. At a flow rate of 100 ml·min^{-1}, the characteristic stripping time is 5.2 min. Thus, a stripping time of 40 min is sufficient to quantitatively flush CH_4 from the can.

Methane was combusted to CO_2 and H_2O by passage through a 25 cm x 16.6 mm i.d. Vycor tube packed with wire form CuO heated to $800^{\circ}C$. Attachment of an FID to the effluent of the combustion tube demonstrated that combustion efficiency was greater than 99.9% for all quantities of

CH_4 encountered in this study. The combustion products were collected in two traps cooled to $-196^{o}C$, the first trap collecting more than 95% of the CO_2.

When CH_4 stripping and combustion were complete, the noncondensible gases were pumped from the circulating loop and the CO_2 was transferred to the reservoir section of the manifold. The H_2O resulting from CH_4 combustion was retained in a trap cooled to $-89^{o}C$ and collected for future hydrogen isotope ratio analysis. The CO_2 was allowed to expand into a volume yielding a pressure between 50 and 600 mm Hg, quantified by measuring the pressure and temperature, and flame-sealed in a 20 cm x 1/4" o.d. Pyrex tube.

Contaminants. The CH_4 analysis is not specific for CH_4 but includes any carbon compound having a significant vapor pressure at liquid nitrogen temperature $(-196^{o}C)$. There are few naturally occurring carbon compounds that do not condense at $-196^{o}C$. Ethane and carbon monoxide are the two most likely to be present in recently deposited sediments. There are no data on carbon monoxide in anoxic marine sediments but concentrations are likely to be small relative to CH_4. Likewise, the ratio of ethane to CH_4 is less than 10^{-3} (Whiticar and Faber, 1986) in recent sediments where the CH_4 is of biogenic origin.

Preliminary experiments showed that about 20% of the DIC was purged from the sediment during the CH_4 analysis. Because CH_4 has low concentrations and is isotopically light relative to DIC ($[CH_4]/[DIC]=0.002$ in the surface sediments; $\delta^{13}C-CH_4=-70^o/oo$, $\delta^{13}C-DIC=-10^o/oo$), it is important that CH_4 and CO_2 be quantitatively separated. If 0.1% of the DIC were to escape entrapment, it would lead to an artificial increase

in the CH_4 concentration of 10% and cause an isotopic bias as large as $6^o/oo$. Although the vapor pressure of CO_2 at -196^oC is infinitesimally small, at the high flow rates used in this study, quantitative CO_2 entrapment is difficult because: (a) the short residence time of the gas stream in the trap; (b) lack of thermal equilibrium between the trap and the liquid nitrogen bath; and (c) solid CO_2 aerosol transport out of the trap.

Two CO_2 traps in series were employed (Fig. 2.7; #13 and #14). The primary trap was constructed of Pyrex and contained a sintered glass frit on the outlet that was kept submerged in liquid nitrogen. This trap had a large volume (100 ml) and was "ribbed" to improve mixing of the gas stream. If the gas in the trap was well mixed, the average residence time was about 3 min. The sintered glass frit on the outlet served to retain particulate CO_2 carried in the gas stream. The secondary CO_2 trap was constructed of six 20 cm long loops of 1/8" stainless steel tubing that were kept half submerged in liquid nitrogen (DesMarais, 1983). The high surface area to volume ratio and stainless steel construction assured rapid heat transfer between the carrier gas and the liquid nitrogen bath. By submerging the loops only half-way in liquid nitrogen, each loop functioned as an independent trap (D. DesMarais, NASA Ames, personal communication). The primary trap collected most the CO_2 and prevented clogging of the secondary trap, which served to catch traces of CO_2 that escaped the primary trap. Blanks run with and without DIC present were identical, indicating that negligible quantities of CO_2 were escaping the two traps.

Methane may be trapped as a clathrate at -196^oC if H_2O vapor is

present in the gas stream (N. Blair, North Carolina State Univ., personal communication). Thus, H_2O must be completely removed before the gas stream encounters the CO_2 traps. Methane standards run with and without H_2O present gave identical recoveries and $\delta^{13}C$ values indicating that CH_4 was not being trapped in the CO_2 traps.

DIC Analysis

Particulate-dissolved separation. Pore water was separated from solid material using a gas-operated (Ultra-pure N_2) sediment squeezer (Reeburgh, 1967). The sediment was quickly transferred from the can to the squeezer to minimize contact with air. Pore water was filtered through two precombusted 0.6 um glass fiber filters (Whatman EPM 1000) directly into a N_2-flushed reaction vessel (Fig. 2.9). The Pyrex reaction vessel (approximate volume 180 ml) had vacuum o-ring stopcocks on the inlet and outlet and a sintered-glass gas dispersion tube to accelerate the gas stripping process. Just prior to squeezing the sediment, the reaction vessel was flushed with N_2 and filled with 30 ml of carbon-free 0.01 N NaOH solution which served to trap the DIC. Atmospheric CO_2 was prevented from contacting the pore water by an Ascarite trap attached to the outlet of the reaction vessel.

Stripping of DIC. The reaction vessel was attached to the manifold and the pore water was acidified with 10 ml carbon-free H_3PO_4 (2 N). The acid was added to the reaction vessel using an in-line reservoir placed between the manifold outlet and the reaction vessel inlet. A small magnetic Teflon-coated stir bar throughly mixed the pore water and the acid solution. The resulting CO_2 was stripped from solution (N_2 flowing
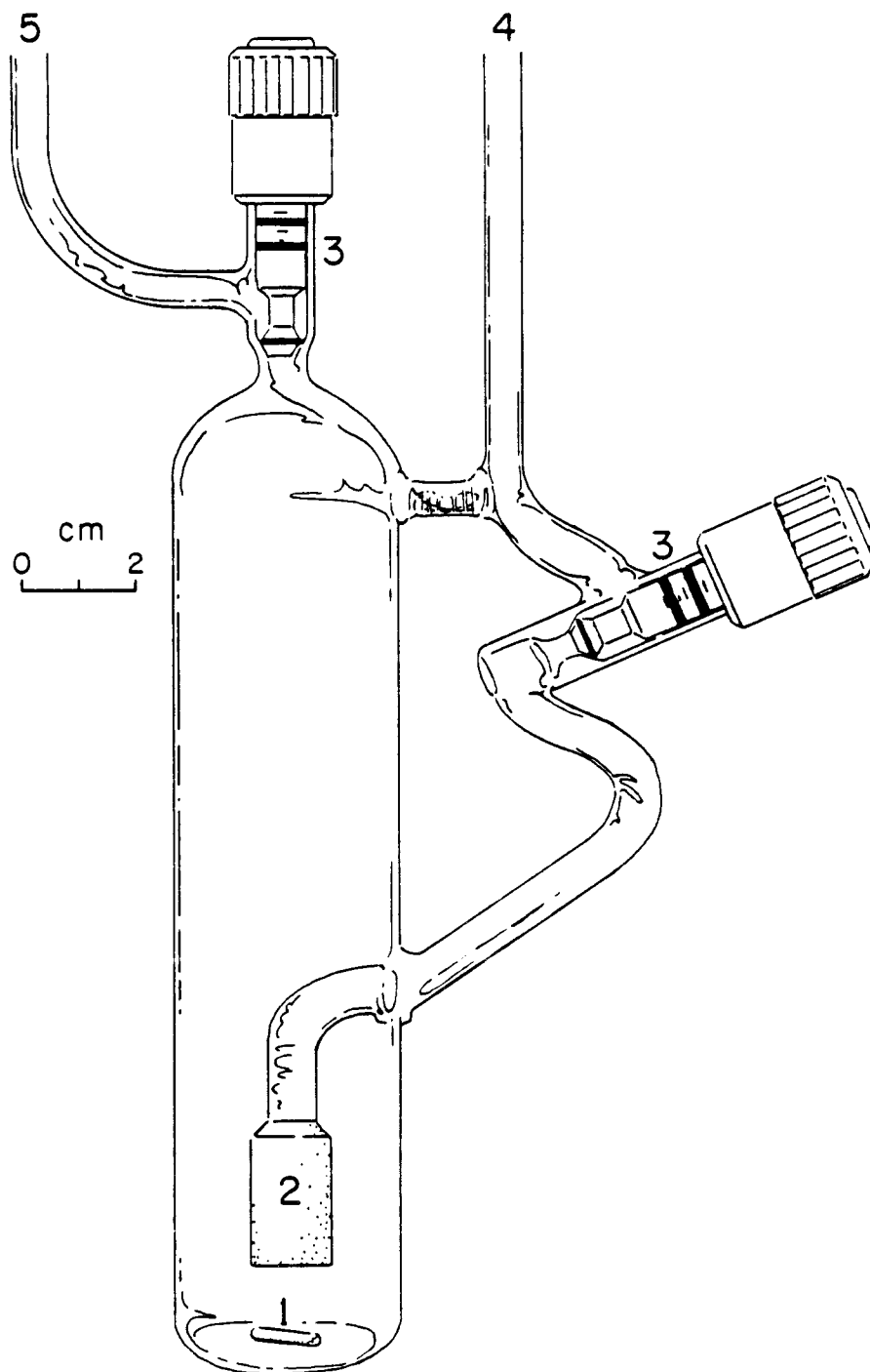
Fig. 2.9. Pyrex reaction vessel for DIC and DOC analyses. (1) Teflon-coated magnetic stir bar, (2) sintered-glass gas dispersion tube, (3) vacuum o-ring stopcocks, (4) gas inlet, (5) gas outlet.

at 100 ml·min^{-1}) and combined with the DIC collected during the CH_4 analysis. Water was removed with a trap cooled to $-89^{\circ}C$ and H_2S was trapped in a U-tube packed with $CuSO_4$-coated Chromosorb. Protocol for collection and quantification of the DIC was the same as for CH_4.

The characteristic stripping time (t) for a dissolved gas is given by $t=\beta VP/F$ (Weiss and Craig, 1973) where β is the Bunsen solubility coefficient, V is the volume of solution, P is the pressure inside the stripper, and F is the flow rate of carrier gas. For CO_2 dissolved in sea water at room temperature, $\beta=0.7$ atm^{-1} (Stumm and Morgan, 1970), V=100 ml, P=1 atm, and F=100 ml min^{-1}. This gives a characteristic stripping time of 0.7 min. Removal of dissolved CO_2 from solution is complete within 5 min, but additional time is required to purge the gas from the reaction vessel headspace. Tests showed that a 40 min stripping period completely removed DIC from the reaction vessel.

Contaminants. The efficiency of the H_2S trap was tested by mass spectrometry. DIC samples from actual sediment analyses were monitored for an ion current at m/e=34. No peak was detected, indicating that samples were H_2S-free.

DOC Analysis

Oxidation of DOC and stripping. DOC was oxidized using a procedure similar to Wilson (1961). Potassium persulfate (Baker "Instra-Analyzed") was ground to a fine powder and 5.0 g was transferred to the reaction vessel containing the acidified, stripped pore water. The stopcocks were closed and the reaction vessel was placed in a boiling water bath for 30 min. A magnetic stir bar mixed the solid oxidant into solution. The

useful oxidation time is limited by the decomposition of $S_2O_8^{2-}$. At the temperature and pH used in the above procedure, the half-life of $S_2O_8^{2-}$ is <6 min (Goulden and Anthony, 1978).

The cooled reaction vessel was attached to the manifold and the CO_2 was purged by flowing N_2 at 100 ml·min^{-1} for 40 min. Water was retained by a trap cooled to -89^oC and the Cl_2, produced by Cl^- oxidation, was trapped on Cuprin (Coleman) heated to 200^oC. Collection and quantification of the CO_2 was as previously described.

Contaminants. Large quantities of Cl_2 were produced during the oxidation. The efficiency of the Cl_2 trap was tested by comparing blanks with permanganate distilled water to those with $35^o/oo$ NaCl solution. (The NaCl was combusted at 550^oC for 8 h to remove traces of organic matter.) Equivalency of these two blanks indicated that the Cl_2 trap was quantitative.

PIC Analysis

Preparation of solid material. The solid (squeezed) portion of the sediment was removed from the squeezer and the glass fiber filters discarded. The sediment was dried at 70^oC for 24 h and ground to a fine powder. About 3 g dried sediment was transferred to a reaction vessel (Fig. 2.10) consisting of a gas stripping bottle (approximate volume 100 ml) with a standard taper (40/50) ground glass joint. This reaction vessel also had a sintered-glass gas dispersion tube to facilitate stripping of dissolved gases.

Acidification and stripping of the PIC. The reaction vessel was attached to the manifold and 58.5 ml of carbon-free 0.4 N H_3PO_4 was
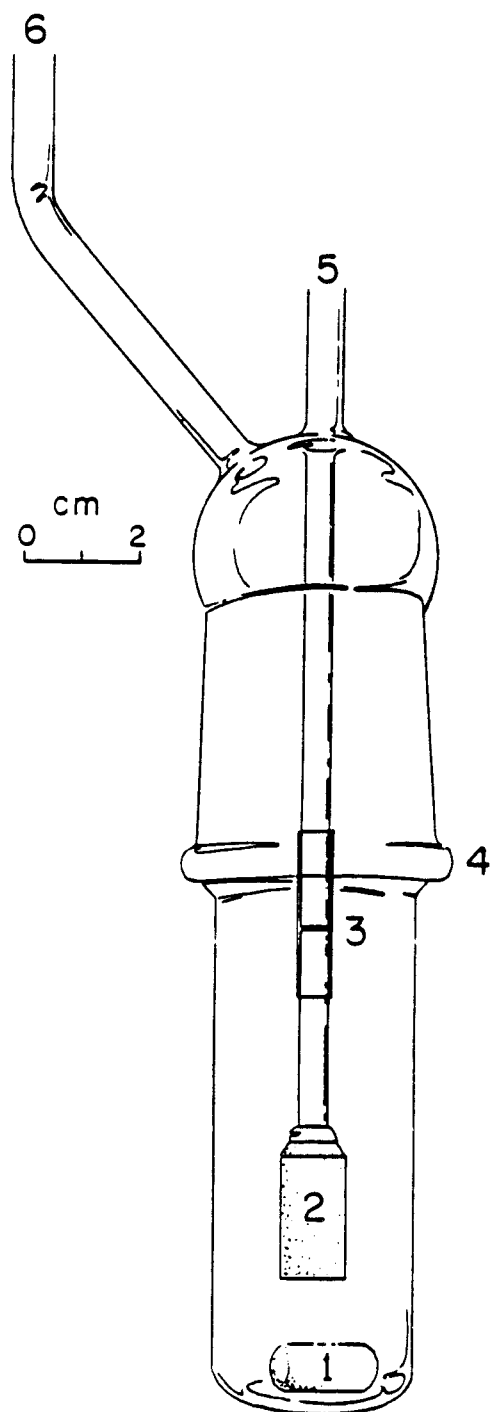
Fig. 2.10. Reaction vessel for PIC analysis. (1) Teflon-coated magnetic stir bar, (2) sintered-glass gas dispersion tube, (3) Teflon sleeve, (4) standard taper 40/50 ground glass joint, (5) gas inlet, (6) gas outlet.

added with an inline reservoir (analogous to the DIC analysis). A Teflon-coated magnetic stir bar throughly mixed the ground sediment with the acid solution. The resulting CO_2 was stripped from solution by N_2 flowing at 100 ml·min^{-1} for 40 min. Methods for removal of H_2O and acid-released sulfides were similar to those for the DIC analysis, while methods for collection and quantification of the CO_2 followed those for the CH_4 analysis.

POC Analysis

Preparation of Acidified Sediment. The acidified, stripped sediment was transferred from the reaction vessel to a glass jar, dried at 70^oC (36 h), and ground to a fine powder. The "double-tube" combustion technique (Minagawa et al., 1984) was employed because H_3PO_4 attacks quartz at high temperatures. An aliquot of the powdered sediment (100 to 200 mg) was transferred to a small cuvette (5 cm) made from 6 mm o.d. quartz tubing. The cuvette was inserted in a Vycor tube (30 cm x 9 mm o.d.) previously flame sealed on the bottom. The Vycor tube was then filled with 2.0 g finely ground CuO, evacuated, and flame sealed. The sealed tubes were placed in a steel rack (Sofer, 1980) and combusted at 850^oC for 6 h (the furnace reached this temperature after 2 h). The furnace was allowed to cool to 300^oC (8 h) before sample removal.

Collection and purification of CO_2. The gaseous combustion products were introduced to the evacuated manifold using a "tube cracker" fashioned from Cajon Ultra-Torr fittings and flexible stainless steel tubing (DesMarais and Hayes, 1976). The Vycor tubing was etched, sealed in the tube cracker, evacuated, and broken.

Water was removed by a trap cooled to -89^oC, Cl_2 was removed by the

Cuprin at $200^{\circ}C$, and CO_2 was trapped at $-196^{\circ}C$. Sulfur oxides were removed by the CuO (Sofer, 1980) and nitrogen compounds were converted to N_2 during combustion (Sofer, 1980). Final collection and quantification of the CO_2 was the same as the CH_4 analysis.

Isotope Ratio Analysis

The dual-inlet ratio mass spectrometer (VG Micromass, Sira 9) was equipped with a 20 port automated sampling system controlled by a Hewlett-Packard 86B desk-top computer. Each sample port had a "tube cracker" fashioned from Cajon Ultra-Torr fittings and flexible stainless steel tubing (DesMarais and Hayes, 1976). Stainless steel turnings and a sintered-glass frit above the point of breakage prevented glass splinters from entering the mass spectrometer. A liquid nitrogen cold-finger concentrated samples smaller than 25 umol CO_2 permitting automated analysis for samples containing more than 2 umol.

An isotope ratio measurement consisted of balancing gas pressures in sample and reference inlets to within 5% by automatic expansion or contraction of stainless steel bellows, followed by twelve ion current measurements alternating between sample and reference gas. Each ion current measurement consisted of ten 1 second voltage integrations; transient voltage surges were filtered by discarding integrations with values that differed from the mean by more than two standard deviations. The eleven $\delta^{13}C$ values calculated from the twelve sample or reference ion current measurements were averaged.

Precision and Accuracy

Sources of error specific to isotope ratio analyses. Variation in

carbon stable isotope ratios in natural carbonaceous material is rather limited. Although compounds at the extreme ends of the $\delta^{13}C$ spectrum span nearly $100^o/oo$, most carbon reservoirs differ by only 10 to $20^o/oo$ (Fig. 1.1) and variation within a reservoir may be as little as 1 to $2^o/oo$. High precision ratio mass spectrometers allow routine measurement of the $\delta^{13}C$ of CO_2 with a precision and accuracy of $\pm0.1^o/oo$. However, the process of converting a particular portion of a complex natural sample to pure CO_2 could introduce random variation or systematic errors in the isotope ratios that are as large or larger than the natural variation. Three types of analytical problems could bias stable isotope results:

1. **Sample contamination.** The contaminant carbon could have a distinct $\delta^{13}C$ so that a relatively small blank contribution could significantly bias the measurement. An appreciable blank could result from either inadequate purification of the fraction of interest, or a source external to the sample (e.g. contaminated storage container, reactant, carrier gas, etc.).

2. **Incomplete sample recovery.** Chemical reactions that occur at normal temperatures generally lead to products enriched in molecules containing the lighter isotope. Likewise, physical processes leave the heavier isotope enriched in the more stable phase. Stable carbon isotope analyses employ chemical and physical processes to separate the component of interest from the complex matrix, convert this component to CO_2, and purify the CO_2 from other gaseous molecules. Isotope ratios may be biased by any non-quantitative

reaction or separation process.

   3.   **Inadequate sample purification.** For optimal accuracy, the mass spectrometer requires that the sample and reference gas be of the same purity.

For measured isotope ratios to be considered reliable, it must be demonstrated that (a) the contribution of CO_2 from the blank is negligible (or consistent so that corrections can be made), (b) sample recovery is quantitative (or that incomplete recovery does not cause isotope fractionation), and (c) the purification procedures are effective.

Blanks. Six steel cans were filled with 60 ml N_2-purged, permanganate-distilled water, stored in the freezer, and periodically analyzed for CH_4, DIC, and DOC. The blank for the CH_4 analysis (0.24 ± 0.04 umol), had insufficient gas for an isotope ratio analysis. The $\delta^{13}C$ of the CH_4 blank was calculated to be -34.4^o/oo by extrapolation to 100% of a plot of $\delta^{13}C$ vs. per cent blank for CH_4 standards. The principle source of this blank was contaminants adsorbed onto CuO in the combustion tube. Air combustion as well as vacuum combustion of the CuO did not reduce the blank.

The quantity and $\delta^{13}C$ of the DIC blank was 14.4 ± 3.4 umol and -17.9^o/oo, respectively. Uncertainty in the $\delta^{13}C$ is not reported because 5 of 6 samples were lost due to mass spectrometer malfunction. The lacquered can appeared to be the major source of DIC blank: degassed permanganate-distilled water added directly to the reaction vessel contained 0.6 ± 0.2 umol DIC (n=6) while the same water sealed in an

N_2-flushed can for a short time (<1 hr) prior to transfer to the reaction vessel contained 11.2 umol (n=1).

The DOC blank was 14.2±3.9 umol with a $\delta^{13}C$ of -25.8±1.1°/oo. The can and squeezer were the major sources of DOC contamination. Permanganate distilled water passed through the squeezer contained 5.7±0.8 umol DOC (n=4). The same water added directly to the reaction vessel contained 1.3±0.2 umol (n=6) derived from contamination in the water (0.3 umol), the Cl_2 trap (0.5 umol), the NaOH solution (0.3 umol), and the potassium persulfate oxidant (0.2 umol). The can presumably contributed the remainder of the DOC blank (ca. 8.5 umol).

The PIC blank, measured by adding acid solution to the empty reaction vessel, was 0.14±0.09 umol (n=6). The POC blank, determined on quartz bombs filled only with CuO, was 0.27±0.08 umol (n=5). Both these blanks provided insufficient gas for isotope ratio analysis.

Carbon isotope ratios were corrected for the effects of blanks using an isotope mass-balance equation:

$$n_S \; \delta^{13}C_S = n_M \; \delta^{13}C_M - n_B \; \delta^{13}C_B \; ,$$

where n is the molar quantity and subscripts represent sample (S), measured (M), and blank (B). This is an approximate version of the general mass-balance equation, but is quite accurate provided sample and blank have isotope ratios that fall within the range of natural materials (Hayes, 1982). The magnitude of the blank correction for CH_4 was <0.5°/oo (average = 0.2°/oo) except for samples within 6 cm of the sediment-water interface where the correction was as large as 2°/oo. The blank correction for DIC and DOC was always less than 0.2°/oo. The $\delta^{13}C$ of the PIC and POC blank was unknown, but assuming that it differed from

the sample by $\leq 20^{o}$/oo, the magnitude of the blank correction is much less than 0.1^{o}/oo.

Standards. Isotope artifacts depend on sample size as well as sample matrix. Therefore, standards were designed to cover the entire range of sample sizes and mimic the sample matrix. Standards were analyzed using previously defined procedures, the only significant difference being the addition of a known quantity of carbon.

Methane standards were analyzed by injecting 2 to 400 umol of pure CH_4 (equivalent to concentrations ranging from 0.025 to 5 mM_{PW}) into cans filled with 100 ml buffered solution (pH 7) containing 50 mM $NaHCO_3$. The HCO_3^- served to mimic pore water DIC that would be stripped with the CH_4. The CH_4 was stripped and oxidized according to the procedures described in "Methane Analysis". The average recovery for standards larger than 6 umol was $100\pm2.1\%$ (n=11). The precision of the $\delta^{13}C$ for these standards was $\pm0.1^{o}$/oo (n=11). Neither the recovery nor the $\delta^{13}C$ showed any systematic variation with the quantity of CH_4 added.

Methane standards containing less than 6 umol of CH_4 (equivalent to concentrations below 0.075 mM_{PW}) could not be quantified manometrically. Alternatively, pressures were measured with a thermocouple gauge calibrated against CO_2. Although accuracies of standards containing less than 6 umol of CH_4 were poor, recoveries were 80 to 100%.

DIC standards were run by injecting 2 to 10 ml of a 0.2835 mM HCO_3^- solution (equivalent to 10 to 50 mM_{PW}) into a reaction vessel containing 30 ml of 0.01 N NaOH solution and 60 ml of CO_2-free water. The standards were analyzed according to the procedure described in "DIC Analysis". The average recovery for the standards was $99.7\pm1.2\%$ (n=8); the

precision of the $\delta^{13}C$ analyses was $<\pm0.1^o/oo$ (n=8).

DOC standards were run by injecting 2 to 8 ml of poisoned (0.1 mM Hg_2Cl_2) sucrose solution (154.9 mmol $C\cdot l^{-1}$) into a reaction vessel containing 30 ml of 0.01 N NaOH and 70 ml $35^o/oo$ NaCl (equivalent to concentrations ranging from 5 to 25 mM_{PW}). The contents of the reaction vessel were acidified and stripped of CO_2 according to the procedures for the DIC analysis. Potassium persulfate was added to the reaction vessel and the DOC analyzed according to the procedures described in "DOC Analysis". The average recovery for standards was $98.8\pm1.8\%$ (n=4). The precision of the $\delta^{13}C$ analyses was $<\pm0.1^o/oo$ (n=4).

PIC standards were run by weighing 2 to 5 mmol $CaCO_3$ (corresponding to PIC concentrations of 0.4 to 1.3 $mmol\cdot g^{-1}$ in 3 g of dried sediment) into the reaction vessel. The reaction vessel was attached to the vacuum manifold, acidified, and the resulting CO_2 was stripped (see "PIC Analysis"). The average recovery for the standards was $99.8\pm0.2\%$ (n=4). The precision of the $\delta^{13}C$ was $<\pm0.1^o/oo$ (n=4).

POC standards were run by weighing 4 to 20 mg sucrose into a precombusted aluminum boat. The amount of carbon generated was equivalent to that in 100 mg dried-acidified sediment containing 1.3 to 6.3 mmol $POC\cdot g^{-1}$ solid matter. The aluminum boat was placed in a quartz cuvette, transferred to a vycor bomb, and combusted (see "POC Analysis"). The average recovery for the standards was $98.5\pm1.8\%$ (n=8). The precision of the $\delta^{13}C$ was $<\pm0.1^o/oo$ (n=8).

Purity of sample gas. The purity of gas introduced to the mass spectrometer was checked by scanning the full range of mass to charge ratio (m/e) available to the Sira 9. Sample and reference gases had

peaks at m/e=28 (N_2), equivalent to approximately 5% of the CO_2 peak. The height of the m/e=28 peak was constant for all gases suggesting that the N_2 represented background pressure in the mass spectrometer analyzer. No peaks other than m/e=28 and m/e=44,45,46 (due to the different isotopic species of CO_2) were detected in gas samples from DIC and POC analyses. However, gas samples from DOC analyses contained trace quantities of compounds with m/e ranging from 47 to 52. The identity of these compounds is unknown.

Potential artifacts. Methane bubble formation after core retrieval may have resulted in some methane loss during sampling and hence underestimated concentrations. It is expected that this effect is most pronounced in the deepest samples. Isotope fractionation between gaseous and aqueous CH_4 is small (0.3^o/oo; Feux, 1980), indicating that CH_4 loss due to bubble formation will not significantly bias stable isotope results.

There is some uncertainty regarding the efficacy of persulfate as an oxidant for DOC. MacKinnon (1978) oxidized seawater DOC by high temperature combustion and persulfate oxidation. He found the persulfate method to give results that were systematically low by 10 to 25%. Gershey et al. (1979) compared three oxidation methods and found that the persulfate method oxidized only 85% of the seawater DOC. The accuracy of the persulfate method for DOC in marine pore water has not been evaluated.

Sediment subjected to stable isotope and pool size analysis was stored frozen. The freezing process could produce transformations between carbon reservoirs that do not reverse during thawing. For example,

freezing could stimulate calcite precipitation in supersaturated pore water. Such an artifact could lead to significant error in DIC and PIC concentration and isotope ratio data. However, alkalinity profiles determined on fresh sediment (A. Devol, Univ. Washington, unpublished data) agreed well with DIC measurements on frozen samples. Only in the uppermost sediment (0-4 cm) was the alkalinity significantly higher than the DIC. Precipitation of carbonate minerals within this region is unlikely as the pore waters are undersaturated with respect to calcite (Fig. 4.18).

Reproducibility of replicate samples. The analyses for CH_4, DIC, and DOC consumed the entire sample, making true replication impossible. However, each sample provided sufficient solid phase material for replicate analyses of PIC and POC. The precision of the PIC pool size and isotope ratio analyses (based on the mean relative standard deviation of triplicate determinations of 3 samples) were $\pm 0.5\%$ (range: 0.2 to 0.8%) and $\pm 0.03^o$/oo (range: 0.02 to 0.04^o/oo), respectively. The precision of the POC pool size and isotope ratio analyses were $\pm 1.1\%$ (range: 0.7 to 1.4%) and $\pm 0.02^o$/oo (range: 0.02 to 0.03^o/oo), respectively. The accuracy of the POC concentration analysis was checked with a Perkin-Elmer CHN elemental analyzer (S. Henrichs, Univ. of Alaska, Fairbanks, unpublished data). The relative difference between POC concentrations determined by the bomb combustion method and the CHN analyzer was $\pm 1.1\%$ (range:-2.4 to +5.2%, n=8).

Mass spectrometer precision and accuracy. Samples were routinely analyzed in duplicate; $\delta^{13}C$ values generally agreed within 0.1^o/oo. The accuracy of an isotope analysis depends on (a) bias in the mass

spectrometer, and (b) the accuracy with which the $\delta^{13}C$ of the reference gas is known. Zero-enrichments demonstrated that for samples larger than 3 umol, mass discrimination between the sample and reference inlets was negligible ($<0.05^o$/oo). Likewise, other sources of mass spectrometer error (abundance sensitivity, valve mixing, and analyzer background [Deines, 1970]) were found to be negligible.

For very small samples (<3 umol), imbalance between the sample and reference gas pressure led to errors as large as 1°/oo. Fortunately, samples this small only occurred for CH_4 samples nearest the sediment-water interface. Because of the large error, the $\delta^{13}C$ data for these very small samples has been discarded.

Aliquots of the isotope reference gas were sent to five laboratories for calibration (Table 2.3). Although the precision of each laboratory was approximately $\pm 0.1^o$/oo, the range between laboratories was almost 0.4^o/oo. The mean value, weighting each laboratory equally, was taken as the best estimate of the $\delta^{13}C$ value of the reference gas. The accuracy with which the $\delta^{13}C$ value of the reference gas is known is taken as $\pm 0.15^o$/oo, the standard deviation of the results from the five laboratories.

Once in the mass spectrometer bellows, the reference gas became isotopically heavier as it was consumed. With each set of samples run on the mass spectrometer, an aliquot of reference gas was analyzed to check for changes in the bellows gas. When bellows and reference gas differed by $\geq 0.05^o$/oo, the bellows were evacuated and refilled with fresh reference gas.

A stable carbon isotope reference material from the National Bureau

Table 2.3. Interlaboratory calibration of isotope reference gas.

==

Laboratory	n	$\delta^{13}C$ (^{o}/oo)	std. dev. (^{o}/oo)
Coastal Science Labs (Port Aransas, TX)	2	-13.0	±0.14
NASA/Ames (Mountain View, Ca.)	3	-12.64	±0.085
Global Geochemistry (Canoga Park, Ca.)	2	-12.87	±0.014
North Carolina State University (Raleigh, NC)	2	-12.83	±0.014
Federal Institute for Geosciences and Natural Resources (Hannover, FRG)	2	-13.0	±0.14
MEAN	5	-12.87	±0.15

of Standards (NBS-22 hydrocarbon oil) was combusted, purified, and
analyzed with each set of samples run on the mass spectrometer. The
average value of the δ^{13}C for NBS-22 was -29.63 ± 0.19^{o}/oo (n=34), in
agreement with the value of -29.61 ± 0.03^{o}/oo (n=7) reported by Coplan et
al. (1983). However, these values differ significantly from the results
of an interlaboratory comparison conducted by Schoell et al. (1983) who
suggested -29.81 ± 0.06^{o}/oo as the best value for NBS-22.

Data Corrections and Conversions

Depth corrections. The mass of whole sediment differed slightly for
parallel samples from the same depth. Since horizontal density gradients
were probably small, mass differences between samples from similar
depths were probably due to differences in the volume of sediment sam-
pled. Sediment was sampled by extruding a cylinder of mud from the core
into a segment of core liner. Variability in sample volume is more
likely due to variability in the length rather than diameter of the
sediment cylinder. The correct sample length was estimated from the
sample mass, the whole sediment density, and the core liner radius. The
whole sediment density (ρ_{WS}) was calculated as a function of cumulative
mass using porosity (ϕ), water content (WC), and pore water density
(ρ_{PW}):

$$\rho_{WS} = \frac{\phi \; \rho_{PW}}{WC} \; .$$

The correct depth interval was calculated by summing the length of each
sample.

Concentration corrections. In addition to subtraction of the blank

contribution, two corrections were applied to the concentration data. First, since squeezing does not quantitatively separate the aqueous and solid phases, the PIC and POC concentrations were corrected for the contribution from DIC and DOC, respectively. The water content of the squeezed sediment was measured and the dissolved contribution to the solid matter pools (1 to 10% for PIC and 0.1 to 0.6% for POC) were subtracted. Second, the PIC and POC concentrations were corrected for the contribution of salts to the mass of the solid matter, and for POC, concentrations were corrected for the mass of added H_3PO_4 and lost CO_2 and H_2O.

Isotope ratio corrections. The contribution from the blank was corrected for as previously described. The contribution to the m/e=45 peak from ^{17}O was corrected according to Craig (1957). All $\delta^{13}C$ values were corrected to the PDB scale (Craig, 1957). The PIC and POC $\delta^{13}C$ values were corrected for the DIC and DOC contribution, respectively, caused by incomplete removal of pore water during squeezing.

Unit conversions. The CH_4 concentrations were measured as $umol \cdot g^{-1}$ whole sediment. The following relationship was used to convert data to pore water concentration units:

$$mM_{PW} = \frac{umol}{g_{WS} \cdot \phi} \cdot \rho_{WS}$$

The DIC and DOC concentrations were measured as $umol \cdot g^{-1}$ pore water. Concentrations were converted to pore water units with a similar relationship:

$$mM_{PW} = \frac{umol}{g_{PW}} \cdot \rho_{PW}$$

Other Analyses

X-radiography. A rectangular subcore was taken by gently inserting an 18 x 2.5 x 60 cm plexiglass container into a box core. The overlying water was siphoned and the subcore was capped and stored upright at room temperture for several months. The seal on the box's bottom was imperfect allowing pore water to drain from the sediment. The subcore was X-rayed by a local veterinarian.

Geochronology. The ^{210}Pb and ^{137}Cs were analyzed by S. Sugai (University of Alaska, Fairbanks, unpublished data). The methods for both these analyses are described in Sugai (1985).

Hydrogen sulfide. Total reduced sulfur, assumed to be composed primarily of ΣH_2S ($[H_2S] + [HS^-] + [S^{2-}]$), was determined by iodimetry (Kolthoff et al., 1969). Sediment obtained by box coring was transferred to squeezers inside N_2-filled glove bags and pore water was squeezed directly into plastic syringes. A known quantity of I_2 was generated in a pore water sample by acidification of a standard IO_3^- solution. The I_2 oxidized ΣH_2S to elemental sulfur and the excess I_2 was back titrated to a starch end-point with thiosulfate.

Analytical Methods: Summary

Analytical methods for concentrations, rates, and isotope ratios were designed to provide accurate, high resolution depth profiles for the upper 40 cm of the sediment column. Whenever possible, multiple analyses were conducted on individual cores to provide a self-consistent data set free from variability caused by lateral sediment heterogeneity. In addition, replicate subcores from within a box core and from

different box cores provided quantitative estimates of small and large

scale heterogeneity (see p. 69). Analytical precision and accuracy are

summarized in Table 2.4.

Table 2.4. Precision and accuracy of analytical methods.

===

Analysis	Precision	Accuracy
Porosity	$<\pm0.5\%$	WLP
Methane Concentrations	$<\pm3\%$	Methane may have been lost from deeper samples
Methane Oxidation Rates	$<\pm16\%$	Agreement between measured and modelled concentration profiles suggests that rates are accurate to $\pm25\%$
Sulfate Concentrations	$\pm2\%$	$\pm2\%$
Sulfate Reduction Rates	$\pm8\%$	Discrepancy between measured and modelled concentration profiles suggests that rates are overestimated by more than a factor of 2
Stable Carbon Isotopes	$\pm0.1^{\circ}/oo$	$\pm0.15^{\circ}/oo$
Pool Sizes		
CH_4	$\pm2\%$ ($>$0.0075 mM) $\pm10\%$ ($<$0.0075 mM)	Methane may have been lost from deeper samples
DIC	$\pm1\%$	WLP
DOC	$\pm2\%$	May be underestimated by 10 to 25% due to incomplete oxidation
PIC	$\pm0.5\%$	WLP
POC	$\pm1\%$	$\pm1\%$

WLP = within the limits of the precison.

CHAPTER 3: RESULTS

Concentration, rate, and isotope ratio depth distributions from Skan Bay sediment are presented in this chapter. Noteworthy features are described and compared with published data from Skan Bay and other anoxic marine environments. Tabulated data are provided in Appendix I.

The magnitude of lateral heterogeneity is evaluated for each sediment property having sufficient data. Small-scale (5 to 15 cm) and large-scale (1 to 100 m) horizontal variability are defined as the intra- and inter-box core precision (i.e. relative standard deviation), respectively, for a particular property at a given depth.

Porosity

Sediment porosity was very high (>0.99) in the upper 3 cm interval (Fig. 3.1) indicative of a floc layer. Porosity generally decreased with depth as the solid phase was compressed by the mass of overlying sediment. An exponential function was fit to data from the upper 40 cm using a least-squares non-linear regression:

$$\phi = 0.136 \exp(-0.0929 z) + 0.864 , \tag{3.1}$$

where z is depth in cm ($r^2 = 0.903$, n=39).

Methane Concentrations

Methane concentrations determined at sea by a headspace equilibration technique are shown in Figs. 3.2 and 3.3. Methane depth distributions in the upper 40 cm were concave up (Fig. 3.2), a common characteristic of profiles from anoxic marine sediments (Reeburgh and
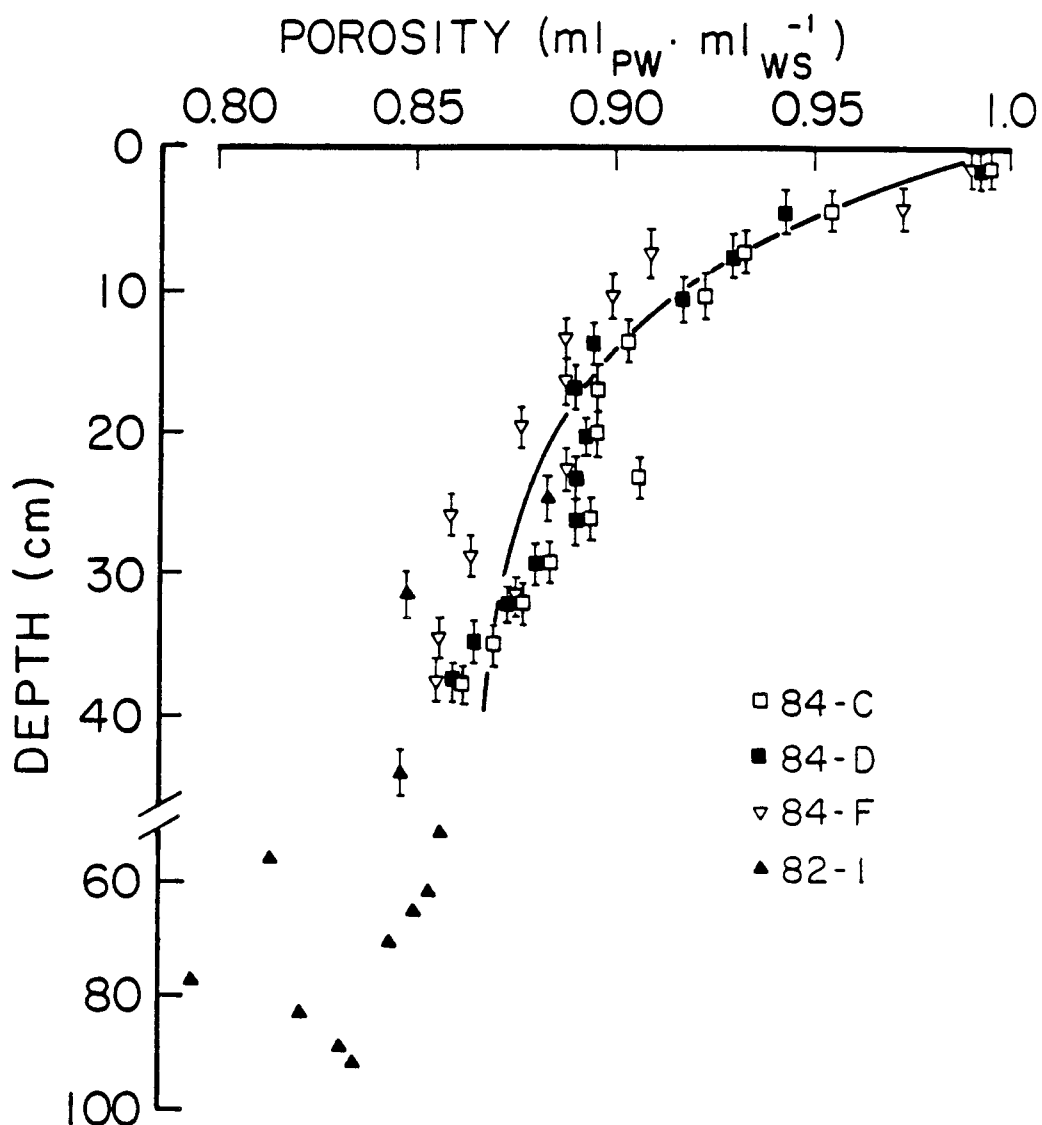
Fig. 3.1. Depth distribution of porosity. Vertical bars represent the sample depth interval; the symbol size represents the depth interval for samples lacking a vertical bar. Subcores 84-C and 84-D are replicates from a single box core, subcore 84-F is from a different box core, and core 82-1 is a gravity core. The solid curve represents an exponential function fit to data from the upper 40 cm. Note the break and change of scale on the depth axis.
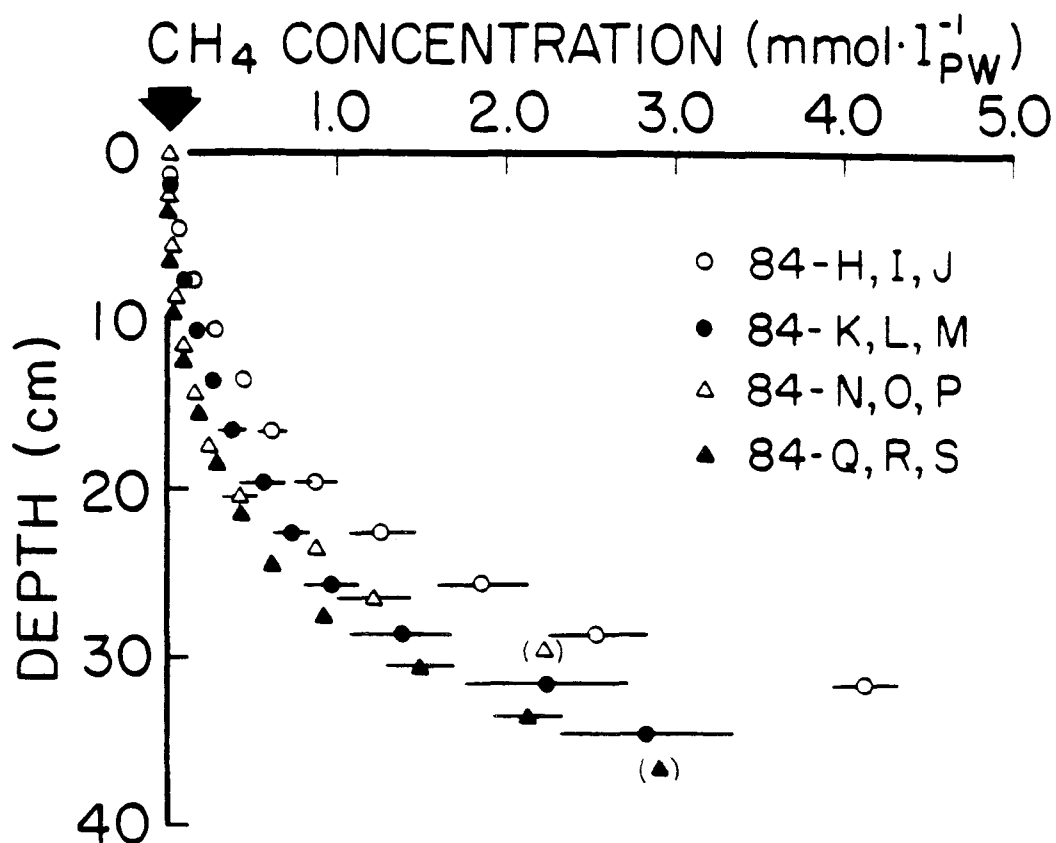
Fig. 3.2. Depth distribution of methane concentration in the upper 40 cm determined at sea by a headspace equilibration technique. Each data point represents average concentrations for triplicate subcores from a single box core. Horizontal error bars represent ±1 standard deviation. The absence of an error bar indicates standard deviations smaller than the symbol size. Data points bracketed by parentheses represent samples for which replicates were absent. The vertical sampling interval is represented by the size of the symbol. The large arrow represents bottom water concentration.

Heggie, 1977) indicating net CH_4 consumption (Reeburgh, 1976; Martens
and Berner, 1977). Small-scale horizontal variability for triplicate CH_4
profiles from a single box core averaged 13% (range: 2 to 28%, n=42).
The estimated precision of the method was $\pm3\%$ (Table 2.4), suggesting
that most of the small-scale horizontal variability could be attributed
to lateral heterogeneity in the sediment. Large-scale horizontal varia-
bility of CH_4 concentration profiles from four different box cores
averaged 50% (range: 37 to 70%, n=12). Inter-core variability of this
magnitude has been observed in other studies (Devol et al., 1984;
Kuivila, 1986) which used an in situ sampler (Sayles et al., 1976) and
established that the variability was not a sampling artifact.

Methane concentrations continued to increase below 40 cm, reaching
a maximum ca. 65 cm (Fig. 3.3). Scatter in the data makes it impossible
to determine whether the profile was linear (indicating no net reaction)
or concave down (indicating net production) between 35 and 50 cm. It is
not clear whether CH_4 production occurs at (a) relatively slow rates
between 35 and 65 cm, or (b) faster rates in a deeper, narrower zone (50
to 65 cm). The anoxic sediments of Saanich Inlet have linear CH_4 concen-
tration profiles below the region of upward concavity, suggesting that
CH_4 production is somehow inhibited in this region (Kuivila, 1986).

Methane Oxidation Rates

Methane oxidation rates were low near the sediment-water inter-
face, reached a maximum in a narrow subsurface zone, and decreased with
depth (Fig. 3.4). This pattern is consistent with earlier Skan Bay
studies (Reeburgh, 1980; Alperin and Reeburgh, 1984) and studies of
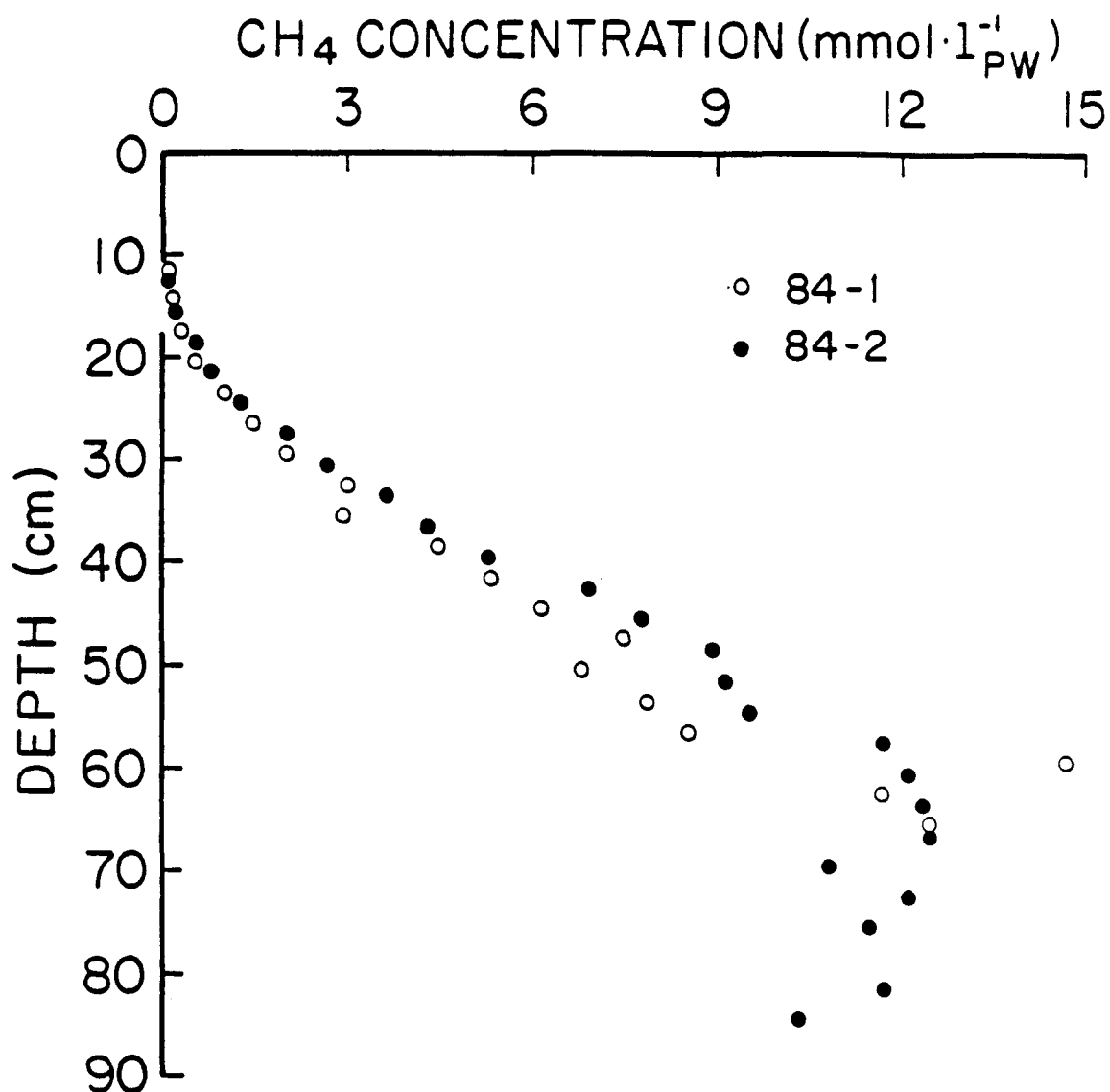
Fig. 3.3. Depth distribution of methane concentration in deep gravity cores determined at sea by a headspace equilibration technique. The depth scale was established by aligning the methane concentration profiles of sediment sampled by gravity corer and box corer.
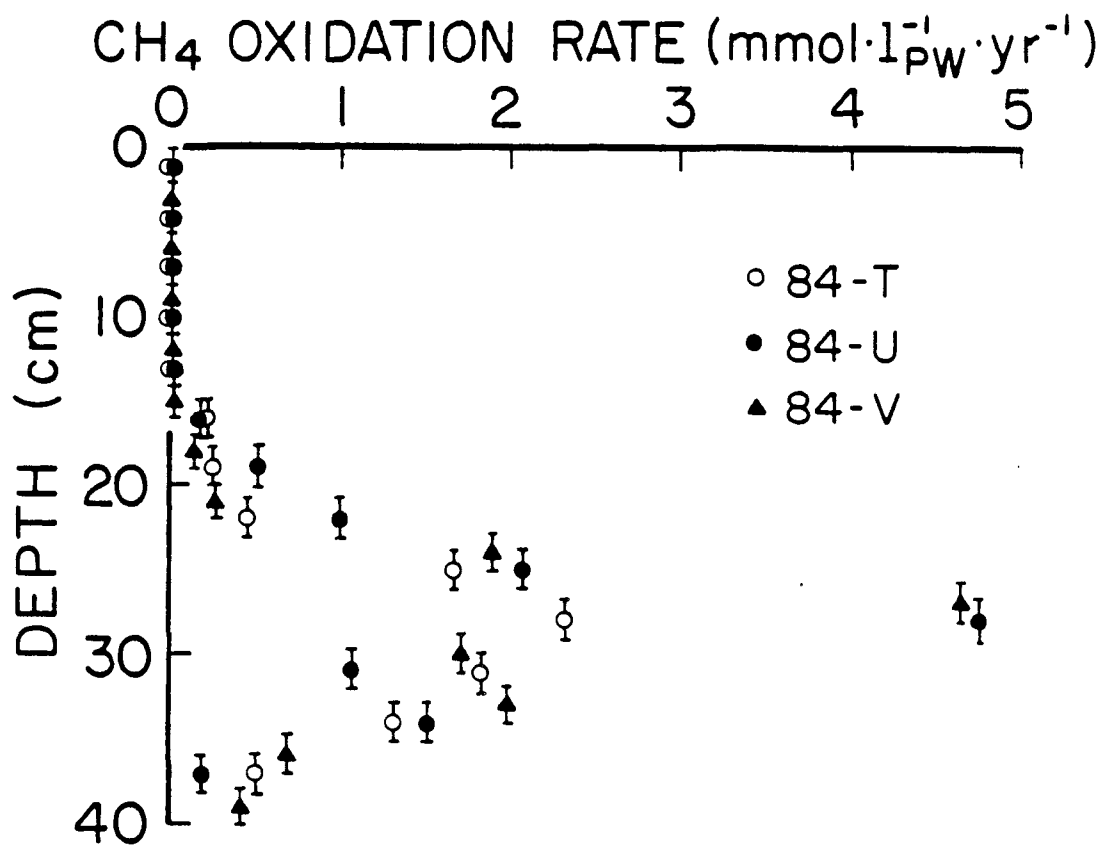
Fig. 3.4. Depth distribution of methane oxidation rate for triplicate subcores from a single box core. Vertical bars represent the sample depth interval.

other anoxic marine sediments (Devol, 1983; Iversen and Jørgensen, 1985). Small-scale horizontal variability was greater for CH_4 oxidation rates than concentrations. Subcores from the same box core had maximum rates that differed by a factor of two.

Sulfate Concentrations

The SO_4^{2-} depth distribution was linear or slightly concave up above 18 cm and concave down at greater depths (Fig. 3.5). This shape conflicts with theoretical models (Berner, 1964, 1980; Jørgensen, 1978b) which predict that SO_4^{2-} profiles in anoxic marine sediment should be concave down. However, disagreement between measured and modeled SO_4^{2-} profiles is common. A survey by Jørgensen (1978b) found that only 10 of 50 SO_4^{2-} depth distributions from coastal and oceanic sediments showed the consistent downward curvature predicted by models. Berner (1971) suggested that linearity in the SO_4^{2-} profile may be due to a decrease in surface SO_4^{2-} reduction rates with time. Jørgensen (1978b) noted that this could not explain all deviations and suggested that compaction, which decreases the diffusion coefficient with depth, could linearize SO_4^{2-} profiles. Devol et al. (1984) pointed out that the subsurface maxima in their SO_4^{2-} reduction rates would reduce downward concavity in the SO_4^{2-} profile. Although these mechanisms reduce curvature near the sediment-water interface, none are capable of producing a linear or concave up SO_4^{2-} depth distribution. Possible causes for the anomalous SO_4^{2-} depth distribution in Skan Bay sediment are discussed in "Chapter 4: The Diagenetic Model" (p. 150).

Horizontal variability for triplicate SO_4^{2-} profiles from a single
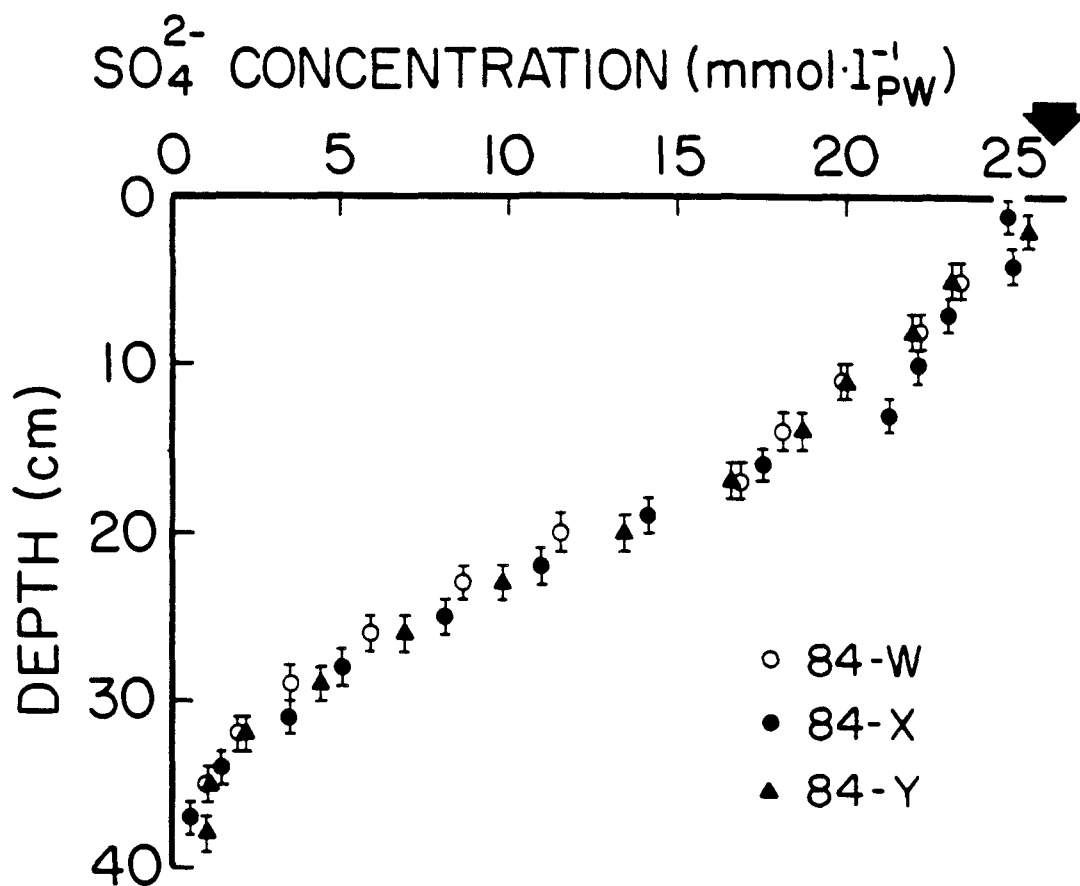
Fig. 3.5. Depth distribution of sulfate concentration for triplicate subcores from a single box core. Vertical bars represent the sample depth interval. The large arrow represents bottom water concentration.

box core averaged 7% (range: 1 to 19%, n=13). The analytical precision was ±2% (Table 2.4) indicating that most horizontal variability was due to lateral sediment heterogeneity.

Sulfate Reduction Rates

Sulfate reduction rates (Fig. 3.6) were low near the sediment-water interface and had two maxima, a primary maximum near the surface and a secondary maximum located just below the CH_4 oxidation rate maximum (Fig. 3.4). A secondary maximum in the SO_4^{2-} reduction rate has been previously observed (Devol and Ahmed, 1981; Iversen and Jørgensen, 1985; Crill and Martens, 1987) and is generally coincident with the maximum methane oxidation rate (Devol, 1983; Iversen and Jørgensen, 1985).

Sulfate reduction rate profiles showed the greatest lateral variability just above or below the primary and secondary maxima. Like the CH_4 oxidation rate profiles, SO_4^{2-} reduction rate measurements in triplicate subcores from the same box core differed by as much as a factor of two in the vicinity of the maxima. Away from the maxima, horizontal variability decreased to about 10%, approximately equal to the analytical precision (Table 2.4).

Stable Carbon Isotope Ratios and Pool Sizes

Methane Analysis

Methane concentrations for subcores subjected to stable isotope ratio analysis are shown in Fig. 3.7. Methane depth distributions in the upper 40 cm were essentially identical to those analyzed by the headspace technique (Fig. 3.2) while at greater depths, CH_4 concentrations were a factor of two lower than those analyzed by the headspace
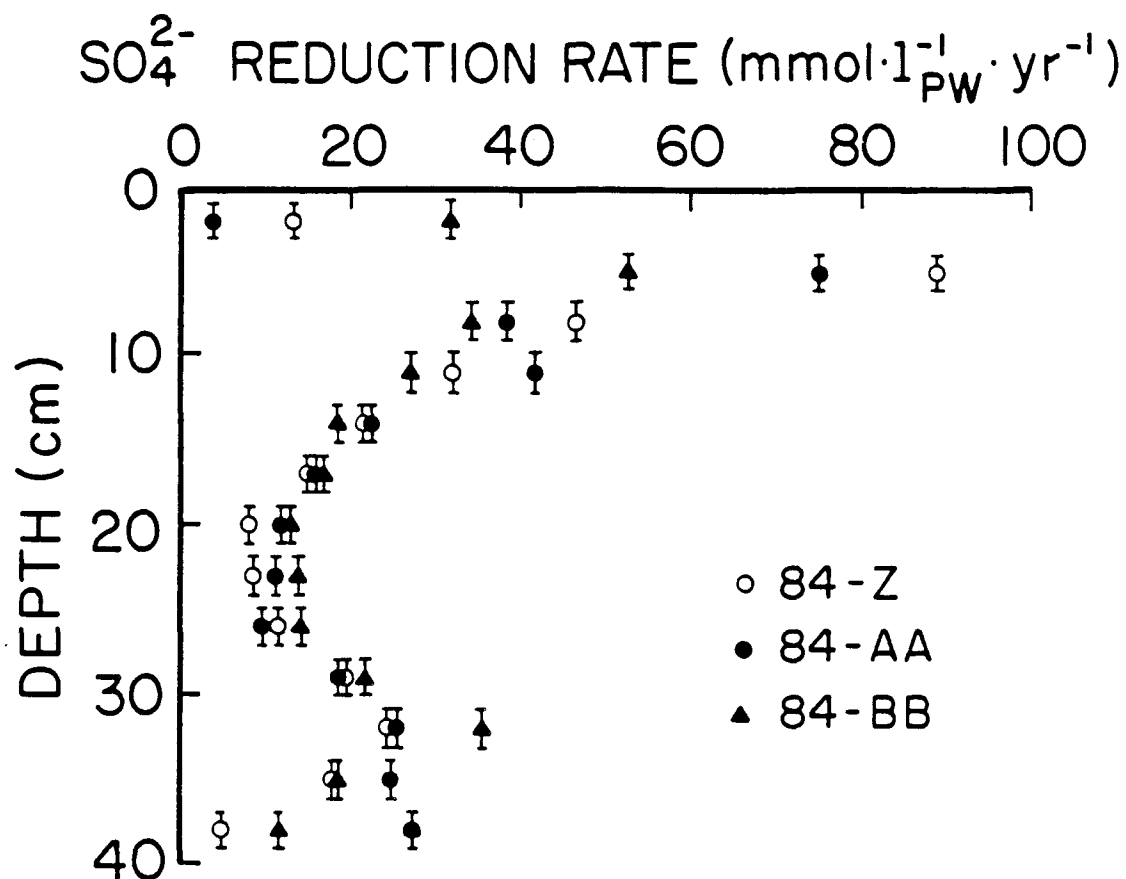
Fig. 3.6. Depth distribution of sulfate reduction rate for triplicate subcores from a single box core. Vertical bars represent the sample depth interval.

Fig. 3.7 Depth distributions of methane and δ^{13}C-CH$_4$. Vertical bars represent the sample depth interval; the symbol size represents the depth interval for points lacking a vertical bar. Subcores 84-A and 84-B are replicates from a single box core, subcore 84-E is from a different box core, and core 82-1 is a gravity core. The large arrow represents the bottom water concentration. Note the break and change of scale on the depth axis.

method (Fig. 3.3). This discrepancy is probably due to CH_4 loss from gravity core 82-1 which was frozen prior to sectioning. The deep sediment was supersaturated with CH_4 and freezing may have excluded CH_4 bubbles. Thus, methane concentrations for the deep samples are suspect.

Methane $\delta^{13}C$ values were relatively constant below 30 cm and became isotopically heavier between 30 and 20 cm as the CH_4 concentration decreased (Fig. 3.7). A similar shift in $\delta^{13}C-CH_4$ has been reported in other studies (Doose, 1980; Oremland and DesMarais, 1983; Alperin and Reeburgh, 1984; Whiticar and Faber, 1986), and has been attributed to CH_4 oxidation: $^{12}CH_4$ is oxidized faster than $^{13}CH_4$ leaving the residual CH_4 isotopically heavier. The depth interval of the isotopic shift coincides with the zone of CH_4 oxidation (cf. Fig. 3.7 and Fig. 3.4). The direction of the shift in $\delta^{13}C-CH_4$ reverses above 20 cm for subcores 84-A and 84-B. Possible causes for this reversal are discussed in "Chapter 4: The Diagenetic Model" (p. 147).

The $\delta^{13}C-CH_4$ profiles of subcores from the same box core (84-A, 84-B) agreed within $1^o/oo$. The subcore from a different box core (84-E) had a similar $\delta^{13}C-CH_4$ profile but was offset by about $-6^o/oo$.

DIC Analysis

The shape of the DIC depth distribution was a mirror image of the SO_4^{2-} depth distribution (cf. Fig. 3.8 and Fig. 3.5). It was linear or slightly concave up above 18 cm and concave down at greater depths. DIC concentrations continued to increase below 40 cm and appeared to reach a constant value between 80 and 90 cm.

Fig. 3.8 Depth distributions of DIC and δ^{13}C-DIC. Vertical bars represent the sample depth interval; the symbol size represents the depth interval for points lacking a vertical bar. Subcores 84-A and 84-B are replicates from a single box core, subcore 84-E is from a different box core, and core 82-1 is a gravity core. The large arrows represent bottom water values. Note the break and change of scale on the depth axis.

The small-scale horizontal variability (subcores 84-A and 84-B) was similar to that for the SO_4^{2-} depth distribution, averaging about 10% (range: 1 to 20%, n=13). Large- and small-scale horizontal variability were about the same magnitude.

The $\delta^{13}C$-DIC ranged from +1 to -21°/oo (Fig. 3.8), the largest span of the five major carbon reservoirs. Bottom water DIC had a $\delta^{13}C$ of about 0, consistent with the value expected for ocean water. The sediment DIC became isotopically lighter with depth reaching a minimum at about 20 cm. At greater depths, the DIC became isotopically heavier reaching the same $\delta^{13}C$ as the bottom water at about 90 cm. A similar minimum in $\delta^{13}C$-DIC has been observed in other anoxic marine sediments (Claypool and Kaplan, 1974; Miller, 1980; Boehme and Blair, 1986), and has been explained in two ways:

1. Organic matter remineralization in the upper sediments produces DIC with a $\delta^{13}C$ of approx. -20°/oo, resulting in the DIC pool becoming isotopically lighter with depth. At greater depth, isotope fraction associated with CH_4 production from DIC results in the residual DIC pool becoming isotopically heavier with depth (Claypool and Kaplan, 1974).

2. Methane oxidation results in a localized input of isotopically light DIC (Reeburgh, 1982).

The relative importance of organic matter remineralization, CH_4 production, and CH_4 oxidation in controlling the $\delta^{13}C$-DIC profile can be resolved only by a model calculation since all three processes are occurring within Skan Bay sediment (see p. 185).

The δ^{13}C-DIC profiles of subcores from the same box core (84-A and 84-B) generally agreed within 1 to 2°/oo. Subcore 84-E, from a different box core, had δ^{13}C-DIC values that were isotopically lighter by 3 to 5°/oo.

DOC Analysis

The DOC concentration (Fig. 3.9) increased dramatically just below the sediment surface, a common feature of anoxic marine sediments (Orem et al., 1986). DOC concentrations reached a maximum between 7 and 10 cm, (just below the primary maximum in the SO_4^{2-} reduction rate [Fig. 3.6]), and generally decreased at greater depth. The data hint that DOC concentrations increased below 30 cm, (coinciding with the secondary maximum in the SO_4^{2-} reduction rate [Fig. 3.6]), but the magnitude of the increase does not appear to be appreciably larger than scatter in the data.

There is a paucity of data on DOC concentrations in anoxic marine sediments, and the depth resolution of much of the available data is insufficient to define the shape of the depth profile. While most studies report that pore water DOC concentrations increase with depth (e.g. Krom and Sholkovitz, 1977; Barcelona, 1980), there are data showing DOC profiles with constant concentrations (e.g. Brown et al., 1972) and mid-depth DOC maxima (e.g. Orem et al., 1986).

Small- and large-scale horizontal variability in DOC concentrations were approximately equal, averaging 15% (range: 5 to 37%, n=13). Unlike the other dissolved pools (CH_4, SO_4^{2-}, and DIC), which showed systematic variations between subcores, horizontal variability in DOC concentrations was random.
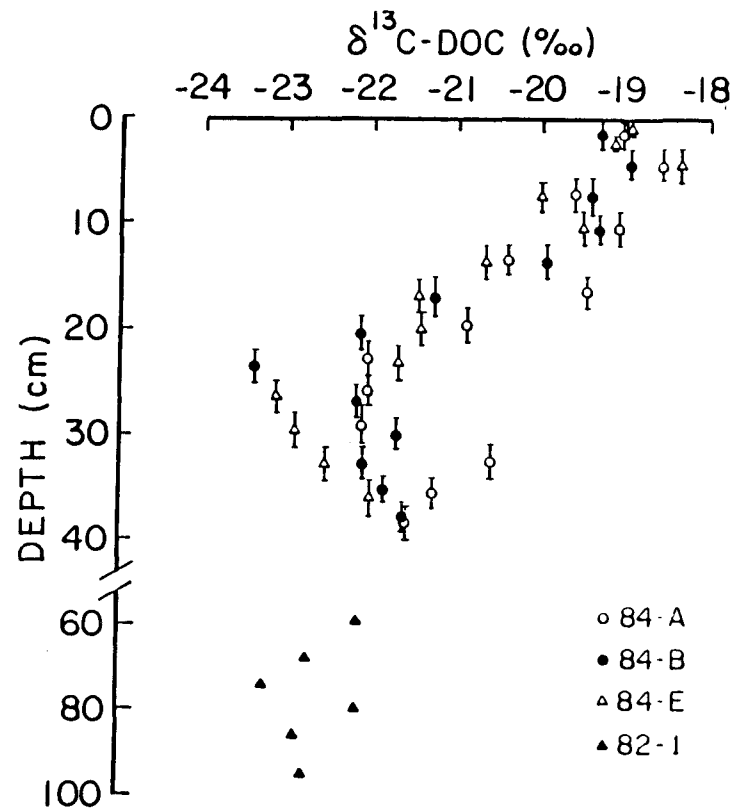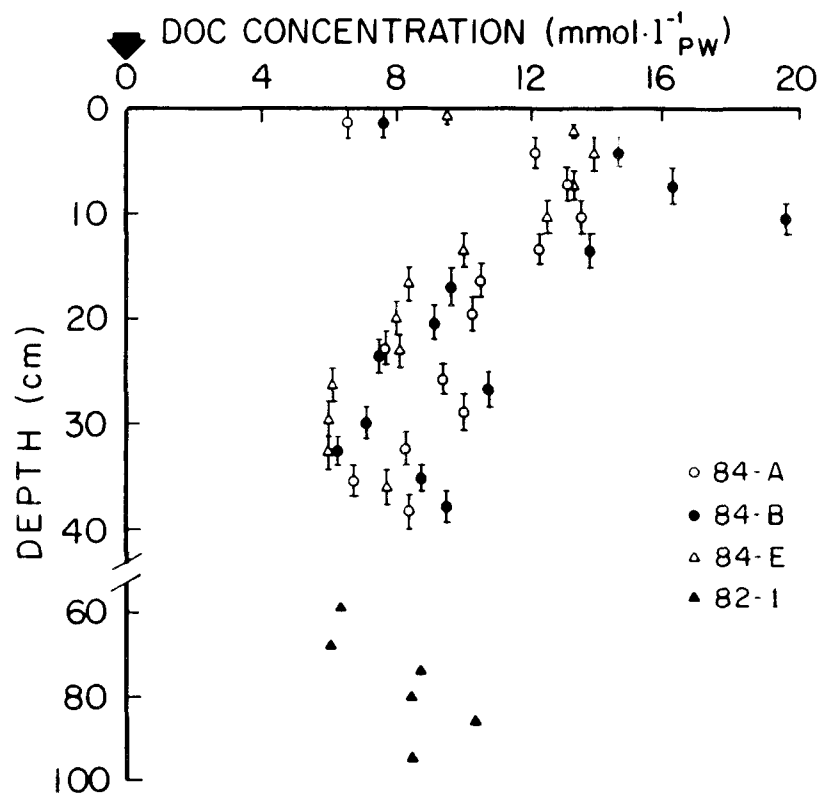
Fig. 3.9 Depth distributions of DOC and δ^{13}C-DOC. Vertical bars represent the sample depth interval; the symbol size represents the depth interval for points lacking a vertical bar. Subcores 84-A and 84-B are replicates from a single box core, subcore 84-E is from a different box core, and core 82-1 is a gravity core. The large arrow represents the bottom water concentration. Note the break and change of scale on the depth axis.

There was considerable random variability in the δ^{13}C-DOC depth distribution but significant trends are apparent (Fig. 3.9). DOC in samples closest to the sediment surface was isotopically similar to the POC from this interval (cf. Figs. 3.9 and 3.11). Proceeding down core, DOC became isotopically heavier between 0 and 5 cm and isotopically lighter between 5 and 25 cm. DOC isotope ratios were relatively constant between 25 and 40 cm (although one subcore [84-E] appeared to become isotopically heavier in this zone). Within the sediment column, the δ^{13}C-DOC reached values of -23 to -24°/oo, while the δ^{13}C-POC was never less than -21°/oo (Fig. 3.11).

There have been very few studies of δ^{13}C-DOC in anoxic marine sediments. Brown et al. (1972) reported that DOC from Saanich Inlet sediments is isotopically lighter than the bulk organic matter by as much as 4°/oo, although the average difference between DOC and POC is much less (-0.6^o/oo). Several studies have measured the δ^{13}C of the high molecular weight fraction of DOC concentrated by dialysis through ultrafiltration membranes (Nissenbaum, et al. 1971; Orem et al., 1986). None of the above studies had adequate depth resolution to define the shape of the δ^{13}C-DOC profile.

PIC Analysis

PIC concentrations appeared to decrease to a depth of about 10 cm and increase at greater depth (Fig. 3.10). Coccolithophore and foraminifera tests were found to be absent from the sediment after careful microscopic analysis (J. Hilgert, Institute of Northern Forestry, Fairbanks, Ak., personal communication), suggesting that terrestrial
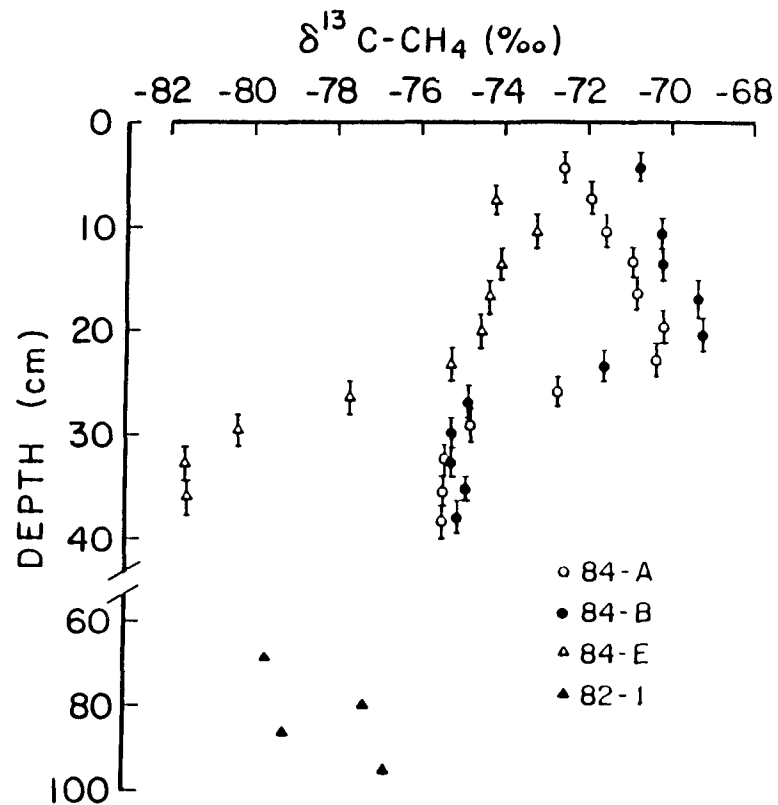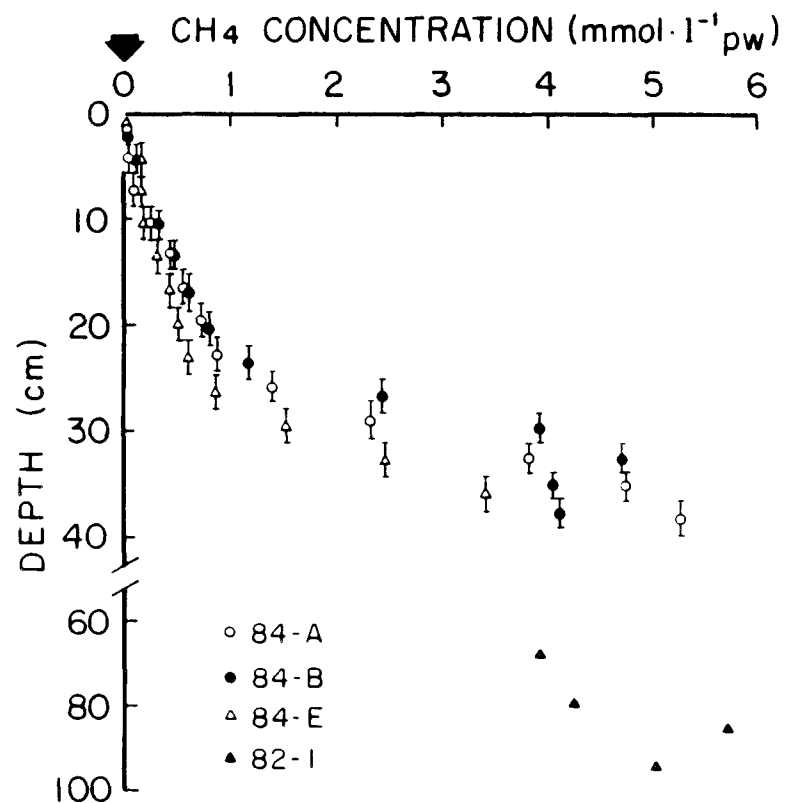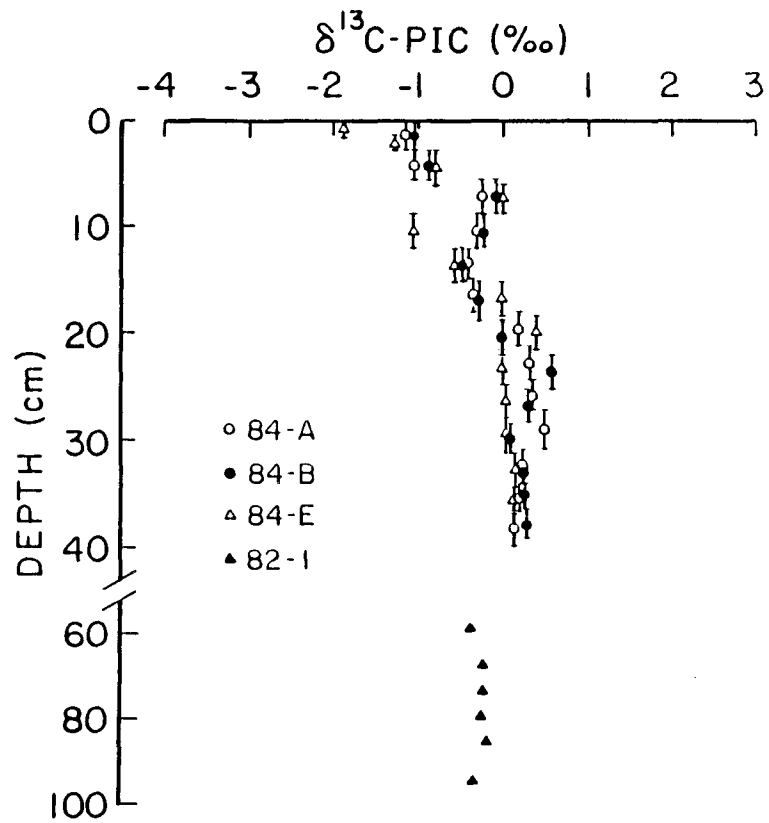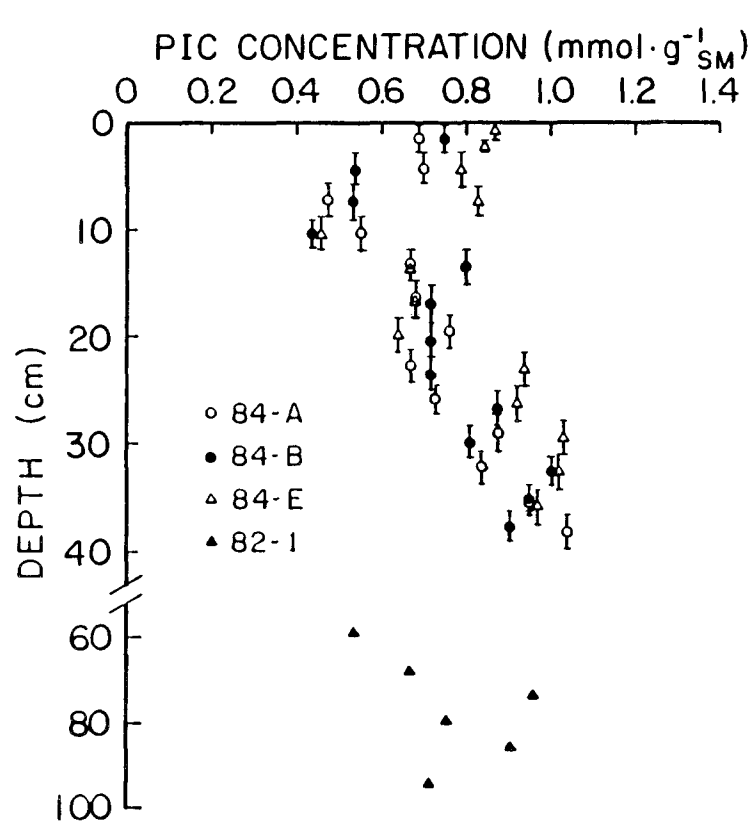
Fig. 3.10 Depth distributions of PIC and δ^{13}C-PIC. Vertical bars represent the sample depth interval; the symbol size represents the depth interval for points lacking a vertical bar. Subcores 84-A and 84-B are replicates from a single box core, subcore 84-E is from a different box core, and core 82-1 is a gravity core. Note the break and change of scale on the depth axis.

derived carbonates and/or mollusc shells serve as principle sources of sediment PIC. Fragments of mollusc shells were found in sediment and are visible in the X-radiograph (Fig. 3.12).

Small- and large-scale horizontal variability were approximately equal, averaging 11% (range: 5 to 20%, n=13). Vertical and horizontal variability were not appreciably different, with approximately 75% of the data points falling within 20% of the overall mean.

The δ^{13}C of the PIC pool (Fig. 3.10) covered a narrow range, with most samples falling between +0.5 and $-1^o/oo$. These δ^{13}C values are typical of marine invertebrates (Lloyd, 1964), and suggest that Skan Bay PIC has not been diagenetically altered. The δ^{13}C-PIC values became slightly more positive in the upper 20 cm and were essentially constant at greater depth. The δ^{13}C-PIC values for replicate subcores generally differed by less than $0.5^o/oo$.

POC Analysis

POC concentrations decreased rapidly just below the sediment-water interface so that by 10 cm, the concentration was about half its initial value (Fig. 3.11). Assuming the organic matter to have an empirical formula of CH_2O, the POC concentration near the sediment surface (8 mmol·g_{SM}^{-1}) is equivalent to 24% organic matter, an extremely high value even for organic-rich marine sediments. Small- and large-scale horizontal heterogeneity were approximately equal, averaging 8% (range: 2 to 13%, n=13).

The δ^{13}C-POC ranged from -19 to $-21^o/oo$ (Fig. 3.11), typical values for marine sediment (Deines, 1980). The POC became isotopically
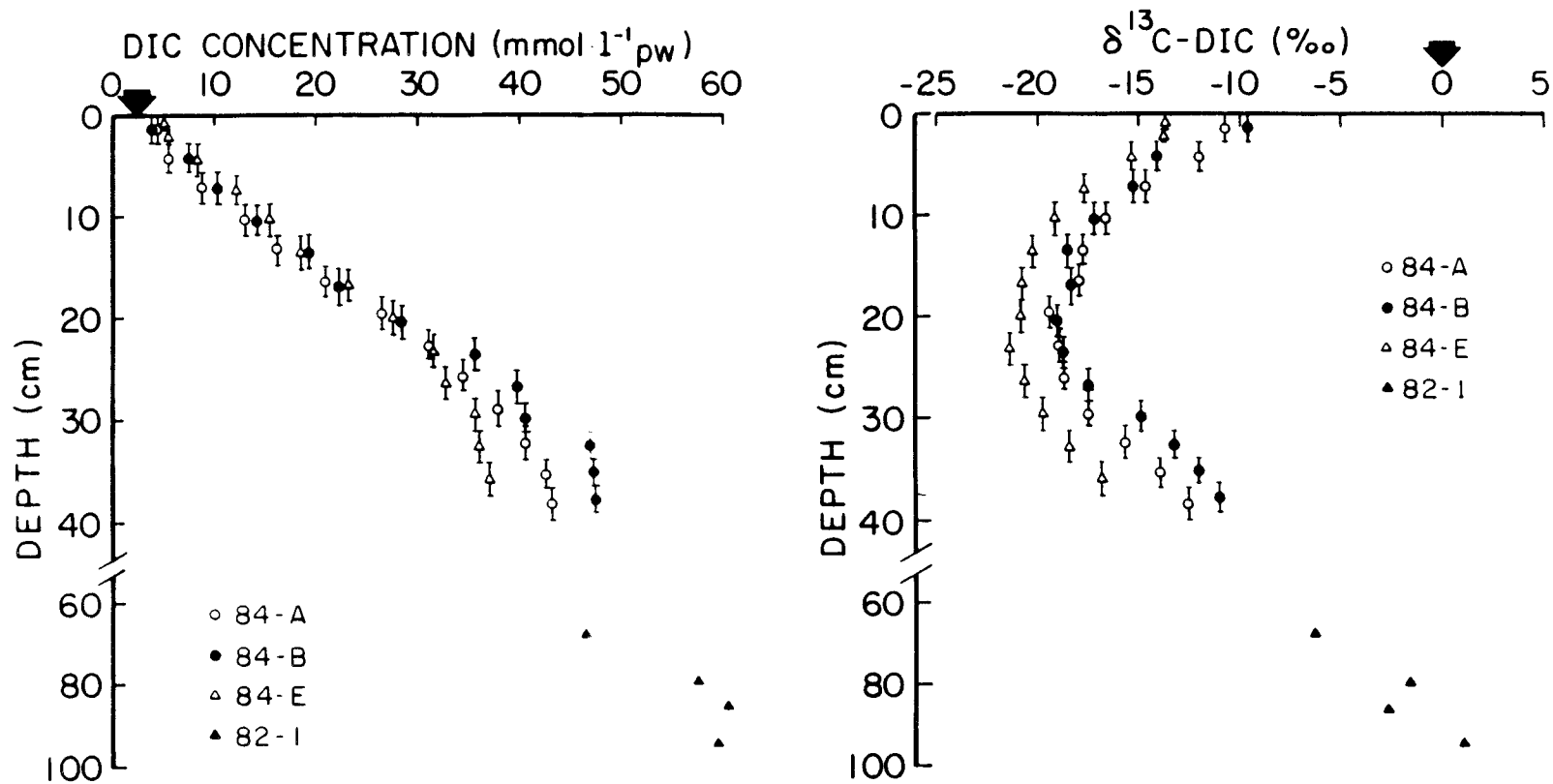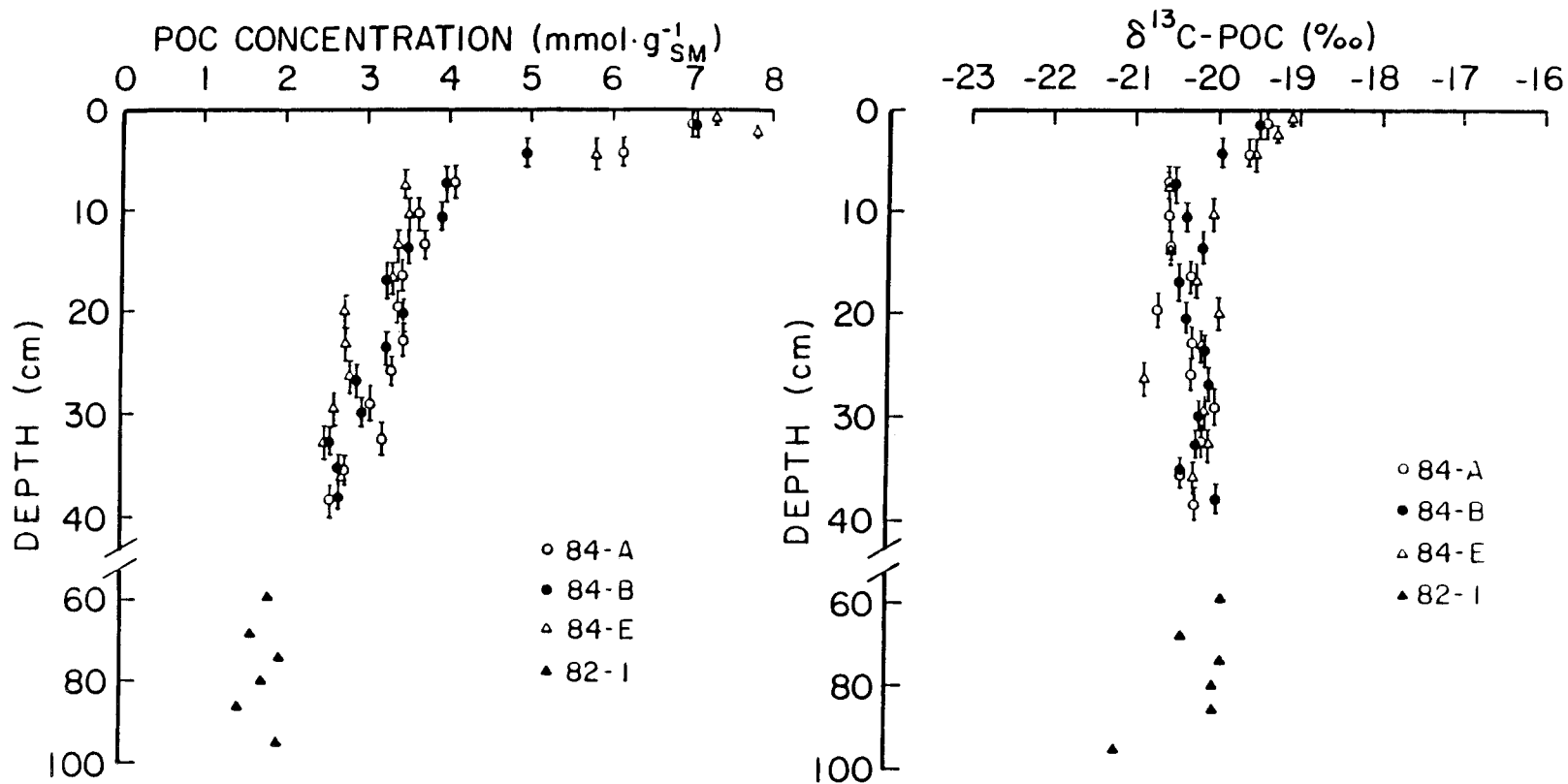
Fig. 3.11 Depth distributions of POC and δ^{13}C-POC. Vertical bars represent the sample depth interval; the symbol size represents the depth interval for points lacking a vertical bar. Subcores 84-A and 84-B are replicates from a single box core, subcore 84-E is from a different box core, and core 82-1 is a gravity core. Note the break and change of scale on the depth axis.

lighter with depth in the region where the POC concentration change was largest and showed little change below 10 cm. The δ^{13}C-POC values for replicate subcores generally agreed within 0.5^{o}/oo.

There are a number of possible explanations for a shift in δ^{13}C-POC with depth (Spiker and Hatcher, 1984): (a) temporal fluctuations in the isotopic composition of the source material, (b) selective utilization of isotopically distinct components of the POC, and (c) isotope fractionation during organic matter remineralization. The role that each of these processes plays in controlling the sediment δ^{13}C-POC depth distribution in Skan Bay is discussed in "Chapter 4: The Diagenetic Model" (p. 164).

Kelp and Water Column Particulates

Carbon content and δ^{13}C values of kelp and water column particulates are summarized in Table 3.1. The kelp samples appeared to be partially decomposed, as they had a lower carbon content than live, healthy kelp (30 to 35% C, K. Dunton, Univ. of Texas, Port Aransas, personal communication). Decomposition did not appear to alter the stable isotope ratios; two kelp samples with different carbon contents (i.e. different degrees of decomposition) had similar δ^{13}C values. The stipe had a higher carbon content and was isotopically lighter than the blade.

The δ^{13}C values of acidified and unacidified water column particulates were similar, indicating that PIC was not an important component of the material filtered from the water column. The filter was green and did not have visible kelp fragments, suggesting that the sample was composed primarily of phytoplankton.

Table 3.1. Carbon content and δ^{13}C of kelp and water column (WC) POC.

==

Sample	Date Collected	%C	δ^{13}C (^{o}/oo)	n
Whole kelp	Sept. 1980	22.2±0.2	-16.8±0.03	2
Whole kelp	Sept. 1981	26.9±0.1	-16.5±0.01	2
Stipe	Sept. 1982	25.2±0.7	-16.5±0.04	2
Blade	Sept. 1982	23.1±0.1	-15.8±0.01	2
WC POC	Sept. 1981		-21.5	1
WC POC (acidified)	Sept. 1981		-21.6	1

Other Analyses

X-radiography

The X-radiograph shows distinct layers indicating that sediment particles were not mixed by bioturbation (Fig. 3.12). Approximately 10 X-radiographs were taken in the course of this study. All show similar features: light and dark striations at approximately regular intervals. The absence of burrows or tubes extending to the surface suggests that bioirrigation and methane ebullition are not active.

The X-radiograph is a positive image; light and dark regions correspond to X-ray transparent and X-ray opaque sediment, respectively. The sediment appeared uniformly black to the naked-eye; the laminations are visible only by X-radiography. The white vertical crescent in the lower right is a split in the sediment caused by dessication. The slits that become prominent below 25 cm were created by CH_4 bubbles that formed when the sediment decompressed. The small black circular objects scattered throughout the X-radiograph are probably fragments of mollusc shells.

Geochronology

The supply of the natural radionuclide ^{210}Pb to the marine environment is approximately steady-state (Benninger, 1978), while prior to the explosion at the Chernobyl nuclear power plant (April, 1986), introduction of ^{137}Cs to the environment was restricted to the period of atmospheric bomb testing (early 1960's). These two radio-tracers, having source functions with distinct time dependence, provide independent estimates of sediment accumulation rates.

^{137}Cs profiles. The observed maximum in the ^{137}Cs profiles

Fig. 3.12. Representative X-radiograph of Skan Bay sediment.

0   CM   5

(Fig. 3.13) was assumed to represent the 1963 peak in atmospheric nuclear bomb testing (USERDA Health and Safety Laboratory, 1977). When corrected for the 4 years that lapsed between collection of subcores 84-B and 80-WP, both profiles had similar patterns. Higher maximum activities for subcore 80-WP may have resulted from the smaller sampling interval (1 cm as opposed to 3 cm for 84-B) leading to less dilution of the narrow ^{137}Cs maximum. The cause of the small peak in ^{137}Cs activity near the sediment surface is unknown.

The solid matter flux was calculated by dividing the cumulative mass at the ^{137}Cs maximum by the years elapsed between 1963 and the date of sediment sampling. The sediment accumulation rate, calculated from two ^{137}Cs profiles representing subcores collected 4 years apart, was 0.35 ± 0.01 g·cm^{-2}·yr^{-1}.

^{210}Pb profiles. The ln excess ^{210}Pb profile (Fig. 3.13) was approximately linear below a cumulative mass of 3.0 (corresponding to a depth of 17 cm). At shallower depths, the ^{210}Pb data showed considerable lateral heterogeneity.

In the absence of particle mixing, a linear ln excess ^{210}Pb profile indicates a constant rate of sediment accumulation over a time scale similar to the ^{210}Pb half-life (22.3 yr). The solid matter flux was calculated by dividing the ^{210}Pb decay constant by the slope of a line fitted to the natural logarithm of excess ^{210}Pb vs. cumulative mass data. Separate lines were fit to each subcore and all data points not enclosed in parenthesis (Fig. 3.13) were included in the regression. Correlation coefficients averaged 0.94 (range: 0.92 to 0.96, n=3), indicating that the ln excess ^{210}Pb vs. cumulative mass data show a
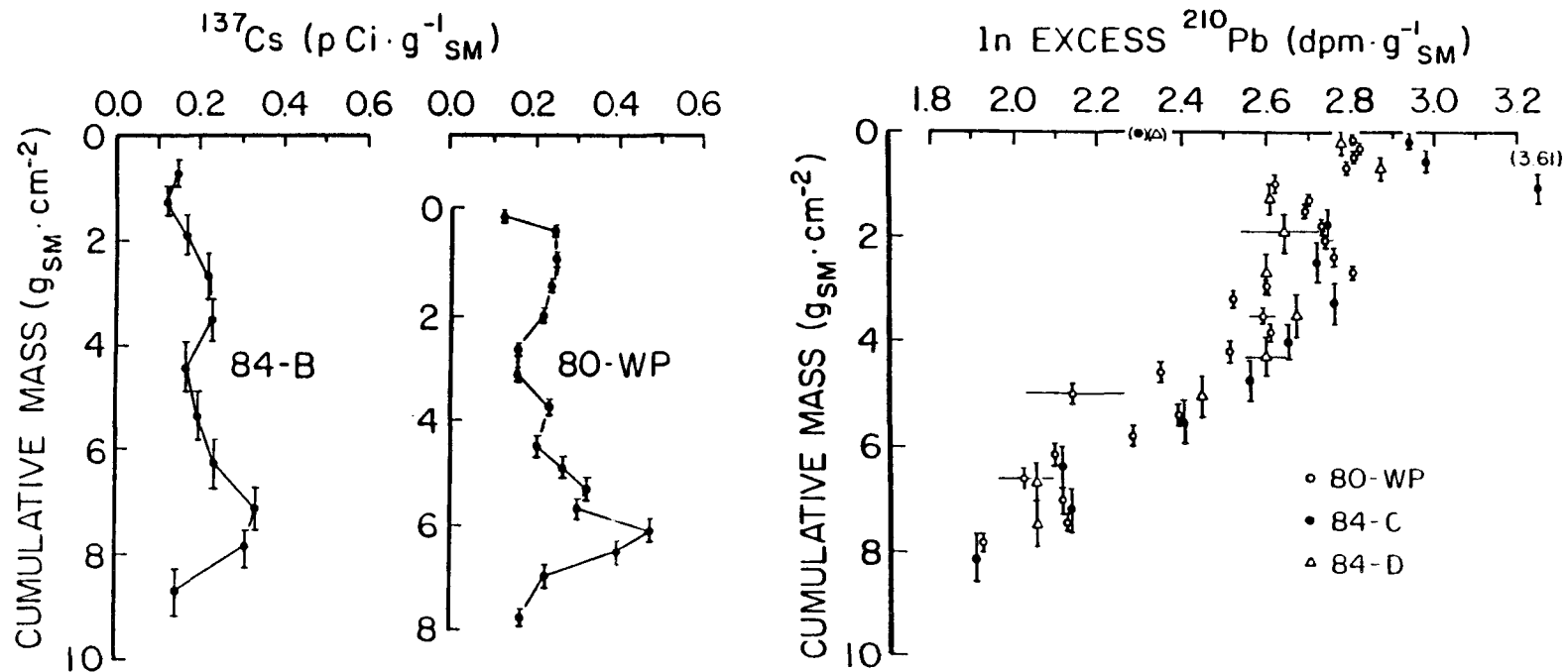
Fig. 3.13. Depth distributions of ^{137}Cs and ln excess ^{210}Pb. Vertical bars represent the sample depth interval. Subcores 84-B, 84-C, and 84-D are replicates from a single box core, while subcore 80-WP is from a different box core. The depth scales for the Cs profiles were aligned to account for sediment deposited during the 4 years between sampling of 80-WP and 84-B. The off-set in the depth scale was calculated from average Cs-137 sediment accumulation rates (Table 3.2). Data points bracketed by parenthesis are taken to be anomalous. Note that the depth scale is presented as cumulative mass.

strong linear correlation. The sedimentation rate calculated from the three ^{210}Pb profiles was 0.27 ± 0.03 g·cm^{-2}·yr^{-1}.

The cause of the extreme scatter in surficial ^{210}Pb activity is unknown. Sediment mixing to depths of 17 cm by bioturbating organisms is inconsistent with the laminations apparent in the X-radiograph (Fig. 3.12). Steep porosity gradients in the upper 10 cm (Fig. 3.1) argue against a major slumping event. Low surface concentrations of ^{210}Pb in non-bioturbated, anoxic marine sediments have been reported previously and may result from Pb redistribution by reaction with sulfide (Murray et al., 1978). It is also possible that the ^{210}Pb profile in Skan Bay sediment is influenced by the floc layer at the sediment-water interface.

Geochronology: Summary. Sedimentation rates calculated from ^{137}Cs and ^{210}Pb profiles are summarized in Table 3.2. Sediment accumulation rates estimated by the two tracers agree reasonably well, the ^{137}Cs rates being about 23% higher. Agreement of two geochronologies based on radio-tracers subject to processes having very different time constants argues against an unknown sedimentary process. In addition, close agreement between ^{137}Cs profiles from subcores collected 4 years apart indicates that the sediment accumulation rate between 1980 and 1984 was approximately equal to the average rate since 1963.

<div align="center">Hydrogen Sulfide</div>

Pore water ΣH_2S concentrations were high throughout the sediment column (Fig. 3.14). Samples closest to the sediment surface had ΣH_2S concentrations approaching 1 mM$_{PW}$, indicating that sediments were anoxic at or just below the sediment-water interface.

Table 3.2. Sediment accumulation rates estimated from ^{137}Cs and ^{210}Pb depth distributions.

===

| Core | ----Sediment Accumulation Rate $(g \cdot cm^{-2} \cdot yr^{-1})$---- | |
	from ^{137}Cs	from ^{210}Pb
80-WP	0.36	0.26
84-B	0.34	
84-C		0.24
84-D		0.30
MEAN	0.35±0.01 (n=2)	0.27±0.03 (n=3)
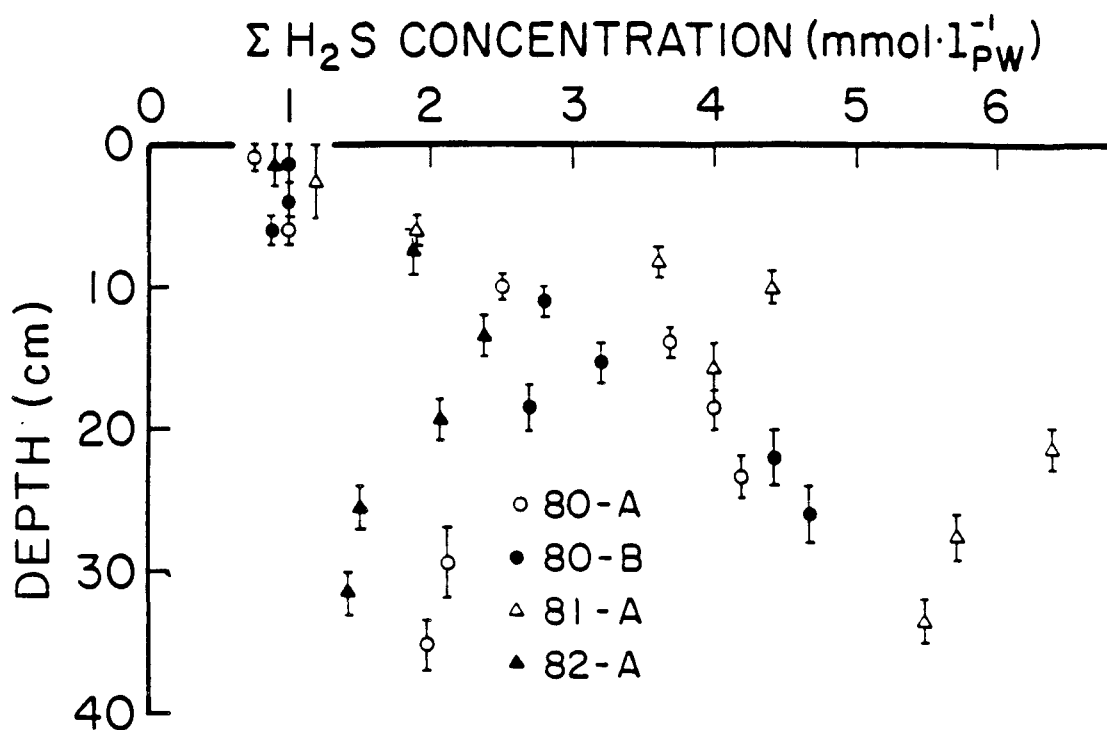
Fig. 3.14. Depth distribution of hydrogen sulfide. Each subcore came from a different box core; samples collected in 1980, 1981, and 1982 are represented. Vertical bars represent the sample depth interval.

CHAPTER 4: THE DIAGENETIC MODEL

A quantitative description of the sediment carbon cycle requires knowledge of exchange rates between major reservoirs. The purpose of this chapter is to quantify depth-dependent chemical reaction rates by means of a theoretical model. Concentration and isotope ratio depth distributions represent a composite record of the physical, biological, and chemical processes operating in a sedimentary environment. The diagenetic model provides a means of decoupling physical and chemical influences, so that if physical processes and chemical distributions are known, quantitative information on the chemical reactions can be predicted. The diagenetic model supplies reaction rates for processes that are difficult to measure experimentally, and serves to complement and augment those reactions where experimental rate data are available.

The chapter is divided into three sections: (a) **General Diagenetic Models** details the theory underlying the diagenetic model and the assumptions necessary to make the model equations tractable, (b) **Techniques for Solving the Diagenetic Equations** describes two complementary procedures for deriving predictive information from the diagenetic model, and (c) **Diagenetic Model Results** presents the results of applying the diagenetic model to the reservoirs involved in the Skan Bay carbon cycle.

General Diagenetic Models

Diagenesis refers to the physical, chemical, and biological changes that occur in sediment after deposition but prior to exposure to

the elevated temperatures and pressures characteristic of metamorphism. The diagenetic model is a concise, idealized representation of the physical and chemical processes that affect unconsolidated sediment. The model is based on the equation of motion, a mass-balance equation common in physical and chemical oceanographic studies. Berner (1964) was first to apply the equation to sediment and coined the term "diagenetic model" (Berner, 1971). A thorough summary of the theory and applications of diagenetic modelling is presented in Berner (1980).

The diagenetic model employs mathematical equations to represent the major processes that regulate mass transfer in the sediment system: diffusion (which may include "biodiffusion" [i.e. random mixing caused by benthic organisms] as well as molecular diffusion), advection, and reaction. The model can be conceptualized by dividing the sediment column into a number of contiguous boxes. Since matter can neither be produced nor destroyed within a box, the rate at which compound C accumulates must equal the difference between the rate at which it enters or is produced and the rate at which it leaves or is consumed. If the dimensions of the boxes are infinitely reduced, the rate of mass transfer can be represented by a partial differential equation in which diffusion (diff), advection (adv), and reaction (rxn) are represented by separate terms:

$$\frac{\partial [C]_{WS}}{\partial t} = \left\{\frac{\partial [C]_{WS}}{\partial t}\right\}_{diff} + \left\{\frac{\partial [C]_{WS}}{\partial t}\right\}_{adv} + \left\{\frac{\partial [C]_{WS}}{\partial t}\right\}_{rxn} . \qquad (4.1)$$

The brackets denote concentration in terms of molarity, the subscript (WS) indicates that concentrations are in whole sediment units (mmol l^{-1} whole sediment), and t is time. By expressing diffusion, advection, and

reaction processes as depth dependent functions and making simplifying assumptions, eq. 4.1 can be transformed into a linear differential equation solvable by standard techniques.

The diagenetic model is a vastly simplified representation of the sedimentary system. The assumptions necessary to produce a tractable model could lead to a distorted view of sediment processes. The likelihood of such misrepresentation will be reduced by considering the following guidelines in model formulation:

1. The model should be physically, chemically, and microbiologically realistic.

2. Simplifying assumptions should be stated and evaluated.

3. Quantitative model predictions should take into account uncertainty in the parameters.

4. The model should avoid introducing artifacts by dividing the system with arbitrary boundaries.

Each term on the right-hand side of eq. 4.1 will be considered separately. Concentration will be expressed in pore water units ($mmol \cdot l^{-1}$ pore water) for dissolved constituents and solid matter units ($mmol \cdot g^{-1}$ solid matter) for solid phase constituents. The symbols used in the following discussion are defined in Table 4.1.

Diffusion

Diffusion is a process "which leads to an equalization of

Table 4.1. List of commonly used symbols and their units.

==

$[C]_{WS}$ = whole sediment concentration (mmol$\cdot$l^{-1} whole sediment)

$[C]_{PW}$ = pore water concentration (mmol$\cdot$l^{-1} pore water)

$[C]_{SM}$ = solid matter concentration (mmol$\cdot$g^{-1} solid matter)

D_o = free solution diffusion coefficient (cm$^2\cdot$yr^{-1})

D_{WS} = whole sediment diffusion coefficient (cm$^2\cdot$yr^{-1})

$f = {}^{12}D_o/{}^{13}D_o$ (molecular diffusivity ratio for ^{12}C and ^{13}C)

F_{SM} = solid matter flux (g solid matter cm$^{-2}\cdot$yr^{-1})

ω = burial velocity of solid particles (cm$\cdot$yr^{-1})

ν = burial velocity of pore water (cm$\cdot$yr^{-1})

ϕ = porosity (ml$_{PW}\cdot$ml$_{WS}^{-1}$)

θ = tortuosity (unitless)

ρ_{SM} = solid matter density (g$_{SM}\cdot$ml$_{SM}^{-1}$)

t = time (yr)

x,y = horizontal distances (cm)

z = vertical distance below the sediment-water interface (cm)

∞ (subscript) = depth where dϕ/dz = 0

----

concentrations within a single phase" (Jost, 1960). In a sedimentary environment, diffusion may result from random advective mixing associated with physically active macroscopic organisms (biodiffusion) as well as random molecular motions driven by thermal energy (molecular diffusion). The following discussion is limited to molecular diffusion.

Molecular diffusion in the pore water is described by Fick's Second Law (Jost, 1960):

$$\left\{\frac{\partial [C]_{PW}}{\partial t}\right\}_{diff} = \frac{\partial (D_o \partial [C]_{PW}/\partial x)}{\partial x} + \frac{\partial (D_o \partial [C]_{PW}/\partial y)}{\partial y} + \frac{\partial (D_o \partial [C]_{PW}/\partial z)}{\partial z}, \quad (4.2)$$

where the subscript (PW) indicates pore water concentration units, D_o is the free solution diffusion coefficient, and x, y, and z are spatial coordinates (x and y represent horizontal distances and z represents the vertical distance below the sediment surface). If horizontal concentration gradients are small relative to vertical, eq. 4.2 simplifies to:

$$\left\{\frac{\partial [C]_{PW}}{\partial t}\right\}_{diff} = \frac{\partial (D_o \partial [C]_{PW}/\partial z)}{\partial z} . \quad (4.3)$$

Whole sediment is a two-phase system composed of solid material and pore water solution, but molecular diffusion occurs only within the dissolved phase. To describe diffusion in whole sediment, a porosity term must be incorporated into Fick's Second Law:

$$\left\{\frac{\partial [C]_{WS}}{\partial t}\right\}_{diff} = \frac{\partial (\phi D_{WS} \partial [C]_{PW}/\partial z)}{\partial z} , \quad (4.4)$$

where D_{WS} is the whole sediment diffusion coefficient. The presence of solid material restricts random molecular motions, reduces the rate of diffusion, and causes the value of D_{WS} to be less than D_o (Berner, 1980):

$$D_{WS} = D_o/\theta^2 \ . \tag{4.5}$$

Tortuosity (θ) is the distance traveled by a molecule diffusing through whole sediment divided by the straight line distance. In high porosity ($\phi > 0.7$) marine sediments, tortuosity may be estimated by the following empirical relationship (Ullman and Aller, 1982):

$$\theta = 1/\phi. \tag{4.6}$$

Therefore, from eqs. 4.5 and 4.6,

$$D_{WS} = \phi^2 D_o. \tag{4.7}$$

Substituting eq. 4.7 into eq. 4.4,

$$\left\{\frac{\partial[C]_{WS}}{\partial t}\right\}_{diff} = \frac{\partial(\phi^3 D_o \partial[C]_{PW}/\partial z)}{\partial z} \ . \tag{4.8}$$

If D_o is constant with depth, it can be factored outside the derivative and the right-hand side expanded:

$$\left\{\frac{\partial[C]_{WS}}{\partial t}\right\}_{diff} = \phi^3 D_o \frac{\partial^2[C]_{PW}}{\partial z^2} + 3\phi^2 D_o \frac{\partial\phi}{\partial z}\frac{\partial[C]_{PW}}{\partial z} \ . \tag{4.9}$$

Advection

Advection is the flow of material relative to a defined reference frame (Lerman, 1979). Geochemists consider the fixed reference frame to be the sediment-water interface. Thus, as sediment accumulates, particles at a given depth appear to "flow" downward. For a solid phase constituent, the concentration change due to advection is given by:

$$\left\{\frac{\partial[C]_{WS}}{\partial t}\right\}_{adv} = \frac{-\partial(\omega[C]_{WS})}{\partial z} \ , \tag{4.10}$$

where ω is the burial velocity of solid particles below the sediment surface. The results of the solid phase analyses are reported in solid

matter concentration units; the diagenetic equation for a solid phase
constituent should be expressed in equivalent units. Whole sediment and
solid matter concentrations are related by the following equation:

$$[C]_{WS} = \rho_{SM}(1-\phi)[C]_{SM} , \qquad (4.11)$$

where the subscript (SM) indicates solid matter concentration units and
ρ_{SM} is solid matter density. Substituting eq. 4.11 into eq. 4.10:

$$\left\{\frac{\partial[C]_{WS}}{\partial t}\right\}_{adv} = \frac{-\partial(\omega\rho_{SM}(1-\phi)[C]_{SM})}{\partial z} . \qquad (4.12)$$

If the density of the material comprising the solid fraction does not
change with depth, ρ_{SM} can be factored and the derivative expanded:

$$\left\{\frac{\partial[C]_{WS}}{\partial t}\right\}_{adv} = -\rho_{SM}\omega(1-\phi)\frac{\partial[C]_{SM}}{\partial z} - \rho_{SM}[C]_{SM}\frac{\partial[\omega(1-\phi)]}{\partial z} . \qquad (4.13)$$

Pore water is incorporated with solid matter as sediment accumu-
lates giving rise to pore water "flow". In addition to the downward
"flow" of pore water caused by sediment accumulation, there is an upward
flux due to compaction. Thus in sediments undergoing compaction, the
burial velocity of pore water is less than that of the solid particles.
Advection of a pore water constituent is described by:

$$\left\{\frac{\partial[C]_{WS}}{\partial t}\right\}_{adv} = \frac{-\partial(\nu[C]_{WS})}{\partial z} , \qquad (4.14)$$

where ν is the burial velocity of pore water relative to the sediment-
water interface. Pore water analyses are reported in pore water concen-
tration units and the advection equation for a pore water constituent
should be expressed in similar units. Whole sediment and pore water
concentrations are related by the following equation:

$$[C]_{WS} = \phi [C]_{PW} .\tag{4.15}$$

Substituting eq. 4.15 into eq. 4.14 and expanding the derivative:

$$\left\{\frac{\partial [C]_{WS}}{\partial t}\right\}_{adv} = -\phi v \frac{\partial [C]_{PW}}{\partial z} - [C]_{PW} \frac{\partial (\phi v)}{\partial z} .\tag{4.16}$$

Reaction

The reaction term is the most problematic aspect of the diagenetic equation. In recent anoxic marine sediments, most reactions involving carbon are bacterially mediated and the kinetics of such reactions are poorly understood. A great number of factors influence the rate of biological reactions including: concentration and bio-availability of carbon compounds, concentration of electron acceptors, bacterial population densities, enzyme affinities, and interspecies competition and symbiosis. Berner (1980) discussed the difficulties of understanding rates of bacterially mediated carbon remineralization reactions:

> In sediments we must deal with many different interacting micro-organisms and a whole series of simultaneous reactions, with the product of one being the reactant or the inhibitor (poison) of one or more others. Generally, we do not know the nature of the inter-mediate organic molecules transferred from one group of bacteria to another... In fact, we do not have a very good idea of the nature of the complex starting materials in organic decomposition, the biopolymers ... and we know even less about the relatively non-degradable complex molecules that may form abiologically during decomposition, the so-called 'geopolymers'. (p. 84)

Nevertheless, as a first approach to understanding a complex problem, Berner proposed that sediment organic matter be approximated by a relatively small number of components each having pseudo-first order decomposition kinetics:

$$\left\{\frac{\partial [POC]}{\partial t}\right\}_{rxn} = -(k_1 [POC]_1 + k_2 [POC]_2 + k_3 [POC]_3 + \ldots) ,\tag{4.17}$$

where the subscripts (1,2,3) represent components of the POC pool with differing reactivities, and the k's represent first-order rate constants for each component. First-order kinetics is the most often applied rate law in diagenetic models. The rate constants are calculated so that concentration-depth distributions predicted by the diagenetic model best fit the data. Although many valuable insights have emerged from these models, first-order rate laws contain features inconsistent with the modelling guidelines set forth earlier in this chapter (p. 100). Two drawbacks of first-order kinetic rate laws are described below.

1. Rate laws are difficult to confirm experimentally. Rigorous verification requires detailed chemical knowledge of the reactants, elucidation of the bacterial species involved in the reaction, an understanding of the enzymes that catalyze the reaction, and a knowledge of how the overall process is influenced by micro-organism interactions. Because of the intractable nature of the verification procedure, many geochemical models have used first-order rate laws without experimental justification. However, unless the kinetic laws have an experimental or theoretical foundation, the predicted rate constants have meaning only as empirical curve-fitting parameters.

Westrich and Berner (1984) have attempted to verify first-order kinetics for POC remineralization using a laboratory "feeding" experiment. They found that SO_4^{2-} reduction rates were directly proportional to the quantity and quality of phytoplankton added to anoxic sediment. Although these results show that SO_4^{2-} reduction rates are stimulated when sediment is enriched with organic matter, the predicted rate

constants are only rigorously applicable to a sediment system amended with phytoplankton.

2. **The number of terms in the first-order rate law (eq. 4.17) necessary to provide a chemically and microbiologically realistic description of POC remineralization is difficult to evaluate.** The POC in Skan Bay sediment appears to have two main sources: phytoplankton and kelp (see p. 165). However, to describe remineralizaton by a two term rate law ignores the fact that phytoplankton and kelp are composed of many different biomolecules, each of which is metabolized according to unique reaction kinetics. Without a considerable extension of organic geochemical knowledge, it is impossible to link each term of the rate law to an actual compound or class of chemicals.

Predictions derived from diagenetic models are strongly dependent on the formulation of the rate term. Given our limited knowledge regarding kinetics of bacterially mediated reactions in anoxic marine sediment, it is preferable to utilize diagenetic models without employing an uncertain representation of the reaction term. This can be accomplished in two ways: (a) if estimated reaction rates are available, a numerical representation of the rate data can be input into the diagenetic equation; (b) if reaction rates are unknown, the diagenetic equation can be inverted and the reaction rate expressed as the solution to the equation. Both approaches will be utilized in this study; presently, the reaction term will be written in its most general form.

A reaction can lead to production or consumption of a particular sediment constituent. The reaction term in eq. 4.1 was written so that

positive and negative values represent production and consumption, respectively. A reaction that consumes a solid phase constituent such as POC leads to production of a pore water constituent (e.g. DOC). Since solid phase and pore water reactions are directly related, reaction rates for both phases should be expressed in equivalent units. For convenience, pore water units are used. Equation 4.15 describes the relationship between pore water and whole sediment concentration units. Substitution into the reaction term from eq. 4.1 yields:

$$\left\{\frac{\partial [C]_{WS}}{\partial t}\right\}_{rxn} = \left\{\frac{\partial(\phi[C]_{PW})}{\partial t}\right\}_{rxn} . \tag{4.18}$$

The Diagenetic Equations

The diffusion, advection, and reaction terms can be combined to form diagenetic equations for solid phase and pore water constituents. For solid phase constituents, the advection (eq. 4.13) and reaction (eq. 4.18) terms are combined:

$$\frac{\partial [C]_{WS}}{\partial t} = -\rho_{SM}\omega(1-\phi)\frac{\partial [C]_{SM}}{\partial z} - \rho_{SM}[C]_{SM}\frac{\partial(\omega(1-\phi))}{\partial z} + \left\{\frac{\partial(\phi[C]_{PW})}{\partial t}\right\}_{rxn}. \tag{4.19}$$

For pore water constituents, diffusion (eq. 4.9), advection (eq. 4.16), and reaction (eq. 4.18) terms are combined:

$$\frac{\partial [C]_{WS}}{\partial t} = \phi^3 D_o \frac{\partial^2 [C]_{PW}}{\partial z^2} + 3\phi^2 D_o \frac{\partial \phi}{\partial z}\frac{\partial [C]_{PW}}{\partial z}$$

$$- \phi\nu \frac{\partial [C]_{PW}}{\partial z} - [C]_{PW}\frac{\partial(\phi\nu)}{\partial z} + \left\{\frac{\partial(\phi[C]_{PW})}{\partial z}\right\}_{rxn} . \tag{4.20}$$

Due to compaction, the burial velocity of solid matter (ω) and pore water (ν) relative to the sediment-water interface change with depth.

The rate of compaction is most pronounced in the surface sediment and decreases exponentially with depth. At some depth, the compaction rate approaches zero, porosity approaches an asymptotic value (ϕ_∞), sediment accumulation rates approach a constant (ω_∞), and solid matter and pore water velocities become equal. The following identities simplify the advection terms in eqs. 4.19 and 4.20 (Berner, 1980):

$$\omega(1-\phi) = \omega_\infty(1-\phi_\infty) \ , \qquad (4.21)$$

$$\phi\nu = \phi_\infty\omega_\infty \ , \qquad (4.22)$$

The diagenetic equations can be simplified by assuming that the sediment system is at steady-state, i.e. the composition of the sediment does not change with time. This implies that

$$\partial[C]_{WS}/\partial t = 0 \ , \qquad (4.23)$$

$$\partial\phi/\partial t = 0 \ . \qquad (4.24)$$

$$\partial(\phi\nu)/\partial z = 0 \ , \qquad (4.25)$$

$$\partial(\omega(1-\phi))/\partial z = 0 \ . \qquad (4.26)$$

With eqs. 4.21 thru 4.26, eqs. 4.19 and 4.20 reduce to:

$$-\rho_{SM}\omega_\infty(1-\phi_\infty) \ \frac{d[C]_{SM}}{dz} + \phi \ \{\frac{d[C]_{PW}}{dt}\}_{rxn} = 0 \ , \qquad (4.27)$$

$$\phi^2 D_o \ \frac{d^2[C]_{PW}}{dz^2} + (3\phi D_o \ \frac{d\phi}{dz} - \frac{\omega_\infty\phi_\infty}{\phi}) \ \frac{d[C]_{PW}}{dz} + \{\frac{d[C]_{PW}}{dt}\}_{rxn} = 0 \ . \qquad (4.28)$$

Equations 4.27 and 4.28 are the steady-state, one-dimensional diagenetic equations for solid phase and pore water constituents, respectively.

Model Assumptions

The assumptions incorporated into eqs. 4.27 and 4.28 are stated and evaluated in the following section.

1. **Molecular diffusion and advection were the only important mass transport processes in Skan Bay sediments.** Other mass transport processes in marine sedimentary environments include: (a) bioturbation, (b) bioirrigation, (c) CH_4 ebullition, (d) wind and current mixing, and (e) forced advection due to ground water intrusion.

Bioturbation refers to the crawling and burrowing activities of benthic organisms which can lead to mixing and homogenization of shallow sediment. The sediment X-radiograph (Fig. 3.12) provides evidence that any sediment reworking in Skan Bay was limited to the sediment-water interface. The striations that occur at regular 1 to 2 cm intervals represent sediment layers of differing X-ray opacity; these layers would be homogenized if bioturbating organisms were active below the sediment surface.

Benthic organisms can also enhance sediment-overlying water exchange by bioirrigation, i.e. active or passive irrigation by burrow-dwelling organisms. There is strong evidence that irrigating organisms were not active in Skan Bay sediments at the time of sampling. A benthic chamber deployed during the September 1984 cruise provided in situ flux measurements for alkalinity, PO_4^{3-}, NH_4^+, and $Si(OH)_4$ (Devol, 1987). Measured fluxes agreed quite well with those calculated from pore water concentration profiles assuming molecular diffusion to be the only mass-transport process (Table 4.2). Furthermore, tritiated water (HTO), injected into the overlying water a short time after closure of the deployed benthic chamber, mixed with pore water at a rate in accordance with molecular diffusion.

Table 4.2. Comparison of measured and calculated benthic fluxes[a].

==

Pore Water Constituent	Benthic Flux Measured/Calculated[b]	n
Alkalinity	1.1±0.2	7
PO_3^{3-}	1.1±0.2	8
NH_4^+	0.9±0.1	8
$Si(OH)_4$	0.9±0.2	8
HTO	1.0±0.2	2
MEAN	1.0±0.1	5

----

[a]Data from Devol (1987).

[b]Measured fluxes were based on data from an in situ benthic chamber experiment. Fluxes were calculated from sediment-water concentration gradients using Fick's Law modified for sediment porosity and tortuoisty. Details of the calculations are given in Devol (1987).

Methane ebullition can transport dissolved gases through the sediment column. In addition, bubble tubes formed by CH_4 ebullition can significantly enhance molecular diffusion of all pore water constituents by increasing the sediment surface area in contact with the overlying water column (Martens and Klump, 1980). In situ bubble formation occurs when the CH_4 partial pressure exceeds that exerted by the overlying sediment, water column, and atmosphere. The 65 m water column contributed a pressure of 6.5 atmospheres (the hydrostatic pressure of 10 m of seawater is approximately 1 atm) so that the total pressure at the sediment surface was 7.5 atm. This partial pressure is equivalent to a CH_4 concentration of >14 mM (calculated from Henry's Law using solubility data from Yamamoto et al. [1976]). Methane distributions from gravity cores (Fig. 3.3) showed that concentrations peaked at about 12.5 mM_{PW}. Only one anomolous sample had a concentration high enough to cause in situ bubble formation. The absence of visible bubble tubes in the X-radiograph (Fig. 3.12) confirms that ebullition was not an important transport mechanism in Skan Bay sediment.

Sediment mixing by currents or wind-induced waves was probably negligible. The 10 m sill prevents bottom currents from entering the basin. Skan Bay is well protected from the wind and the pycnocline restricts wave energy to the upper water column.

Finally, the effect of ground water intrusion is considered. Ion chromatographic analyses of pore water Cl^- showed constant concentrations with depth, indicating that ground water percolation into the sediment did not occur.

2. **Horizontal concentration gradients for pore water constituents were small relative to vertical.** All concentration profiles had greater lateral variability than expected from analytical error. This "patchiness" suggests that there was a horizontal as well as vertical component to the diffusive flux. The ratio of horizontal to vertical concentration gradients for pore water constituents examined in this study are summarized in Table 4.3. For CH_4, SO_4^{2-}, and DIC reservoirs, vertical dominated over horizontal concentration gradients. The horizontal component of the diffusive flux was simulated in the models by incorporating uncertainty in the diffusion coefficient.

3. **The free solution diffusion coefficient was constant with depth.** According to the Stokes-Einstein equation (Lerman, 1979), the free solution diffusion coefficient for a given spherical molecule depends only on solution temperature and viscosity. The viscosity, in turn, is a function of temperature and salinity. Thus, to the extent that the Stokes-Einstein equation is accurate, D_o will change with sediment depth only if vertical temperature and salinity gradients are present. Since annual temperature variation in Skan Bay sediment is probably $\leq 3^o C$ (see p. 16), thermal gradients within the sediment are unlikely. As discussed above, a pore water salinity gradient was not observed.

4. **The density of solid matter was constant with depth.** The sediment is primarily composed of clay particles for which the density is not likely to change during diagenesis (prior to thermal alteration). This was confirmed by measurements which showed that solid matter

Table 4.3. Ratio of horizontal to vertical concentration gradients
for pore water constituents.[a]

Depth (cm)	CH_4[b]	SO_4^{2-}[c]	DIC[d]	DOC[d]
1.5	0.10	0.13	0.02	0.02
4.5	0.13	0.15	0.16	3.13
7.5	0.07	0.05	0.08	0.47
10.5	0.06	0.20	0.04	1.35
13.5	0.11	0.21	0.14	0.12
16.5	0.14	0.02	0.03	0.11
19.5	0.18	0.07	0.01	0.37
22.5	0.09	0.08	0.14	0.10
25.5	0.08	0.07	0.33	0.19
28.5	0.18	0.07	0.20	0.17
31.5	0.06	0.09	0.49	0.73
34.5	0.14	0.02	0.73	0.22
37.5	0.12	0.44	0.56	0.25
MEAN	0.11	0.12	0.22	0.56

[a]Horizontal concentration gradients were calculated as the standard deviation at a particular depth divided by the average distance between replicate subcores from the same box core (10 cm). Vertical concentration gradients were estimated from the slope of the concentration-depth distribution.

[b]Subcores 84-T, 84-U, and 84-V.

[c]Subcores 84-W, 84-X, and 84-Y.

[d]Subcores 84-A and 84-B.

densities of surface and deep samples were essentially identical (see p. 22).

5. **Equation 4.7 ($D_{WS} = \phi^2 D_o$) accurately describes the relationship between the free-solution and whole-sediment diffusion coefficients.** Several studies have measured D_{WS} for SO_4^{2-} and CH_4 in high porosity marine sediment. These results were compared with D_{WS} values predicted from eq. 4.7 (Table 4.4). The average difference between measured and predicted values was -3% indicating no large systematic bias, while the magnitude of the relative error averaged 13%. Whole sediment diffusion coefficients predicted by eq. 4.7 were assumed to be accurate to $\pm15\%$.

6. **Concentrations within carbon reservoirs are at steady-state.** Steady-state is probably the most common assumption in diagenetic models and is also the most difficult to verify. In theory, steady-state could be validated by repetitive measurements at one location over a period of time. However, even in a high deposition environment like Skan Bay, sediment collected in a typical box core represents several decades' accumulation. Direct observation of long-term temporal variability is obviously impractical. Also, the same sediment cannot be sampled twice, so that time-series studies are confounded by lateral heterogeneity.

The reservoirs that comprise the sediment carbon cycle will maintain a steady-state if input and output fluxes remain constant. The carbon input flux is ultimately controlled by the sediment deposition rate. The output flux, consisting of decomposed organic matter that diffuses to the overlying water, is also ultimately controlled by the supply of sediment material. Geochronological data from Skan Bay suggest

Table 4.4. Comparison of measured and predicted values for D_{WS}.

===

Study	ϕ	Temp (^{o}C)	D_{WS} (x10^{-6}cm^{2}s^{-1}) Measured	Predicted[a]	Relative error (%)
SULFATE					
Li and Gregory (1974)	0.68[b]	5	3.3	2.7	18
Jørgensen (1978b)	0.9[c]	10	4.5[c]	5.6[d]	-24
	0.8		4.0	4.4	-10
	0.7		3.5	3.4	-3
Krom and Berner (1980)	0.72	20	5.0	4.6	8
Iversen and Jørgensen (1985)	0.9[c]	8	4.8[c]	5.3[e]	-33
	0.8		3.6	4.2	-17
	0.7		3.2	3.2	0
METHANE					
Iversen and Jørgensen (1985)	0.9[c]	8	8.0[c]	7.6[e]	5
	0.8		7.1	6.0	15
	0.7		5.2	4.6	12

Average relative error (%)   -3
Average magnitude of relative error (%)   13

[a]D_{WS} values were predicted by eq. 4.7. Values of D_o for sulfate and methane from Li and Gregory (1974) and Sahores and Witherspoon (1970), respectively, were corrected to the experimental temperature and salinity according to the Stokes-Einstein equation using seawater viscosities reported in Knauss (1978).

[b]Calculated from reported water content and solid matter density.

[c]Calculated from linear regression of D_{WS} vs. ϕ data.

[d]Salinity ranged from 23 to 29°/oo; 26°/oo was used in calculations.

[e]Salinity ranged from 26 to 35°/oo; 30°/oo was used in calculations.

that the sediment accumulation rate has been relatively constant over a period of years to decades (see p. 95). It is reasonable to assume that concentrations within carbon reservoirs have remained relatively constant over this time-scale.

Non-steady-state variability over shorter (i.e. seasonal) time-scales is more difficult to evaluate. Unfortunately, seasonal sampling in Skan Bay was not possible because of its remote location. Seasonal changes in solar luminosity probably have minimal impact on the Skan Bay carbon cycle. Skan Bay sediment is well below the euphotic zone and annual variation in sediment temperature is minimal (see p. 16). The quality and quantity of deposited organic matter undoubtedly change with season, but this variability should have minimal impact on carbon cycling rates below the surface sediment.

Periodic ventilation of Skan Bay bottom water could create a seasonal oxidized surface layer in the sediment. Carbon degradation rates in oxic and anoxic sediment appear to be comparable (Henrichs and Reeburgh, 1987), so oxic conditions at the surface would not profoundly affect overall remineralization rates. However, oxygen-rich bottom water could allow temporary habitation by benthic macrofauna, which would significantly increase rates of organic matter decompositon reactions (Kristensen and Blackburn, 1987).

Without seasonal data, periodic habitation of Skan Bay sediment by macrofauna cannot be ruled out. Unlike bioturbation, bioirrigation does not leave a permanent sedimentary record. Small burrows may collapse and essentially disappear after abandonment. Likewise, pore water profiles quickly change following the demise of a benthic community.

Techniques for Solving the Diagenetic Equations

Solving the diagenetic equations (eqs. 4.27 and 4.28) requires that system boundaries be defined. An obvious choice for the upper boundary is the sediment-water interface. A natural discontinuity is not available for the lower boundary which is therefore established by the sampling method. Since the deepest sample provided by the box corer covers the 36-39 cm interval, the lower boundary was set at 37.5 cm.

The lower boundary is not as arbitrary as it may seem. Carbon remineralization rates at depths greater than 37.5 cm are much slower than in shallower sediment and the transition from SO_4^{2-} reduction to CH_4 production, which occurs at depths greater than 30 to 40 cm makes this location somewhat of a natural boundary.

Two complementary approaches are available for solving the diagenetic equations: (a) direct solution, and (b) derivative estimation of concentration-depth profiles. The utility and merits of both approaches are discussed below.

Direct Solution of the Diagenetic Equation

Direct solution of the diagenetic equation requires a priori knowledge of the reaction term. Because of the difficulties of validating assumed kinetic rate laws, this approach was employed only for reservoirs in which depth dependent reaction rates had been measured experimentally (i.e. CH_4 and SO_4^{2-}).

Experimental rate data were incorporated into the diagenetic equation by fitting depth distributions with a natural cubic spline. A cubic spline is a function consisting of multiple cubic polynomials joined

together with the condition of continuous first and second derivatives (Cheney and Kincaid, 1980). The result is a smooth curve that passes through each data point. Cubic splines are discussed in more detail in a later section (p. 126).

The diagenetic equation for a particular reservoir was numerically solved and the predicted concentration-depth distribution compared with experimental data. Agreement between modelled and measured concentration profiles substantiates the experimental rate data and indicates that reactions important in controlling the concentration-depth distribution have been considered. On the other hand, failure of the model to predict the essential features of a measured depth distribution points to errors in experimental rate measurements, the existence of important but un-quantified chemical or biological reactions, and/or unjustified assump-tions regarding the physical processes that influence sediment chemistry.

Prescribed Conditions

The diagenetic equation for pore-water constituents (eq. 4.28) is a second-order differential equation and thus requires two prescribed conditions to define a unique solution. If both conditions are specified at the same boundary, the equation is said to be an "initial value problem". If the conditions are at the two boundaries, the equation is said to be a "boundary value problem". An initial value problem normally requires that the dependent variable (in this case concentration) and its first derivative (the concentration gradient) be known at one of the system's boundaries, while a boundary value problem requires knowledge of the concentration at the two system boundaries.

For pore water constituents, establishing concentrations at system boundaries is relatively straightforward. Since eddy diffusion ensures that bottom waters are well-mixed, the concentration at the sediment-water interface can be estimated from the bottom water concentration. The concentration at the lower boundary is the concentration at the depth of the deepest sample (36-39 cm).

Conversely, concentration gradients at the system boundaries are difficult to estimate. High-resolution measurements above and below the boundary are required to accurately establish a concentration gradient. Measurements of this type are only available for parameters such as pH, O_2, and H_2S that can be measured by microelectrodes (ultra-small, fast-response electrodes that are inserted into the sediment using a micrometer-type device to control the depth of penetration [Revsbech et al., 1980]). Because of the problems associated with accurately estimating gradients at the system boundaries, the boundary value approach was selected.

Numerical Techniques

An analytical solution to a differential equation has the advantage of being exact but, unfortunately, many differential equations of practical interest cannot be solved explicitly. Numerical methods, on the other hand, can be applied to virtually any differential equation. An added advantage to numerical techniques is that sophisticated commercial software is available. The IMSL Mathematical and Statistical Library (IMSL Software Systems, Houston, Tx), the source of numerical subroutines in this study, is widely available.

Two numerical techniques are commonly used to solve boundary value problems: finite difference and shooting methods (Cheney and Kincaid, 1980). Although both are based on a Taylor Series, they differ significantly in their actual mode of computation and each is subject to independent systematic errors.

The finite difference approach involves dividing the system with a grid and approximating the differential equation between each grid point with a separate numerical representation. The numerical representations are then solved simultaneously and the solution at each grid point is calculated.

The shooting method is a modification of the Runge-Kutta method for initial value problems. The Runge-Kutta formula provides an estimate of the solution to the differential equation at the point $(x+\Delta x)$ if the value at x (the initial condition) is known. The solution at $(x+\Delta x)$ is then used as the initial condition for a new problem and a solution at $(x+2\Delta x)$ is attained. This procedure is repeated until the lower system boundary is reached. The shooting method converts the Runge-Kutta initial value routine into a boundary value problem solver. The shooting method "guesses" an initial condition, solves the initial value problem using the Runge-Kutta equation, and compares the solution at the boundary to the specified boundary condition. If agreement is poor, a new guess at the initial condition is made and the procedure is repeated until the guessed initial condition is consistent with the specified boundary condition.

Both finite difference and shooting methods are convergent (Hornbeck, 1975) which implies that a "solution" will be reached for

virtually any differential equation. However, the availability of a so-
lution does not ensure its accuracy. A solution must be considered sus-
pect until all sources of error have been thoroughly scrutinized.

There are three main sources of error in a numerical solution to a
differential equation: truncation error, round-off error, and insta-
bility. Most algorithms used to solve differential equations are based
on an infinite Taylor Series; truncation error arises because it is
impossible to include every term of the series. The "order" of a parti-
cular algorithm increases and the truncation error decreases with inclu-
sion of additional terms. Round-off error occurs because of the thou-
sands of calculations required to numerically solve a differential
equation, and can be minimized by programming with double precision (8
digit) real numbers. Instabilities occur when "parasitic solutions",
(i.e. solutions that "feed" on truncation and round-off errors), over-
power the fundamental solution. An instability will lead to a numerical
solution that bears no resemblance to the true solution.

In general, the shooting method is of higher order than the finite
difference method and thus is more accurate, while the finite difference
method has better stability. In this study, the finite difference method
was used to solve the diagenetic equation, while the shooting method was
used occasionally to check finite difference solutions.

Testing the Numerical Solution

The following tests were performed to check the accuracy of the
finite difference routine:

1. Simplified versions of the diagenetic equation were solved

analytically and numerically using the finite difference method; computer plots of the true (analytical) and numerical solution agreed exactly.

2. Varying the grid size by a factor of two did not affect the solution. Insensitivity of the solution to the grid size indicated a stable solution (Hornbeck, 1975).

3. Increasing and decreasing the tolerated global error by an order of magnitude did not affect the solution, indicating that the solution had converged rapidly.

4. Solutions obtained by finite difference and shooting methods agreed to within four significant digits.

Rate Estimation by Derivative Evaluation

Evaluating the derivatives of the concentration-depth distribution provides a means of estimating reaction rates when experimental rate data are not available. This becomes apparent upon rearranging eqs. 4.27 and 4.28:

$$\left\{\frac{d[C]_{PW}}{dt}\right\}_{rxn} = -\rho_{SM}\omega_\infty \phi(1-\phi_\infty)\frac{d[C]_{SM}}{dz} , \qquad (4.29)$$

$$\left\{\frac{d[C]_{PW}}{dt}\right\}_{rxn} = \phi^2 D_o\frac{d^2[C]_{PW}}{dz^2} + \left(3\phi D_o\frac{d\phi}{dz} - \frac{\omega_\infty\phi_\infty}{\phi}\right)\frac{d[C]_{PW}}{dz} . \qquad (4.30)$$

Reaction rates can be estimated directly if the first and second derivatives of the concentration vs. depth profile can be evaluated.

Derivatives are easily evaluated if the concentration profile can be represented by a suitable numerical function. Goldhaber et al. (1977) fit a fourth-order polynomial to their SO_4^{2-} depth distribution and

calculated SO_4^{2-} reduction rates that corroborated rates measured by a jar experiment. Chanton (1985) fit SO_4^{2-} depth distributions with several polynomial and exponential functions. He found that all functions faithfully reproduced the SO_4^{2-} depth distribution, but the predicted reaction rates varied widely depending on the function used.

Derivatives estimated by fitting simple functions (e.g. exponentials) to concentration data are not reliable. Simple functions do not possess sufficient flexibility to reproduce features that may be present in a concentration distribution. Rather than conforming to nuances contained within the data, the simple function "forces" the data to take a predefined shape.

The CH_4 data provide an example of the distortion that may occur when rates are estimated using derivatives calculated by differentiating a simple function fit to the concentration data. An exponential function was fit to the CH_4 concentration data by least-squares, non-linear regression (Fig. 4.1a). The CH_4 oxidation rate was predicted by differentiating the exponential and substituting the calculated derivatives into eq. 4.30. The predicted and measured rates bear no resemblance to one another (Fig. 4.1b). Rates predicted from the concentration data increased exponentially with depth while actual measurements showed a pronounced mid-depth maximum.

Derivatives estimated by polynomial regression of the concentration data are also subject to substantial error. In contrast to an exponential equation, polynomials possess "too much" flexibility. For example, fit of a fourth-order polynomial to 10 equally spaced points derived
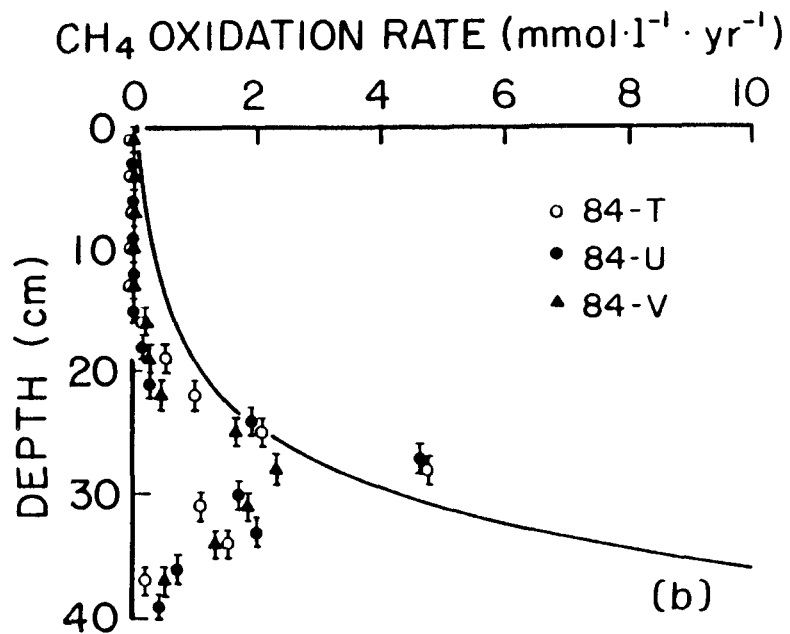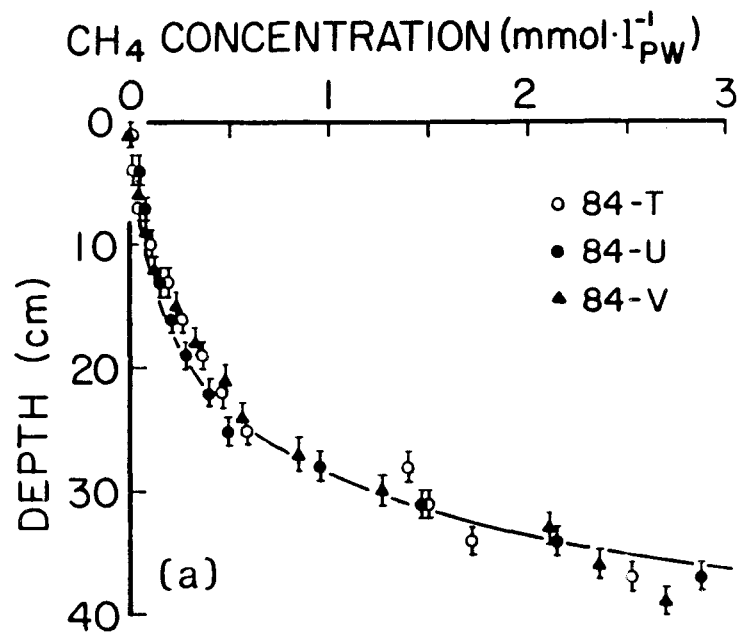
Fig. 4.1. Depth distribution of methane oxidation rates predicted by differentiating an exponential curve fit to the methane data. (a) Exponential curve fit to methane data, (b) measured (data points) and modelled (solid curve) methane oxidation rates.

from a Gaussian-type function reproduced the basic features of the curve although it underestimated the maximum and predicted negative values not present in the original function (Fig. 4.2a). However, the first and second derivatives calculated from the fourth-order polynomial deviated substantially from the true values (Fig. 4.2b,c). By increasing the order of the polynomial to six, the fit to the original Gaussian function improved but distortion in the derivatives got substantially worse (Fig. 4.2a,b,c). In fact, near the tails of the original Gaussian curve, the error in the second derivative predicted from the sixth-order polynomial approached three orders of magnitude.

This illustrates a serious defect with polynomial functions: they are highly oscillatory. For the purpose of evaluating derivatives from concentration vs. depth data, a flexible and non-oscillating function is desired. These are precisely the characteristics of cubic splines. Oscillatory behavior arises when the magnitude of the second derivative is large. In contrast, the second derivatives of a spline that interpolates a data set are less than or equal to the second derivatives of any other function that fits the same data (Cheney and Kincaid, 1980). Cubic splines are perhaps the best functions for curve-fitting because they possess continuous first and second derivatives, have the flexibility to reproduce the features of nearly any data set, and produce a function with minimum curvature. Ahlberg et al. (1967) have demonstrated that the cubic spline is an effective tool for estimating derivatives. The spline provided an almost perfect fit to the original Gaussian function and the first and second derivatives were faithfully reproduced (Fig. 4.3a,b,c).
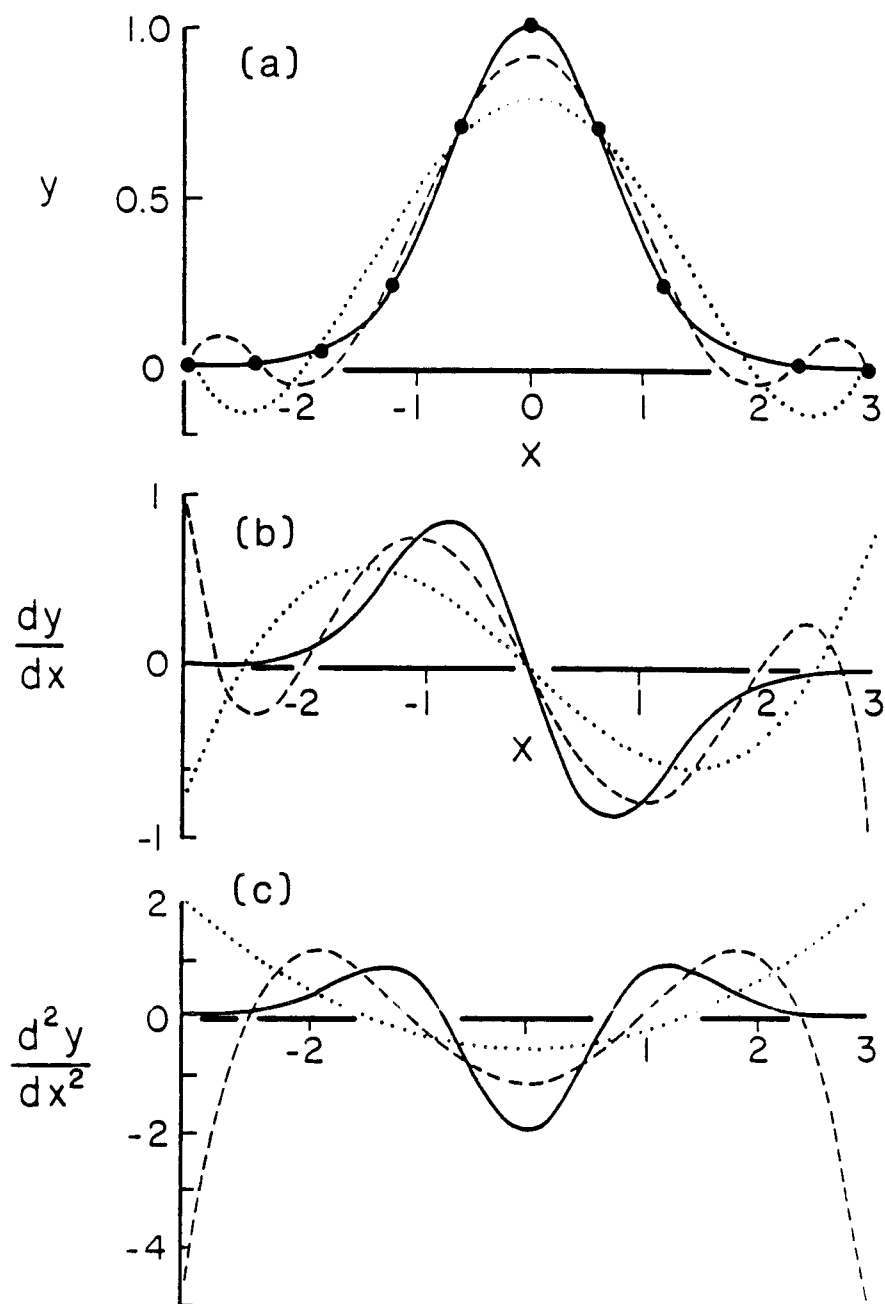
Fig. 4.2. Derivatives estimated by polynomial regression. (a) Fourth-
(dotted curve) and sixth- (dashed curve) order polynomials fit to 10
points derived from a Gaussian-type function (solid curve), (b) first
derivatives of Gaussian function (solid curve) and those predicted by
differentiating fourth- (dotted curve) and sixth- (dashed curve) order
polynomials, (c) second derivatives of Gaussian function (solid curve)
and those predicted by differentiating fourth- (dotted curve) and sixth-
(dashed curve) order polynomials.
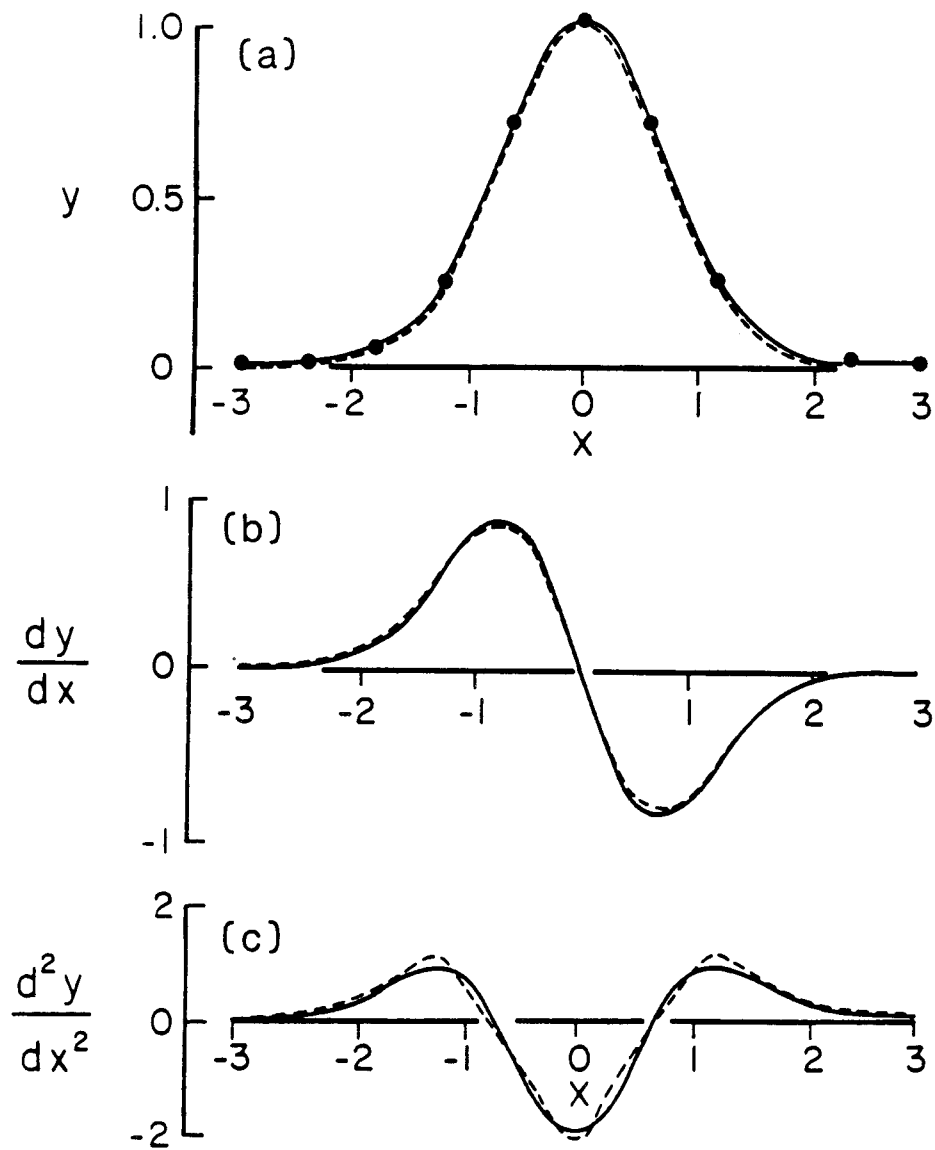
Fig. 4.3. Derivatives estimated by cubic splines. (a) Cubic spline (dashed curve) fit to 10 points derived from Gaussian-type function (solid curve), (b) first derivatives of Gaussian function (solid curve) and those predicted by differentiating the spline (dashed curve), (c) second derivatives of Gaussian finction (solid curve) and those predicted by differentiating the spline (dashed curve).

Derivative End Conditions

A cubic spline is a function consisting of n-1 cubic polynomials, where n is the number of points to be fit by the spline function. Each cubic polynomial (Ax^3+Bx^2+Cx+D) has four unknown coefficients, so a cubic spline passing through n points will have $4(n-1)$ unknown coefficients. Thus, $4(n-1)$ conditions must be specified in order for the spline function to be unique. The requirement that each polynomial segment must pass through two points provides $2(n-1)$ conditions; that the first and second derivatives must be continuous at the $(n-2)$ interior points provides an additional $2(n-2)$ conditions. This adds up to $4(n-1)-2$ conditions. The two additional conditions necessary to define a unique spline are the first or second derivatives at the end-points. If the second derivatives at the endpoints are set equal to zero, the resulting spline is called a "natural spline". However, there is no a priori reason why the second derivative of a concentration-depth profile should equal zero at the system boundaries.

It is preferable to use empirical data and the diagenetic equations (eqs. 4.27 and 4.28) to calculate derivatives at the system boundaries. For a solid phase constituent, the first derivatives of the concentration profile are given by:

$$\frac{d[C]_{SM}}{dz} = \frac{\phi}{\rho_{SM}\omega_\infty(1-\phi_\infty)} \{\frac{d[C]_{PW}}{dt}\}_{rxn} \cdot$$

For a pore water constituent, the second derivatives of the concentration profile are given by:

$$\frac{d^2[C]_{PW}}{dz^2} = \frac{-1}{\phi^2 D_o} (3\phi D_o \frac{d\phi}{dz} - \frac{\omega_\infty \phi_\infty}{\phi}) \frac{d[C]_{PW}}{dz} + \{\frac{d[C]_{PW}}{dt}\}_{rxn} \ .$$

In addition to the model parameters that define the physical con-
stants and bulk composition of the sediment system (i.e. ρ_{SM}, ϕ, w_∞,
and D_o), estimation of the derivatives at the boundaries requires
knowledge of reaction rates and concentration gradients. Rates of carbon
cycling at the system boundaries were assumed to be slow (i.e. approx-
imately 0) relative to rates within the system. The rationale behind
this assumption is as follows. Reaction rates within the sediment are
generally much faster than in the water column due to higher substrate
concentrations and the presence of solid surfaces (Fenchel and
Blackburn, 1979). Reaction rates in an infinitesimal volume of sediment
located just at the interface will be intermediate between bottom water
and sediment, i.e. slow relative to immediately below the sediment-water
interface. At the lower sediment boundary, a decrease in quantity and
quality of organic matter leads to reduced decomposition rates. Depth
distributions of SO_4^{2-} reduction rate (Fig. 3.6) and ATP biomass
(see p. 213) were consistent with low rates at the system boundaries.

Concentration gradients were calculated from the slope of a line
through the two points closest to the boundary. Reaction rates predicted
by estimating derivatives of the concentration profile were not sensi-
tive to errors in the derivative end conditions. Sensitivity analysis
demonstrated that large errors in the estimated boundary derivatives
($\pm$50%) had little effect on predicted rates 2 to 3 cm away from the
system boundaries.

Data Smoothing

All experimental data are to some degree contaminated by error. Relatively small levels of random error can lead to "wiggles" in the concentration vs. depth profile which will be reproduced when the data are fit with a cubic spline. Minor "wiggles" in the concentration profile will translate to oscillations in the second derivative which, in turn, will lead to wild fluctuations in the predicted rate distribution.

This problem can be minimized by smoothing or filtering the experimental data. The effect of smoothing is shown schematically in Fig. 4.4. A cubic spline was fit to a data set containing random error (Fig. 4.4a). To satisfy the requirements of passing through each point and having continous first and second derivatives, the spline function was forced to "wiggle". The calculated second derivative oscillated accordingly with a wavelength exactly twice the sampling interval (Fig. 4.4b). If the cubic spline was not required to pass directly through each point, but allowed to miss a point by an amount less than or equal to the specified error, the resulting curve was free of wiggles (Fig. 4.4c) and the calculated second derivatives did not show wild oscillations (Fig. 4.4d).

There are hazards associated with data smoothing; it tends to reduce the magnitude of the second derivatives and therefore affects the predicted reaction rates. The concentration profiles were filtered by selecting the minimum degree of smoothing sufficient to eliminate the short-wavelength oscillations in the second derivative. Concentration profiles with large vertical changes and little horizontal scatter required very little smoothing to filter the noise; the error allowed
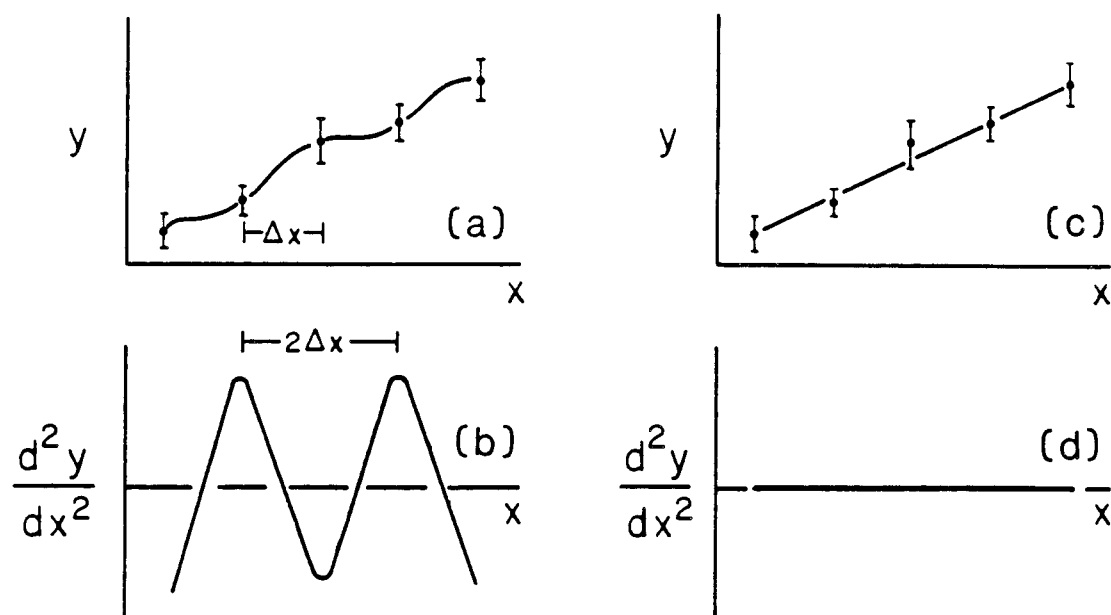
Fig. 4.4. Effect of data smoothing on derivatives estimated by cubic splines. (a) Cubic spline fit to data contaminated by random error, (b) second derivatives predicted by differentiating the spline, (c) cubic spline fit to same data after smoothing, (d) second derivatives predicted by differentiating the smoothed spline. The distance between data points is represented by Δx.

for the spline fit was less than analytical error in the data. On the other hand, concentration profiles with substantial horizontal variability and relatively little vertical trend retained wild oscillations in the second derivative even after the degree of smoothing exceeded the analytical error. For this reason, rate estimation by derivative evaluation was not applied to concentration profiles showing substantial horizontal scatter.

Testing the Spline Derivative Estimates

The following tests were performed to check the accuracy of derivatives predicted by the spline function:

1. Four distinct functions (exponential, sine wave, fifth-order polynomial, and Gaussian) were represented by 14 equally spaced points (analogous to 14 samples per core), fit by a spline, and the derivatives evaluated. In all cases, predicted and true (analytical) derivatives were essentially identical.

2. The diagenetic equation was solved by the finite difference technique employing an arbitrary rate term. Rates were then estimated by spline derivative evaluation of the concentration profile that resulted from the initial solution of the diagenetic equation. The rates derived from derivative evaluation were identical to those originally input into the diagenetic equation.

Model Results

In this section, three different applications of the diagenetic model provide complementary information regarding reaction rates in Skan Bay sediment. For reservoirs having experimental rate data (CH_4 and

$SO_4{}^{2-}$), the diagenetic equation is solved to check for inconsistencies between the rate and concentration distributions. For reservoirs having concentration profiles with minimal horizontal scatter (CH_4, $SO_4{}^{2-}$, POC, and DIC), depth-dependent reaction rates are estimated by the derivative evaluation technique. And for reservoirs having stable isotope ratio data (CH_4, POC, DOC, PIC, and DIC), diagenetic or mass-balance equations provide an independent constraint on the processes operating within the reservoirs.

The model parameters are summarized in Table 4.5. The diagenetic model for solid phase constituents is not sensitive to uncertainty in ρ_{SM} or ϕ, but is strongly influenced by possible error in ω_∞. The model for pore water constituents is not responsive to uncertainty in ϕ and ω_∞, but is quite sensitive to small errors in D_0. Therefore, model predictions for solid phase and pore water constituents consider error in ω_∞ and D_0, respectively.

The Methane Reservoir

Methane concentration profiles in anoxic marine sediment are controlled by two processes: oxidation and production. Anaerobic CH_4 oxidation is confined to a narrow subsurface zone, but appears to be a nearly quantitative sink for CH_4 in non-bubbling sedimentary environments (Reeburgh, 1976; Alperin and Reeburgh, 1984). Although there is substantial geochemical evidence supporting anaerobic CH_4 oxidation (Alperin and Reeburgh, 1984), the biochemical mechanism remains a mystery. The electron acceptor has not been identified (Alperin and Reeburgh, 1985) and bacteria responsible for the process have not been

Table 4.5. Model parameters.

===

ρ_{SM} = 2.33$\pm$0.01 g$\cdot$cm^{-3} [a]

ϕ = 0.135 exp(-0.0929 z) + 0.864 [b]

dϕ/dz = -0.0126 exp(-0.929 z)

ϕ_{∞} = 0.864

F_{SM} = 0.31$\pm$0.06 g$\cdot$cm$^{-2}\cdot$yr^{-1} [c]

ω_{∞} = 1.0$\pm$0.2 cm$\cdot$yr^{-1} [d]

Diffusion Coefficients[e]

D_o(CH$_4$) = 250$\pm$60 cm$^2\cdot$yr^{-1} [f]

D_o(SO$_4^{2-}$) = 170$\pm$44 cm$^2\cdot$yr^{-1} [g]

D_o(HCO$_3^-$) = 177$\pm$44 cm$^2\cdot$yr^{-1} [g]

----

[a]See p. 22.

[b]See p. 69.

[c]Average of ^{137}Cs and ^{210}Pb sediment accumulation rates (Table 3.2).

[d]ω_{∞} = F_{SM}/[ρ_{SM}(1-ϕ_{∞})] (Berner, 1980).

[e]The uncertainty in D_o represents a composite of experimental error (±10%), uncertainty in the tortuosity correction (±15%, Table 4.4), and horizontal diffusion (±15%, Table 4.3). Error propagation yields a total estimated uncertainty in diffusivity of 25%.

[f]D_o was taken from Sahores and Witherspoon (1970) and corrected to in situ salinity as described in Table 4.4.

[g]D_o for bicarbonate and sulfate were taken from Li and Gregory (1974) and corrected to in situ temperature and salinity as described in Table 4.4.

isolated.

Methane production is thought to occur via two principle pathways: (a) DIC reduction with H_2 and (b) acetate fermentation (Fenchel and Blackburn, 1979). In anoxic marine sediments, tracer experiments suggest that DIC/H_2 is the preferred substrate (Crill and Martens, 1987). Kinetic studies show that sulfate reducing bacteria out-compete methanogenic bacteria for H_2 and CH_3COOH (Capone and Kiene, 1987), suggesting that most CH_4 production will occur in sulfate-depleted sediment. Other methanogenic substrates have been identified (formate, methanol, methyl-amines, and methylated sulfur compounds [Oremland, 1987]) and may serve as CH_4 precursors in sulfate-rich environments.

Direct Solution of the Diagenetic Equation

Methane oxidation rate data (subcores 84-T, 84-U, and 84-V) were averaged and curve-fit with a natural cubic spline (Fig. 4.5a). The diagenetic equation (eq. 4.28) for CH_4 was solved, and the predicted concentration profile compared with concentration measurements (Fig. 4.5b). The three curves demonstrate model sensitivity to the value of the diffusion coefficient. Given the uncertainty in D_o (Table 4.5), modelled and measured concentration-depth distributions were in reasonable agreement. This agreement suggests that the $^{14}CH_4$ tracer technique provided accurate estimates of in situ CH_4 oxidation rates. Furthermore, the fact that the CH_4 concentration distribution was accurately reproduced by a model that considered oxidation as the only source of reaction is evidence that CH_4 production rates in these subcores were minimal.
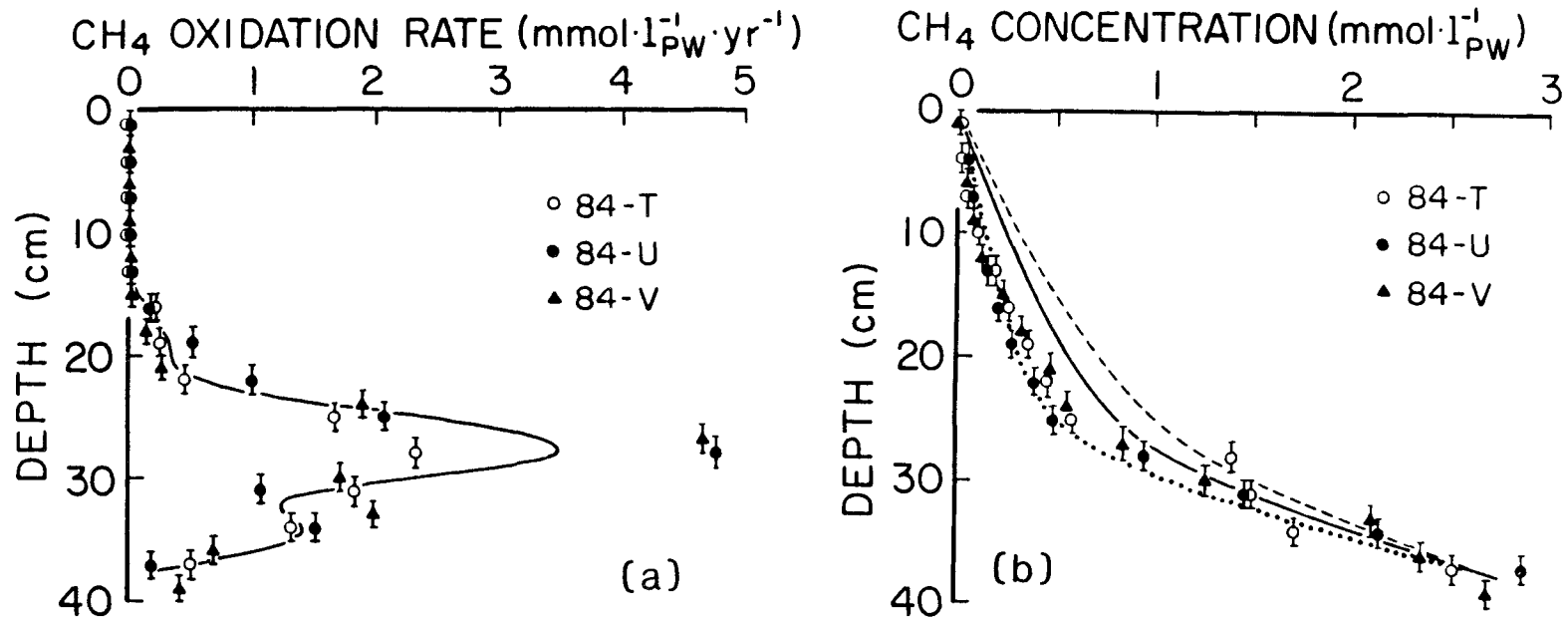
Fig. 4.5. Methane depth distribution predicted by direct solution of the dia-
genetic equation. (a) Cubic spline fit to averaged methane oxidation rate data,
(b) measured (data points) and modelled (curves) methane concentrations for
three values of D_o (cm^2/yr): 250 (solid curve), 190 (dotted curve), and 310
(dashed curve).

Rate Estimation by Derivative Evaluation

The well characterized CH_4 reservior provides an opportunity to test the accuracy of rates calculated using spline-estimated derivatives. The CH_4 concentration data (subcores 84-T, 84-U, and 84-V) were averaged and fit with a smoothed cubic spline (Fig. 4.6a). The first and second derivatives were estimated by differentiation, and reaction rates were calculated according to eq. 4.30 (Fig. 4.6b). The modelled CH_4 oxidation rate distribution accurately reproduced the main features in the data: low rates near the sediment surface, a mid-depth maximum, and reduced rates at greater depth. Agreement between measured and modelled rates indicates that the derivative evaluation technique provides accurate estimates of depth-dependent reaction rates.

Methane reaction rates for subcores subjected to stable isotope analysis (84-A, 84-B, and 84-E) were also estimated by spline derivative evaluation. The two deepest samples from subcore 84-B (Fig. 3.7) were not included in the model as they showed a decrease in CH_4 concentration below 30 cm, probably the result of CH_4 loss caused by bubble formation after core retrieval. Reaction rates predicted by differentiating the spline functions had a distinct maximum in CH_4 oxidation between 20 and 30 cm (Fig. 4.7), in agreement with rates measured by the $^{14}CH_4$ tracer technique (Fig. 4.5a). Negative reaction rates below 30 cm were predicted for subcores 84-A and 84-B, indicating high CH_4 production rates just below the CH_4 oxidation zone (curve not plotted). Net CH_4 production in subcore 84-E, like subcores 84-T, 84-U, and 84-V, did not occur over the depth interval represented by the core (0 to 35 cm).

Differences in the magnitude of the predicted rate maxima between
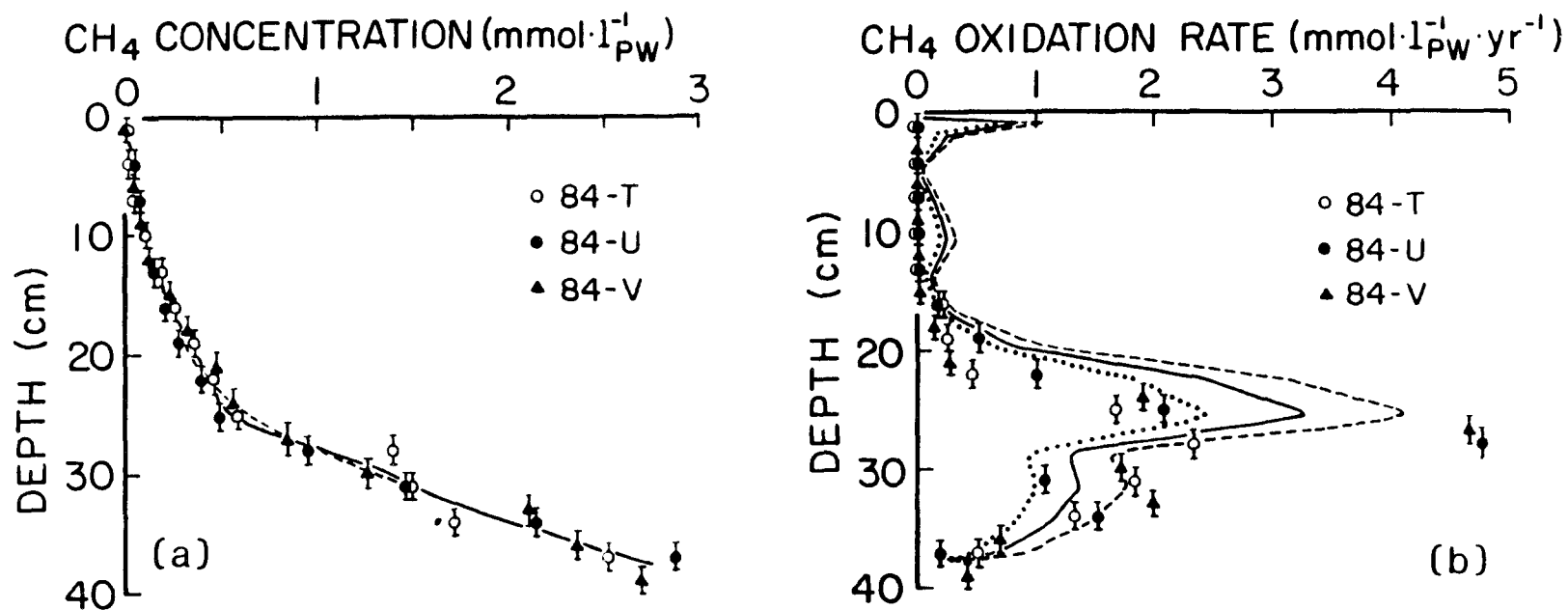
Fig. 4.6. Depth distribution of methane oxidation rate predicted by derivative evaluation. (a) Unsmoothed (solid curve) and smoothed (dashed curve) cubic spline fit to averaged methane concentration data, (b) measured (data points) and modelled (curves) methane oxidation rates for three values of D_o (cm^2/yr): 250 (solid curve), 190 (dotted curve), and 310 (dashed curve).
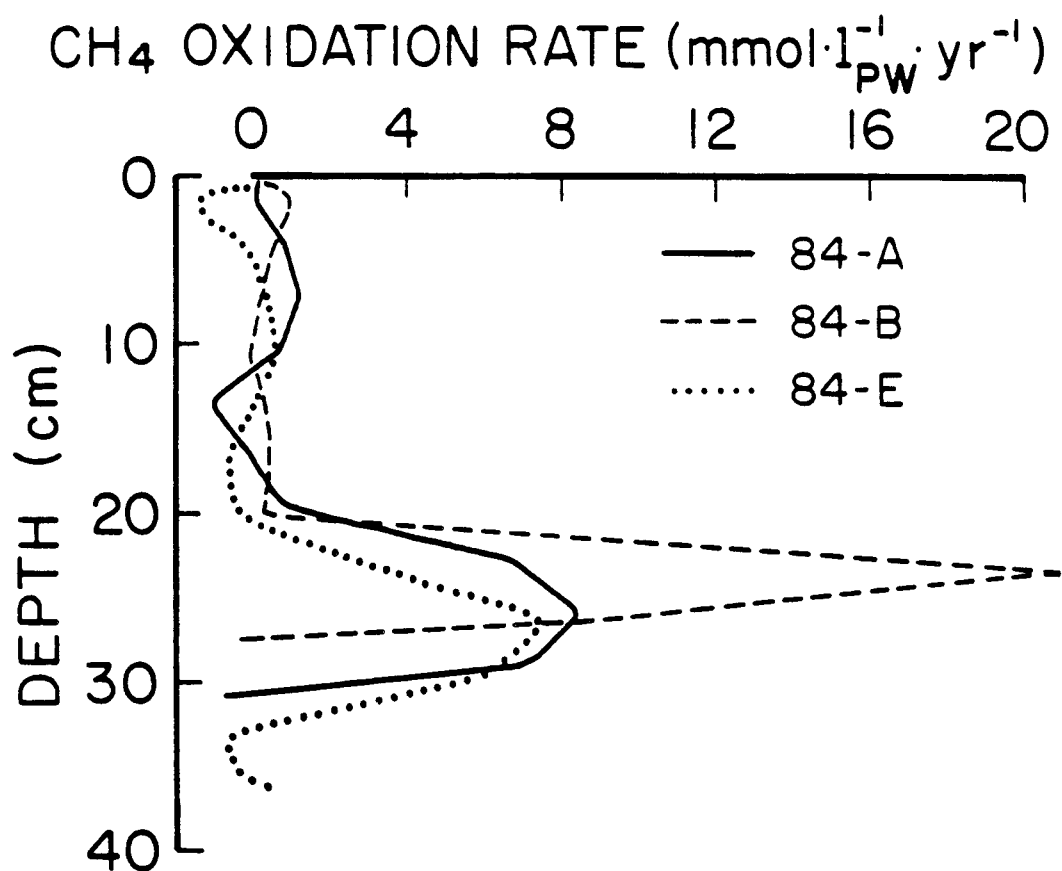
Fig. 4.7. Depth distribution of methane oxidation rate (for subcores subjected to stable isotope ratio analyses) predicted by derivative evaluation.

subcores 84-A and 84-B were consistent with the variability in measured rates (e.g. subcores 84-T and 84-U, Fig. 4.5a) and appear to result from sediment heterogeneity. Methane oxidation rates for subcores 84-A, 84-B, and 84-E were generally 2 to 3 times higher than for subcores 84-T, 84-U, and 84-V. The different rates reflect large-scale lateral heterogeneity apparent in the CH_4 concentration data. Methane concentrations at a depth of 34.5 cm were 3.0 to 4.5 mM_{PW} for subcores 84-A, 84-B, and 84-E (Fig. 3.7), and 1.8 to 2.3 mM_{PW} for subcores 84-T, 84-U, and 84-V (Fig. 4.6a). Since CH_4 concentrations for all subcores approached 0 at the sediment-water interface, subcores 84-A, 84-B, and 84-E must have had higher oxidation rates.

The low amplitude oscillations in the upper 20 cm of the predicted CH_4 oxidation rate profiles (Figs. 4.6b and 4.7) reflect very subtle changes in curvature of the concentration profiles (Figs. 4.6a and 3.7) and are not considered to be reliable estimates of in situ reaction rates.

Isotope Ratio Depth Distributions

A model of $\delta^{13}C$-CH_4 depth distributions serves as an additional constraint on the CH_4 system and an independent check on experimental and model-derived reaction rates. Furthermore, a model of isotope ratio profiles for the CH_4 reservoir can provide an estimate of the magnitude of the kinetic isotope effect associated with CH_4 oxidation (isotope effects are described in "Chapter 1: Introduction" [p. 6]).

Concentration-depth distributions for $^{12}CH_4$ and $^{13}CH_4$ may be represented by two diagenetic equations analogous to eq. 4.28:

$$\phi^2 \; D_o \; \frac{d^2[CH_4]_{PW}}{dz^2} + (3\phi \; D_o \; \frac{d\phi}{dz} - \frac{\omega_\infty \phi_\infty}{\phi}) \; \frac{d[CH_4]_{PW}}{dz} + \{\frac{d[CH_4]_{PW}}{dt}\}_{rxn} . \quad (4.31)$$

$$\phi^2 \; {}^{13}D_o \; \frac{d^2[{}^{13}CH_4]_{PW}}{dz^2} + (3\phi \; {}^{13}D_o \; \frac{d\phi}{dz} - \frac{\omega_\infty \phi_\infty}{\phi}) \; \frac{d[{}^{13}CH_4]_{PW}}{dz}$$

$$+ \{\frac{d[{}^{13}CH_4]_{PW}}{dt}\}_{rxn} . \quad (4.32)$$

Since $^{12}CH_4$ represents about 99% of the total CH_4, concentrations and reaction rates for $^{12}CH_4$ and total CH_4 were assumed to be equal.

Reaction rates for CH_4 and $^{13}CH_4$ are related by the kinetic isotope fractionation factor (α) (eq. 1.2):

$$\{\frac{d[{}^{13}CH_4]_{PW}}{dt}\}_{rxn} = \{\frac{d[CH_4]_{PW}}{dt}\}_{rxn} \; \frac{[{}^{13}CH_4]_{PW}}{\alpha[CH_4]_{PW}} . \quad (4.33)$$

Diffusion coefficients for CH_4 and $^{13}CH_4$ are related by the following expression:

$$f = {}^{12}D_o / {}^{13}D_o . \quad (4.34)$$

Substituting eqs. 4.33 and 4.34 into 4.32, and assuming that α is constant with depth, yields:

$$\phi^2 \; \frac{D_o}{f} \; \frac{d^2[{}^{13}CH_4]_{PW}}{dz^2} + (3\phi \; \frac{D_o}{f} \; \frac{d\phi}{dz} - \frac{\omega_\infty \phi_\infty}{\phi}) \; \frac{d[{}^{13}CH_4]_{PW}}{dz}$$

$$+ \{\frac{d[CH_4]_{PW}}{dt}\}_{rxn} \; \frac{[{}^{13}CH_4]_{PW}}{\alpha[CH_4]_{PW}} = 0 . \quad (4.35)$$

It is well established that gaseous diffusion coefficients for the different CH_4 isotopic species vary inversely as the square-root of their reduced masses (Mason and Marrero, 1970). However, for CH_4 in aqueous solution, the effect of isotopic substitution on the diffusion coefficient is uncertain. The diffusion coefficient for dissolved $^{13}CH_4$

has not been determined experimentally and current theories of tracer diffusion in aqueous solution are inadequate for demonstrating either the presence or absence of a small diffusion isotope effect (Mills and Harris, 1976).

Of the available experimental data on aqueous diffusion coefficients for isotopically related solutes, CO_2 is probably the best CH_4 analogue. O'Leary (1984) measured a small difference between $^{12}CO_2$ and $^{13}CO_2$ diffusion coefficients ($f=1.0007\pm0.0002$), suggesting that a measurable effect also exists for the different isotopic species of CH_4. However, the magnitude of this effect, which is probably strongly dependent on CH_4-H_2O interactions, cannot be predicted. Therefore, two extreme cases will be considered: (a) aqueous diffusion coefficients for CH_4 are unaffected by isotopic substitution (i.e. $f=1.0000$); and (b) CH_4-H_2O interactions are sufficiently small that diffusion coefficients for isotopic species follow the inverse square-root reduced mass relationship applicable to a gaseous system (i.e. $f=1.016$).

The diagenetic equations for isotopically light and heavy CH_4 (eqs. 4.31 and 4.35) were solved using CH_4 reaction rates derived by spline derivative evaluation of CH_4 concentration profiles from subcores 84-A, 84-B, and 84-E (Fig. 4.7). The boundary conditions were different than those used above. Because $\delta^{13}C$-CH_4 data did not extend to the sediment-water interface, the upper boundary condition was established by the shallowest sample having sufficient CH_4 for isotope ratio analysis (Fig. 3.7). Due to uncertainties regarding CH_4 production rates and methanogenic substrates, the CH_4 production zone was excluded from the model. Therefore, the lower boundary was set at the base of the CH_4

oxidation zone, defined as the depth below which there was no further net oxidation (Fig. 4.7).

Solution of the two equations yielded predictions of depth distributions of isotopically light and heavy CH_4. Isotope ratio depth distributions were then calculated from the "del"-scale definition (eq. 1.3). The fractionation factor was adjusted until the model-predicted profiles reproduced the shift in $\delta^{13}C-CH_4$ observed in the data.

Sensitivity of the stable isotope model to α is shown in Fig. 4.8. In the absence of a kinetic isotope effect ($\alpha=1.000$), isotope ratio profiles were approximately constant from the base of the oxidation zone to within 10 cm of the sediment surface, where diffusive mixing at the upper boundary became important. A value of α greater than unity produced a shift toward isotopically heavier CH_4 through the oxidation zone. The extent of the shift was quite sensitive to the magnitude of α; a change of ±0.001 shifted the predicted $\delta^{13}C-CH_4$ profile by approximately $\pm0.5^{\circ}/oo$. Above the oxidation zone, $\delta^{13}C-CH_4$ values were relatively constant until shallow depths where diffusive mixing occurred. Since the $\delta^{13}C-CH_4$ values represent a ratio of model-derived concentrations, the predicted isotope ratio profiles were not sensitive to uncertainty in the absolute value of D_o.

Results of the isotope model for two diffusion coefficient cases ($f=1.000$ and $f=1.016$) are shown in Fig. 4.9. The magnitude of the predicted fractionation factors were strongly influenced by the ratio of diffusion coefficients for isotopically light and heavy species. In the absence of a diffusion isotope effect ($f=1.000$), predicted values ranged
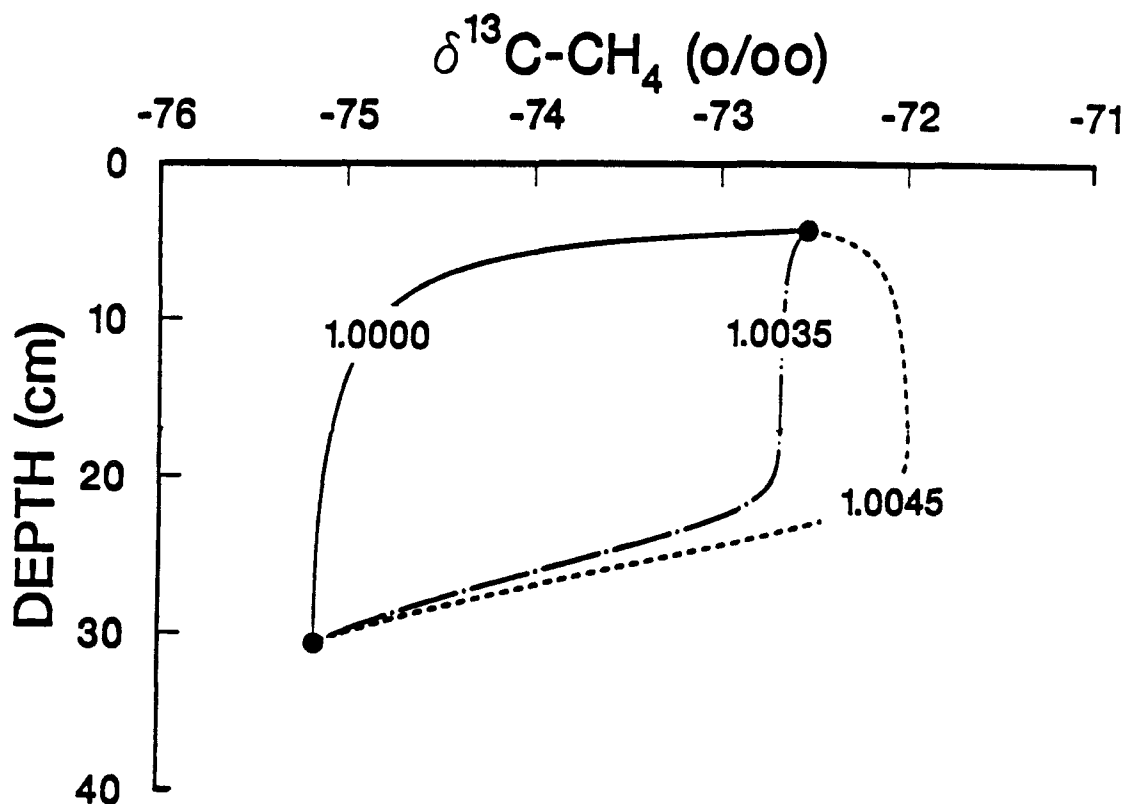
Fig. 4.8. Sensitivity of model-predicted δ^{13}C-methane profile to the magnitude of the isotope fractionation factor. The filled circles represent arbitrary boundary conditions. The curves represent predicted isotope ratio profiles for three values of α. The methane reaction rate profile was assumed to equal that of subcore 84-A (Fig. 4.7). For this sensitivity analysis, diffusion coefficients for both isotopic species were assumed to be equal (i.e. f=1.000).
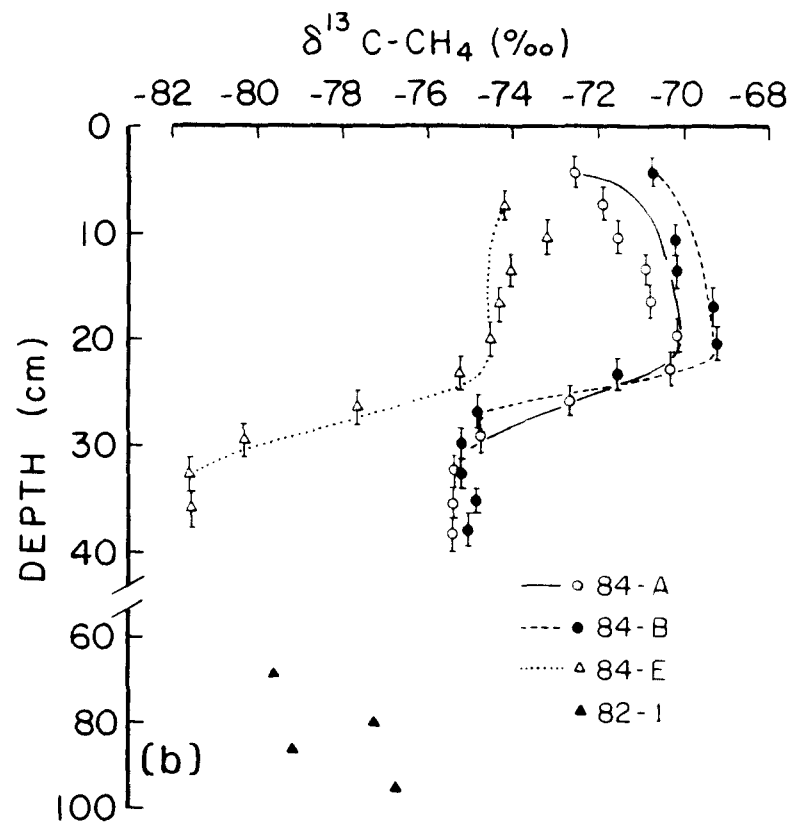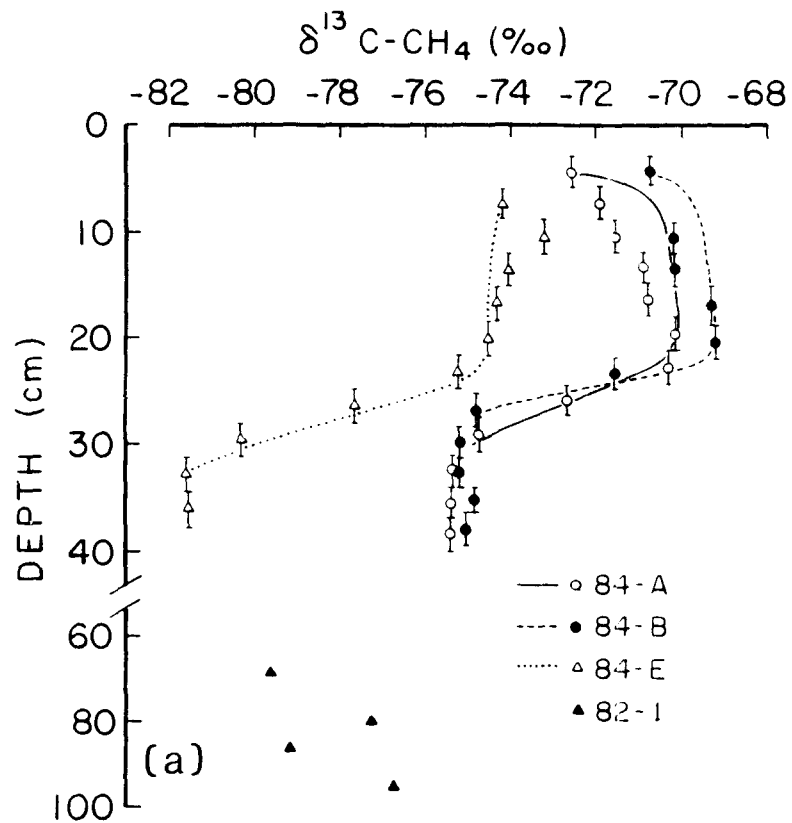
Fig. 4.9. Depth distributions of δ^{13}C-CH$_4$ predicted by the isotope model. (a) No diffusion isotope effect (f=1.0000); α = 1.0073, 1.0098, and 1.0093 for subcores 84-A, 84-B, and 84-E, respectively, (b) diffusion isotope effect (f=1.016); α = 1.024, 1.026, and 1.026 for subcores 84-A, 84-B, and 84-E, respectively. Note the break and change of scale on the depth axis.

from 1.0073 to 1.0098; assuming that diffusion coefficients for different isotope species of CH_4 vary according to the inverse square-root law (f=1.016) yielded values that ranged from 1.024 to 1.026.

The model-predicted $\delta^{13}C-CH_4$ profiles generally reversed direction above the CH_4 oxidation zone (Fig. 4.9a,b). This was caused by diffusive mixing of CH_4 made isotopically heavy by oxidation and isotopically light CH_4 present at the upper boundary. In subcore 84-E, the model did not show a reversal in $\delta^{13}C-CH_4$ because CH_4 at the top of the oxidation zone and the upper boundary had similar $\delta^{13}C-CH_4$ values.

Although the model reproduced the reversal in isotope ratio profiles seen in the data, it does not explain the cause of isotopically light CH_4 at the upper boundary. Bottom water cannot be a significant source of isotopically light CH_4 because concentrations were too low (0.0003 mM_{PW}). Likewise, a diffusion isotope effect (i.e. larger diffusion coefficient for isotopically light species) could account for only a portion of the observed reversal.

The reversal in $\delta^{13}C-CH_4$ values above 20 cm could be explained by production of isotopically light CH_4 in the upper sediment. Approximately linear CH_4 concentration profiles (Figs. 4.6a, 3.7) and negligible $^{14}CH_4$ oxidation rates (Figs. 4.5a) in the upper 20 cm indicate that CH_4 production rates were slow relative to diffusion. The trend toward isotopically light CH_4 in the shallow sediments may be due to a relatively slow input of CH_4 highly enriched in isotopically light carbon. High SO_4^{2-} reduction rates in this sediment region (Fig. 3.6) suggest that this CH_4 may be derived from a non-competitive substrate (i.e. a substrate not utilized by SO_4^{2-} reducing bacteria). Slow rates

of methanogenesis from CH_3OH, a non-competitive substrate with an extremely large kinetic isotope effect (α>1.070) (Rosenfeld and Silverman, 1959; Krzycki et al., 1987), is a possible cause of the reversal observed in the isotope ratio data. Methane production from CH_3OH is supported by the isolation of a CH_3OH-utilizing methanogenic bacterium from the CH_4 oxidation zone of Skan Bay (K. Sandbeck, Univ. of Alaska., Fairbanks, personal communication). If production of isotopically light CH_4 is occurring within the CH_4 oxidation zone, isotope fractionation factors predicted by the model will underestimate the in situ values.

The average values of model-predicted isotope fractionation factors for the two diffusion coefficient cases are 1.0088±0.0013 (f=1.000) and 1.0253±0.0012 (f=1.016). Fractionation factors associated with anaerobic CH_4 oxidation have not been measured in the laboratory because organisms responsible for the process have not been isolated. Previous estimates derived from models include 1.004 (Alperin and Reeburgh, 1984) and 1.002 to 1.014 (Whiticar and Faber, 1986). Both studies estimated fractionation factors using closed-system models that neglected the effects of diffusion. Diffusion can influence isotope ratio depth distributions in two ways. First, the kinetic isotope effect leads to preferential oxidation of isotopically light CH_4, thereby steepening the concentration gradient and enhancing the diffusive flux of light CH_4 relative to heavy CH_4 (Jørgensen, 1979; Goldhaber and Kaplan, 1980; Chanton et al., 1987). Second, there may be preferential diffusion of $^{12}CH_4$ due to a larger diffusion coefficient for the isotopically lighter molecule. Since differential diffusion counteracts the effect of isotope fractionation (i.e. in a region affected by CH_4 oxidation, diffusion preferentially

supplies while oxidation preferentially consumes the light isotope), fractionation factors estimated by closed-system models tend to be underestimated. A closed-system Rayleigh distillation model (Alperin and Reeburgh, 1984) applied to the $\delta^{13}C-CH_4$ data from subcores 84-A, 84-B, and 84-E yielded fractionation factors of 1.002 to 1.004.

The Methane Cycle

Methane oxidation is restricted to a relatively narrow depth interval (20 to 35 cm) but appears to dominate the CH_4 cycle in the upper 30 cm. Isotope ratio profiles suggest input of isotopically light CH_4 in the upper 20 cm, but a model of the CH_4 reservoir indicates that production rates over this depth interval must be very slow.

The exact location and vertical extent of the CH_4 production zone is uncertain. Several subcores (84-A and 84-B, Fig. 3.7) showed pronounced upward concavity below 30 cm suggesting high rates of CH_4 production just below the oxidation zone. Other subcores (84-T, 84-U, and 84-V, Fig. 4.6a) had relatively linear profiles and low $^{14}CH_4$ oxidation rates between 30 and 40 cm, suggesting that oxidation and production zones are not contiguous. The lower extent of the CH_4 production zone is well below the depth of most cores used in this study; increasing CH_4 concentrations down to 65 cm (Fig. 3.3) indicate that production continues at least to this depth.

The CH_4 cycle in Skan Bay sediment can be divided into four zones. In the first zone (0 to 20 cm), the rate of CH_4 oxidation is apparently limited due to low CH_4 concentrations while methanogens are inhibited by competition with SO_4^{2-} reducing bacteria. Very slow rates of CH_4

production appear to be occurring and may represent CH_4 derived from substrates not utilized by sulfate reducing bacteria. The second zone (20 to 35 cm) is the region of CH_4 oxidation. Approximately 90% of the upward diffusive flux of CH_4 is consumed within this zone. The third zone (35 to >40 cm) marks the transition between CH_4 oxidation and production. This narrow region, where neither oxidation nor production are occurring at significant rates, is not apparent in all subcores. Finally, the forth zone (40 to >65 cm) is the region of CH_4 production. High CH_4 concentrations in sediment collected by piston corer (unpublished data) indicate that this zone may extend to depths of meters.

The Sulfate Reservoir

Since oxidation and reduction reactions must occur in parallel, the oxidation processes that fuel the carbon cycle require compounds that serve as oxidants. Sulfate is generally considered to be the dominant electron acceptor in anoxic marine sediments (Henrichs and Reeburgh, 1987). During the final stage of organic matter remineralization, sulfate reducing bacteria oxidize material derived from POC degradation and reduce SO_4^{2-} to H_2S. In marine sediment, acetate appears to be the preferred substrate for sulfate reducing bacteria, although other fatty acids, as well as H_2, are also utilized (Sørensen et al., 1981).

Relatively little attention has been focused on a process that complements SO_4^{2-} reduction: sulfide oxidation by microaerophilic bacteria. These organisms, which form large multicellular filaments, live at the oxic-anoxic interface and exploit the chemical energy available in the H_2S-O_2 couple. The role that these bacteria play in the carbon

and sulfur cycle of marine sediment has not been quantified.

Direct Solution of the Diagenetic Equation

The diagenetic equation (eq. 4.28) for SO_4^{2-} was solved using a cubic spline representation of the averaged SO_4^{2-} reduction rate data as the reaction term (Fig. 4.10). The predicted concentration profile bears little resemblance to the actual data. Unrealistically steep concentration gradients near the sediment-water interface and "negative concentrations" below 10 cm were necessary for the model to attain a mass balance. The three curves show the model's sensitivity to uncertainty in the diffusion coefficient.

Rate Estimation by Derivative Evaluation

Sulfate reduction rates predicted by the derivative evaluation technique provide a different perspective on the apparent inconsistency between SO_4^{2-} concentration and reduction rate data. Sulfate concentration data were averaged, fit with a smoothed spline function (Fig. 4.11a), and depth-dependent reaction rates were calculated by the derivative evaluation technique (Fig. 4.11b). Predicted SO_4^{2-} reduction rates had primary and secondary maxima that coincided with maxima in the measured rates. However, the magnitude of the predicted rates in the upper 10 cm were approximately 10 times slower than the measured rates. In the 10 to 20 cm depth interval, the model predicted net SO_4^{2-} production.

Sources of Discrepancy in the Sulfate Reservoir

The model results indicate that SO_4^{2-} concentration and reduction
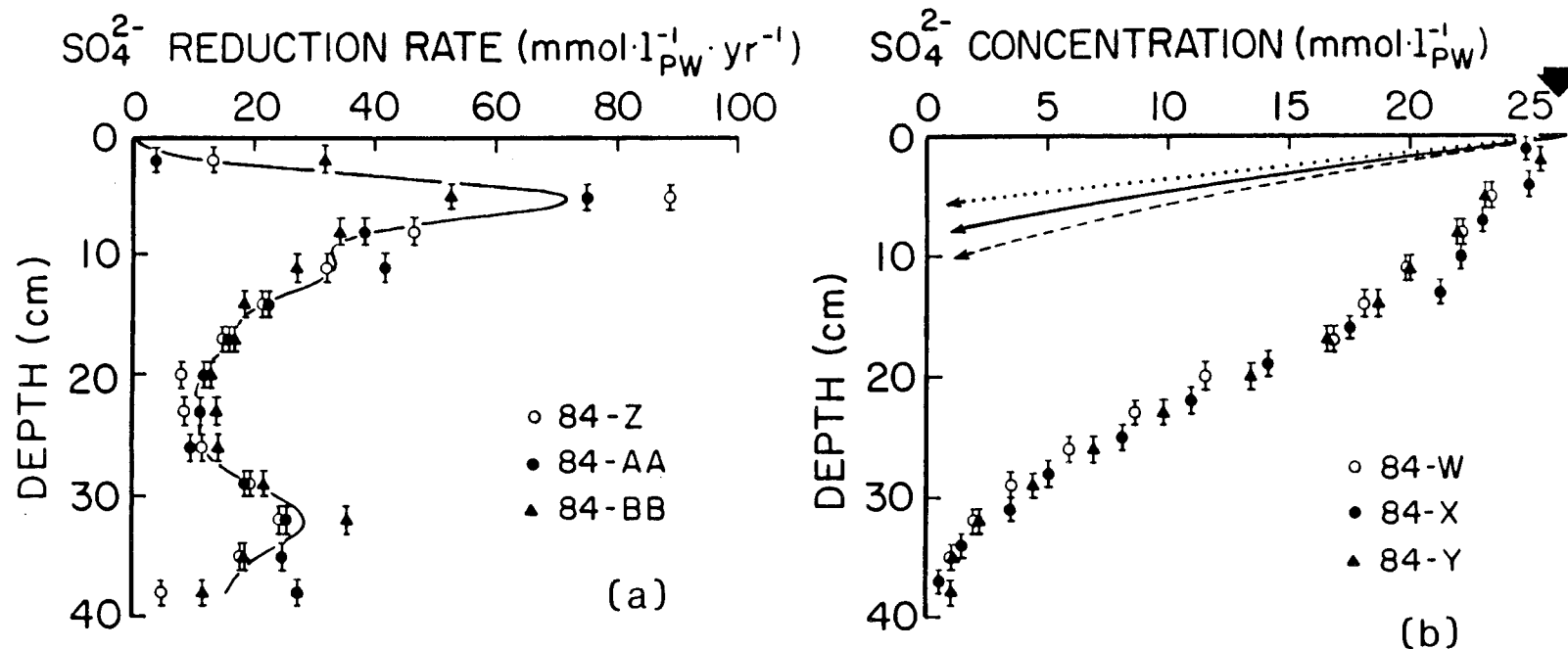
Fig. 4.10. Sulfate depth distribution predicted by direct solution of the dia-
genetic equation. (a) Cubic spline fit to averaged sulfate reduction rate data,
(b) measured (data points) and modelled (curves) sulfate concentrations for
three values of D_o (cm^2/yr): 170 (solid curve), 126 (dotted curve), and 214
(dashed curve). The modelled concentration profiles return to the lower bound-
ary at 37.5 cm (not shown). The large arrow represents the bottom water con-
centration.
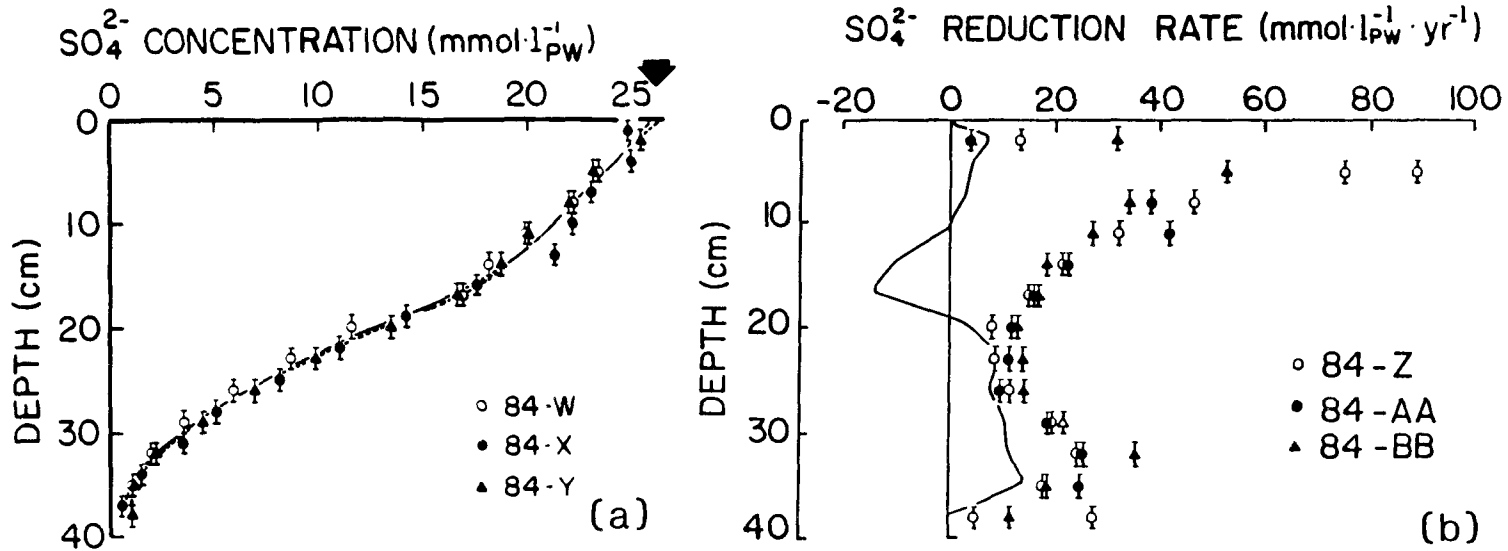
Fig. 4.11. Depth distribution of sulfate reduction rate predicted by derivative evaluation. (a) Unsmoothed (solid curve) and smoothed (dashed curve) cubic spline fit to averaged sulfate concentration data (the large arrow represents the bottom water concentration), (b) measured (data points) and modelled (curve) sulfate reduction rates.

rate profiles are inconsistent with the processes assumed to be active in Skan Bay sediments. Possible explanations for the discrepancy are discussed in the following section.

1. Measured sulfate reduction rates overestimated in situ activity. Sources of error in the SO_4^{2-} reduction rate analysis were discussed in "Chapter 2: Study Site and Analytical Methods" (p. 35). There is no apparent analytical error that would lead to overestimated rates. Incomplete recovery of reduced $^{35}SO_4^{2-}$, the most likely analytical error, would cause measured rates to be underestimated. Most perturbations caused by sediment manipulation (e.g. introduction of trace quantities of O_2, disruption of sediment-microbial associations, etc.) would also result in underestimated rates. A temperature increase during the incubation period could significantly enhance SO_4^{2-} reduction rates (Jørgensen, 1978a). However, samples were removed from the incubation bath for <5 min, suggesting that significant warming did not occur. The measured SO_4^{2-} reduction rates were qualitatively and quantitatively consistent with POC consumption rates predicted from a model of the POC concentration profile (see p. 165). Although this agreement provides direct evidence that measured rates were not grossly inaccurate, there is some indication that the agreement may be fortuitous (see p. 207).

2. Important biological or chemical processes have been neglected. Linear or concave-up SO_4^{2-} concentration profiles (Fig. 4.11a) in the zone of active SO_4^{2-} reduction (Fig. 4.10a) suggest that SO_4^{2-} concentrations in Skan Bay sediments are not controlled solely by molecular diffusion, advection, and SO_4^{2-} reduction. An additional process must be

supplying SO_4^{2-} to the sediment. Hydrogen sulfide produced by sulfate reducing bacteria could be chemically (Cline and Richards, 1969; Aller and Rude, 1986) or biologically (Jørgensen, 1982) oxidized to SO_4^{2-}. Sulfate production in the sediment column could have a substantial impact on concentration profiles.

Rates of SO_4^{2-} production were estimated by combining modelled and experimental rate data. Sulfate reaction rates predicted by a model applied to concentration-depth distributions represent net (i.e. reduction plus production) rates. Conversely, rates measured using the $^{35}SO_4^{2-}$ tracer technique approximate gross reduction rates. Therefore, gross production rates may be calculated as the difference between modelled (Fig. 4.11b) and measured (Fig. 4.10b) rates. The results of this calculation are shown in Fig. 4.12. Sulfate production and reduction rates were approximately equal in the upper 10 cm, while production exceeded reduction between 10 and 18 cm. The integrated SO_4^{2-} production rate was 790 $umol \cdot cm^{-2} \cdot yr^{-1}$.

Oxidation of H_2S to SO_4^{2-} requires an electron acceptor. Iron and manganese oxides can react with sulfide to form reduced metals and SO_4^{2-} (Aller and Rude, 1986). However, fluxes of Fe (110 $umol \cdot cm^{-2} \cdot yr^{-1}$) and Mn (7 $umol \cdot cm^{-2} \cdot yr^{-1}$) in Skan Bay were insufficient to account for the SO_4^{2-} production predicted by the model. (Flux calculations were based on maximum solid phase Fe and Mn concentrations [J. Cornwell, Univ. of Maryland, Hornpoint, unpublished data] and sediment accumulation rates [Table 3.2]. Note that 8 mol Fe oxide and 4 mol Mn oxide are required to oxidize 1 mol H_2S to SO_4^{2-}.)

Filamentous sulfur bacteria (e.g. _Beggiatoa_) oxidize H_2S to SO_4^{2-}
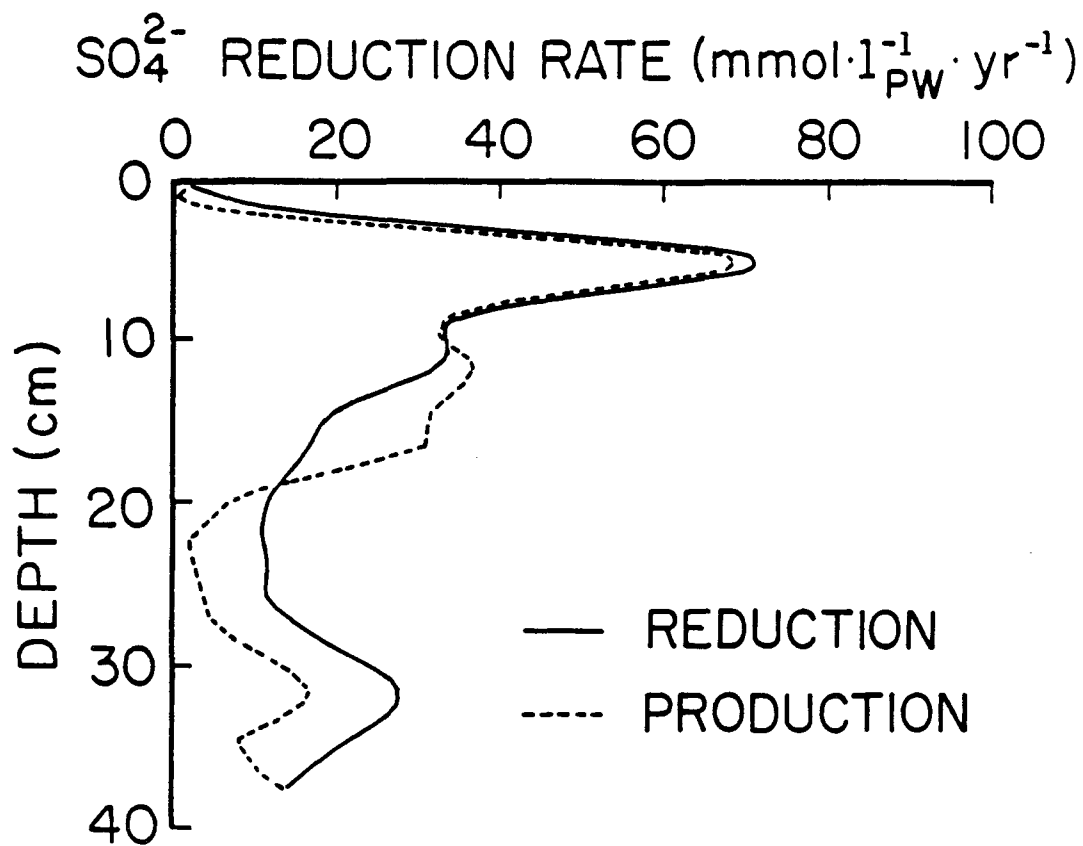
Fig. 4.12. Depth distributions of sulfate reduction and sulfate pro-
duction rates. The reduction rate profile is a cubic spline fit to the
averaged sulfate reduction rate data. The production rate profile was
calculated as described in the text.

under microaerophilic conditions (Fenchel and Blackburn, 1979). These bacteria are commonly visible at the sediment surface in freshly sampled Skan Bay cores and form dense mats when left in sealed core liners for several days. Laboratory cultures of Beggiatoa grow in horizontal plates at the oxic-anoxic interface often with the bulk of the bacterial plate occupying the anoxic region (Nelson et al., 1986). Beggiatoa are highly motile with gliding speeds approaching 2 $cm \cdot hr^{-1}$ (Nelson et al., 1986). Their high motility and preference for anoxia led Nelson et al. (1986) to propose that "filaments might migrate randomly" between oxic and anoxic environments in order to secure access to both O_2 and H_2S.

The ability of Beggiatoa to migrate at rates much greater than molecular diffusion may allow some H_2S oxidation to occur within anoxic sediment. Beggiatoa filaments could assimilate O_2 at the sediment surface then glide into anoxic sediment for H_2S uptake and metabolism. However, in Skan Bay, where O_2 is depleted and H_2S is abundant at or just below the sediment-water interface (Figs. 2.2b and 3.14), it is unlikely that SO_4^{2} production by Beggiatoa would extend to depths of 18 cm as predicted by the model.

The discrepancy between SO_4^{2-} concentration and rate data may result from non-steady-state SO_4^{2-} production linked to seasonal changes in the depth of the oxic-anoxic interface. During the winter, high winds generated by Aleutian storms mix the Skan Bay water column and introduce oxygen-rich water to the sediment-water interface (see p. 16). Formation of a wintertime oxidized zone would inhibit SO_4^{2-} reduction and permit sulfide oxidation to extend deeper into the sediment. In order to test this hypothesis, a time-dependent version of the diagenetic equation

(eq. 4.20) was used to predict seasonal changes in the SO_4^{2-} concentration profile resulting from wintertime SO_4^{2-} production in oxidized surface sediment.

In this model, SO_4^{2-} reduction and production rates were assumed to vary seasonally according to the following scenario:

During the winter, the sediment was assumed to have an oxidized surface layer extending to a depth of 5 cm. Sulfide oxidation was restricted to this oxidized surface layer. The SO_4^{2-} production rate profile was assumed to follow a gaussian distribution, similar to the <u>Beggiatoa</u> biomass profile for Limfjorden sediment (Jørgensen, 1977). The integrated rates for SO_4^{2-} reduction and production were assumed to be equal. Since the total Fe flux was less than 10% of the integrated SO_4^{2-} reduction, sulfide burial as an iron-sulfide compound was neglected. Sulfate reduction rates were assumed to be zero in the oxidized zone and equal to measured values at depths greater than 5 cm.

During the summer, the sediment was assumed to be anoxic at the sediment-water interface. Sulfate production was assumed to occur only at the sediment surface where the resulting SO_4^{2-} was rapidly mixed into the water column. Sulfate reduction rates were set equal to measured values (Fig. 3.6).

The time-dependent diagenetic equation was solved at bimonthly intervals. The upper and lower boundaries were set equal to the SO_4^{2-} concentration in the bottom water and deepest sample, respectively. A

line between boundary conditions was arbitrarily chosen for the initial profile. The model was begun under "winter conditions" and allowed to proceed for 8 months. The model was then switched to "summer conditions".

The model predicted that wintertime sulfide oxidation would produce a SO_4^{2-} concentration maximum near the sediment surface (Fig. 4.13). However, downward diffusion from the SO_4^{2-} maximum was too slow to prevent unrealistic depletion of the SO_4^{2-} reservoir at depth. At the onset of "summer conditions" (cessation of sedimentary SO_4^{2-} production), the SO_4^{2-} maximum quickly disappeared and concentrations at depth became "negative" (not shown). At no time did modelled profiles and data coincide.

3. Important mass-transport processes have been neglected. Models of the sedimentary SO_4^{2-} reservoir that consider molecular diffusion, pore water advection, SO_4^{2-} reduction, and steady-state and seasonal SO_4^{2-} production were unable to reconcile the concentration and reduction rate data. This suggests that mass-transport processes in addition to molecular diffusion and advection may be important in Skan Bay sediments.

Other mass transport processes include: (a) bioturbation, (b) bio-irrigation, (c) CH_4 ebullition, (d) wind and current mixing, and (e) forced advection due to ground water intrusion. Each process was evaluated and shown to be unimportant in Skan Bay sediment (see p. 110). However, seasonal habitation by irrigating benthic macrofauna could not be ruled out (see p. 117).

As discussed above, oxygen-rich bottom water blankets the sediment
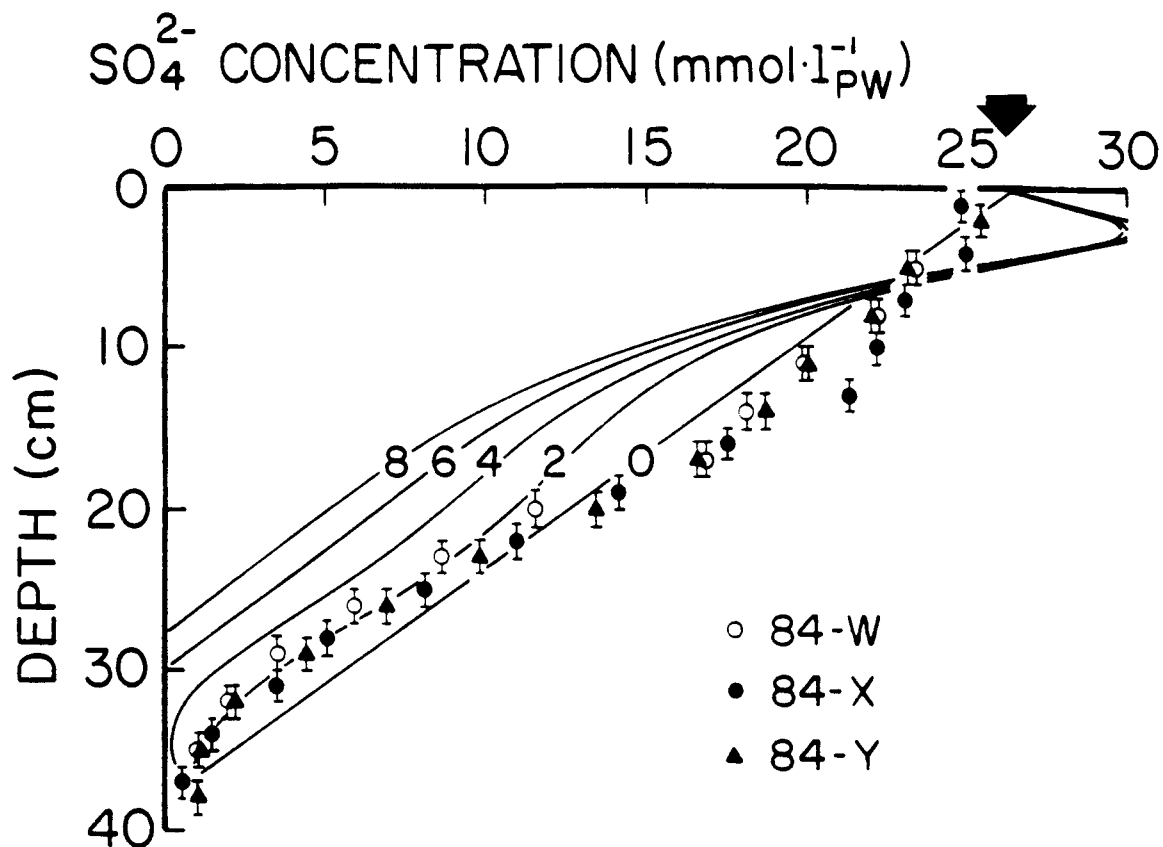
Fig. 4.13. Seasonal changes in sulfate depth distribution resulting from wintertime sulfate production in oxidized surface sediment. The curves represent the sulfate profile after 0, 2, 4, 6, and 8 months of winter conditions. The large arrow represents bottom water concentration.

during the wintertime and may provide a favorable environment for benthic macrofauna. A time-dependent model was run to test the hypothesis that the Skan Bay SO_4^{2-} reservoir was affected by periodic bioirrigation. In this model, bioirrigation was assumed to vary seasonally according to the following scenario:

During the winter, the upper 12 cm of sediment was actively bioirrigated. The bioirrigation rate was assumed to be fast relative to reaction processes so that concentrations in the upper 12 cm were equal to bottom water.

During the summer, the Skan Bay water column stratified leading to O_2 depletion in the bottom water. The sediment environment became anoxic and was evacuated by the bioirrigating organisms. Sulfate reduction rates were assumed to equal measured values (Fig. 3.6).

The model was begun at the start of "summer conditions" and run for 4 months. Sulfate concentration profiles 2 weeks to 4 months after the onset of summer conditions are shown in Fig. 4.14. The model predicted that SO_4^{2-} concentration profiles would change rapidly after bioirrigation ceased. After 2 weeks of "summer conditions", the change in SO_4^{2-} concentrations in the upper 12 cm would be measurable. Approximately 1 month after bioirrigation ceased, the model-derived profile coincided with SO_4^{2-} concentration measurements. After 4 months of "summer conditions", SO_4^{2-} became depleted at depth so that measured SO_4^{2-} reduction rates could not be supported. The model demonstrates
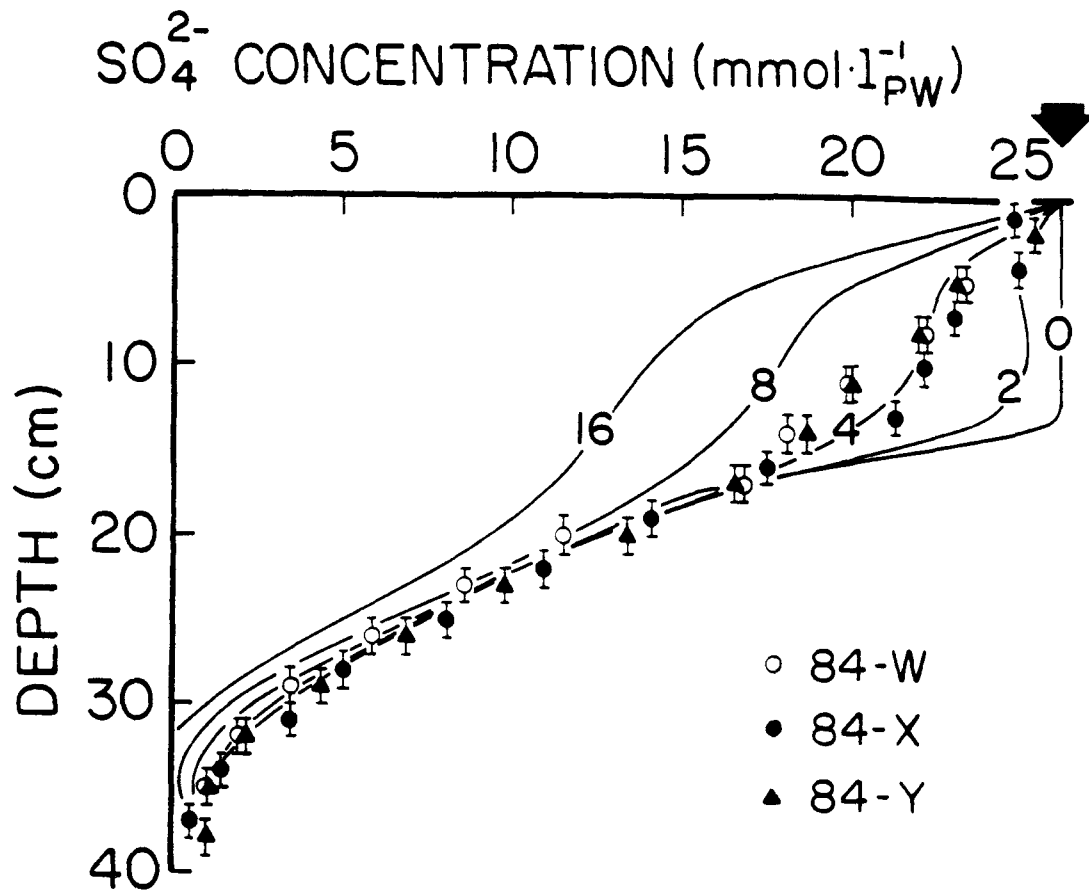
Fig. 4.14. Seasonal changes in sulfate depth distribution resulting from periodic bioirrigation in the upper 12 cm of the sediment column. The curves represent the sulfate profile 0, 2, 4, 8, and 16 weeks after cessation of bioirrigation. The large arrow represents bottom water concentration.

that the discrepancy between SO_4^{2-} concentration and reduction rate data can be reconciled by assuming that Skan Bay sediment is subject to extensive bioirrigation except during a short (<4 months) "summer" period that begins about 1 month before the September cruise.

The Sulfate Cycle

The inconsistencies between rate and concentration data make it difficult to elucidate the details of the Skan Bay SO_4^{2-} cycle. However, measured (Fig. 4.10a) and modelled (Fig. 4.11b) SO_4^{2-} reduction rate profiles both suggest that the SO_4^{2-} cycle is composed of three major zones. The first zone (0 to 15 cm) corresponds to the primary rate maxima and represents a region of intense SO_4^{2-} reduction. The second zone (15 to 30 cm) is a region of relatively slow SO_4^{2-} reduction rates. The third zone (30 to 40 cm), which corresponds to the secondary rate maxima, has reduction rates that are intermediate between the first two zones.

There are indications that the discrepancy between measured and modelled reduction rates is due to multiple causes. The measured rates appear to be unrealistically high when compared with the overall carbon cycle (see p. 207), although the source of error in the $^{35}SO_4^{2-}$ technique could not be identified. There is considerable circumstantial evidence that sulfide oxidation plays a significant role in the sediment SO_4^{2-} cycle. The large ΣH_2S reservoir in Skan Bay sediment (Fig. 3.14) represents a sizable energy source and dense bacterial mats, visible at the sediment surface in sealed cores, probably represent a significant biomass of sulfide oxidizing bacteria. Finally, Skan Bay SO_4^{2-}

concentration distributions are probably influenced by bioirrigation during a portion of the year.

The POC Reservoir

The POC reservoir is a very complex mixture of organic compounds. Most studies of sediment organic matter composition fall into one of two catagories: (a) characterization of gross, operationally defined components (e.g. humic acid, fulvic acid, humin, lignin, lipid, etc.) or (b) identification of specific compounds (e.g. biomarkers). This section emphasizes organic matter sources and reactivity rather than composition.

Sedimentary POC can be allochthonous (derived from the water column) or autochthonous (formed in situ). Water column organic matter has three possible origins: phytoplankton, kelp, or terrestrial organic matter. POC can be formed in situ by adsorption, geopolymerization, or assimilation of DOC or DIC by heterotrophic or autotrophic organisms. In a nontectonic, aphotic environment like Skan Bay sediments, all POC is ultimately allochthonous.

The sedimentary POC reservoir is controlled by two processes: deposition and degradation. Sediment deposition rates are a function of water column productivity, river input, terrestrial runoff, and basin morphology and hydrography. POC degradation is the breakdown of complex polymeric material to soluble compounds. It is assumed that all degraded POC enters the DOC reservoir, i.e. POC is not subject to direct decarboxylation reactions.

Rate Estimation by Derivative Evaluation

A smoothed cubic spline was fit to the average POC concentration data (Fig. 4.15a) and the first derivative estimated by differentiating the spline function. POC consumption rates were calculated according to eq. 4.29 (Fig. 4.15b). The three curves show the model's sensitivity to uncertainty in the sediment accumulation rate (Table 4.1).

The POC consumption rate profile had a shape that approximately paralleled the SO_4^{2-} reduction rate distribution (Fig. 3.6). The model predicted a sharp maximum in POC consumption at about 5 cm, coinciding with the primary maximum in the SO_4^{2-} reduction rate. A quantitative discussion of the relationship between POC consumption and SO_4^{2-} reduction is reserved for the final chapter (see p. 207). About 80% of the total integrated POC consumption occurred in the upper 10 cm.

Isotope Ratio Depth Distributions

Isotope mass-balance models provide a means of identifying the principle sources of sedimentary POC. In addition, the reactivity of POC derived from different sources can be estimated by combining isotope mass-balance and diagenetic models. Before applying a quantitative model to Skan Bay sediment, it is necessary to discuss the principle factors that control stable carbon isotope ratios in the POC reservoir.

1. **The sources of sedimentary organic matter.** Phytoplankton and kelp are the principle sources of POC in Skan Bay sediment. The C:N ratio of the sedimentary organic material averaged 7.7±0.1 (n=6) with no systematic depth variation (S. Henrichs, Univ. of Alaska, Fairbanks, unpublished data), indicating that terrestrial organic matter, with C:N
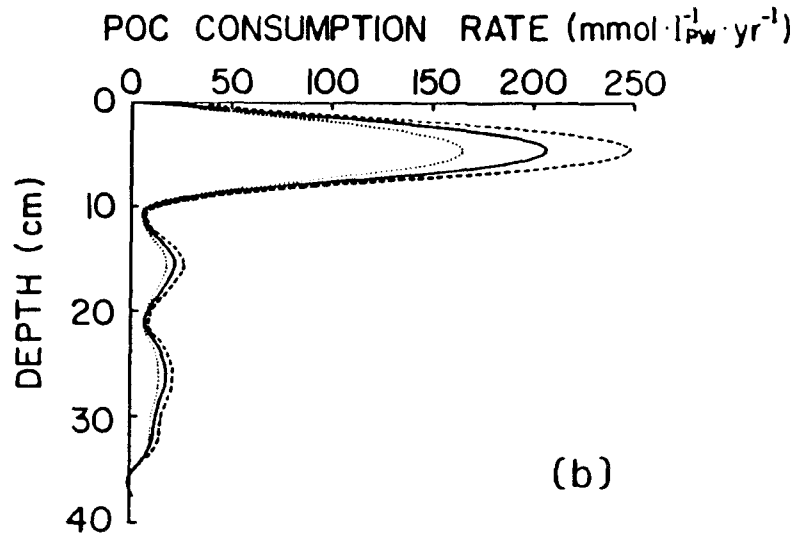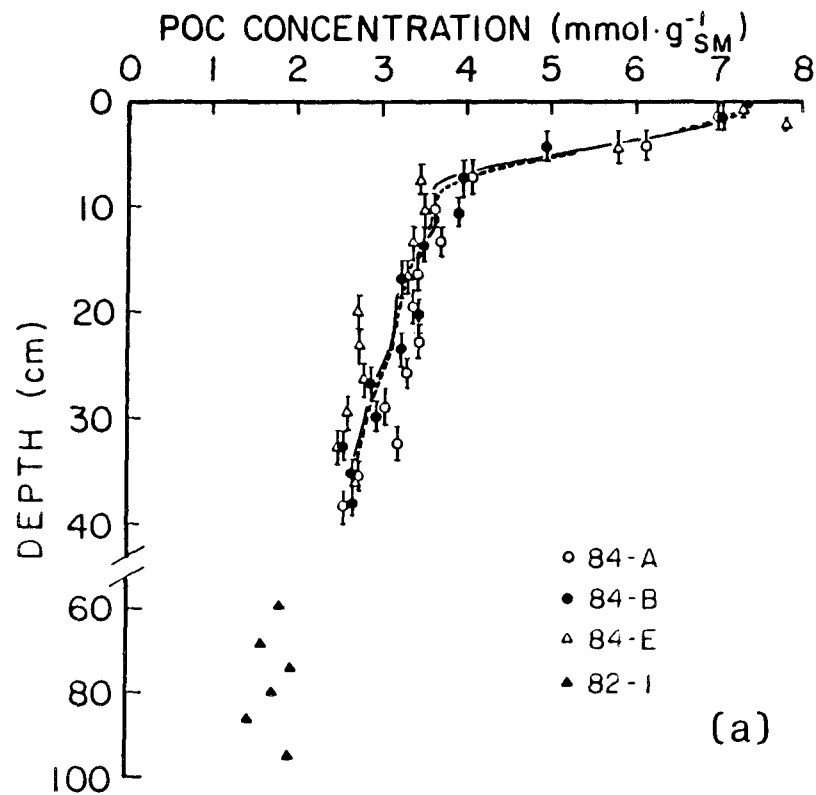
Fig. 4.15. Depth distribution of POC consumption rate predicted by derivative evaluation. (a) Unsmoothed (solid curve) and smoothed (dashed curve) cubic spline fit to averaged POC concentration data (the POC concentration at the sediment-water interface was estimated by linear extrapolation), (b) modelled POC consumption rates for three values of ω_1 (cm/yr): 1.0 (solid curve), 0.8 (dotted curve), and 1.2 (dashed curve). Note the break and change of scale on the depth axis of the POC concentration plot.

ratios of 100 to 1000 (Fenchel and Blackburn, 1979), was not a major component. Autochthonous organic matter, produced by chemoautotrophic bacteria, is assumed to compⅼise a negligible fraction of the total POC reservoir.

2. **Temporal variations in the quantity and isotopic composition of each sedimentary source.** There is solid evidence that the quality and quantity of organic matter deposited in Skan Bay has been approximately constant over the time interval relevant to this study. Agreement between ^{210}Pb and ^{137}Cs geochronologies (Table 3.2) suggests relatively constant rates of sediment accumulation. The POC concentration and δ^{13}C-POC profiles (Fig. 3.11) were monotonic, showing no evidence of episodic fluctuations in the quality or quantity of the deposited organic matter. The isotopic composition of the kelp and phytoplankton is primarily controlled by the δ^{13}C-DIC of the surface water which is in continuous communication with the Bering Sea, and thus not subject to large temporal variations. Short-term (i.e. seasonal) fluctuations in fluxes or isotopic compositions of deposited organic matter were integrated by sampling at 3 cm intervals (equivalent to approx. 3 yr accumulation).

3. **Isotope effects during diagenesis.** Three factors can lead to diagenetic alteration of isotope ratios in Skan Bay POC:

(i) **Different decomposition rates <u>and</u> isotopic compositions for phytoplankton and kelp.** There are a number of morphological and compositional differences between phytoplankton- and kelp-derived organic matter that could lead to different decomposition rates. Phytoplankton are relatively rich in protein while the biochemical

composition of kelp is dominated by carbohydrate. Larger surface area:volume ratios for phytoplankton result in slower settling velocities and hence greater decomposition in the water column. Kelp-derived particles, which reach the sediment as macroscopic fragments, provide good surfaces for bacterial colonization. Since the isotopic composition of these two POC sources differ, changes in δ^{13}C-POC due to differential decomposition of phytoplankton and kelp are expected.

(ii) **Different decomposition rates <u>and</u> isotopic compositions of the biochemical components of phytoplankton and kelp.** Marine organisms are primarily composed of proteins and carbohydrates with minor amounts of lipids (Romankevich, 1984). Within an organism, the protein and carbohydrate pools have similar isotopic compositions while the lipid fraction is approximately 5°/oo lighter than the whole organism (Deines, 1980; Galimov, 1985).

The isotopic conformity in the protein and carbohydrate pools suggests that isotopic alteration of POC by selective decomposition of biochemical components will be minimal. Since the lipid fraction typically accounts for <10% of the organic carbon in marine organisms (Romankevich, 1984), selective decomposition or preservation of lipid will have little effect on the δ^{13}C value of the POC reservoir.

Additional evidence suggesting minimal isotopic alteration during decomposition is derived from kelp isotope analyses (Table 3.1). Kelp samples with different carbon content

(i.e. different degrees of decomposition) had similar isotopic compositions. Furthermore, the stipe and blade portions of the kelp, which presumably decompose at different rates, had $\delta^{13}C$ values that differed by less than $1^o/oo$.

(iii) A kinetic isotope effect associated with the decomposition reactions. As particulate organic matter decomposes, $^{12}C-^{12}C$ bonds will rupture at a faster rate than $^{12}C-^{13}C$ bonds (see p. 6). The net result is preferential decomposition of isotopically lighter material and concentration of isotopically heavier material in the residual, undecomposed organic matter. Although this process is undoubtedly occuring to some degree, it does not appear to exert a major influence on the POC reservoir in Skan Bay, where the $\delta^{13}C$-POC profile shifted toward isotopically lighter carbon with depth (Fig. 3.11).

The ^{12}C and ^{13}C content of the Skan Bay POC reservoir may be represented by two mass-balance equations (Hayes, 1982):

$$\delta^{13}C\text{-POC [POC]} = \delta^{13}C\text{-KELP [KELP]} + \delta^{13}C\text{-PHYTO [PHYTO]} , \quad (4.36)$$

$$[POC] = [KELP] + [PHYTO] , \quad (4.37)$$

where the bracketed terms represent concentrations of total POC, kelp, and phytoplankton. The significant assumptions involved in application of these equations are: (a) phytoplankton and kelp are the major sources of POC to Skan Bay sediments, (b) the flux and isotopic composition of phytoplankton and kelp have been constant over the time span represented by the upper 40 cm of Skan Bay sediment, (c) the isotopic composition of the phytoplankton and kelp are not altered by decomposition, and (d) the

kinetic isotope effect associated with the decomposition reactions is negligible.

Using a kelp and phytoplankton $\delta^{13}C$ of -16.4 and -21.5^o/oo, respectively (Table 3.1), and averaged values of [POC] and $\delta^{13}C$-POC, the two mass-balance equations were solved to yield kelp and phytoplankton concentrations as a function of depth (Fig. 4.16a). The model predicted that phytoplankton was the major source of sedimentary organic matter, accounting for 60 to 80% of the total POC.

Kelp and phytoplankton consumption rates were estimated by derivative evaluation of a spline function fit to each concentration profile (Fig. 4.16b). Kelp decomposition dominated POC consumption in the upper 10 cm while phytoplankton decomposition proceeded at lower, relatively constant rates throughout the sediment column.

The POC Cycle

POC degradation in Skan Bay sediments occurs predominantly in the upper 10 cm. Less than 50% of the organic matter deposited at the sediment surface persists below this depth. The organic matter that does persist is much less reactive, decomposing at rates that are slower by an order of magnitude.

Phytoplankton is the principle source of sedimentary POC. However, it is the kelp that dominates POC decomposition. The greater reactivity of kelp-derived organic matter may stem from (a) bacterial preference for carbohydrate, (b) less decomposition of kelp prior to deposition, or (c) kelp's large surface which is suitable for bacterial colonization.
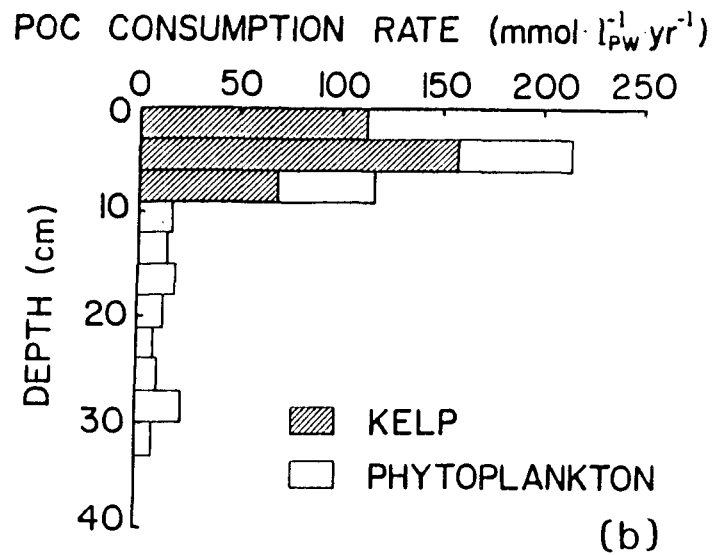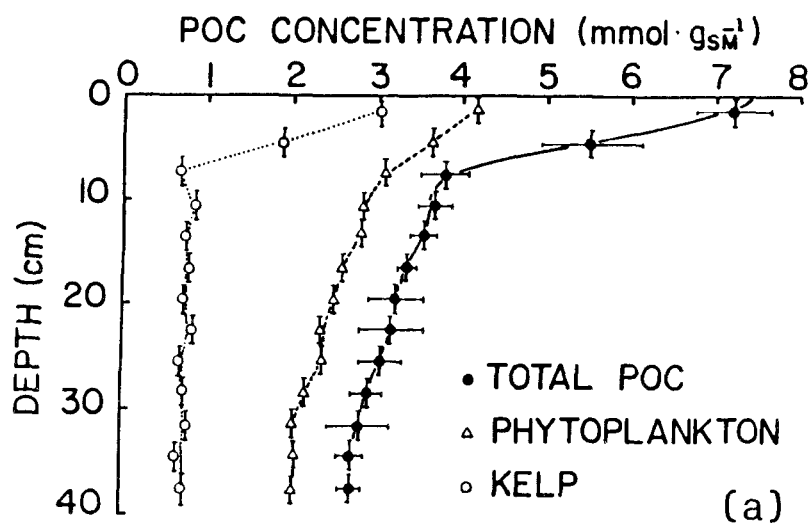
Fig. 4.16. Depth distributions of consumption rates of POC derived from phyto-
plankton and kelp. (a) Depth distributions of total, phytoplankton-derived, and
kelp-derived POC estimated by an isotope mass-balance model (total POC points
represent averaged values from subcores 84-A, 84-B, and 84-E; horizontal bars
represent +1 standard deviation while vertical bars represent the sample depth
interval), (b) consumption rates of POC derived from kelp and phytoplankton
estimated by derivative evaluation.

The DOC Reservoir

Bacteria utilize low molecular weight dissolved organic material that can diffuse through the cell membrane. Organic matter arrives at the sediment surface as POC and must be hydrolyzed by extracellular enzymes prior to bacterial uptake. The DOC reservoir plays a central role in sediment biogeochemistry acting as a repository for the initial products of POC hydrolysis, a source of organic carbon for fermentation and terminal metabolism, and possibly, a reactor for synthesis of refractory geopolymers. DOC is a complex mixture of molecules that range from simple short-chain fatty acids (e.g. acetic acid, mol wt=60) to complex macroscopic bio- and geopolymers with molecular diameters equal to the pore size of the filter used for POC-DOC separation (0.6 um); the molecular weight of a particle this size is approximately 10^{10} (based on molecular weight vs. molecular diameter data [Lehninger, 1975]).

Rate Estimation by Derivative Evaluation

The DOC concentration-depth distribution was not suitable for modelling by the spline derivative evaluation technique. There was considerable random variability in the DOC concentration profile (Fig. 3.9a) which led to wild oscillations in predicted reaction rates. Horizontal and vertical concentration gradients were of comparable magnitude (Table 4.3) so that the oscillations could not be filtered without substantial distortion of the data.

Isotope Ratio Depth Distributions

Three processes that regulate the isotopic compositon of the DOC reservoir are described in the following section.

1. DOC production from decomposition of POC. The $\delta^{13}C$ value of DOC produced from POC decomposition is influenced by the same factors that control the isotopic composition of the POC reservoir. For Skan Bay sediment, these appear to be the quantity and reactivity of sedimentary organic material derived from phytoplankton and kelp.

2. DOC consumption by oxidation to DIC or condensation to POC. The effect of DOC consumption on the $\delta^{13}C$-DOC depth distribution is complex. There is a great deal of inter- and intra-molecular isotopic hetero-geneity within the DOC reservoir. For example, the $\delta^{13}C$ values of individual amino acids isolated from a single organism differ by more than $15^o/oo$, while carboxyl groups are 10 to $20^o/oo$ heavier than the remainder of the molecule (Abelson and Hoering, 1961). Therefore, the isotopic composition of the bulk DOC will be influenced by decar-boxylation reactions or selective oxidation of particular molecules. In addition, DOC oxidation reactions are subject to large and highly vari-able kinetic isotope effects (Kaplan and Rittenberg, 1964; O'Leary, 1969).

3. Diffusion. The effect of diffusion on the $\delta^{13}C$-DOC depth distri-bution cannot be quantified. Concentration and $\delta^{13}C$ gradients of indi-vidual components of the DOC reservoir are unknown and are likely to differ substantially from those of bulk DOC.

There is too much uncertainty with respect to the factors that control $\delta^{13}C$-DOC depth distributions in marine sediments to permit quantitative modelling. However, $\delta^{13}C$-DOC data provide qualitative

information on the nature of the organic material undergoing decomposition. Since sediment DOC is derived from the reactive components within the POC reservoir, the δ^{13}C-DOC depth distributions allow an independent check on the differential decomposition of phytoplankton and kelp predicted by the POC isotope mass-balance model.

The difference between δ^{13}C-DOC and δ^{13}C-POC at each depth is plotted in Fig. 4.17. In the upper 15 cm, the DOC was isotopically heavier than the POC indicating that an isotopically heavy component of the POC reservoir was preferentially decomposed. Below 15 cm, the DOC was isotopically lighter than the POC indicating preferential decomposition of an isotopically light component of the POC reservoir. Thus, the δ^{13}C-DOC depth distributions are consistent with the results of the isotope mass-balance model for the POC reservoir (Fig. 4.16b), which indicated preferential decomposition of isotopically heavy kelp (-16.4^{o}/oo) in the upper 10 cm followed by decomposition of isotopically light phytoplankton (-21.5^{o}/oo) at depth.

The DOC Cycle

DOC is produced by POC degradation and is converted to DIC or CH_4 by fermentation and terminal metabolism. Although the DOC cycle is poorly understood, it is often assumed that DOC is quantitatively converted to metabolic end-products (DIC and CH_4). This assumption does not appear to be justified in Skan Bay sediment. Accumulation of high concentrations of DOC creates a large concentration gradient at the sediment-water interface (Fig. 3.9) indicating that some DOC leaves the sediment prior to complete oxidation.
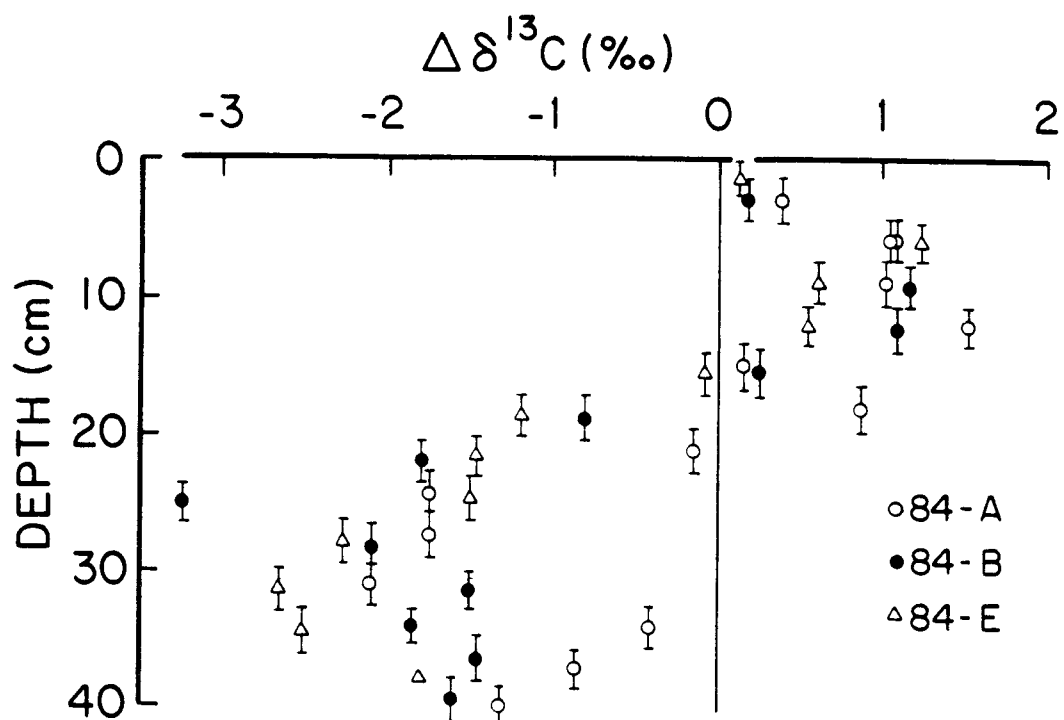
Fig. 4.17 Depth distribution of $\Delta\delta^{13}C$, defined as the difference between $\delta^{13}C$ values for DOC and POC. Positive values represent DOC that is isotopically heavier than POC. Negative values represent DOC that is isotopically lighter than POC.

The maximum in the DOC concentration profile (Fig. 3.9) suggests that the Skan Bay DOC cycle is comprised of two zones. The first zone (0 to 10 cm) is a region of net DOC accumulation where production outstrips consumption. The second zone (10 to 40 cm) is a region of net DOC consumption. A portion of the DOC consumed in the second zone is supplied by downward diffusion from the first zone.

The PIC Reservoir

DIC precipitation or PIC dissolution could occur wherever the DIC reservoir is out of equilibrium with respect to carbonate minerals. Equilibrium calculations indicate that shallow sediments (<12 to 18 cm) are undersaturated with respect to calcite, whereas deeper sediments are supersaturated (Fig. 4.18). The PIC depth distribution (Fig. 3.10) seems to support the thermodynamic calculations. PIC concentrations decrease in the upper 12 cm and increase at greater depths.

Isotope Ratio Depth Distributions

A stable isotope mass-balance model provides a definitive test for authigenic PIC precipitation. The isotopic composition of the PIC reservoir is very sensitive to DIC precipitation because of large differences between $\delta^{13}C$-DIC and $\delta^{13}C$-PIC profiles (c.f. Figs. 3.8 and 3.10).

An isotope mass-balance calculation was performed to see if the increase in PIC concentration below 12 cm could be attributed to DIC precipitation. The model assumed that (a) the increase in PIC concentration below 12 cm (Fig. 3.10) was due to authigenic calcite precipitation, and (b) the carbonate precipitate was at isotopic equilibrium with the DIC reservoir. The thermodynamic isotope fractionation factors for
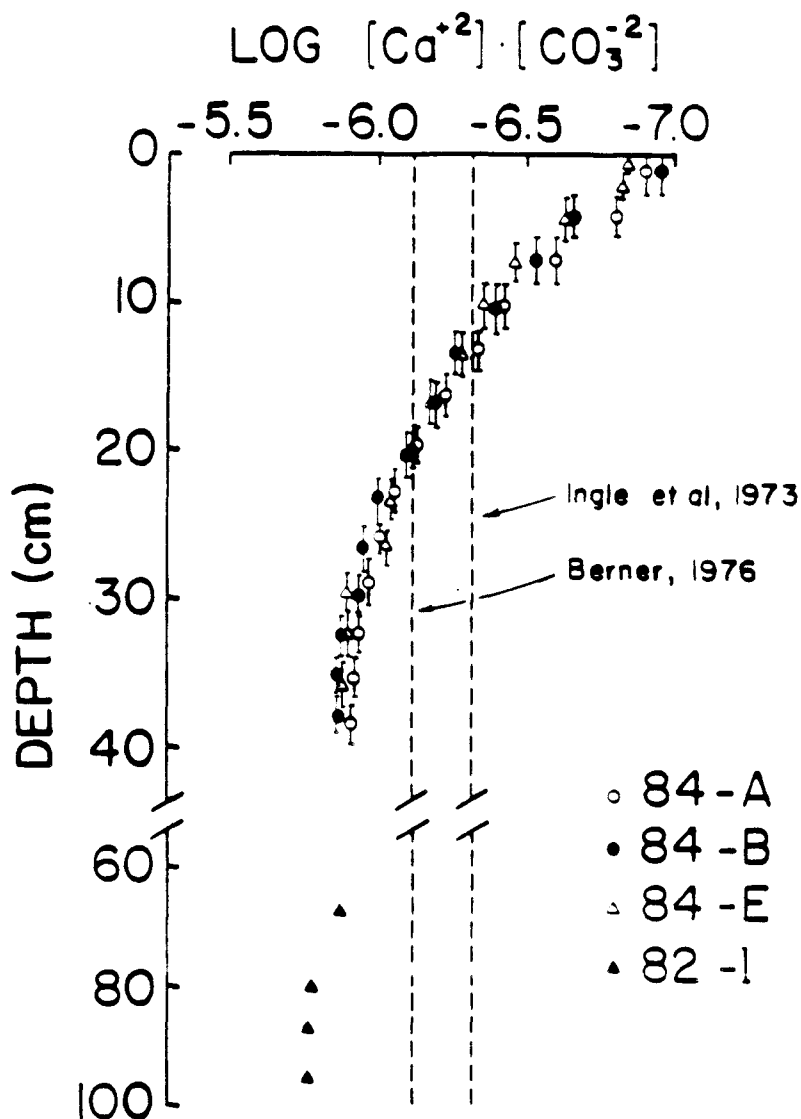
Fig. 4.18. Depth distribution of log ion activity product for calcium and carbonate. Calcium concentrations were estimated from bottom water chlorinity (18°/oo) and a seawater Ca:Cl ratio of 0.02106. Carbonate concentrations were calculated from DIC concentrations (Fig. 3.8) at a pH of 7 (unpublished data) using apparent dissociation constants for seawater at 3^oC (Mehrbach et al., 1973). The dashed vertical lines indicate the equilibrium solubility product for calcite (at the temperature and pressure of Skan Bay sediment) reported by two authors. Pore waters are undersaturated with respect to calcite where the log of the ion activity product is more negative than the solubility product. Note the break and change of scale on the depth axis.

the PIC-DIC system were taken from Grossman (1969) and corrected to in situ temperature according to Emrich et al. (1970). The mass-balance equations were analogous to those used for the POC isotope mass-balance (eqs. 4.36 and 4.37).

The isotope mass-balance model predicted that δ^{13}C-PIC values would range from -3 to -11°/oo if the increase in PIC concentration below 12 cm was due to authigenic precipitation (Fig. 4.19). The results conflict sharply with measured δ^{13}C-PIC values of approximately 0. The results of the model were similar if precipitation of aragonite was assumed.

The PIC Cycle

Although Skan Bay pore waters were supersaturated with respect to calcite at depths greater than 12 cm, isotope mass-balance calculations argue against authigenic precipitation. This is consistent with laboratory and field studies which show that DIC precipitation in marine sediments is inhibited by humic acid and phosphate ion (Berner, 1980).

Dissolution of PIC is a more difficult process to quantify because it has minimal effect on δ^{13}C-PIC depth distributions. However, it is reasonable to assume that in the absence of DIC precipitation, dissolution would lead to a decrease in PIC concentrations with depth. The PIC concentrations did not show an overall decrease with depth (Fig. 3.10) suggesting that PIC dissolution was not an active process.

Changes in the PIC concentration with depth may represent non-steady-state input of PIC. Fragments of mollusc shells appear to be a major source of PIC to Skan Bay sediment (see p. 85). The distribution
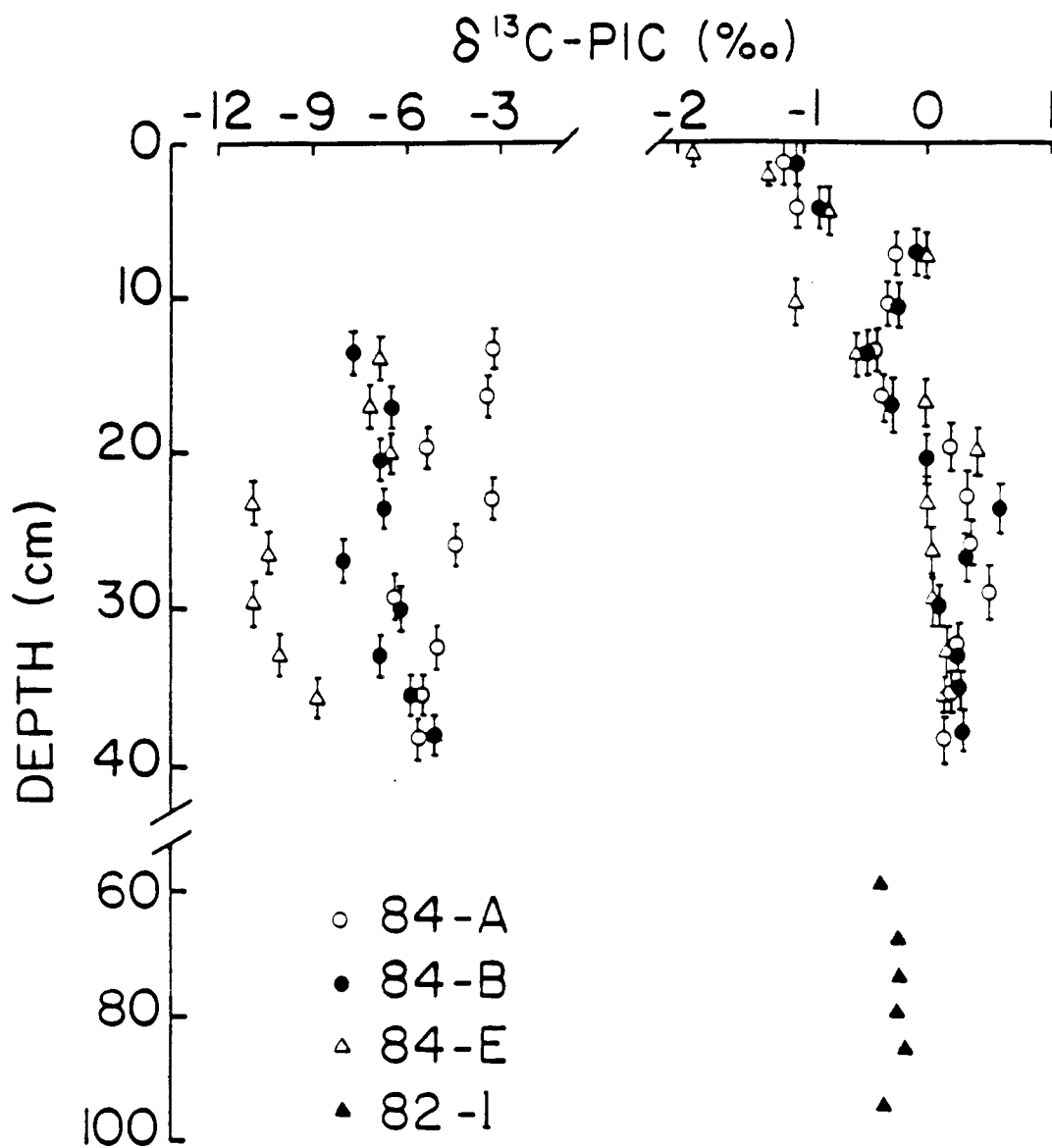
Fig. 4.19. Measured (right panel) and modelled (left panel) δ^{13}C-PIC depth distribution predicted by isotope mass-balance model assuming the increase in PIC concentration below 12 cm was due to authagenic precipitation. Note the break and change of scales in both axes.

and deposition rate of these large particles is expected to be heterogeneous and variable.

The DIC Reservoir

The DIC reservoir is the hub of the sediment carbon cycle. All carbon reservoirs, with the exception of POC, have the potential to communicate directly with DIC. DIC may be produced from CH_4 oxidation, DOC oxidation, and PIC dissolution. Likewise, DIC may be consumed during methanogenesis, acetogenesis, and carbonate mineral formation.

Three chemical species comprise the DIC reservoir: CO_2, HCO_3^-, and CO_3^{2-}. At the pH of Skan Bay sediment (7.1$\pm$0.1, n=8 [unpublished data]), CO_2, HCO_3^-, and CO_3^{2-} account for 11%, 88% and 0.4% of the DIC, respectively (Stumm and Morgan, 1970). Sediment pH, and thus DIC speciation, do not change with depth.

Rate Estimation by Derivative Evaluation

The DIC production rates were estimated by differentiating a smoothed cubic spline function fit to the DIC concentration data (Fig. 4.20). The DIC reservoir was assumed to be pure HCO_3^- in order to simplify the model. The three curves represent model sensitivity to the value of D_o.

The shape of the DIC production rate profile was consistent with the SO_4^{2-} reduction rate data (Fig. 4.10a), having a primary maxima near the sediment-water interface and a secondary maxima at depth. However, there is a severe imbalance between DIC production and POC consumption rates (c.f. Figs. 4.20b and 4.15b). The integrated rates of POC consumption and DIC production were 1558 and 331 $umol \cdot cm^{-2} \cdot yr^{-1}$, respectively.
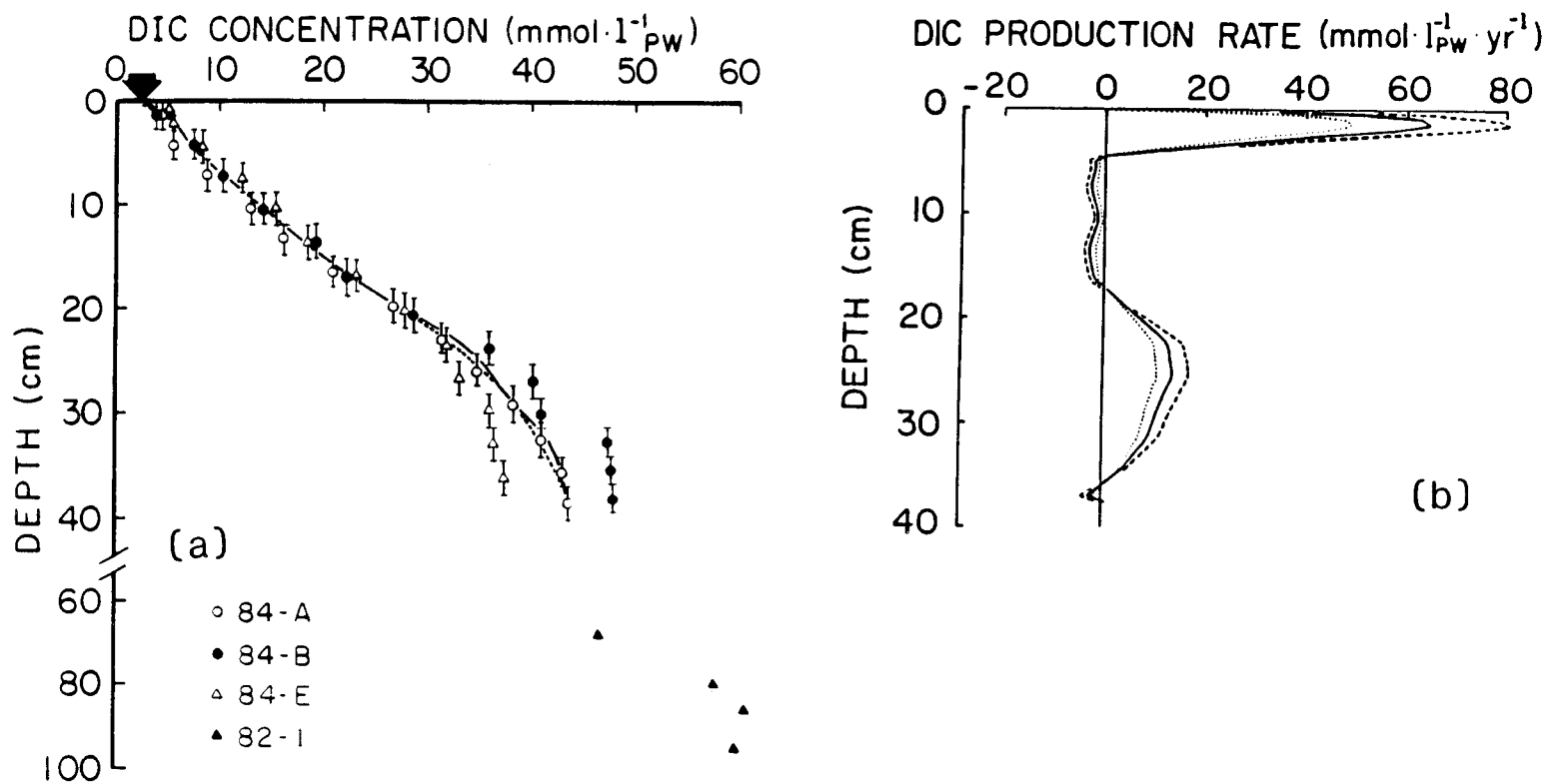
Fig. 4.20. Depth distribution of DIC production rate estimated by derivative evaluation. (a) Unsmoothed (solid curve) and smoothed (dashed curve) cubic spline fit to averaged DIC concentration data (the large arrow indicates bottom water DIC concentration), (b) modelled DIC production rates for three values of D_0 (cm^2/yr): 177 (solid curve), 133 (dotted curve), 221 (dashed curve).

Possible explanations for this discrepancy are discussed in the following section.

1. **Gross DIC consumption within the sediment column.** Biogeochemical processes that consume DIC include: methanogensis, acetogenesis, carbon fixation, and PIC formation.

Methanogenic bacteria consume a portion of the DIC produced during organic matter remineralization and reduce it to CH_4 by reaction with molecular hydrogen (Fenchel and Blackburn, 1979). However, oxidation of CH_4 within the sediment column is nearly quantitative, so that CH_4 production has no net effect on the POC-DIC mass-balance.

Acetogenic bacteria produce acetate by reduction of DIC with molecular hydrogen (Fenchel and Blackburn, 1979). Very little is known of the ecology of these bacteria, but studies using laboratory chemostats suggest that acetogenesis is active only in environments where SO_4^{2-} reducing and methanogenic bacteria are absent (Thompson et al., 1983). Furthermore, acetate turnover to DIC is very rapid in Skan Bay sediment (ca. 1 hr [Shaw et al., 1984]), implying that acetogenesis would have little effect on the DIC depth distribution.

Chemoautotrophic metabolism by a marine strain of Beggiatoa has recently been confirmed (Nelson and Jannasch, 1983). Indirect evidence that Beggiatoa or other white sulfur bacteria may be active near the sediment-water interface in Skan Bay sediment was presented above (p. 155). However, chemoautotrophic production would lead to an equal reduction of POC consumption and DIC production rates and would not affect the mass-balance.

Precipitation of DIC to form PIC could occur at depths greater than 10 to 20 cm where pore waters were supersaturated with respect to calcite (Fig. 4.18). It was shown above that DIC precipitation was inconsistent with the δ^{13}C-PIC data (p. 176). However, reservoirs of different sizes have different sensitivities to mass-balance calculations. Evidence that the PIC reservoir is not affected by authigenic precipitation does not imply a priori that the DIC reservoir is also unaffected. The difference between integrated POC consumption and DIC production is about 1200 umol·cm^{-2}·yr^{-1}. If this carbon were to enter the PIC reservoir via authigenic precipitation, PIC concentrations would exceed 4 mmol·g$_{SM}^{-1}$ ([PIC]=flux/sediment accumulation rate). In contrast, measured PIC concentrations were generally <1 mmol·g$_{SM}^{-1}$ (Fig. 3.10). This suggests that the "missing" carbon from POC decomposition is not "hiding" as carbonate minerals.

2. **Loss of organic matter from the sediment system via DOC diffusion.** The DOC reservoir contains a large, concentrated inventory of organic matter. The residence time in the DOC pool is sufficiently long for significant quantities of DOC to exit the sediment via diffusion across the interface. DOC lost from the sediment system represents POC consumption not coupled to DIC production. A quantitative estimate of DOC loss from the sediment system is presented in "Chapter 5: The Carbon Cycle" (see p. 198).

3. **Seasonal bioirrigation of surface sediments.** A model of the SO_4^{2-} reservoir required intense, periodic irrigation in the upper sediment column in order to reconcile concentration and rate data

(p. 159). The non-steady-state model predicted that irrigation ceased about one month prior to the September 1984 criuse. Thus, sediment sampling may have occurred during a transition period when pore water profiles were adjusting to new physical conditions. DIC production rates, derived from a model that assumed steady-state concentration profiles, would be underestimated if DIC concentrations in the upper sediments were rapidly increasing. The imbalance between POC consumption and DIC production may be an artifact linked to non-steady-state conditions.

The seasonal bioirrigation model predicted that during the first month of non-irrigating conditions, measurable changes in concentration profiles would occur over periods of less than two weeks. However, this prediction is inconsistent with time-series data for the DIC reservoir. Five cores sampled over a two week period showed no sytematic increase in alkalinity (A. Devol, Univ. Washington, Seattle, unpublished data). These data suggest that during the September 1984 cruise, the DIC reservoir was at steady-state, at least over a time-scale of several weeks.

The discrepancy between POC consumption and DIC production rates could be explained by either DOC diffusion or seasonal bioirrigation. It is likely that both processes occur, but it is difficult to establish which is most important. It is clear that DOC diffusion has the potential to deprive sediments of significant quantities of reduced carbon. It is also clear that the DIC reservoir is not changing as fast as the seasonal bioirrigation model suggests.

Isotope Ratio Depth Distributions

Skan Bay DIC is produced primarily from oxidation of DOC and CH_4. Since these reservoirs have distinct carbon isotope ratios (Fig. 1.1), the isotopic composition of the DIC reservoir will depend on relative production rates from each source. An isotope mass-balance model provides a means of resolving the effects of DOC and CH_4 oxidation on the $\delta^{13}C$-DIC depth distribution.

The model is similar to that used for CH_4 (p. 141). The ^{12}C-DIC and ^{13}C-DIC concentration distributions were represented by two diagenetic equations (analogous to eqs. 4.31 and 4.35). Given estimates of DIC production rates from DOC and CH_4, the two equations could be solved to yield a prediction of the $\delta^{13}C$-DIC depth distribution. The importance of a particular DIC source could be inferred by simulating the $\delta^{13}C$-DIC profile that would result if that process were not occurring.

The rate of DIC production from CH_4 was estimated by averaging the model-derived CH_4 oxidation rate profiles in Fig. 4.7. The isotopic composition of methane-derived DIC was calculated trom $\delta^{13}C$-CH_4 data (Fig. 3.7), and a kinetic isotope fractionation factor for CH_4 oxidation of 1.018 (average value for the two diffusion isotope effect cases [Fig. 4.9]).

The rate of DIC production from DOC was estimated by the difference between total DIC production (Fig. 4.20b, solid curve) and DIC production from CH_4. The $\delta^{13}C$ value of DOC-derived DIC was assumed to equal that of DOC (Fig. 3.9). This assumption is crude as there is isotopic heterogeneity within the DOC reservoir as well as isotope fractionation during oxidation. However, it is likely that the difference between $\delta^{13}C$

values for DOC and DIC derived from DOC is small relative to the difference between DOC and CH_4 reservoirs (>50°/oo).

Additional assumptions specific to this model are: (a) the DIC reservoir is pure HCO_3^-, (b) the isotope diffusivity ratio, f, for HCO_3^- and CO_2 are the same, (c) DOC and CH_4 are the only DIC sources, and (d) gross DIC consumption (i.e. methanogenesis, acetogenesis, chemoautotrophic assimilation, or precipitation of carbonate minerals) is not occurring within the model boundaries (0 to 37.5 cm).

Results of the isotope model are shown in Fig. 4.21. The model reproduced the sharp δ^{13}C-DIC gradient near the sediment-water interface and correctly predicted the location of the distinct minimum. However, the model overestimated the magnitude of the δ^{13}C-DIC minimum by 1 to 4°/oo. This error could be the result of overestimated CH_4 oxidation rates, underestimated DIC production rates, or preferential oxidation of isotopically light DOC.

The reversal in the model-derived δ^{13}C-DIC profile below 20 cm is the result of diffusive mixing with isotopically heavy DIC at depth. Isotopically heavy DIC can be produced by carbonate dissolution or methanogenesis. PIC concentrations show no decrease below 40 cm (Fig. 3.10), implying that the isotopically heavy DIC is derived from isotope fractionation during CH_4 production. Even though methanogenesis in Skan Bay sediment is not active in the upper 35 cm (p. 149), it strongly influences the shape of the δ^{13}C-DIC profile.

A mid-depth minimum in the δ^{13}C-DIC depth distribution is a common feature in anoxic marine sediments (Claypool and Kaplan, 1974; Miller, 1980; Alperin and Reeburgh, 1984; Boehme and Blair, 1986). Two
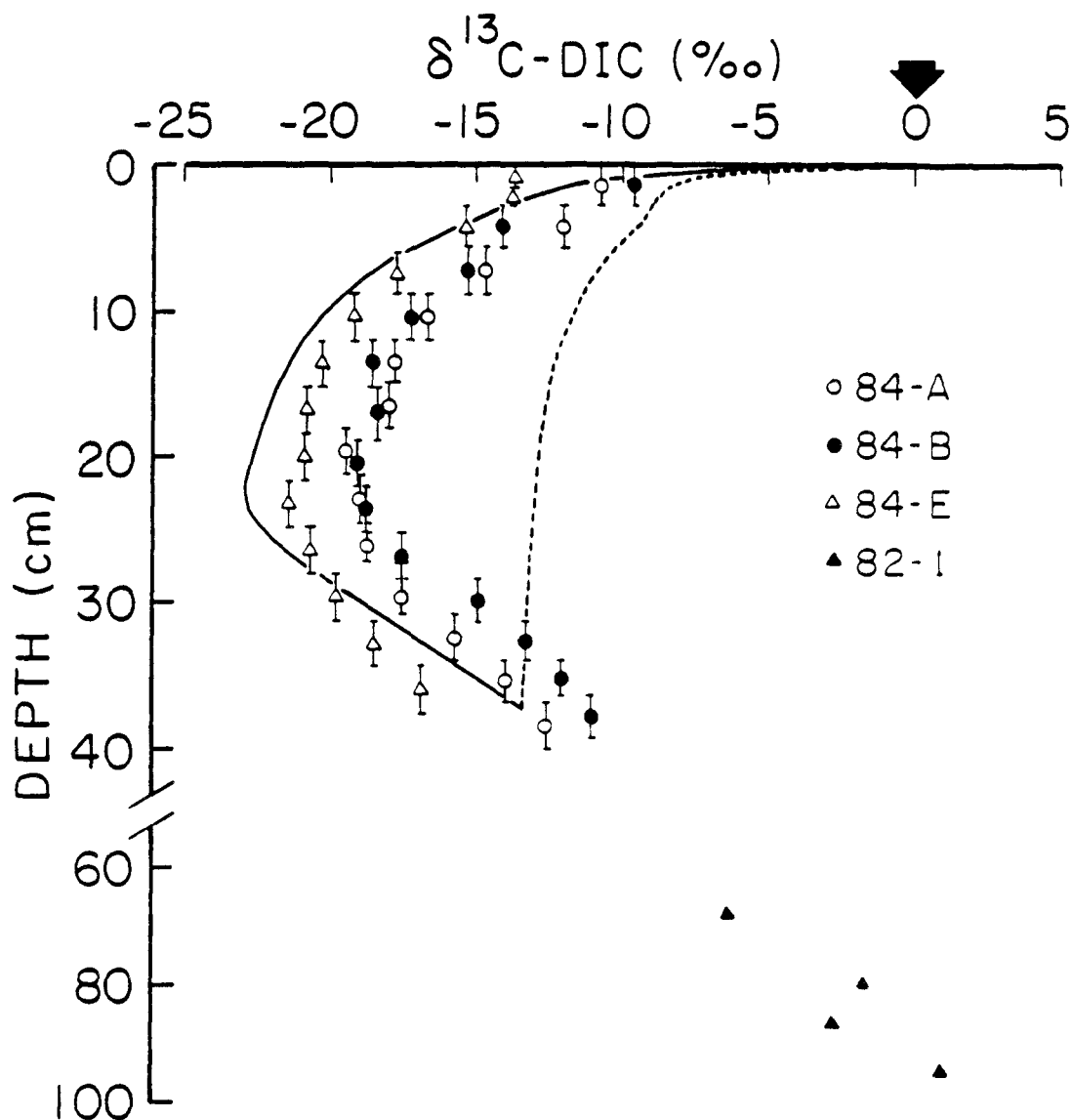
Fig. 4.21. Depth distribution of δ^{13}C-DIC predicted by the isotope model with (solid curve) and without (dashed curve) the input of isotopically light DIC derived from methane oxidation. The large arrow represents the isotopic composition of the bottom water.

explanations of the minimum have been proposed. Claypool and Kaplan (1974) hypothesized that the minimum resulted from organic matter decomposition in the upper sediment (input of DIC with $\delta^{13}C$ of about $-20^{o}/oo$) and methanogenesis at depth (preferential reduction of isotopically light DIC). Reeburgh (1982) postulated that localized input of isotopically light DIC derived from CH_4 oxidation contributed to the minimum.

The model was used to test the influence of CH_4 oxidation on the $\delta^{13}C$-DIC profile in Skan Bay sediments. Methane oxidation rates were set equal to zero, and the $\delta^{13}C$-DIC depth distribution was predicted (Fig. 4.21). In the absence of CH_4 oxidation, the profile did not show an intense minimum, indicating that input of methane-derived DIC plays a significant role in establishing the $\delta^{13}C$-DIC minimum.

The DIC Cycle

The DIC cycle in Skan Bay sediment can be divided into three zones. The first zone (0 to 5 cm) is a region of intense DIC production, presumably from DOC oxidation. Approximately 60% of the integrated DIC production occurs within this zone. The second zone (5 to 20 cm) appears to have very low DIC production rates. The very low rates may, in part, be an artifact caused by seasonal irrigation of the sediment. The third zone (20 to 40 cm) corresponds to the maximum in CH_4 oxidation rates and the secondary maxima in SO_4^{2-} reduction rates. The DIC produced in this zone is a mixture of oxidized DOC and CH_4.

Although DOC oxidation dominates DIC production (approximately 80% of the DIC production is derived from DOC), CH_4 oxidation and production play a significant role in controlling the $\delta^{13}C$-DIC profile. This is

because of very large isotopic signals associated with the CH_4 reservoir. Since DIC derived from CH_4 oxidation is 60 to 80°/oo lighter than DIC derived from DOC (assuming a kinetic isotope effect for CH_4 oxidation of 1.018 [p. 185]), relatively slow rates of CH_4 oxidation have a disproportionate effect on the isotopic signature of the DIC reservoir. Likewise, a large isotope effect associated with DIC reduction to CH_4 is probably the cause of the isotopically heavy DIC at depth (Fig. 3.8).

Model Results: Summary

The sources and sinks for reservoirs involved in the Skan Bay sediment carbon cycle are summarized in Table 4.6. Measured and/or model-derived reaction rates are available for CH_4 oxidation, SO_4^{2-} reduction, POC degradation, and DIC production. Most CH_4 production appears to be confined to depths greater than 40 cm, and thus outside the adopted boundaries (0 to 37.5 cm [p. 118]). Isotope mass-balance calculations suggest that the PIC reservoir is relatively unreactive. The one important reservoir for which exchange rates are lacking is DOC. Since all other processes are known, rates of DOC production and consumption can be evaluated by mass-balance considerations.

Several inconsistencies in the data have become apparent. Measured SO_4^{2-} reduction rates are higher than predicted from the concentration data. Also, only a minor portion of the degraded POC finds its way into the DIC reservoir. By synthesizing rate estimates into a comprehensive depth-dependent model of the carbon cycle, overall and isotope mass-balance constraints may help to locate the causes of the inconsistencies.

Table 4.6. Reservoirs and chemical processes involved in the Skan Bay
sediment carbon cycle.

==

Reservoir	Chemical Process	Reaction Rates[a] Measured	Modelled	Depth Interval and Relative Rates[b]
CH_4	oxidation	4.5a	4.6b 4.7	0-20 cm [O] 20-35 cm [F]
	production			0-20 cm [VS] 20-35 cm [O or VS] >40 cm [F]
SO_4^{2-}	reduction	4.10a	4.11b	0-15 cm [F] 15-30 cm [S] 30-40 cm [M]
	production		4.12	[?]
POC	consumption		4.15b	0-10 cm [F] 10-40 cm [S]
DOC	oxidation and production			0-10 cm [Pr>Ox] 10-40 cm [Ox>Pr]
PIC	dissolution			[O]
	mineral formation			[O]
DIC	production		4.20b	0-5 cm [F] 5-20 cm [S] 20-40 cm [M]
	consumption (methanogenesis)			0-40 cm [O] >40 cm [F?]
	(precipitation)			[O]

----

[a]Number corresponds to figure showing measured or modelled rate pro-
files. Blanks in these columns represent chemical processes for which
rates are unavailable.

[b][O]=undetectable, [VS]=very slow, [S]=slow, [M]=medium, [F]=fast,
[?]=uncertain, [Pr]=production, [Ox]=oxidation.

CHAPTER 5: THE CARBON CYCLE

The goal of this study was to construct an operational blueprint diagramming carbon flow in Skan Bay sediment. In this chapter, reaction rates of chemical processes that regulate CH_4, DIC, DOC, PIC, and POC reservoirs are integrated into a quantitative, depth-dependent model of the carbon cycle. Two types of information are required to formulate the model: (a) advective and diffusive fluxes at the system boundaries, and (b) reactive fluxes between carbon reservoirs. A check on the internal consistency of the carbon cycle model is provided by mass-balance calculations. The model of the carbon cycle will serve as a reference for interpreting biogeochemical rate measurements, and will provide guidance for future studies of the sediment carbon cycle in Skan Bay as well as other anoxic environments.

Advective and Diffusive Fluxes at the System Boundaries

This study focused on that portion of the sediment column that lies between the sediment-water interface and a depth of 37.5 cm. This region, of course, represents an open system with material flowing across the upper and lower boundaries. Since the interface serves as a fixed reference frame for the sediment system (see p. 103), material appears to be advected downward as solid matter is deposited at the sediment surface. In addition, diffusion transports dissolved material across the system boundaries.

Advective fluxes (F_{adv}) for solid phase constituents were calculated from the following relationship:

191

$$F_{adv} = F_{SM} \, [C]_{SM} \, . \qquad (5.1)$$

A similar equation was applied to pore water constituents:

$$F_{adv} = \nu \, [C]_{PW} \, . \qquad (5.2)$$

Substituting eq. 4.22 into 5.2,

$$F_{adv} = \frac{(\phi_\infty \omega_\infty)}{\phi} \, [C]_{PW} \, . \qquad (5.3)$$

Diffusive fluxes (F_{diff}) were calculated from Fick's First Law modified for diffusion in porous media (Berner, 1980):

$$F_{diff} = \phi \, D_{WS} \, \frac{d[C]_{PW}}{dz} \, . \qquad (5.4)$$

Substituting eq. 4.7 into eq. 5.2,

$$F_{diff} = \phi^3 \, D_o \, \frac{d[C]_{PW}}{dz} \, . \qquad (5.5)$$

Advective and diffusive fluxes at the boundaries, calculated from eqs. 5.1, 5.3, and 5.5, are compiled in Table 5.1.

Reactive Fluxes between Carbon Reservoirs

Reactive fluxes refer to mass-flow between carbon reservoirs that is driven by chemical reactions. Diagenetic models applied to CH_4, DIC, and POC concentration-depth distributions provided estimates of CH_4 oxidation (Fig. 4.7), DIC production (4.20), and POC consumption rates (Fig. 4.15). The PIC reservoir functions as a spectator rather than an active participant in the Skan Bay carbon cycle. Concentration and $\delta^{13}C$ profiles for PIC and DIC reservoirs indicated that neither carbonate dissolution nor mineral formation were occurring (see p. 178).

DOC production and consumption rates could not be determined by

Table 5.1. Fluxes at the system boundaries[a].

| | Flux ($\mu mol \cdot cm^{-2} \cdot yr^{-1}$) | | | |
| | Upper Boundary (0 cm) | | Lower Boundary (37.5 cm) | |
Reservoir	Diffusive	Advective	Diffusive	Advective
CH_4	-4 ± 2	0	-49 ± 15	5 ± 1
DIC	-306 ± 167	2 ± 0.2	-25 ± 25	43 ± 10
DOC	-456 ± 211	0	-22 ± 20	9 ± 2
PIC	----	250 ± 60	----	300 ± 60
POC	----	2290 ± 480	----	840 ± 170

[a] Diffusive and advective fluxes were calculated from eqs. 5.1, 5.3, and 5.5. Values of F_{SM}, ϕ, ω_∞, $D_o(CH_4)$, and $D_o(HCO_3^-)$ were from Table 4.5. The value for $D_o(DOC)$ is estimated in Fig. 5.1. Solid phase concentrations at the sediment-water interface were calculated by linear extrapolation of the uppermost samples. Interface concentrations for dissolved constituents were taken as overlying water values. Concentrations at the lower boundary were interpolated to 37.5 cm. Concentration gradients were calculated from the slope of a line fit to two points adjacent to the upper (overlying water and 1.5 cm) and lower (34.5 and 37.5 cm) boundaries. Negative fluxes are upward, positive fluxes are downward. Uncertainties represent the standard deviation of fluxes calculated for subcores 84-A, 84-B, and 84-E.
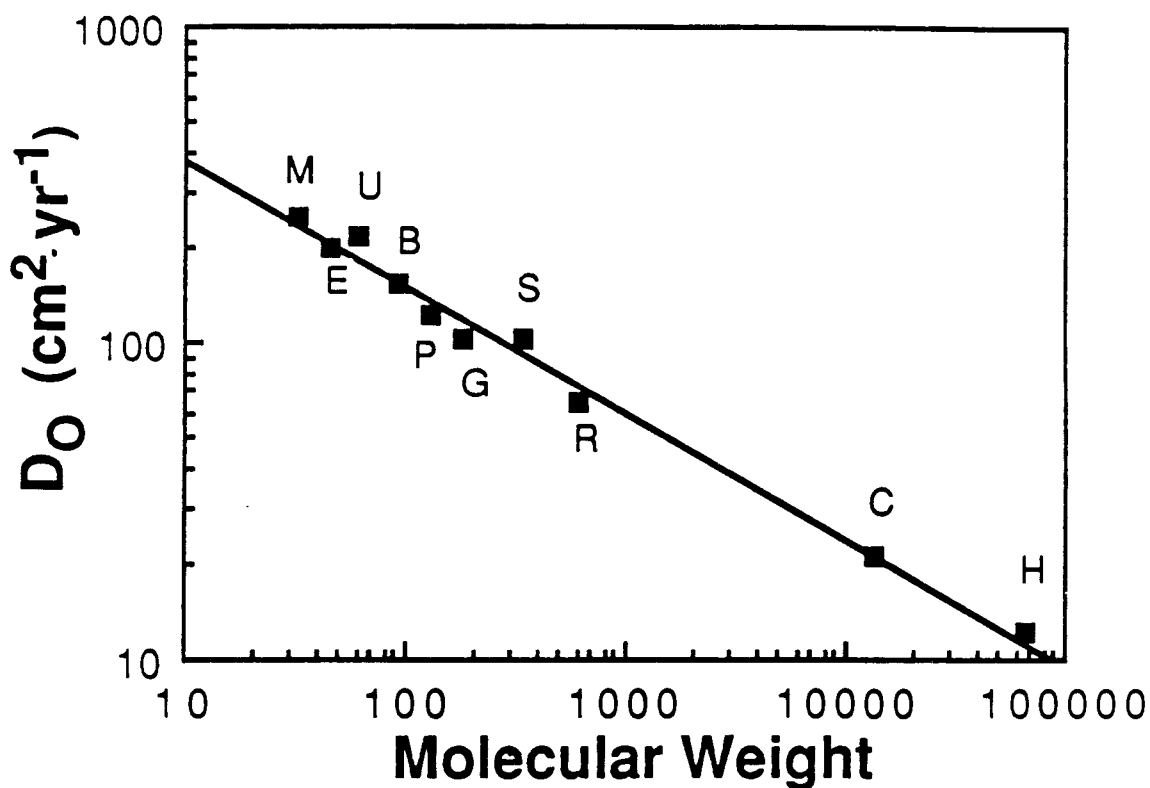
Fig. 5.1. Free solution diffusion coefficient vs. molecular weight for various organic compounds (corrected to $3^{o}C$, $32^{o}/oo$ salinity using the Stokes-Einstein equation): M=methanol, E=ethanol, U=urea, B=butanol, P=pyrogallol, G=glucose, S=sucrose, R=raffinose, C=cytochrome C, and H=hemoglobin (sources: Lehninger, 1975; Jost 1960; Handbook of Chemistry and Physics, 57th edition). Although the bulk of the pore water DOC was shown to have a molecular weight greater than 500 (Orem et al., 1986), the average molecular weight is unknown. Dawson et al. (1981) determined that yellow colored fulvic acids in soil solution and stream waters have an average molecular weight of 800 to 900. Assuming an average molecular weight of Skan Bay DOC of 900, the free solution diffusion coefficient would be about 70 $cm^2 \cdot yr^{-1}$.

diagenetic modelling (see p. 172), but may be inferred from reaction rates of other processes. Assuming that POC is not subject to decarboxylation reactions (i.e. direct oxidation to DIC), degraded POC must enter the DOC reservoir. Therefore, gross DOC production and net POC consumption rates must be equal.

A similar argument provides an estimate of gross DOC consumption rates. Components of the DOC reservoir have three possible fates: (a) conversion to POC by either geopolymerization, adsorption, or bacterial assimilation, (b) fermentation to CH_4, and (c) oxidation to DIC. Conversion of DOC to POC represents a short circuit in the carbon remineralization process and is not detected by diagenetic models that estimate net reaction rates. Methane production occurs primarily at depths greater than 40 cm (see p. 149), which is outside the model boundaries. Since CH_4 and DOC are the only DIC sources (see p. 185), gross DOC consumption must equal the difference between total DIC production and CH_4 oxidation.

Reactive fluxes between the CH_4, DIC, DOC, and POC reservoirs were calculated by integrating model-derived rates at 3 cm depth intervals (Table 5.2). Conversion of reaction rates to flux units ($umol \cdot cm^{-2} \cdot yr^{-1}$) allows direct comparison of reactive, diffusive, and advective fluxes.

The Carbon Cycle Model

A diagram of the carbon cycle in Skan Bay sediment (Fig. 5.2) was constructed by combining boundary fluxes (Table 5.1), reactive fluxes (Table 5.2), and average concentrations (Appendix I) for the five major carbon reservoirs. The diagram provides a quantitative illustration of

Table 5.2. Reactive fluxes between carbon reservoirs[a].

===

| Depth (cm) | Flux (umol·cm^{-2}·yr^{-1}) | | |
	$CH_4 \rightarrow DIC$[b]	$DOC \rightarrow DIC$[c]	$POC \rightarrow DOC$[d]
0-3	0.0	152	301
3-6	0.0	19	594
6-9	0.0	0	325
9-12	0.0	0	32
12-15	0.0	0	46
15-18	0.1	0	59
18-21	2.1	15	31
21-24	23.0	13	32
24-27	26.5	13	50
27-30	13.3	20	44
30-33	2.3	23	34
33-36	0.0	10	11
36-39	0.0	0	0
total	67.3	265	1559

----

[a]Reactive fluxes were calculated by integrating depth-dependent reaction rates at 3 cm intervals.

[b]Methane oxidation rate depth distributions for subcores 84-A, 84-B and 84-E (Fig. 4.7) were averaged.

[c]DIC production from DOC was estimated as the difference between total DIC production (Fig. 4.20b) and methane oxidation (Fig. 4.7).

[d]POC consumption rates were taken from Fig. 4.15b.
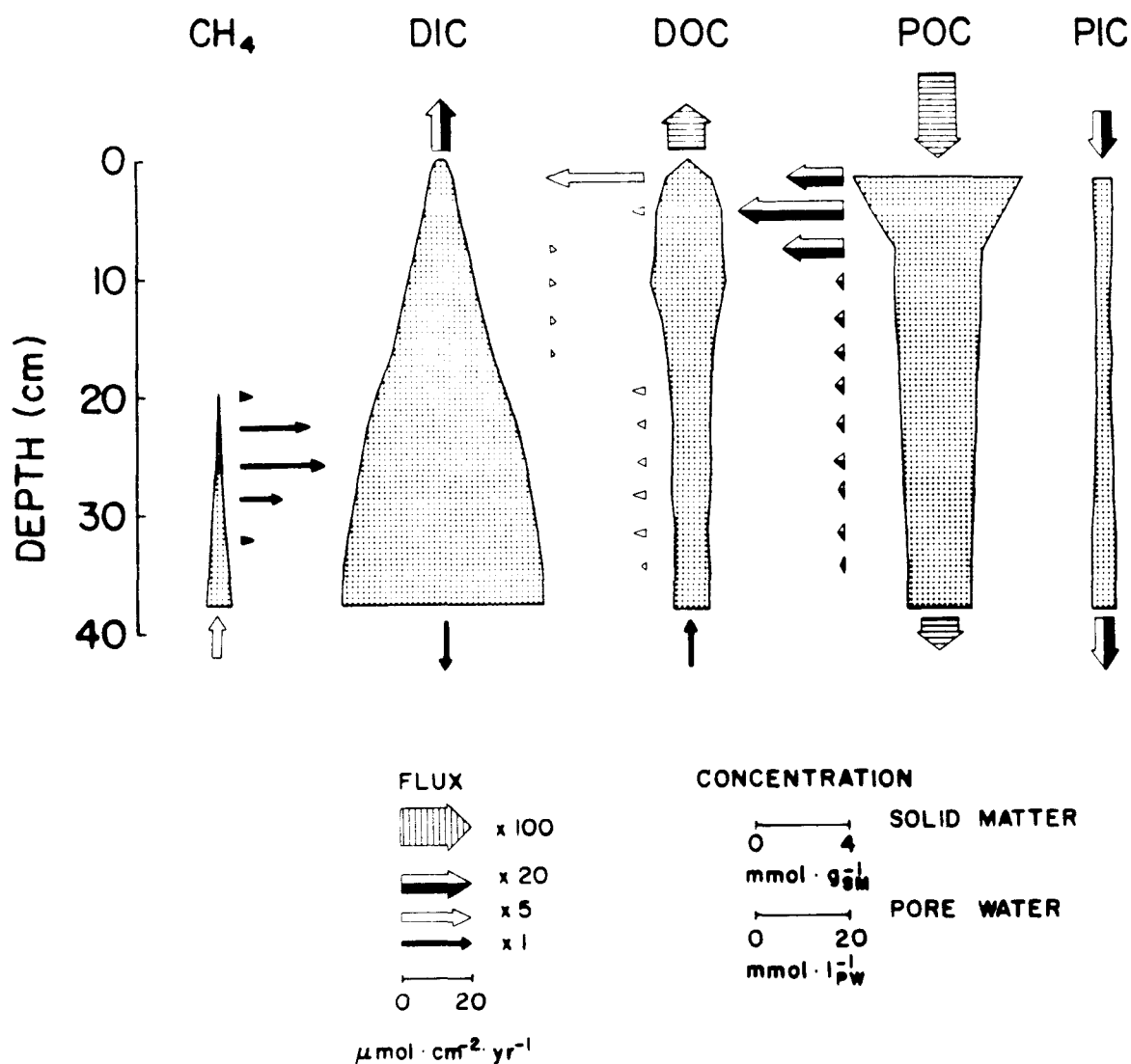
Fig. 5.2. The carbon cycle in Skan Bay sediments. The concentration within a reservoir at a given depth is proportional to the width of the stippled area. The advective (vertical arrows), diffusive (vertical arrows), and reactive (horizontal arrows) fluxes are proportional to the lengths of the arrows. Scaling quantities for converting widths of stippled areas and lengths of arrows to concentrations and fluxes are provided in the legend. All fluxes except for the DOC diffusive flux are from Tables 5.1 and 5.2. The DOC diffusive flux was calculated to impose overall and isotope mass-balance on the carbon cycle (see Table 5.5c). Absence of an arrow indicates a net flux less than 5 umol/cm^{2}yr.

depth-dependent changes in carbon concentrations and reaction rates. Before discussing the implications of the carbon cycle model, accuracy and internal consistency will be checked by material balance calculations.

Total Carbon Mass Balance

Assuming that the sediment column is at steady-state, conservation of mass requires a balance between input and output fluxes for each carbon reservoir. Differences between input and output for CH_4, DIC, and POC reservoirs (Table 5.3) were not significant (95% confidence level). Mass balance is to be expected for these reservoirs since reaction rates were calculated by diagenetic models that balanced advection, diffusion, and reaction.

DOC reactive fluxes, calculated from POC, DIC, and CH_4 reaction rates, were not required to balance with DOC advective and diffusive fluxes, and thus provide an independent check of the carbon cycle model. For the DOC reservoir, inflow was about twice that of outflow (Table 5.3). Possible explanations for this discrepancy are discussed below.

1. **The DOC diffusive flux at the sediment-water interface was underestimated.** In the absence of high-resolution (<0.1 cm) data, benthic fluxes calculated from Fick's First Law must be regarded as lower limits. Reimers and Smith (1986) demonstrated that calculated concentration gradients generally increase as sampling resolution becomes finer. The DOC reservoir, with the largest infacial concentration gradient of any of the dissolved carbon reservoirs, is especially prone to

Table 5.3. Total carbon mass balance[a].

Reservoir	Diffusive	Advective	Reactive	Total
		Flux ($umol \cdot cm^{-2} \cdot yr^{-1}$)		
CH$_4$				
INPUT	49$\pm$15	0	0	49$\pm$15
OUTPUT	4$\pm$2	5$\pm$1	67$\pm$17	76$\pm$17
DIC				
INPUT	25$\pm$25	2$\pm$0.2	333$\pm$83	359$\pm$87
OUTPUT	306$\pm$167	43$\pm$10	0	349$\pm$167
DOC				
INPUT	22$\pm$20	0	1559$\pm$390	1581$\pm$390
OUTPUT	456$\pm$211	9$\pm$2	265$\pm$66	730$\pm$220
PIC				
INPUT	----	250$\pm$60	0	250$\pm$60
OUTPUT	----	300$\pm$60	0	300$\pm$60
POC				
INPUT	----	2290$\pm$480	0	2290$\pm$480
OUTPUT	----	840$\pm$170	1559$\pm$312	2399$\pm$355

[a] Diffusive and advective fluxes are from Table 5.1. Reactive fluxes are from Table 5.2. Error estimates for the reactive fluxes are equal to the uncertainty in the diffusion coefficient ($\pm$25%).

this type of error. In addition, the assumed diffusion coefficient for DOC (Fig. 5.1) may be underestimated.

2. DOC reaction rates could be in error. Net reaction rates for the DOC reservoir were calculated from POC consumption, DIC production, and CH_4 oxidation rates. Of these three rates, DIC production is the one most likely to be in error. POC consumption rates were based on two well-founded assumptions (no bioturbation and steady-state deposition of organic matter [see pp. 110 and 115]), and CH_4 oxidation rates were substantiated by ^{14}C-tracer experiments (see p. 138). On the other hand, the possibility of seasonal bioirrigation (see p. 117) casts doubt on DIC production rates that were calculated from a model that assumed steady-state pore water profiles (see p. 180).

The imbalance in the DOC reservoir may be due to an underestimated diffusive flux, underestimated DIC production rates, or some combination of the two. The distinct isotope ratio depth distributions for DIC and DOC reservoirs (Figs. 3.8 and 3.9) suggest that an isotope mass-balance calculation may provide a clue as to which source of error is dominant.

Stable Isotope Mass Balance

In addition to the requirement of overall material balance for each reservoir, conservation of mass requires that stable isotopes be conserved. If the sediment column is at steady-state, isotope ratios of total input (δ_{IN}) and output (δ_{OUT}) fluxes must be equal. Values for δ_{IN} and δ_{OUT} were calculated as the weighted average $\delta^{13}C$ of material flowing across the boundaries:

$$\delta_{IN} = \frac{{}^a_o(F \cdot \delta)_{CH4} + {}^a_o(F \cdot \delta)_{DIC} + {}^a_o(F \cdot \delta)_{DOC} + {}^a_o(F \cdot \delta)_{POC}}{F_{IN}}$$

$$+ \frac{{}^d_z(F \cdot \delta)CH4 + {}^d_z(F \cdot \delta)DIC + {}^d_z(F \cdot \delta)DOC}{F_{IN}} , \qquad (5.6)$$

$$\delta_{OUT} = \frac{{}^a_z(F \cdot \delta)_{CH4} + {}^a_z(F \cdot \delta)_{DIC} + {}^a_z(F \cdot \delta)_{DOC} + {}^a_z(F \cdot \delta)_{POC}}{F_{OUT}}$$

$$+ \frac{{}^d_o(F \cdot \delta)_{CH4} + {}^d_o(F \cdot \delta)_{DIC} + {}^d_o(F \cdot \delta)_{DOC}}{F_{OUT}} , \qquad (5.7)$$

where $(F \cdot \delta)$ is the product of the advective (superscript a) or diffusive (superscript d) flux and its $\delta^{13}C$ value, F_{IN} and F_{OUT} are the sum of input and output fluxes from each carbon reservoir, and the characters preceding each term represent upper (subscript o) and lower (subscript z) boundaries. PIC fluxes were not included in eqs. 5.6 and 5.7.

The $\delta^{13}C$ values for fluxes at the system boundaries are summarized in Table 5.4. The isotopic composition of advective fluxes was taken as the $\delta^{13}C$ value at the boundaries. The isotopic composition of diffusive fluxes was calculated from the following equation (derived in Appendix II):

$$\delta_{diff} = ([C]_{PW} \frac{d\delta}{d[C]_{PW}} + \delta) + (1-f) \, 1000 . \qquad (5.8)$$

where δ_{diff} is the $\delta^{13}C$ value of material diffusing through a boundary, δ is the $\delta^{13}C$ value of material at the boundary, and other symbols are as previously defined (Table 4.1). It is clear from eq. 5.8 that the isotopic composition of material transported across a boundary by diffusion generally differs from the $\delta^{13}C$ value of the material at the boundary. This effect, known as "differential isotopic diffusion", was

Table 5.4. $\delta^{13}C$ values of fluxes at the system boundaries.

| | $\delta^{13}C$ (°/oo) | | | |
| | Upper Boundary (0 cm) | | Lower Boundary (37.5 cm) | |
Reservoir	Diffusive	Advective	Diffusive	Advective
CH_4	-79.3[a,b]	-73.0[b]	-84.0[a]	-77.3[c]
DIC	-21.9[a]	$+0.3$[d]	$+25.0$[a]	-13.4[c]
DOC	-19.2[a,b]	-19.3[b]	-21.1[a]	-21.7[c]
PIC	----	-1.5[e]	----	$+0.2$[f]
POC	----	-19.2[e]	----	-20.2[f]

[a] The isotopic composition of diffusive fluxes was estimated from eq. 5.8 (see Appendix II). At the upper boundary, $d\delta/d[C]$ was calculated from isotope ratio and concentration data for bottom water and a sediment depth of 1.5 cm. At the lower boundary, $d\delta/d[C]$ was calculated from isotope ratio and concentration data at 34.5 and 37.5 cm. The value of f was taken as 1.008 for methane, 1.0007 for DIC, and 1.000 for DOC.

[b] The $\delta^{13}C$ value of the bottom water was not measured. The isotopic composition at the upper boundary was estimated from pore water data by linear extrapolation to the sediment-water interface.

[c] The isotopic composition of pore water advective fluxes at the lower boundary was calculated from $\delta^{13}C$ data at 37.5 cm.

[d] The isotopic composition of pore water advective fluxes at the upper boundary was taken as bottom water values.

[e] The isotopic composition of solid phase advective fluxes at the upper boundary was calculated by linear extrapolation of $\delta^{13}C$ data to the sediment-water interface.

[f] The isotopic composition of solid phase advective fluxes at the lower boundary was calculated from $\delta^{13}C$ data at 37.5 cm.

first predicted by Goldhaber (1974) and has since been confirmed by Chanton et al. (1987).

Boundary fluxes (Table 5.1) and $\delta^{13}C$ values (Table 5.4) were input into eqs. 5.6 and 5.7 to calculate δ_{IN} and δ_{OUT} values for the upper 37.5 cm of the Skan Bay sediment column (Table 5.5a,b). Based on these data, the material flowing into and out of the sediment system had $\delta^{13}C$ values of $-20.1^{\circ}/oo$ and $-20.4^{\circ}/oo$, respectively. However, the total input flux (F_{IN}) exceeded the output flux (F_{OUT}) by approximately 700 $umol \cdot cm^{-2} \cdot yr^{-1}$ (Table 5.5a,b). As described above, this imbalance is linked to the DOC reservoir (Table 5.3), and may be due to (a) an underestimated DOC diffusive flux, or (b) underestimated DIC production rates.

Imposing overall mass-balance on the carbon cycle by increasing the DOC diffusive flux to 1190 $umol \cdot cm^{-2} \cdot yr^{-1}$ allows the $\delta^{13}C$ of input and output fluxes to match at $-20.1^{\circ}/oo$ (Table 5.5c). Conversely, if DIC production rates (and consequently the DIC diffusive flux) are increased so that total carbon input and output fluxes balance, the $\delta^{13}C$ ot the output flux becomes isotopically lighter than the input flux by $0.7^{\circ}/oo$ (Table 5.5c). Therefore, simultaneous mass balance for ^{12}C and ^{13}C can be achieved only by increasing the DOC flux. The isotope mass-balance calculation suggests that the DOC diffusive flux calculated from Fick's First Law was underestimated.

The Carbon Cycle Model: Summary

The carbon cycle in Skan Bay sediment (Fig. 5.2) is analogous to a chemical processing plant. Raw material from the water column (a 60:40

Table 5.5. Isotopic compositions of fluxes into and out of each
reservoir.

==

a. Fluxes into the system

Reservoir[a]	Flux ($umol \cdot cm^{-2} \cdot yr^{-1}$)	$\delta^{13}C$ (°/oo)
$^{d}_{z}(CH_4)$	49±15	−84.0
$^{a}_{o}(DIC)$	2±0.2	+0.3
$^{d}_{z}(DIC)$	25±25	+25.0
$^{d}_{z}(DOC)$	22±20	−21.1
$^{a}_{o}(POC)$	2290±480	−19.2
	F_{IN} = 2338±480	δ_{IN} = −20.1

b. Fluxes out of system

Reservoir[a]	Flux ($umol \cdot cm^{-2} \cdot yr^{-1}$)	$\delta^{13}C$ (°/oo)
$^{d}_{o}(CH_4)$	4±2	−79.0
$^{a}_{z}(CH_4)$	5±2	−77.3
$^{d}_{o}(DIC)$	306±167	−21.9
$^{a}_{z}(DIC)$	43±10	−13.4
$^{d}_{o}(DOC)$	456±211	−19.2
$^{a}_{z}(DOC)$	9±2	−21.7
$^{a}_{z}(POC)$	840±170	−20.2
	F_{OUT} = 1663±480	δ_{OUT} = −20.4

Table 5.5. Isotopic compositions of fluxes into and out of each reservoir (continued).

==

c. δ_{OUT} after imposing mass-balance by increasing DOC or DIC flux

Reservoir[a]	Flux ($umol \cdot cm^{-2} \cdot yr^{-1}$)	δ_{OUT} ($^o/oo$)
^d_o(DOC)	1190	-20.1
^d_o(DIC)	1013	-20.8

[a]Superscripts that precede the reservoir refer to advective (a) or diffusive (d) fluxes. Subscripts that precede the reservoir refer to upper (o) and lower (z) boundaries.

mixture of phytoplankton and kelp) is continuously fed into a primary reactor (POC reservoir) where it is converted to soluble products by means of enzyme-catalyzed reactions. About 60% of the material that enters the POC reservoir is labile. The material derived from kelp is degraded preferentially, accounting for greater than 60% of the total POC consumption.

The soluble products are transferred to a secondary reactor (DOC reservoir) where they are subjected to a series of fermentation and oxidation reactions. About 80% of the material that enters the DOC reservoir is transferred back to the water column prior to complete oxidation. The DOC fraction that is completely oxidized enters a final reactor (DIC reservoir) before leaving the sediment system by diffusion.

Additional raw material enters a tertiary reactor (CH_4 reservoir) by diffusion from depth. This material is nearly quantitatively oxidized, transferred to the DIC reservoir, and mixed with DOC-derived material prior leaving the system.

In addition, relatively small quantities of materials in the form of DIC and DOC enter the system via diffusion from depth. Organic carbon that resists degradation is enriched in phytoplankton-derived material and leaves the POC reservoir as refractory "sludge". PIC deposited in the sediment column does not appear to undergo reactions that are significant to the overall carbon cycle.

The possibility that Skan Bay sediment is inhabited by irrigating macrofauna during a portion of the year cannot be ruled out (see pp. 117 and 159). Therefore, it is necessary to consider the effect of seasonal bioirrigation on the carbon cycle model. The PIC and POC reservoirs

would be affected very little by burrow-dwelling organisms. The sediment X-radiograph (Fig. 3.12) documented that the solid phase was not bioturbated. Bioirrigation would influence pore water constituents by, in effect, increasing the diffusion coefficient. Methane fluxes would be affected little because concentrations in the irrigation zone are very low. Both DIC and DOC fluxes at the sediment-water interface would increase at the onset of bioirrigation. However, the DIC and DOC boundary fluxes are constrained by the rate of POC consumption, so the flux increase would be temporary.

Biogeochemical Rate Measurements

The carbon cycle (Fig. 5.2) provides a framework for integrating and evaluating biogeochemical rate measurements. In addition to SO_4^{2-} reduction rates, which were measured as part of this study, other published measurements of biogeochemical processes in Skan Bay sediment include acetate turnover rates (Shaw et al., 1984), H_2 production rates (Novelli et al., 1987), and total bacterial biomass and nucleic acid turnover (Craven, 1984). In this section, these measurements are interpreted in terms of the carbon cycle presented above.

Sulfate Reduction Rates

Sulfate is the dominant electron acceptor for organic matter remineralization in anoxic marine sediments (Henrichs and Reeburgh, 1987). The link between the carbon and sulfur cycles is often described by the following reaction (Berner, 1980):

$$2 \text{ POC } (CH_2O) + SO_4^{2-} = 2 \text{ DIC } (HCO_3^-) + HS^- + H^+. \qquad (5.9)$$
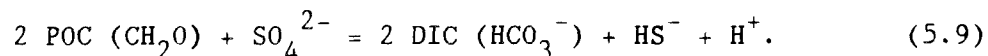
This equation contains three implicit assumptions: (a) POC has an average oxidation state (O) equal to that of carbohydrate carbon, (b) SO_4^{2-} is the only electron acceptor involved in organic matter remineralization, and (c) all POC consumed is oxidized to DIC.

The assumption that POC has an average oxidation state of zero is well-founded. Sediment POC is derived from phytoplankton and kelp material that is composed primarily of polysaccharides, proteins, and nucleic acids. The carbon in these biomolecules has an average oxidation state approximately equal to carbohydrate carbon.

The assumption that SO_4^{2-} is the dominant electron acceptor in anoxic marine sediments is also reasonable. Other possible electron acceptors include NO_3^- and metal oxides. Nitrate reduction does not contribute substantially to the sediment carbon cycle because of its low concentration. Metal oxides have been shown to play a minor role in the organic carbon oxidation process (Henrichs and Reeburgh, 1987).

The assumption that all consumed POC is oxidized to DIC does not appear to be valid for Skan Bay sediments. The average residence time for carbon in the DOC reservoir, calculated from the total DOC inventory (377 $umol \cdot cm^{-2}$) and total input flux (1580 $umol \cdot cm^{-2} \cdot yr^{-1}$), is about 90 days. This relatively slow turnover, along with large concentration gradients, suggests that dissolved organic material undergoes significant vertical transport during the time that it resides in the DOC reservoir (the mean diffusion distance for DOC in a 90 day period is about 5 cm). Diffusive migration of DOC is consistent with the carbon cycle model (Fig. 5.2), which predicted that a large proportion of the degraded POC diffuses across the sediment-water interface and is not

oxidized to DIC within the sediment column.

The relationship between SO_4^{2-} reduction and carbon remineralization (eq. 5.9) should be amended to acknowledge that (a) DOC production and consumption may not be tightly coupled, and (b) sulfate reducing bacteria utilize dissolved rather than particulate organic compounds (Fenchel and Blackburn, 1979):

$$2 \text{ DOC} + SO_4^{2-} = 2 \text{ DIC } (HCO_3^-) + HS^- + H^+ . \qquad (5.10)$$
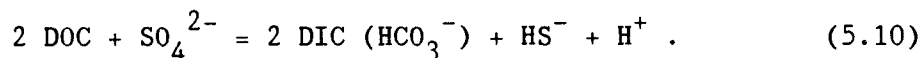
In addition, the relationship should recognize a possible link between anaerobic CH_4 oxidation and SO_4^{2-} reduction:

$$CH_4 + SO_4^{2-} = \text{DIC } (HCO_3^-) + HS^- + H_2O . \qquad (5.11)$$
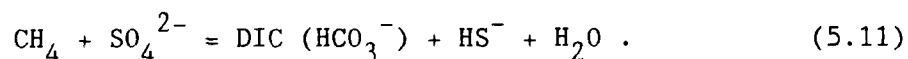
Although there is no experimental proof that CH_4 oxidation in nature is directly mediated by sulfate reducing bacteria, considerable circumstantial evidence suggests that the two processes are somehow linked (Alperin and Reeburgh, 1985).

Equations 5.10 and 5.11 provide a means of calculating sulfate reduction rates from DOC consumption and CH_4 oxidation rate data (Table 5.2):

$$\left\{\frac{d[SO_4^{2-}]}{dt}\right\}_{rxn} = 0.5\left\{\frac{d[DOC]}{dt}\right\}_{rxn} + \left\{\frac{d[CH_4]}{dt}\right\}_{rxn} . \qquad (5.12)$$

The SO_4^{2-} reduction rate profile calculated from eq. 5.12 (Fig. 5.3a) is qualitatively similar to that measured by the $^{35}SO_4^{2-}$ tracer technique (Fig. 3.6). Both profiles have a large primary maxima near the sediment-water interface, a secondary maxima located near the CH_4 oxidation zone, and low reaction rates at depths between the two maxima. However, modelled rates at the maxima are systematically lower than measured rates by a factor of 2 to 3.
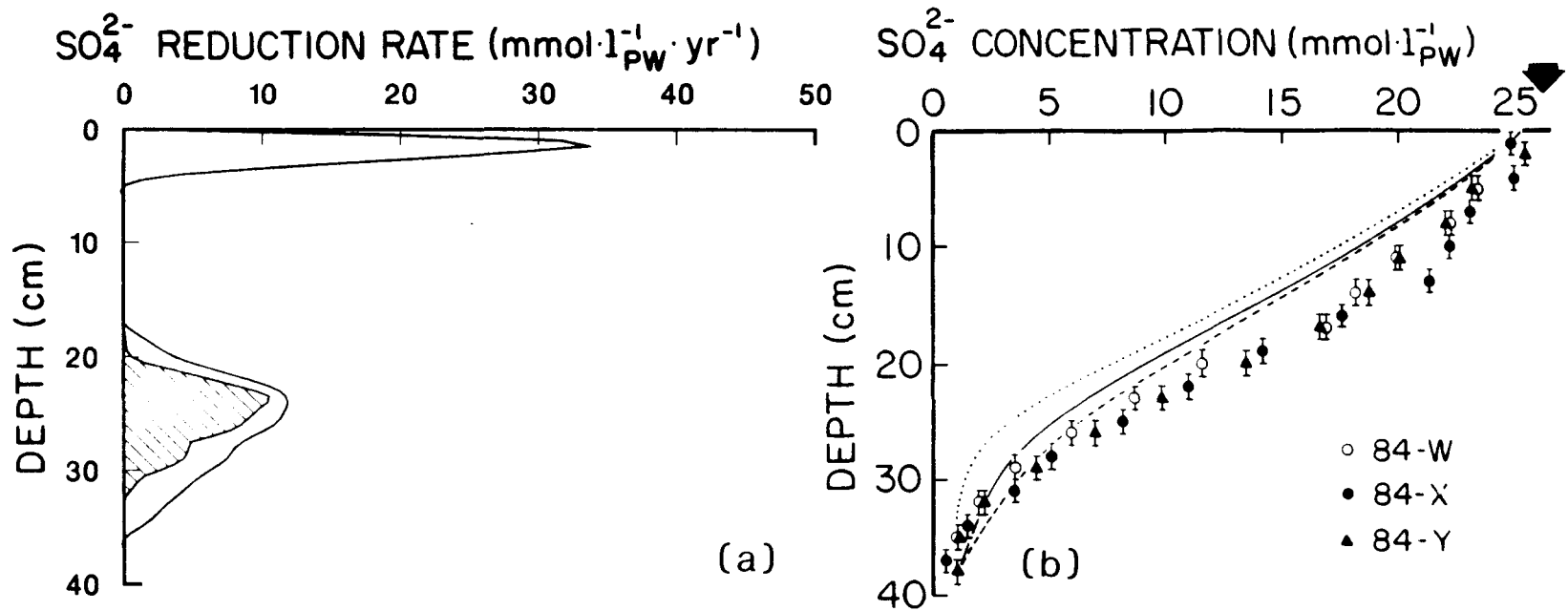
Fig. 5.3. Depth distributions of sulfate reduction rate and sulfate concentration predicted by the carbon cycle model. (a) Sulfate reduction rate (curve) and methane oxidation rate (hatched area) profiles, (b) measured (data points) and modelled (curve) sulfate profiles for three values of D_o (cm^2/yr): 170 (solid curve), 126 (dotted curve), and 214 (dashed curve). The large arrow represents the bottom water concentration.

The diagenetic equation (eq. 4.28) for SO_4^{2-} was solved using the SO_4^{2-} reduction rate profile predicted from eq. 5.12. The model-derived concentration profile agreed reasonably well with measured concentrations (Fig. 5.3b), suggesting that rates determined by the tracer technique were significantly overestimated. However, the model failed to reproduce the upward concavity apparent in the concentration data. The shape of the measured concentration profile requires that SO_4^{2-} be supplied to the sediment column by processes in addition to advection and molecular diffusion. As discussed in the previous chapter (p. 163), the Skan Bay SO_4^{2-} cycle may be influenced by sulfide oxidation and/or seasonal bioirrigation.

A secondary maxima in SO_4^{2-} reduction rate coincident with the maximum in CH_4 oxidation rate has been observed in several sediment systems (Devol et al., 1984; Iversen and Jørgensen, 1985; Alperin and Reeburgh, 1985), and is perhaps the strongest evidence of a link between the two processes. Crill and Martens (1987) suggested that oxidation of short-chain fatty acids may also contribute to the secondary rate maxima. In Skan Bay sediment, the model predicts that CH_4 oxidation accounts for about 60% of the SO_4^{2-} reduction at the secondary maxima (Fig. 5.3a).

Acetate Turnover Rates

Acetate is a key intermediate in the organic matter remineralization process, representing an end product of fermentation and a substrate for terminal metabolism (Fenchel and Blackburn, 1979). Acetate concentrations in Skan Bay sediment ranged from 4 to 12 uM (Shaw et al., 1984), accounting for a very small portion (0.2%) of the total DOC.

Acetate turnover rates were measured by a ^{14}C-acetate tracer technique. Rapid acetate oxidation relative to SO_4^{2-} reduction led Shaw et al. (1984) to suggest that measured acetate turnover rates were overestimated. A similar conclusion is reached when measured acetate oxidation rates are compared with the carbon cycle model (Fig. 5.2). The integrated acetate oxidation rate (0 to 36 cm) was 2600 umol·cm^{-2}·yr^{-1}. Since one mole acetate contains two moles carbon, the measured acetate oxidation is equivalent to production of 5200 umol C·cm^{-2}·yr^{-1}, which exceeds total POC consumption by a factor of three and DIC production by more than an order of magnitude (Table 5.3).

Hydrogen Production Rates

Fermentation is a metabolic process in which an organic substrate serves as both electron acceptor and electron donor (Fenchel and Blackburn, 1979). Fermenting bacteria are believed to be responsible for the breakdown of complex organic compounds to a form suitable for terminal metabolism. Many fermenting microorganisms dispose of "excess" electrons by passing H_2 to the environment (Doelle, 1975). Thus, H_2 production rates provide a measure of fermentation rates.

Hydrogen production rates in Skan Bay sediment were measured by monitoring H_2 accumulation in sediment samples amended with inhibitors of microbial H_2 consumption (Novelli et al., 1987). The integrated H_2 production rate for the upper 30 cm was estimated at <3 umol·cm^{-2}·yr^{-1}. This low rate suggests that hydrogen-producing fermenting bacteria play a quantitatively minor role in the overall Skan Bay carbon cycle.

The trend toward isotopically heavier DIC at depths greater than

25 cm (Fig. 3.8) is probably the result of isotope fractionation during CH_4 production from DIC (Claypool and Kaplan, 1974). Assuming that (a) DIC reduction with H_2 is the principle CH_4 producing pathway, (b) total CH_4 production and oxidation are equal (67.3 $umol \cdot cm^{-2} \cdot yr^{-1}$, Table 5.2), and (c) four moles H_2 react with one mole DIC to form one mole CH_4 (Fenchel and Blackburn, 1979), the integrated H_2 production rate required to support the CH_4 production is about 270 $umol \cdot cm^{-2} \cdot yr^{-1}$. Assuming that H_2 production rates in the CH_4 production zone (40 to >65 cm) are comparable to those in the upper 30 cm, rates measured by the inhibition method appear to be underestimated.

Nucleic Acid Turnover

Craven (1984) estimated microbial biomass and production in Skan Bay sediment by measuring ATP concentrations and rates of nucleic acid biosynthesis, respectively. Depth distributions of ATP biomass, POC consumption rate (Fig. 4.15b), and SO_4^{2-} reduction rate (Fig. 4.10a) have similar shapes with low values at the sediment surface, a sharp maximum at 5 cm, and diminished values at depth (the biomass data do not extend to the depth of the secondary maxima in SO_4^{2-} reduction rate). Assuming a biomass-carbon:ATP ratio of 250 (Karl, 1980), the living microbial biomass represents <0.05% of the total POC.

Nucleic acid synthesis rates, measured by a tracer technique employing ^{3}H-adenine, also had a depth distribution similar to POC consumption and SO_4^{2-} reduction. However, bacterial carbon production (2.3×10^5 $umol \cdot cm^{-2} \cdot yr^{-1}$), estimated from rates of nucleic acid biosynthesis, exceeded total POC consumption (1.6×10^3 $umol \cdot cm^{-2} \cdot yr^{-1}$) by two

orders of magnitude. Although POC recycling in the sediment (i.e. chemo-autotrophy) may be occurring, the magnitude of the discrepancy suggests that nucleic acid synthesis rates may be systematically overestimated.

Rate Measurements: Summary

The rate measurements and the carbon cycle model are not self-consistent: (a) measured SO_4^{2-} reduction rates are 2 to 3 times greater than those predicted from DOC and CH_4 oxidation, (b) acetate oxidation is 10 times greater than DIC production and 3 times greater than measured SO_4^{2-} reduction, (c) H_2 production rates are 100 times too slow to support the CH_4 production, and (d) bacterial carbon production is 100 times greater than total POC consumption and measured SO_4^{2-} reduction. These discrepancies underscore the difficulty of accurately determining in situ metabolic rates for a complex natural system. Lack of agreement for acetate turnover, H_2 production, and biomass production is not surprising. Experimental artifacts can result from manipulating, injecting, inhibiting, and incubating the sediment. However, measured SO_4^{2-} reduction rates in subtidal, anoxic marine sediments generally give results consistent with diagenetic models (Jørgensen, 1978b) and overall carbon budgets (Crill and Martens, 1987). The carbon cycle model for Skan Bay may be subject to revision when the exact cause of the "sulfate problem" (see p. 151) is identified.

The Carbon Cycle in Skan Bay Sediments: Epilogue

The objective of this study was to determine how the carbon cycle in an anoxic marine sediment "works". The operations that control carbon remineralization were deciphered by modelling concentration and isotope

ratio depth-distributions, and when possible, integrating the models with direct rate measurements. The approach that was taken here differs from other studies of organic-rich marine sediments in several respects. First, pool sizes and $\delta^{13}C$ values were determined for five carbon reservoirs (CH_4, DIC, DOC, PIC, and POC), so that all carbon within the sediment column was accounted for. Second, model-derived reaction rates were not biased by assuming simple kinetic rate laws for bacterially mediated reactions. And third, the sediment system was not arbitrarily divided into biogeochemical zones; rather, zonation emerged as a result of the data.

The results of this study differ from conventional wisdom in two ways. First, POC decomposition and DIC production were not tightly coupled. A portion of the hydrolyzed POC was lost from the sediment system by diffusion at the interface, while DOC remaining in the pore water was subject to redistribution prior to complete oxidation. This conclusion is supported by the following evidence: (a) the carbon budget requires a loss of DOC from the sediment system in order to achieve ^{12}C and ^{13}C mass-balance, (b) the very large DOC concentration gradient at the sediment-water interface, combined with a reasonable estimate for diffusion coefficient, argues for a sizable flux, and (c) the average residence time in the DOC reservoir (90 days) is sufficient for diffusive transport of DOC from the site where it was initially produced.

The carbon cycle presented in this study differs from conventional models in one other way: POC consumption and DIC production rates do not decrease monotonically with depth. Carbon remineralization in Skan Bay can be resolved into three distinct zones (Fig. 5.2). The first zone

(0 to 10 cm) is characterized by pronounced maxima in POC and DOC consumption rates. The second zone (10 to 20 cm) is a region where these processes slow down dramatically and rates change little with depth. In the third zone (20 to 35 cm), POC consumption maintains a slow rate while DIC production is augmented by oxidation of CH_4 diffusing up from depth.

Diagenetic changes in the isotopic composition of Skan Bay organic matter provided a means of linking POC decomposition rates to the source and reactivity of sediment organic matter. Diagenetic and isotope mass-balance models applied to POC and $\delta^{13}C$-POC depth distributions predicted that POC consumption in the uppermost zone is dominated by rapid kelp degradation while decomposition of planktonic algae occurs at relatively slow rates throughout the sediment column. Therefore, the zonation apparent in the Skan Bay carbon cycle is linked to the quantity and quality of carbon substrate. This "fine structure" is superimposed on biogeochemical zonation that results from sequential depletion of electron acceptors (Stumm and Morgan, 1970).

Future biogeochemical studies of organic-rich marine sediments should investigate the role of DOC in the organic matter remineralization process. Specifically, what is the composition of material in the DOC reservoir and how fast do different components turnover. Direct measurements of the DOC flux at the sediment-water interface would also be useful. Investigations of pore water DOC will require improved sampling and analytical methods that provide accurate measurements of the total pool size.

Sediment-water interface processes are another promising area of study. The role of motile (and possibly chemoautotrophic) sulfide oxidizing bacteria in the carbon and sulfur cycles is poorly understood. The release of ^{134}Cs and ^{137}Cs during the Chernobyl nuclear accident may provide an extremely sensitive tracer of particulate deposition rates at the interface (S. Sugai, Univ. of Alaska, personal communication).

Direct biogeochemical rate measurements require improved methods that better mimic in situ conditions. In addition, accurate rate measurements require a method of discriminating between microbially available and unavailable substrates.

Future studies in Skan Bay will require an understanding of how pore water chemical profiles are influenced by seasonal bottom water renewal. High resolution measurements of sediment ^{222}Rn distributions would provide information regarding temporal bioirrigation rates. Time series measurements of SO_4^{2-} concentration and reduction rates, even over a relatively short time period (e.g. 1 month), would help to constrain the extent of non-steady-state processes.

REFERENCES

Abelson, P. H. and Hoering, T. C. (1961) Carbon isotope fractionation in formation of amino acids by photosynthetic organisms. Proceed. Nat. Acad. Sci., 47, 623-632.

Ahlberg, J., Nilson, E. and Walsh, J. (1967) The Theory of Splines and Their Applications. Academic Press, 284 p.

Aller, R. C. and Rude, P. (1986) Anoxic oxidation of sulfides in surficial sediments. In Report on the Chemistry of Seawater, Chalmers University of Technology and University of Goteborg, Sweden.

Alperin, M. J. and Reeburgh, W. S. (1984) Geochemical observations supporting anaerobic methane oxidation. In Microbial Growth on C-1 Compounds (eds. R. L. Crawford and and R. S. Hanson), pp. 282-289, American Society for Microbiology.

Alperin, M. J. and Reeburgh, W. S. (1985) Inhibition experiments on anaerobic methane oxidation. Appl. Environ. Microbiol., 50, 940-945.

Barcelona, M. J. (1980) Dissolved organic carbon and volatile fatty acids in marine sediment pore waters. Geochim. Cosmochim. Acta, 44, 1977-1984.

Benninger, L. K. (1978) ^{210}Pb balance in Long Island Sound. Geochim. Cosmochim. Acta, 42, 1165-1174.

Berner, R. A. (1964) An idealized model of dissolved sulfate in recent sediments. Geochim. Cosmochim. Acta, 28, 1497-1503.

Berner, R. A. (1971) Principles of Chemical Sedimentology. Mcgraw-Hill, 240 p.

Berner, R. A. (1976) The solubility of calcite and aragonite in seawater at atmospheric pressure and 34.5^{o}/oo salinity. Am. J. Sci., 276, 713-730.

Berner, R. A. (1980) Early Diagenesis: a Theoretical Approach. Princeton University Press, 241 p.

Bigeleisen, J. (1965) Chemistry of isotopes. Science, 147, 463-471.

Bigeleisen, J. and Wolfsberg, M. (1958) Theoretical and experimental aspects of isotope effects in chemical kinetics. Adv. Chem. Phys., 1, 15-76.

Boehme, S. E. and Blair, N. E. (1986) Biogeochemical control of coastal sediment pore water CO_2 carbon isotopic composition. EOS, 67, 1058.

Broecker, W. S. and Peng, T.-H. (1982) Tracers in the Sea. Eldigio Press, 690 p.

Brown, F. S., Baedecker, M. J., Nissenbaum, A. and Kaplan, I. R. (1972) Early diagenesis in a reducing fjord, Saanich Inlet, British Columbia III. Changes in organic constituents of sediment. Geochim. Cosmochim. Acta, 36, 1185-1203.

Capone, D. G. and Kiene, R. P. (1987) Comparison of microbial dynamics in marine and freshwater sediments: pathways of anaerobic carbon catabolism. In Proceedings of the Symposium on the Comparative Ecology of Freshwater and Coastal Marine Ecosystems (ed. S. Nixon), in press.

Chanton, J. P. (1985) Sulfur mass balance and isotopic fractionation in an anoxic marine sediment. Ph.D. thesis, Univ. North Carolina, Chapel Hill.

Chanton, J. P., Martens, C. S. and Goldhaber, M. B. (1987) Biogeo-chemical cycling in an organic-rich coastal marine basin. 8. A sulfur isotopic budget balanced by differential diffusion across the sediment-water interface. Geochim. Cosmochim. Acta, 51, 1201-1208.

Cheney, W. and Kincaid D. (1980) Numerical Mathematics and Computing. Brooks/Cole Publishing Co., 362 p.

Christensen, D. and Blackburn (1982) Turnover of ^{14}C-labelled acetate in marine sediments. Mar. Biol., 71, 113-119.

Claypool, G. E. and Kaplan, I. R. (1974) The origin and distribution of methane in marine sediments. In Natural Gases in Marine Sediments, (ed. I. R. Kaplan), pp. 99-139, Plenum Publishing Corp.

Cline, J. D. and Richards, F. A. (1969) Oxygenation of hydrogen sulfide in seawater at constant salinity, temperature, and pH. Env. Sci. Technol., 3, 838-843.

Coplan, T. B., Kendall, C. and Hopple, J. (1983) Comparison of stable isotope reference samples. Nature, 302, 236-238.

Craig, H. (1953) The geochemistry of stable carbon isotopes. Geochim. Cosmochim. Acta, 3, 53-92.

Craig, H. (1957) Isotopic standards for carbon and oxygen and correction factors for mass-spectrometric analysis of carbon dioxide. Geochim. Cosmochim. Acta, 12, 133-149.

Craven, D. B. (1984) Nucleic acid synthesis measurements in sediment

microbial communities: methods developement and field application. MS thesis, Univ. Hawaii.

Crill, P. M. and Martens, C. S. (1987) Biogeochemical cycling in an organic-rich coastal marine basin. 6. Temporal and spatial variations in sulfate reduction rates. Geochim. Cosmochim. Acta, **51**, 1175-1186.

Dawson, H. J., Hrutfiord, B. F., Zasoski, R. J. and Ugolini, F. C. (1981) The molecular weight and origin of yellow organic acids. Soil Science, **132**, 191-199.

Deines, P. (1970) Mass spectrometer correction factors for the determination of small isotopic composition variations of carbon and oxygen. Int. J. Mass Spectrom. Ion Phys., **4**, 283-295.

Deines, P. (1980) The isotopic composition of reduced organic carbon. In Handbook of Environmental Isotope Geochemistry, Vol. 1 (eds. P. Fritz and J. Ch. Fontes), pp. 329-406, Elsevier.

DesMarais, D. J. (1983) Methods for stable carbon isotopic analysis. In Planetary Biology and Microbial Ecology: Biochemistry of Carbon and Early Life (eds. L. Margulis, K. H. Nealson and I. Taylor), pp. 123-125, NASA Technical Memorandum 86043.

DesMarais, D. J. and Hayes, J. M. (1976) Tube cracker for opening glass-sealed ampoules under vacuum. Anal. Chem., **48**, 1651-1652.

Devol, A. H. (1983) Methane oxidation rates in the anaerobic sediments of Saanich Inlet. Limnol. Oceanogr., **28**, 738-742.

Devol, A. H. (1987) Verification of flux measurements made with in situ benthic chambers. Deep-Sea Res., **34**, 1007-1026.

Devol, A. H. and Ahmed, S. I. (1981) Are high rates of sulfate reduction associated with anaerobic oxidation of methane? Nature, **291**, 407-408.

Devol, A. H., Anderson, J. J., Kuivila, K. and Murray, J. W. (1984) A model for coupled sulfate reduction and methane oxidation in the sediments of Saanich Inlet. Geochim. Cosmochim. Acta, **48**, 993-1004.

Doelle, H. W. (1975) Bacterial Metabolism. Academic Press, 738 p.

Doose, P. R. (1980) The bacterial production of methane in marine sediments. Ph.D. thesis, Univ. California, Los Angeles.

Emrich, K., Ehhalt, D. H., Vogel, J. C. (1970) Carbon isotope fractionation during the precipitation of calcium carbonate. Earth Planet. Sci. Lett., **8**, 363-371.

Fenchel, T. and Blackburn, T. H. (1979) Bacterial and Mineral Cycling. Academic Press, 225 p.

Feux, A. N. (1980) Experimental evidence against an appreciable isotopic fractionation of methane during migration. Phys. Chem. Earth, 12, 725-732.

Flett, R. J., Hamilton, R. D. and Campbell, E. N. (1976) Aquatic acetylene-reduction techniques: solutions to several problems. Can. J. Microbiol., 22, 43-51.

Galimov, E. M. (1985) The Biological Fractionation of Isotopes. Academic Press, 261 p.

Gershey, R. M., MacKinnon, M. D., Williams, P. J. le B. and Moore, R. M. (1979) Comparison of three oxidation methods used for the analysis of the dissolved organic carbon in seawater. Mar. Chem., 7, 289-306.

Goldhaber, M. B. (1974) Equilibrium and dynamic aspects of the marine geochemistry of sulfur. Ph.D. thesis, Univ. California, Los Angeles.

Goldhaber, M. B., Aller, R. C., Cochran, J. K., Rosenfeld, J. K., Martens, C. S., and Berner, R. A. (1977) Sulfate reduction, diffusion, and bioturbation in Long Island Sound sediments: report of the FOAM group. Am. J. Sci., 277, 193-237.

Goldhaber, M. B. and Kaplan, I. R. (1980) Mechanisms of sulfur incorporation and isotope fractionation during early diagenesis in sediments of the Gulf of California. Mar. Chem., 9, 95-143.

Goulden, P. D. and Anthony, D. H. J. (1978) Kinetics of uncatylzed peroxydisulfate oxidation of organic material in fresh water, Anal. Chem.. 50, 953-958.

Grossman, E. L. (1984) Carbon isotopic fractionation in live benthic formanifera - comparison with inorganic precipitate studies. Geochim. Cosmochim. Acta, 48, 1505-1512.

Hayes, J. M. (1982) Fractionation, et al.: an introduction to isotopic measurements and terminology. Spectra, 8, 3-8.

Henrichs, S. M. and Reeburgh, W. S. (1987) Anaerobic mineralization of marine sediment organic matter: rates and role of anaerobic processes in the oceanic carbon economy. Geomicrobiol. J., 5, 191-237.

Hoefs, J. (1980) Stable Isotope Geochemistry, Springer-Verlag, 241 p.

Hornbeck, R. W. (1975) Numerical Methods. Quantum Publishers, 310 p.

Howarth, R. W. and Jørgensen, B. B. (1984) Formation of ^{35}S-labelled elemental sulfur and pyrite in coastal marine sediments (Limfjorden and Kysing Jford, Denmark) during short-term sulfate reduction measurements. Geochim. Cosmochim. Acta, 48, 1807-1818.

Ingle, S. E., Culberson, C. H., Hawley, J. and Pytkowicz, R. M. (1973) The solubility of calcite in seawater at atmospheric pressure and 35°/oo salinity. Mar. Chem., 1, 295-307.

Iversen, N. and Jørgensen, B. B. (1985) Anaerobic methane oxidation rates at the sulfate-methane transition in marine sediments from Kattegat and Skagerrak (Denmark). Limnol. Oceanogr., 30, 944-955.

Jørgensen, B. B. (1977) Bacterial sulfate reduction within reduced microniches of oxidized marine sediments. Mar. Biol., 41, 7-17.

Jørgensen, B. B. (1978a) A comparsion of methods for the quantification of bacterial sulfate reduction in coastal marine sediments. I. Measurement with radiotracer techniques. Geomicrobiol. J., 1, 11-27.

Jørgensen, B. B. (1978b) A comparsion of methods for the quantification of bacterial sulfate reduction in coastal marine sediments. II. Calculation from mathematical models. Geomicrobiol. J., 1, 29-47.

Jørgensen, B. B. (1979) A theoretical model of the stable sulfur isotope distribution in marine sediments. Geochim. Cosmochim. Acta, 43, 363-374.

Jørgensen, B. B. (1982) Ecology of the bacteria of the sulfur cycle with special reference to anoxic-oxic interface environments. Phil. Trans. R. Soc. Lond., B 298, 543-561.

Jørgensen, B. B. (1983) Processes at the sediment-water interface. In The Major Biogeochemcial Cycles and Their Interactions (eds. B. Bolin and R. B. Cook), pp. 477-509, J. Willey.

Jost, W. (1960) Diffusion in Solids, Liquids, and Gases. Academic Press, 558 p.

Kaplan, I. R. and Rittenberg, S. C. (1964) Carbon isotope fractionation during metabolism of lactate by Desulfovibrio desulfuricans. J. Gen. Microbiol., 34, 213-217.

Karl, D. M. (1980) Cellular nucleotide measurements and application in microbial ecology. Microbiol. Rev., 44, 739-796.

Kiene, R. P. and Capone, D. G. (1985) Degassing of pore water methane during sediment incubations. Appl. Environ. Microbiol., 49, 143-147.

King, G. M. (1986) Characterization of β-glucosidase activity in intertidal marine sediments. Appl. Environ. Microbiol., 51, 373-380.

Knauss, J. A. (1978) Introduction to Physical Oceanography. Prentice-Hall, 338 p.

Kolthoff, I. M., Sandell, E. B., Meehan, E. J. and Bruckenstein, S. (1969) Quantitative Chemical Analysis. Macmillan, 1199 p.

Kristensen, E. and Blackburn, T. H. (1987) The fate of organic carbon and nitrogen in experimental marine sediment systems: influence of bioturbation and anoxia. J. Mar. Res., 45, 231-257.

Krom, M. D. and Berner, R. A. (1980) The diffusion coefficients of sulfate, ammonium, and phosphate ions in anoxic marine sediments. Limnol. Oceanogr., 25, 327-337.

Krom, M. D. and Sholkovitz, E. R. (1977) Nature and reactions of dissolved organic matter in the interstitial waters of marine sediments. Geochim. Cosmoschim. Acta, 41, 1565-1573.

Krom, M. D. and Westrich, J. T. (1980) Dissolved organic matter in the pore waters of recent marine sediments; a review. In Biogochimie de la Matiere Organique a l'Interface Eau-sediment Marin, Colloques Internationaux du C.N.R.S., pp. 103-111.

Krumbein, W. E. and Swart, P. G. (1983) The microbial carbon cycle. In Microbial Geochemistry (ed. W. E. Krumbein), pp. 5-62, Blackwell Scientific.

Krzycki, J. A., Kenealy, W. R., DeNiro, M. J. and Zeikus, J. G. (1987) Stable carbon isotope fractionation by Methanosarcina barkeri during methanogenesis from acetate, methanol, or carbon dioxide-hydrogen. Appl. Environ. Microbiol., 53, 2597-2599.

Kuivila, K. M. (1986) Methane production and cycling in marine and freshwater sediments. Ph.D. thesis, Univ. Washington.

Lehninger, A. L. (1975) Biochemistry. Worth Publishers, 1104 p.

Lerman, A. (1979) Geochemical Processes: Water and Sediment Environments. Wiley, 481 p.

Li, Y.-H. and Gregory, S. (1974) Diffusion of ions in sea water and in deep-sea sediments. Geochim. Cosmochim. Acta, 38, 703-714.

Linkens, A. E., Melillo, J. M. and Sinsabaugh, R. L. (1984) Factors affecting cellulase activity in terrestrial and aquatic ecosystems. In Current Perspectives in Microbial Ecology (eds. M. J. Klug and C. A. Reddy), pp. 572-579, American Society for Microbiology.

Lloyd, R. M. (1964) Variations in the oxygen and carbon isotope ratios of Florida Bay mollusks and their environmental significance. J. Geol., 72, 84-111.

Lovelock, J. E. (1979), Gaia: A New Look at Life on Earth. Oxford University Press, 157 p.

MacKinnon, M. D. (1978) A dry method for the analysis of the TOC in seawater. Mar. Sci., 7, 17–37.

Martens, C. S. (1984) Recycling of organic carbon near the sediment-water interface in coastal environments. Bull. Mar. Sci., 35, 566–577.

Martens, C. S. and Berner, R. A. (1977) Interstitial water chemistry of Long Island Sound sediments. I. Dissolved gases. Limnol. Oceanogr., 22, 10–25.

Martens, C. S. and Klump, J. V. (1980) Biogeochemical cycling in an organic-rich coastal marine basin - 1. Methane sediment-water exchange processes. Geochim. Cosmochim. Acta, 44, 471–490.

Martens, C. S. and Klump, J. V. (1984) Biogeochemical cycling in an organic-rich coastal marine basin. 4. An organic carbon budget for sediments dominated by sulfate reduction and methanogenesis. Geochim. Cosmochim. Acta, 48, 1987–2004.

Mason, E. A. and Marerro, T. J. (1970) The diffusion of atoms and molecules. Adv. At. Mol. Phys., 6, 155–232.

Mehrbach, C., Culberson, C. H., Hawley, J. E. and Pytkowicz, R. M. (1973) Measurements of the apparent dissociation constants of carbonic acid in seawater at atmospheric pressure. Limnol. Oceanogr., 18, 897–907.

Miller, L. G. (1980) Dissolved inorganic carbon isotope ratios in reducing marine sediments. M.S. thesis, Univ. South. California.

Mills, R. and Harris, K. R. (1976) The effect of isotopic substitution on diffusion in liquids. Chem. Soc. Rev., 5, 215–231.

Minagawa, M., Winter, D. A., and Kaplan, I. R. (1984) Comparison of Kjeldahl and combustion methods for measurement of nitrogen isotope ratios in organic matter. Anal. Chem., 56, 1859–1861.

Murray, J. W., Grundmanis, V. and Smethie, W. M. Jr. (1978) Interstitial water chemistry in the sediments of Saanich Inlet. Geochim. Cosmochim. Acta, 42, 1011–1026.

Nelson, D. C. and Jannasch, H. W. (1983) Chemoautotrophic growth of a marine Beggiatoa sulfide-gradient cultures. Arch. Microbiol., 136, 262–269.

Nelson, D. C., Revsbech, N. P. and Jørgensen, B. B. (1986) Microoxic-anoxic niche of Beggiatoa spp.: microelectrode survey of marine and freshwater strains. Appl. Environ. Microbiol., 52, 161–168.

Nissenbaum, A., Baedecker, M. J. and Kaplan, I. R. (1971) Studies on dissolved organic matter from interstital water of a reducing marine fjord. In Advances in Organic Geochemistry, 1971, (eds. H. R. v. Gaertner and H. Wehner), pp. 427-440, Pergamon Press.

Nissenbaum, A., Presley, B. J. and Kaplan, I. R. (1972) Early diagenesis in a reducing fjord, Saanich Inlet, British Columbia - I. Chemical and isotopic changes in major components of interstitial water. Geochim. Cosmochim. Acta, 36, 1007-1027.

Novelli, P. C., Scranton, M. I. and Michener, R. H. (1987) Hydrogen in marine sediments. Limnol. Oceanogr., 32, 565-576.

O'Leary, M. H. (1969) The carboxyl carbon isotope effect on the enzymatic decarboxylation of glutamic acid. J. Amer. Chem. Soc., 91, 6886-6887.

O'Leary, M. H. (1984) Measurement of the isotope fractionation associated with diffusion of carbon dioxide in aqueous solution. J. Phys. Chem., 88, 823-825.

Orem, W. H., Hatcher, P. G., Spiker, E. C., Szeverenyi, N.M. and Maciel, G. E. (1986) Dissolved organic matter in anoxic pore waters from Mangrove Lake, Bermuda. Geochim. Cosmochim. Acta, 50, 609-618.

Oremland, R. S. (1987) The biogeochemistry of methanogenic bacteria. In Environmental Microbiology of Anaerobes (ed. A. J. B. Zehnder), J. Wiley and Sons, pp. 405-467

Oremland, R. S. and DesMarais, D. J. (1983) Distribution, abundance, and carbon isotopic composition of gaseous hydrocarbons in Big Soda Lake, Nevada: an alkaline, meromictic lake. Geochim. Cosmochim. Acta, 47, 2107-2114, 1983.

Reeburgh, W. S. (1967) An improved interstitial water sampler. Limnol. Oceanogr. 12, 163-165.

Reeburgh, W. S. (1976) Methane consumption in Cariaco Trench waters and sediments. Earth Planet. Sci. Lett., 28, 337-344.

Reeburgh, W. S. (1980) Anaerobic methane oxidation: rate depth distributions in Skan Bay sediments. Earth Planet. Sci. Lett., 47, 345-352.

Reeburgh, W. S. (1982) A major sink and flux control for methane in marine sediments: anaerobic consumption. In The Dynamic Environments of the Ocean Floor (eds. K. Fanning and F. T. Manheim), pp. 203-217, Heath.

Reeburgh, W. S. (1983) Rates of biogeochemical processes in anoxic sediments. Ann. Rev. Earth Planet. Sci., 11, 269-297.

Reeburgh, W. S. and Heggie, D. T. (1977) Microbial methane consumption reactions and their effect on methane distributions in fresh water and marine environments. Limnol. Oceanogr., 22, 1-9.

Rees, C. E. (1973) A steady-state model for sulphur isotope fractionation in bacterial reduction processes. Geochim. Cosmochim. Acta, 37, 1141-1162.

Reimers, C. E. and Smith, K. L. Jr. (1986) Reconciling measured and predicted fluxes of oxygen across the deep sea sediment-water interface. Limnol. Oceanogr., 31, 305-318.

Revsbech, N. P., Sørensen, J., Blackburn, T. H. (1980) Distribution of oxygen in marine sediments measured with microelectrodes. Limnol. Oceanogr., 25, 403-411.

Romankevich, E. A. (1984) Geochemistry of organic matter in the ocean. Springer-Verlag, 334 p.

Rosenfeld, W. D. and Silverman, S. R. (1959) Carbon isotope fractionation in bacterial production of methane, Science, 130, 1658-1659.

Sahores, J. J. and Witherspoon, P. A. (1970) Diffusion of light paraffin hydrocarbons in water from $2^{\circ}C$ to $80^{\circ}C$. In Advances in Organic Geochemistry, 1966 (ed. G. C. Spears), pp. 219-230, Pergamon Press.

Sansone, F. J. (1986) Depth distribution of short-chain organic acid turnover in Cape Lookout Bight sediments. Geochim. Cosmochim. Acta, 50, 99-105.

Sayles, F. L., Mangelsdorf, P. C. Jr., Wilson, T. R. S. and Hume D. N. (1976) A sampler for in situ collection of marine sedimentary pore waters. Deep-Sea Res., 23, 259-264.

Schoell, M., Faber, E. and Coleman, M. L. (1983) Carbon and hydrogen isotopic compositions of the NBS 22 and NBS 21 stable isotope reference materials: an inter-laboratory comparison. Org. Geochem., 5, 3-6.

Shaw, D. G., Alperin, M. J., Reeburgh, W. S. and McIntosh, D. J. (1984) Biogeochemistry of acetate in anoxic sediments of Skan Bay, Alaska. Geochim. Cosmochim. Acta, 48, 1819-1825.

Sofer, Z. (1980) Preparation of carbon dioxide for stable carbon isotope analysis of petroleum fractions. Anal. Chem., 52, 1389-1391.

Sørensen, J., Christensen, D. and Jørgensen, B. B. (1981) Volatile fatty acids and hydrogen as substrates for sulfate-reducing bacteria in anaerobic marine sediment. Appl. Environ. Microbiol., 42, 5-11.

Spiker, E. C. and Hatcher, P. G. (1984) Carbon isotope fractionation of sapropelic organic matter during early diagenesis. Org. Geochem., 4, 283-290.

Stern, M. J. and Vogel, P. C. (1971) Relative $^{14}C-^{13}C$ kinetic isotope effects. J. Chem. Phys., 55, 2007-2013.

Stumm, W. and Morgan, J. J. (1970) Aquatic Chemistry. Wiley-Interscience, 583 p.

Sugai, S. F. (1985) Processes controlling trace metal and nutrient geochemistry in two southeastern Alaskan Fjords. Ph.D. thesis, Univ. of Alaska.

Thompson, L. A., Nedwell, D. B., Balba, M. T., Banat, I. M. and Senior, E. (1983) The use of multiple-vessel, open flow systems to investigate carbon flow in anaerobic microbial communities. Microbiol. Ecol., 9, 189-199.

Ullman, W. J. and Aller, R. C. (1982) Diffusion coefficients in near-shore marine sediments. Limnol. Oceanogr., 27, 552-556.

USERDA Health and Safety Laboratory environmental quarterly (1970) HASL 329, Final tabulation of monthly Sr-90 fallout data: 1954-1976 (National Technical Information Service).

Weiss, R. F. and Craig, H. (1973) Precise shipboard determination of dissolved nitrogen, oxygen, argon, and total inorganic carbon by gas chromatography. Deep-Sea Res., 20, 291-303.

Westrich, J. T. and Berner, R. A. (1984) The role of sedimentary organic matter in bacterial sulfate reduction: the G model tested. Limnol. Oceanogr., 29, 236-249.

Whiticar, M. J. and Faber, E. (1986) Methane oxidation in sediment and water column environments - isotope evidence. Org. Geochem., 10, 759-768.

Wilson, R. F. (1961) Measurement of organic carbon in sea water. Limnol. Oceanogr., 6, 251-261.

Woeller, F. H. (1961) Liquid scintillation counting of $^{14}CO_2$ with phenethylamine. Anal. Biochem., 2, 508-511.

Yamamoto, S., Alcauskas, J. B. and Carozier, T. E. (1976) Solubility of methane in distilled water and seawater. J. Chem. Eng. Data, 21, 78-80.

APPENDIX I: DATA TABLES

Table A.1. Porosity.

===

Subcore 84-C		Subcore 84-F	
Depth (cm)	ϕ	Depth (cm)	ϕ
0-2.8	0.995	0-2.9	0.991
2.8-5.8	0.955	2.9-5.8	0.973
5.8-8.8	0.934	5.8-8.9	0.909
8.8-12.0	0.924	8.9-11.9	0.899
12.0-15.2	0.903	11.9-15.0	0.877
15.2-18.6	0.896	15.0-18.3	0.877
18.6-21.7	0.896	18.3-21.3	0.876
21.7-24.7	0.907	21.3-24.3	0.889
24.7-27.8	0.894	24.3-27.3	0.859
27.8-30.8	0.884	27.3-30.4	0.864
30.8-33.7	0.878	30.4-33.2	0.876
33.7-36.6	0.870	33.2-36.0	0.857
36.6-39.4	0.862	36.0-39.0	0.855

Subcore 84-D		Gravity core 84-1	
Depth (cm)	ϕ	Depth (cm)	ϕ
0-2.9	0.993	23.2-26.5	0.883
2.9-6.0	0.943	30.0-33.4	0.847
6.0-9.1	0.930	42.6-46.1	0.846
9.1-12.3	0.918	49.1-52.2	0.856
12.3-15.4	0.895	54.6-57.6	0.813
15.4-18.7	0.891	61.1-63.7	0.853
18.7-21.8	0.895	63.7-66.6	0.850
21.8-24.8	0.891	69.8-72.9	0.844
24.8-27.9	0.892	75.9-79.0	0.794
27.9-30.9	0.881	81.7-84.7	0.821
30.9-33.4	0.875	88.0-90.6	0.831
33.4-36.2	0.866	90.6-93.4	0.835
36.2-39.0	0.860		

Table A.2. Methane concentrations.

Depth (cm)	Methane Concentration (mM_{PW}) Subcore		
	84-H	84-I	84-J
Bottom Water	ND	ND	ND
1-2	ND	0.010	0.051
4-5	0.073	0.032	0.115
7-8	0.129	0.129	0.204
10-11	0.262	0.284	0.317
13-14	0.443	0.421	0.509
16-17	0.560	0.604	0.705
19-20	0.801	0.835	0.993
22-23	1.23	1.10	1.46
25-26	1.68	1.69	2.18
28-29	2.30	2.38	2.91
31-32	3.99	NA	4.23

Depth (cm)	Methane Concentration (mM_{PW}) Subcore		
	84-K	84-L	84-M
1-2	0.020	0.031	0.011
4-5	0.073	0.094	0.031
7-8	0.086	0.129	0.118
10-11	0.131	0.197	0.175
13-14	0.221	0.310	0.277
16-17	0.313	0.459	0.369
19-20	0.463	0.699	0.530
22-23	0.647	0.829	0.704
25-26	0.844	1.16	0.901
28-29	1.28	1.68	1.18
31-32	NA	2.58	1.88
34-35	NA	3.18	2.45

NA = Data not available.
ND = Not detectable.

Table A.2. Methane concentrations (continued).

===

| | Methane Concentration (mM_{PW}) | | |
| | ------------------Subcore------------------ | | |
Depth (cm)	84-N	84-O	84-P
2-3	0.021	0.010	0.010
5-6	0.042	0.042	0.021
8-9	0.065	0.065	0.043
11-12	0.110	0.110	0.077
14-15	0.189	0.167	0.133
17-18	0.236	0.281	0.247
20-21	0.486	0.452	0.351
23-24	0.875	0.898	0.853
26-27	1.07	1.37	NA
29-30	2.22	NA	NA

| | Methane Concentration (mM_{PW}) | | |
| | ------------------Subcore------------------ | | |
Depth (cm)	84-Q	84-R	84-S
0-1	ND	ND	ND
3-4	ND	ND	ND
6-7	0.011	0.021	0.011
9-10	0.033	0.054	0.033
12-13	0.110	0.132	0.066
15-16	0.178	0.201	0.178
18-19	0.270	0.315	0.315
22-23	0.408	0.431	0.478
24-25	0.604	0.604	0.660
27-28	0.937	0.869	0.960
30-31	1.42	1.35	1.70
33-34	2.13	1.99	2.26
36-37	2.90	NA	NA

NA = Data not available.
ND = Not detectable.

Table A.2. Methane concentrations (continued).

```
==================================================================
          Gravity Core 84-1              Gravity Core 84-2
      Depth (cm)    [CH₄] (mM_PW)     Depth (cm)    [CH₄] (mM_PW)
      ----------    ------------      ----------    ------------
```

Gravity Core 84-1		Gravity Core 84-2	
Depth (cm)	$[CH_4]$ (mM_{PW})	Depth (cm)	$[CH_4]$ (mM_{PW})
11-12	0.110	12-13	0.088
14-15	0.167	15-16	0.223
17-18	0.337	18-19	0.551
20-21	0.543	21-22	0.782
23-24	1.03	24-25	1.28
26-27	1.50	27-28	2.03
29-30	2.03	30-31	2.69
32-33	3.03	33-34	3.64
35-36	2.95	36-37	4.33
38-39	4.49	39-40	5.30
41-42	5.35	42-43	6.93
44-45	6.16	45-46	7.79
47-48	7.49	49-50	8.94
50-51	6.80	51-52	9.14
53-54	7.87	54-55	9.54
56-57	8.55	57-58	11.7
59-60	14.7	60-61	12.1
62-63	11.7	63-64	12.4
65-66	12.5	66-67	12.5
		69-70	10.8
		72-73	12.1
		75-76	11.5
		81-82	11.7
		84-85	10.3

Table A.3. Methane oxidation rates.

Subcore	Depth (cm)	[CH_4] (mM$_{PW}$)	Rate (mM$_{PW}$·yr^{-1})
84-T	0-2	0.010	0.0002
	3-5	0.010	0.0003
	6-8	0.043	0.0064
	9-11	0.098	0.0060
	12-14	0.188	0.0137
	15-17	0.257	0.187
	18-20	0.361	0.233
	21-23	0.454	0.428
	24-26	0.581	1.59
	27-29	1.40	2.20
	30-32	1.49	1.74
	33-35	1.71	1.26
	36-38	2.52	0.484
84-U	0-2	0.020	0.0009
	3-5	0.042	0.0020
	6-8	0.064	0.0034
	9-11	0.098	0.0051
	12-14	0.144	0.0068
	15-17	0.201	0.165
	18-20	0.270	0.494
	21-23	0.386	0.944
	24-26	0.490	1.97
	27-29	0.949	4.52
	30-32	1.46	1.02
	33-35	2.14	1.44
	36-38	2.87	0.181
84-V	2-4	0.021	0.0009
	5-7	0.042	0.0023
	8-10	0.076	0.0048
	11-13	0.121	0.0148
	14-16	0.234	0.0182
	17-19	0.326	0.127
	20-22	0.475	0.248
	23-25	0.558	1.80
	26-28	0.845	4.42
	29-31	1.26	1.62
	32-34	2.10	1.89
	35-37	2.36	0.655
	38-40	2.70	0.397

Table A.4. Sulfate concentrations.

Subcore	Depth (cm)	$[SO_4^{2-}]$ (mM_{PW})
Bottom Water		26.1
84-W	1-3	25.4
	4-6	23.3
	7-9	22.1
	10-12	19.9
	13-15	18.1
	16-18	16.8
	19-21	11.5
	22-24	8.6
	25-27	5.9
	28-30	3.5
	31-33	2.0
	34-36	1.0
	37-39	0.96
84-X	0-2	24.8
	3-5	24.9
	6-8	23.0
	9-11	22.1
	12-14	21.2
	15-17	17.5
	18-20	14.1
	21-23	10.9
	24-26	8.1
	27-29	5.1
	30-32	3.4
	33-35	1.4
	36-38	0.56
84-Y	1-3	25.4
	4-6	23.2
	7-9	22.0
	10-12	20.0
	13-15	18.7
	16-18	16.6
	19-21	13.4
	22-24	9.8
	25-27	6.9
	28-30	4.4
	31-33	2.1
	34-36	1.1
	37-39	0.99

Table A.5. Sulfate reduction rates.

==

| Depth (cm) | $[SO_4^{2-}]$ (mM_{PW}) | Sulfate Reduction Rate ($mM_{PW} \cdot yr^{-1}$) | | |
| | | --------------Subcore--------------- | | |
		84-Z	84-AA	84-BB
1-3	25.2	12.8	3.55	31.6
4-6	23.6	88.6	75.1	52.5
7-9	22.3	46.4	38.1	34.0
10-12	20.6	31.8	41.5	27.1
13-15	18.9	21.6	22.0	18.4
16-18	16.5	15.1	15.4	16.8
19-21	12.6	8.04	11.8	12.5
22-24	9.4	8.47	11.0	13.7
25-27	6.7	11.5	9.60	14.1
28-30	4.1	19.2	18.7	21.8
31-33	2.3	24.5	25.2	35.6
34-36	1.1	18.2	24.7	18.5
37-39	0.82	5.28	27.6	11.9

Table A.6. Stable carbon isotope ratios and pool sizes.

Bottom Water

$[CH_4]$ (mM$_{PW}$)	$\delta^{13}C-CH_4$ ($^o/oo$)	$[DIC]$ (mM$_{PW}$)	$\delta^{13}C-DIC$ ($^o/oo$)	$[DOC]$ (mM$_{PW}$)	$\delta^{13}C-DOC$ ($^o/oo$)
0.0003	NA	2.23	−0.1	ND	NA
		2.13	0.6		

Subcore 84−A

Depth (cm)	$[CH_4]$ (mM$_{PW}$)	$[DIC]$ (mM$_{PW}$)	$[DOC]$ (mM$_{PW}$)	$[PIC]$ (mmol·g$_{SM}^{-1}$)	$[POC]$ (mmol·g$_{SM}^{-1}$)
0−2.8	0.014	4.43	6.44	0.689	6.97
2.8−5.7	0.042	5.58	12.1	0.699	6.14
5.7−8.8	0.114	8.85	13.1	0.476	4.08
8.8−11.9	0.241	13.1	13.5	0.551	3.62
11.9−14.9	0.423	16.1	12.3	0.670	3.70
14.9−18.0	0.537	21.0	10.5	0.679	3.43
18.0−21.1	0.706	26.3	10.2	0.764	3.39
21.1−24.3	0.869	31.0	7.67	0.666	3.45
24.3−27.3	1.40	34.3	9.35	0.723	3.29
27.3−30.8	2.33	37.8	10.0	0.886	3.03
30.8−34.0	3.82	40.6	8.23	0.831	3.21
34.0−37.0	4.73	42.6	6.77	0.946	2.72
37.0−39.8	5.26	43.1	8.37	1.04	2.55

Depth (cm)	$\delta^{13}C-CH_4$ ($^o/oo$)	$\delta^{13}C-DIC$ ($^o/oo$)	$\delta^{13}C-DOC$ ($^o/oo$)	$\delta^{13}C-PIC$ ($^o/oo$)	$\delta^{13}C-POC$ ($^o/oo$)
0−2.8	NA	−10.7	−19.0	−1.2	−19.4
2.8−5.7	−72.5	−12.0	−18.6	−1.0	−19.6
5.7−8.8	−71.9	−14.7	−19.6	−0.3	−20.6
8.8−11.9	−71.6	−16.7	−19.1	−0.3	−20.6
11.9−14.9	−70.9	−17.7	−20.4	−0.4	−20.6
14.9−18.0	−70.8	−17.9	−19.4	−0.3	−20.3
18.0−21.1	−70.2	−19.4	−20.9	0.2	−20.7
21.1−24.3	−70.3	−18.9	−22.0	0.3	−20.3
24.3−27.3	−72.6	−18.7	−22.1	0.3	−20.3
27.3−30.8	−74.8	−17.5	−22.1	0.5	−20.0
30.8−34.0	−75.4	−15.3	−20.6	0.2	−20.2
34.0−37.0	−75.4	−13.9	−21.3	0.2	−20.4
37.0−39.8	−75.4	−12.6	−21.6	0.1	−20.3

NA = Data not available.
ND = Not detectable.

Table A.6. Stable carbon isotope ratios and pool sizes (continued).

===

Subcore 84-B

Depth (cm)	$[CH_4]$ (mM_{PW})	$[DIC]$ (mM_{PW})	$[DOC]$ (mM_{PW})	$[PIC]$ $(mmol \cdot g_{SM}^{-1})$	$[POC]$ $(mmol \cdot g_{SM}^{-1})$
0-2.8	0.020	3.98	7.60	0.750	6.97
2.8-5.8	0.088	7.64	14.6	0.540	4.95
5.8-9.0	NA	10.4	16.3	0.534	3.96
9.0-12.2	0.315	14.1	19.7	0.452	3.91
12.2-15.3	0.445	19.2	13.8	0.801	3.50
15.3-18.7	0.602	22.1	9.62	0.717	3.25
18.7-21.9	0.795	28.2	9.09	0.719	3.43
21.9-25.1	1.17	35.6	7.50	0.718	3.25
25.1-28.3	2.43	39.8	10.8	0.871	2.87
28.3-31.3	3.92	40.5	7.16	0.806	2.95
31.3-34.0	4.70	46.8	6.23	1.01	2.55
34.0-36.4	4.06	47.2	8.79	0.948	2.69
36.4-39.3	4.12	47.4	9.47	0.906	2.71

Depth (cm)	$\delta^{13}C-CH_4$ $(^o/oo)$	$\delta^{13}C-DIC$ $(^o/oo)$	$\delta^{13}C-DOC$ $(^o/oo)$	$\delta^{13}C-PIC$ $(^o/oo)$	$\delta^{13}C-POC$ $(^o/oo)$
0-2.8	NA	-9.6	-19.3	-1.1	-19.5
2.8-5.8	-70.8	-14.1	-19.0	-0.9	-20.0
5.8-9.0	NA	-15.0	-19.4	-0.1	-20.5
9.0-12.2	-70.2	-17.2	-19.3	-0.3	-20.4
12.2-15.3	-70.1	-18.5	-20.0	-0.5	-20.2
15.3-18.7	-69.3	-18.3	-21.3	-0.3	-20.5
18.7-21.9	-69.2	-19.0	-22.2	0.0	-20.4
21.9-25.1	-71.6	-18.7	-23.4	0.6	-20.1
25.1-28.3	-74.8	-17.5	-22.2	0.3	-20.1
28.3-31.3	-75.2	-14.9	-21.7	0.1	-20.2
31.3-34.0	-75.2	-13.3	-22.1	0.2	-20.2
34.0-36.4	-74.9	-12.0	-21.9	0.3	-20.4
36.4-39.3	-75.1	-11.0	-21.6	0.3	-20.0

NA = Data not available.

Table A.6. Stable carbon isotope ratios and pool sizes (continued).

==

Subcore 84-E

Depth (cm)	$[CH_4]$ (mM_{PW})	$[DIC]$ (mM_{PW})	$[DOC]$ (mM_{PW})	$[PIC]$ $(mmol \cdot g_{SM}^{-1})$	$[POC]$ $(mmol \cdot g_{SM}^{-1})$
0-1.4	0.023	5.09	9.51	0.871	7.30
1.4-2.9	0.033	5.37	13.3	0.844	7.81
2.9-5.9	0.071	8.28	13.8	0.792	5.85
5.9-9.0	0.130	12.2	13.2	0.830	3.45
9.0-12.1	0.204	15.4	12.5	0.461	3.51
12.1-15.4	0.308	18.5	10.1	0.672	3.37
15.4-18.6	0.420	23.1	8.33	0.683	3.31
18.6-21.6	0.512	27.6	8.03	0.640	2.74
21.6-24.7	0.601	31.1	8.15	0.939	2.75
24.7-28.0	0.856	32.6	6.15	0.921	2.80
28.0-31.3	1.51	35.6	6.01	1.03	2.60
31.3-34.5	2.46	35.9	5.97	1.01	2.49
34.5-37.8	3.42	36.9	7.77	0.966	2.71

Depth (cm)	$\delta^{13}C-CH_4$ $(^o/oo)$	$\delta^{13}C-DIC$ $(^o/oo)$	$\delta^{13}C-DOC$ $(^o/oo)$	$\delta^{13}C-PIC$ $(^o/oo)$	$\delta^{13}C-POC$ $(^o/oo)$
0-1.4	NA	-13.6	-19.0	-1.9	-19.1
1.4-2.9	NA	-13.8	-19.1	-1.3	-19.3
2.9-5.9	NA	-15.3	-18.4	-0.8	-19.6
5.9-9.0	-74.2	-17.6	-20.0	-0.1	-20.6
9.0-12.1	-73.2	-19.1	-19.5	-1.3	-20.0
12.1-15.4	-74.1	-20.2	-20.7	-0.6	-20.6
15.4-18.6	-74.3	-20.7	-21.5	0.0	-20.3
18.6-21.6	-74.5	-20.9	-21.4	0.4	-20.0
21.6-24.7	-75.3	-21.3	-21.7	0.0	-20.2
24.7-28.0	-77.7	-20.6	-23.1	0.1	-20.9
28.0-31.3	-80.3	-19.8	-22.8	0.2	-20.2
31.3-34.5	-81.6	-18.4	-22.6	0.2	-20.1
34.5-37.8	-81.5	-16.8	-22.1	0.2	-20.3

NA = Data not available.

Table A.6. Stable carbon isotope ratios and pool sizes (continued).

===

Gravity core 82-1

Depth (cm)	$[CH_4]$ (mM_{PW})	$[DIC]$ (mM_{PW})	$[DOC]$ (mM_{PW})	$[PIC]$ $(mmol \cdot g_{SM}^{-1})$	$[POC]$ $(mmol \cdot g_{SM}^{-1})$
57.6-61.1	NA	NA	6.35	0.536	1.82
66.6-69.8	3.94	46.5	6.18	0.686	1.59
72.9-75.9	NA	NA	8.78	0.956	1.94
79.0-81.7	4.26	57.6	8.14	0.761	1.72
84.7-88.0	5.73	60.5	10.32	0.907	1.44
93.4-96.6	5.04	59.5	8.47	0.720	1.93

Depth (cm)	$\delta^{13}C-CH_4$ $(^o/oo)$	$\delta^{13}C-DIC$ $(^o/oo)$	$\delta^{13}C-DOC$ $(^o/oo)$	$\delta^{13}C-PIC$ $(^o/oo)$	$\delta^{13}C-POC$ $(^o/oo)$
57.6-61.1	NA	NA	-22.2	-0.4	-19.9
66.6-69.8	-79.6	-6.3	-22.7	-0.2	-20.4
72.9-75.9	NA	NA	-23.3	-0.2	-19.9
79.0-81.7	-77.2	-1.6	-22.2	-0.2	-20.0
84.7-88.0	-79.2	-2.7	-22.9	-0.2	-20.0
93.4-96.6	-76.7	1.0	-22.8	-0.3	-21.2

NA = Data not available.

Table A.7. Hydrogen sulfide concentrations.

===

Subcore	Depth (cm)	$[H_2S]$ mM$_{PW}$
80-A	0-2	0.77
	5-7	1.01
	9-11	2.49
	13-15	3.68
	17.5-20	4.01
	22-25	4.19
	27-32	2.15
	33.5-37	1.97
80-B	0-2.5	0.98
	2.5-5.0	0.45
	5.0-7.0	0.90
	10-12	2.76
	14-16.5	3.20
	16.5-20	2.87
	20-24	4.43
	24-28	4.68
81-A	0-5	1.18
	5-7	1.90
	7-9	3.55
	9-11	4.44
	14-17	4.02
	20-23	6.44
	26-29	5.75
	32-35	5.47
82-A	0-3	0.87
	6-9	1.87
	12-15	1.95
	18-21	2.07
	24-27	1.47
	30-33	1.42

APPENDIX II: DIFFERENTIAL ISOTOPIC DIFFUSION

From the definition of the $\delta^{13}C$ scale (eq. 1.3), the ratio of ^{13}C to ^{12}C for a pore water constituent is given by:

$$\frac{[^{13}C]_{PW}}{[^{12}C]_{PW}} = \{\frac{\delta}{1000} + 1\} R , \tag{A.1}$$

where δ is the $\delta^{13}C$ value and R is the $^{13}C{:}^{12}C$ ratio for the PDB reference standard. Differentiating both sides of eq. A.1 with respect to depth and rearranging:

$$\frac{d[^{13}C]_{PW}}{dz} = [^{12}C]_{PW} \frac{R}{1000} \frac{d\delta}{dz} + \frac{[^{13}C]_{PW}}{[^{12}C]_{PW}} \frac{d[^{12}C]_{PW}}{dz} . \tag{A.2}$$

The diffusive fluxes for ^{13}C and ^{12}C components of a pore water constituent are given by eq. 5.5:

$$^{13}F_{diff} = \phi^3 \, ^{13}D_o \, d[^{13}C]_{PW}/dz , \tag{A.3}$$

and

$$^{12}F_{diff} = \phi^3 \, ^{12}D_o \, d[^{12}C]_{PW}/dz . \tag{A.4}$$

The $\delta^{13}C$ value of material diffusing through a boundary (δ_{diff}) is given by the following equation (Chanton et al., 1987):

$$\delta_{diff} = \{\frac{^{13}F_{diff}/^{12}F_{diff}}{R} - 1\} \, 1000 . \tag{A.5}$$

Substituting eqs. A.3 and A.4 into eq. A.5:

$$\delta_{diff} = \{\frac{1}{R \, f} \frac{d[^{13}C]_{PW}/dz}{d[^{12}C]_{PW}/dz} - 1\} \, 1000 , \tag{A.6}$$

where f is the molecular diffusivity ratio for ^{12}C and ^{13}C.

Substituting eq. A.2 into eq. A.6 and rearranging,

$$\delta_{diff} = \frac{1}{f} \{ [^{12}C]_{PW} \frac{d\delta}{d[^{12}C]_{PW}} + \delta + (1-f) \ 1000 \} \ . \qquad (A.7)$$

Since $[^{12}C]_{PW} \cong [C]_{PW}$,

$$\delta_{diff} \cong \frac{1}{f} \{ [C]_{PW} \frac{d\delta}{d[C]_{PW}} + \delta + (1-f) \ 1000 \} \ . \qquad (A.8)$$

If the diffusion coefficients for light and heavy isotopic species differ by less than $10^o/oo$, eq. A.8 can be further simplified with little loss of accuracy:

$$\delta_{diff} \cong \{ [C]_{PW} \frac{d\delta}{d[C]_{PW}} + \delta + (1-f) \ 1000 \} \ . \qquad (A.9)$$

If sampling resolution is sufficiently fine that the $\delta^{13}C-[C]_{PW}$ gradient between two adjacent data points can be taken as constant, the differentials in eq. A.9 can be approximated by differences:

$$\delta_{diff} \cong \{ [C]_{PW} \frac{\Delta\delta}{\Delta[C]_{PW}} + \delta + (1-f) \ 1000 \} \ , \qquad (A.10)$$

where $\Delta\delta$ and $\Delta[C]_{PW}$ are the differences in $\delta^{13}C$ and concentration for two adjacent data points, δ and $[C]_{PW}$ are average $\delta^{13}C$ and concentration for the two data points, and δ_{diff} is the $\delta^{13}C$ value of material diffusing through a horizon half-way between the two data points.

Chanton et al. (1987) demonstrated that differential isotopic diffusion leads to intuitively surprising results. For example, if concentrations and $\delta^{13}C$ values change from 8 to 10 mM and -10 to $-12^o/oo$, respectively, eq. A.10 predicts that material diffusing through a horizon intermediate between the two points will have a $\delta^{13}C$ value of $-20^o/oo$ (D_o values for both isotopic species were assumed to be equal).